AXISYMMETRIC TURHULENT JETS

W.M. VOGEL

AXISYMMETRIC TURBULENT JETS
AND WAKES THAT ARE SELF-PRESERVING

By

William M. Vogel

A thesis submitted to the Faculty of Graduate Sudies and Research in partial fulfilment of the requirements for the degree of Doctor of Philosophy

Department of Mechanical Engineering
McGill University
Montreal, P.Q. June, 1974

Summary

Axisymmetric free turbulent jets and wakes may be self-similar if the external flow has a suitable adverse pressure gradient. Five such flows were measured; one wake and four jets. All flows were found to be satisfactorily self-preserving in both mean and turbulent quantities and the non-dimensional turbulence levels are also found to be almost the same for all flows.

An open-jet wind tunnel was built and a perforated working section was added to produce the desired pressure gradients. The flows were measured using hot-wire anemometer connected to an on-line computer.

Two integral theories are developed to predict the growth. The first uses Townsend's (1956) original large eddy equilibrium hypthesis. The second, more satisfactory theory uses the integral energy equation by Townsend (1966), but includes a more appropriate relation relating the shear stress to the turbulent energy.

Sommaire

Le développement de jets ou de sillages ronds, dans un milieu fluide en mouvement, peut se faire en équilibre ("self-preserving") si l'écoulement exterieur est modifié par un gradient de pression positif. Cette thèse contient un ensemble de résultats concernant ce type d'écoulement. On a établi en laboratoire cinq jets et un sillage où l'écoulement était en équilibre relatif à la fois au profil des vitesse de l'écoulement moyen et de l'écoulement de fluctuation. On a trouvé, entre autres, que l'intensité relative de la turbulence était semblable dans tous les cas.

Pour effectuer les mesures on a construit une soufflerie ronde dans laquelle le jet ou le sillage évoluait au centre. Le gradient de pression a été établi a la fois en bloquant la sortie de la soufflerie et en entourant l'écoulement exterieur de grillages avec une densité de perforation variable.

Deux théories de type "integral" ont été utilisées pour calculer le développement des écoulements. La premiere utilise l'hypothèse de Townsend (1956) selon laquelle les gros tourbillons sont en équilibre. La deuxième constitue une amélioration d'une autre théorie de Townsend (1966), et utilise: (1) l'equation de la somme de l'énergie moyenne et turbulente; et (2) une relation entre la tension et l'énergie turbulente.

ACKNOWLEDGEMENTS

The author is indebted to Dr. B.G. Newman for his guidance and advice during the course of this work. He never lost his faith that this thesis would be completed while others, including the author, doubted.

Mr. Alex Gustavsen built the traversing gear, helped with the construction of the wind tunnel, and generally provided the skill to build the numerous pieces of apparatus needed for this experiment. The late Einar Hansen did much of the construction of the wind tunnel, and brought to this task the skills from many years as a cabinet maker. The author is indebted to both these men.

Thanks are also due to Mr. L. Vroomen of the DATAC Computing Center. He aided the author in developing a computer-controlled data collecting system on what was then a very new computer system.

The author would like to thank the members of the Aero Group for many interesting informal discussions which were an important part of being a graduate student.

Thanks are also due to Miss Wendy Smith who cheerfully and speedily transformed a much corrected draft into tidy typewritten pages.

During this work the author was the recipient of a Defence Research Board of Canada scholarship, and the work was also supported by this organization under D.R.B. Grant Number 9551-12.

TABLE OF CONTENTS

Note: Due to an error in numbering there is no equation (79) in the main text.

NOTATION

Capital Letters

A - $\frac{\partial U}{\partial y}$ at specified point in flow

B - $\frac{\partial U}{\partial x}$ at specified point in flow

C_0 - $\frac{dL_0}{dx}$

C_1 - scale factor from $U_1=C_1(x-x_0)^m$

C_p - pressure drop coefficient for screens and perforated plates

C_{p_0} - value of C_p for unblocked screen in flow perpendicular to screen or perforated plate

D - diameter of pipe

E - energy dissipation parameter $\left(\frac{L_0\varepsilon}{U_0^3}\right)$

F - general function of x and y

G - $\frac{U_0}{U_1}$

H - turbulent energy parameter $\left(\frac{\overline{q_0^2}}{U_0^2}\right)$

$I_1(\eta)$ - $\int_0^\eta \eta f(\eta)d\eta$

$I_2(\eta)$ - $\int_0^\eta \eta f^2(\eta)d\eta$

$I_3(\eta)$ - $\int_0^\eta \eta f^3(\eta)d\eta$

I_4 - $\int_0^\infty \eta Hh(\eta)d\eta$

I_5 - $\int_0^\infty \eta f(\eta) Hh(\eta) d\eta$

I_6 - $\int_0^\infty \eta E d\eta$

L, L_1 - measure of large eddy size, subscript$_1$ refers to value for B=0

L_0 - distance from centerline of flow to point where velocity increment (or decrement) is half of maximum

M - Mach number

P - kinematic mean pressure, also polynomial in G

P_0 - kinematic total pressure

P_∞ - kinematic ambient pressure

Re - Reynolds number

R_T - turbulent Reynolds number $\left(\frac{U_0 L_0}{\nu_T}\right)$

U - mean velocity in x-direction

U_0 - difference between velocity at centerline of jet or wake and the free stream velocity

U_1 - free stream velocity in x-direction

U_F - mean velocity in x-direction at end of tunnel working section

V - mean velocity in y-direction

Y - radius of working section

Small Letters

a_1, a_2, a_3 - constants from Equ. (44), also coefficients used in fitting velocity for setting up working section tape pattern

b - jet (or wake body) diameter

e_1, e_2, e_3, e_4 - constants used in theory using integral energy equation

f - mean velocity shape factor ($e^{-k\eta^2}$)

g - shear stress parameter $\left(\frac{\overline{uv}}{U_0^2}\right)$

g_0 - shear stress parameter at $y=L_0$

$h(\eta)$ - shape factor for turbulent energy distribution

k - constant$=\ln(2)=.693$

m - growth exponent for self-preserving flow, ($U_1 \propto (x-x_0)^m$)

n - exponent relating shear stress and turbulent kinetic energy to total strain

p - fluctuating kinematic pressure

p* - static pressure when M=1

p_0 - stagnation pressure, also $\frac{\overline{q}^2}{2}+p$

$\overline{q}^2$ - $\overline{u}^2+\overline{v}^2+\overline{w}^2$

$\overline{q}_0^2$ - $\overline{q}^2$ at center of flow

u - fluctuating component of velocity in x-direction

v - fluctuating component of velocity in y-direction

w - fluctuating component of velocity in θ-direction

x - distance along symmetry axis of flow, measured from start of working section

x_0 - x-position of virtual origin of flow

y - distance radially outwards from symmetry axis of flow.

$y_{.5}$ - average position of boundary between vortical and non-vortical fluid in jet or wake

Greek Letters

α - constant in relation for g_0 in large eddy hypothesis, also total strain.

α_{max} - maximum total strain

β, β_Q - constants in relation for g_0 in large eddy hypothesis

γ - constant relating shear stress to turbulent kinetic energy for still air jet, defined in equation (84)

ε - kinematic energy dissipation rate

λ - pipe flow friction factor $\left(\Delta p = \frac{\lambda}{D} \frac{\rho U^2}{2}\right)$

η - similarity parameter $\left(\frac{y}{L_0}\right)$

ρ - fluid density

σ - length for Gaussian weighting in predicting working section flow, also standard deviation of boundary between vortical and non-vortical fluid in jets and wakes

1. Introduction

1-1 Self-preserving Flows

In this thesis jets and wakes in streaming flow are considered and emphasis is placed on predicting their mean flow characteristics. Such flows are of interest in the design of, for example, jet pumps, thrust augmenters, and combustion chambers. Since the difference between the central velocity and the surrounding streaming flow velocity decreases with downstream distance the possibility exists that such flows can be self-preserving (self-similar) if the free stream velocity is also reduced in the downstream direction, i.e., if the jet (or wake) were in a suitable adverse pressure gradient.

A self-preserving flow is of interest because of the theoretical simplicity of its description. Partial differential equations are replaced by ordinary differential equations and since all properties scale with a single velocity and length scale, the non-dimensional properties of the turbulent structure can be unambiguously related to the properties of the mean flow. Consequently, experimental information on such flows can provide useful tests for theories relating such quantities.

The required free-stream velocity for self-preserving flow is obtained from the mean momentum and turbulence energy equations. These define the necessary mean flow conditions for a self-preserving flow to exist. Whether or not such a flow will be self-preserving can only be answered by experiment or further theoretical development. For example, the mean momentum equation says that both the small-deficit two-dimensional and axisymmetric wakes in zero pressure gradient are possible approximately self-preserving flows. The existence of the two-dimensional self-preserving flow is well established experimentally, but the axisymmetric one does not seem to become self-preserving, at least not universally. Work by Baldwin and Sandborn (1968), Gibson et al (1968), Bukreev et al (1973), and Antonia and Bilger (1973) have all lent support to this finding. It is interesting that Townsend (1970) predicts this difference between these two types of wakes.

Another theoretically possible self-preserving flow that does not become self-preserving in practice is the laterally strained two-dimensional wake as studied by Reynolds (1962).

The experimental study of self-preserving free shear flows has naturally had to follow their theoretical recognition. In the case of symmetric jets and wakes the first to be examined was the jet in still surroundings, and axisymmetric and two-dimensional flows have been extensively studied. (Table 4-9 has information on some of the work on the axisymmetric jet in still surroundings). Both these jet flows seem well established as self-preserving cases, although there appear to be unexplainably large variations in measured turbulent quantities from one experiment to another.

Only fairly recently has it been recognized that the still-air jet is but one member of a family of self-preserving jets and wakes in a pressure gradient. Patel and Newman (1962) developed this concept for two-dimensional wall jets and free jets. The concept was then developed in general for both two-dimensional and axisymmetric free jets and wakes by Newman (1967).

Even more recently the small-deficit wake in zero pressure gradient has also been recognized as one member of a family of approximately self-preserving wakes and jets in pressure gradients by Gartshore and Newman (1969).

1-2 Integral Methods of Analysis

One of the most striking characteristics of both two-dimensional and axisymmetric free jets and wakes is the similarity of the mean increment or decrement velocity profiles, both in the streamwise direction in a particular flow and among flows of different character (Halleen (1964), Harsha (1971)). This makes the use of an integral method of analysis particularly attractive, as it not only reduces the motion equations to ordinary differential equations, but also makes the effect of turbulent models more apparent.

A jet in uniform streaming flow, which is physically simple, is theoretically more difficult to analyse. It cannot be self-preserving except close to the jet origin (where it might behave like a jet in still surroundings) and far downstream (where it might be expected to approach a self-preserving small-deficit wake behaviour). But even the latter may not be possible for the axisymmetric jet.

A number of approaches have been used to try and predict the behaviour of this jet flow. Squire and Trouncer (1944) used a mixing length proportional to the flow width and obtained the constant of proportionality from the jet in still surroundings. This does not take into account the substantial change in the turbulent structure as the flow changes from a strong jet to a weak, small-increment jet. See, for example, Bradbury and Riley (1967).

Other workers have explicitly or implicitly used a frame of reference moving with the fluid to deal with the streaming flow cases, using information from the strong jet. Examples are Kruka and Eskinazi (1963) and Patel (1970).

Bradbury and Riley (1967) measured the development of plane jets in zero pressure gradient with varying ratios of initial jet to free stream velocity. They obtained a satisfactory collapse of the results using excess momentum and the distance from a virtual origin as scaling parameters. However, the position of the virtual origin varies so much between flows that the method cannot be used as a basis for prediction.

Bilger (1968) has attempted to predict the plane jet measured by Bradbury and Riley (and others), and the plane wake measured by Townsend and others, using the total energy equation proposed by Townsend (1966). He obtains good correlation between experiment and his theory, but the variation of virtual origin is still not dealt with. In a later work Bilger (1969) attempts to use the same approach for the axisymmetric jet and wake, but without much success. He ascribes this to a lack of strong structure for the small increment jet (and small-deficit wake).

For predicting the behaviour of axisymmetric jets in streaming flow with a pressure gradient, Hill has developed a quite successful method using an integral approach and assuming that R_T (a turbulent Reynolds number defined from a velocity and length scale of the flow and the turbulent viscosity) is a constant and equal to the value for the jet in still surroundings. The theory adequately predicts the static pressure even after the jet has impinged on the walls of the duct and there is some backflow.

Two reviews, by Halleen (1964) and Harsha (1971), are of interest, and the proceedings of a conference on free turbulent shear flows (NASA Langley (1973)) have been published.

1-2-1 The Large Eddy Equilibrium Model

A model used to relate the turbulent structure to the mean motion was proposed by Townsend (1956) and was independently developed and used to predict the behaviour of two-dimensional free jets, wall jets, and wakes by Gartshore (1964), (1965) and Bradbury (1967). This approach postulated that the turbulent Reynolds number (R_T) could be calculated as a function of the ratio of the mean transverse to longitudinal rates of strain at some representative point in the flow.

This function involved two empirical constants which were to be evaluated from the growth rates for the jet in still surroundings and the small-deficit wake in zero pressure gradient.

Since the theory is essentially a mixing length theory, with the mixing length proportional to the large eddy size rather than flow width, the turbulent Reynolds number should be inversely proportional to the square of this eddy size for a given class of flows. Gartshoré (1966) checked this by measuring intermittency in a number of two-dimensional shear flows and assuming that the standard deviation of the bounding surface between turbulent and non-turbulent fluid was a measure of large eddy size. The agreement with theory was quite good.

However, the theoretical basis for the large eddy equilibrium hypothesis is now in some doubt. Townsend (1966) first raised these doubts, and postulated a different mechanism (Section 1-2-2) to control the process of entrainment.

Both models involve an equilibrium between the large eddies which define the shape of the boundary between vortical and non-vortical fluid and the smaller eddies that contain the bulk of the turbulent energy. Also, both models attempt to explain how the entrainment process is controlled by this interaction. The difference is in how this control process is postulated to act.

In the earlier theory, the transfer of energy from the mean flow is envisioned as a two-step process, with energy transferred first from the mean flow to the large eddies by a process of stretching. The stretching is accompanied by rotation which affects the energy transfer by changing the orientation of the eddy until no more energy can be added. The second step is a transfer of energy from these large eddies to the smaller eddies. This second step is also accomplished by stretching, but of the smaller eddies, and may be described by an apparent eddy viscosity. Thus the growth and decay of the large eddies is controlled in a quasi-viscous manner.

Townsend's (1966) later criticisms of his earlier work were threefold. He used a uniform two-dimensional fluid flow around a strip of fluid with a higher viscosity and, possibly, a different density to model the behaviour of the bounding surface of a turbulent wake characterized by an eddy viscosity. He then showed that such a surface is unstable to disturbances of all wave number. This is not in agreement with experiment which indicates that only disturbances of a narrow range of wave number are amplified. Furthermore, the entrainment predicted by this process is shown to vary proportionally to the ratio of the density of the ambient fluid to the mean jet density. While the experimental evidence for this is not so convincing, it does support the belief that the prediction is incorrect.

Thirdly he objected to his earlier theory on the grounds that it fails to provide the reduced entrainment into a boundary layer in zero pressure gradient. According to Gartshore's formulation this reduced entrainment would require a positive $\partial U/\partial x$ which does not exist.

1-2-2 The Townsend Entrainment Model

As an alternative to his previous model, Townsend (1966) advanced a model in which the incremental stresses induced by disturbances of the boundary surface of the turbulence are resisted in a quasi-elastic way by the turbulent structure. If the energy containing eddies are distorted rapidly then the anisotropy and accompanying shearing stress is proportional to the incremental strain, rather than rate of strain, and an elastic model is thus appropriate. This model predicts that only disturbances of a certain wave number are unstable and thus amplified. He shows that this is in qualitative, and, to a reasonable extent, quantitative agreement with the measured experimental behaviour of the boundary surface. Furthermore, this model predicts that the entrainment varies with the square root of the ratio of the densities, and this is in somewhat better agreement with experiment.

In his second paper Townsend (1970) investigated the details of the turbulent structure associated with the quasi-elastic behaviour of the rapid distortion theory. Thus a relation exists connecting the turbulent shearing stress, $\overline{uv}$, to the total turbulent kinetic energy per unit mass $(\overline{q^2}/2)$. This relation is a function of the average total strain experienced by an eddy during its lifetime. The effective strain is predicted by an equation which includes a diffusive term to account for the fact that eddies which arrive at a certain place have been strained by different amounts due to the turbulence itself. It is therefore appropriate to assume that the associated diffusivity coefficient is approximately equal to ν_T, the turbulent eddy viscosity. He showed that for a range of flows the ratio of total strain to turbulent Reynolds number is approximately constant.

Newman (1968), following suggestions from Townsend (1966), used the total energy integral equation and two integrals of the momentum equation to develop two prediction methods for two-dimensional self-preserving free jets and wakes. The first method linked these equations by using the concept of geometric similarity expressed as $\overline{uv}/\overline{q^2}$ = constant at a representative point in the flow. The second method used a mixing length model, expressed as $\overline{uv} \propto \sqrt{\overline{q^2}}\, U_0$ at this representative point, to link the equations.

Fekete (1970) compares the prediction of the large eddy hypothesis and of the two variations on the entrainment model to Gartshore's (1967) self-preserving wake results, and his own measurements on two-dimensional self-preserving jets. He finds that the predictions using the large eddy hypothesis and those of the entrainment model using the mixing length assumption both do a reasonable job of predicting the growth of these flows.

It is worth noting that both models (the large eddy equilibrium model and the entrainment model) by Townsend predict that the lateral displacement of the bounding surface is essentially proportional to a mixing length, so that Gartshore's (1966) work that shows the square of the standard deviation of the bounding surface varying inversely as R_T is in agreement with this newer theory as well.

1-3 Field Methods of Analysis

In recent years the availability of large digital computers has led to the development of boundary layer prediction methods in which the basic, time averaged partial differential equations describing the motion are solved numerically. The methods differ in the number of equations which are modelled. Early methods merely used a mixing length or eddy viscosity formula for the shearing stress (e.g. Mellor and Herring (1968)) and modelled the streamwise momentum equation and the continuity equation. In later methods the shearing stress was obtained from the turbulence energy equation assuming structural similarity of the turbulence (Bradshaw et al (1967), Glushko (1965)). A model equation for the dissipation of turbulence energy has been added (Spalding (1969)), and the latest methods attempt to model the equations for the individual components of the turbulent stress tensor (Launder et al (1973), Donaldson (1972)).

Those methods are capable of handling complex flows and appear to give good results. No doubt the experiments described in this thesis will provide useful test cases for these methods, but the methods themselves have not been considered in the present work.

1-4 Scope of Present Work

1-4-1 Theory

The basic theory describing axisymmetric turbulent jets and wakes that are self-preserving is developed in Section 2-1. Following Newman (1967), (1968) and using an assumed, universal velocity profile, the mean momentum and total energy equations are transformed to integral equations describing these axisymmetric flows.

In Sections 2-2 and 2-3 two prediction methods are developed to use these basic equations to deal with those flows. The previous development and use of these two models, the large eddy equilibrium model and the entrainment model, has already been described in Section 1-2-1 and 1-2-2.

The conversion of the first theory for axisymmetric flow was first given by Vogel (1968), (1969) and is presented in somewhat different form in Section 2-2. Some modifications to the original theory postulated by Gartshore had to be introduced to overcome the prediction of what appeared to be unreasonable values of growth for medium strehgth jets in both two-dimensional and axisymmetric flows. Subsequent measurements by Fekete (1970) on two-dimensional self-preserving jets and the present work on axisymmetric jets support the validity of this choice.

To evaluate certain constants in the theory, measured growth is needed for two self-preserving flows; the jet in still surroundings and the small-deficit wake in zero pressure gradient.

The second model uses Townsend's (1970) theory relating relative stress intensity ($\overline{uv}/\overline{q^2}$) to the turbulent Reynolds number of the flow. From this it is seen that over limited ranges of R_T, $\overline{uv}/\overline{q^2} \propto R_T^{-n}$. Predictions are calculated for the value of n appropriate to the measured flows. It is also shown that the two equations for the relative stress intensity used by Newman for two-dimensional flows are equivalent to the above relation for different values of n (and thus range of R_T). The predictions using these values of n are given, and also the prediction for another value of n that is equivalent to $\frac{\overline{q_0^2}}{U_0^2}$ = constant for the full range of self-preserving flows.

The theory uses a number of empirical constants derived from measurements on the jet in still surroundings. In this it is better than the theory of Section 2-2 which needs empirical information from two flows.

1-4-2 Experimental Program

Five self-preserving flows were studied; one wake with $U_0/U_1 = -.54$, and four jets with $U_0/U_1 = .85$, 1.83, 3.00, and ∞ (the last one is the jet in still surroundings). As well, some measurements were made of the small-deficit wake in zero pressure gradient.

Details of the results of these measurements are presented in Sections 4-1 to 4-3, with general discussion in Section 4-4.

Since the flows have an external stream co-flowing with the jet or wake, a blower cascade wind tunnel with a 30 inch diameter working section was designed and built. It incorporated a test section with controlled air bleed to generate the necessary adverse pressure gradients and prevent boundary layer separation on the walls. The tunnel, working section, jet supply, traversing gear, and instrumentation are described in Sections 3-1 to 3-5. As well, the design and construction of the novel wide-angle expansion used in the wind tunnel is given in Appendix A, and the electrical power and control system is described in Appendix B.

Section 3-6 describes the experimental procedures used.

1-4-3 Claim for Originality

It is reasonable to suggest that the following three areas represent original work and are a contribution to knowledge:

Setting up and measuring one axisymmetric wake and three axisymmetric jets in an adverse pressure gradient such that the flows are self-preserving;

Developing an integral method of predicting the growth of such flows using the large eddy equilibrium hypothesis by Townsend (1956). This involved modifying the two-dimensional formulation of the prediction method by Gartshore (1967) to handle axisymmetric flows, and an improvement of the method of evaluating the ratio of longitudinal to transverse rates of strain. This improved the predictions of growth for medium strength jets;

Following Newman (1968), developing a second integral prediction method using the total energy equation and Townsend's (1966), (1970) entrainment theory. The prediction method was modified to deal with axisymmetric flows. Several relations linking the relative stress intensity to a turbulent Reynolds number were used to predict the growth.

2. THEORY

The development of the theory describing symmetric free turbulent jets and wakes may be roughly divided into two areas, basic theory and auxiliary theory. Basic theory describes the development of the momentum and energy boundary layer equations to describe symmetric free turbulent jets and wakes, their simplification to integral equations and their specialization to treat self-preserving flows. In this the assumptions used are fairly standard and generally quite respectable. The only new feature is the useful demonstration that the introduction of the self-preserving conditions allow the reduction of the ordinary differential equations to algebraic ones.

This approach, of course, always generates more unknowns than equations. This necessitates the development of models and their resultant auxiliary relations. These auxiliary equations usually relate some turbulent quantity (present in the basic equations) to some mean property of the flow, and, together with other auxiliary equations necessary to provide one independent equation for each unknown, allows the growth of the flow to be calculated. In all the models used here the relations lack one or more constants of proportionality, and these are supplied by using measurements made on some 'standard' or 'asymptotic' flow, such as the jet in still air. Such models are usually greeted skeptically and need experimental testing (on flows that differ as much as possible from the 'standard' flow used to define the constants) before they can be used with confidence.

2-1 Basic Theory

The theory presented here follows in part that by Newman (1967), (1968) and is a modification and expansion of the theory given in two publications by the author (1968), (1969).

The first assumption made is that the flows to be studied can be adequately described by boundary layer equations. An adequate measure of the validity of this assumption is the ratio of the mean transverse to longitudinal velocity gradients, and for all the flows measured this ratio is less than .07.

The coordinate system to be used in all the flows is given in Fig. 2-1. The x-axis is along the centreline of the jet or wake, and y is used as the radial direction at right-angles to the x-axis. L_0 is the distance from the centreline of the jet or wake to the point where the mean increment (or decrement) of velocity is half the maximum value. U_0 is the increment (or decrement) of velocity at the centre of the jet (or wake).

2-1-1 Momentum and Energy Boundary Layer Equation

In this coordinate system the time averaged turbulent boundary layer equation for momentum is:

$$U\frac{\partial U}{\partial x}+V\frac{\partial U}{\partial y}+\frac{\partial}{\partial x}(\overline{u}^2-\overline{v}^2)+\frac{1}{y}\frac{\partial}{\partial y}(y\,\overline{uv})=U_1\frac{dU_1}{dx}+\frac{\nu}{y}\frac{\partial}{\partial y}(y\frac{\partial U}{\partial y}) \qquad (1)$$

This assumes axisymmetric flow. Using the usual assumptions that

$$\overline{u}^2 \simeq \overline{v}^2 \simeq \overline{uv}$$

and

$$\frac{\partial}{\partial x}(\overline{}) << \frac{\partial}{\partial y}(\overline{})$$

the term

$$\frac{\partial}{\partial x}(\overline{u}^2-\overline{v}^2)$$

is discarded. The self-preserving relations ((38)-(42)) can be developed with this term left in the equation, but, as it is subsequently discarded it was felt worthwhile to simplify the relation at this stage and only carry along terms that are essential. As well, if the assumption of large Reynolds number is made the term

$$\nu\frac{\partial}{\partial y}(y\frac{\partial U}{\partial y})$$

may be discarded, as the term representing the turbulent transfer of momentum should greatly exceed this term, which represents the viscous transfer due to mean shear.

This then leaves the momentum boundary layer equation as used in this report.

$$U\frac{\partial U}{\partial x}+V\frac{\partial U}{\partial y}+\frac{1}{y}\frac{\partial}{\partial y}(y\overline{uv})=U_1\frac{dU_1}{dx} \tag{2}$$

To the same level of approximation as (1) the time averaged total energy boundary layer equation is,

$$U\frac{\partial}{\partial x}\left(\frac{U^2-U_1^2}{2}+\frac{\overline{q}^2}{2}\right)+V\frac{\partial}{\partial y}\left(\frac{U^2-U_1^2}{2}+\frac{\overline{q}^2}{2}\right)+\frac{1}{y}\frac{\partial}{\partial y}(y\overline{vp_0})+\frac{1}{y}\frac{\partial}{\partial y}(yU\overline{uv})$$

$$+\frac{\partial}{\partial x}[U(\overline{u}^2-\overline{v}^2)]=\frac{\nu}{y}\frac{\partial}{\partial y}\left[y\frac{\partial}{\partial y}\left(\frac{U^2}{2}+\frac{\overline{q}^2}{2}\right)\right]-\varepsilon \tag{3}$$

where $q^2 = u^2 + v^2 + w^2$

$p_0 = \frac{q^2}{2} + p$

and $\varepsilon=\nu\left[\overline{\left(\frac{\partial v}{\partial y}\right)^2}+\overline{\left(\frac{1}{y}\frac{\partial v}{\partial \theta}-\frac{w}{y}\right)^2}+\overline{\left(\frac{\partial v}{\partial x}\right)^2}+\overline{\left(\frac{\partial w}{\partial y}\right)^2}+\overline{\left(\frac{1}{y}\frac{\partial w}{\partial \theta}+\frac{v}{y}\right)^2}\right.$

$$\left.+\overline{\left(\frac{\partial u}{\partial y}\right)^2}+\frac{1}{y^2}\overline{\left(\frac{\partial w}{\partial \theta}\right)^2}+\overline{\left(\frac{\partial u}{\partial x}\right)^2}+\left(\frac{\partial U}{\partial y}\right)^2\right] \tag{4}$$

The latter term is the kinematic dissipation rate of both mean and turbulent energy.

This is a rather complicated expression, and as it is not used explicitly the symbol ε will be used in its place. A further simplification is made by noting that the term

$$\frac{\partial}{\partial x}[U(\overline{u^2}-\overline{v^2})]$$

is generally of higher order than the other turbulent terms, and can be ignored.

This then leaves the total energy boundary layer equation as used in this report.

$$U\frac{\partial}{\partial x}\left(\frac{U^2-U_1^2}{2}+\frac{\overline{q}^2}{2}\right)+V\frac{\partial}{\partial y}\left(\frac{U^2-U_1^2}{2}+\frac{\overline{q}^2}{2}\right)+\varepsilon$$
$$+\frac{1}{y}\frac{\partial}{\partial y}\left[y\overline{vp_0}+yU\overline{uv}-y\nu\frac{\partial}{\partial y}\left(\frac{U^2}{2}+\frac{\overline{q}^2}{2}\right)\right]=0 \quad (5)$$

Also used is the time averaged continuity equation:

$$\frac{1}{y}\frac{\partial}{\partial y}(yV)+\frac{\partial U}{\partial x}=0 \quad (6)$$

This thesis makes use of the momentum and energy equations integrated in a direction transverse to the flow direction. More correctly, this integral is the control volume equation over a disk of radius y transverse to the flow direction, and of thickness dx; axial symmetry is assumed. It is given by:

$$\int_0^y dy \int_0^{2\pi} F(x,y)\,y\,d\phi\,dx$$
$$=2\pi dx \int_0^y yF(x,y)\,dy \qquad (7)$$

where $F(x,y)$ is one of the boundary layer equations. The $2\pi dx$ is subsequently ignored as it is common to all terms in the resultant relations.

It is convenient at this point to change the independent variables, and thus introduce what will become a similarity parameter. This variable is defined as:

$$\eta = \frac{y}{L_0(x)} \qquad (8)$$

$L_0(x)$ being defined as in Fig. 2-1. The change from an x,y system to an x,η system is made by noting the following relations:

$$\left.\frac{\partial \eta}{\partial x}\right|_y = \frac{\partial}{\partial x}\left(\frac{y}{L_0(x)}\right) = \frac{-y\,\partial L_0}{L_0^2\,\partial x} = -\frac{\eta L_0'}{L_0} \qquad (9)$$

$$\left.\frac{\partial F(x,\eta)}{\partial x}\right|_y = \left.\frac{\partial F}{\partial x}\right|_\eta + \left.\frac{\partial F}{\partial \eta}\right|_x \left.\frac{\partial \eta}{\partial x}\right|_y = \left.\frac{\partial F}{\partial x}\right|_\eta - \left.\frac{\eta L_0'}{L_0}\frac{\partial F}{\partial \eta}\right|_x \qquad (10)$$

$$\left.\frac{\partial F(x,\eta)}{\partial y}\right|_x = \left.\frac{\partial F}{\partial \eta}\right|_x \left.\frac{\partial \eta}{\partial}\right|_x = \left.\frac{1}{L_0}\frac{\partial F}{\partial \eta}\right|_x \qquad (11)$$

(where ' indicates differentiation with respect to x and $\left.\frac{\partial}{\partial(\ )}\right|_{(\ )}\left\{\ \right\}$ indicates a partial derivative holding the subscripted variable constant). When these changes are introduced, equations (2), (5) and (6) become:

$$\left.\frac{\partial}{\partial x}\right|_y (U^2)+\frac{1}{L_0\eta}\left.\frac{\partial}{\partial\eta}\right|_x(\eta UV)+\frac{1}{L_0\eta}\left.\frac{\partial}{\partial\eta}\right|_x(\eta\overline{uv})=U_1\frac{dU_1}{dx} \quad . \tag{12}$$

$$\begin{aligned}&U\left.\frac{\partial}{\partial x}\right|_y\left(\frac{U^2-U_1^2}{2}+\frac{\overline{q}^2}{2}\right)+\frac{V\partial}{L_0\partial\eta}\bigg|_x\left(\frac{U^2-U_1^2}{2}+\frac{\overline{q}^2}{2}\right)+\varepsilon\\&+\frac{1}{L_0\eta}\left.\frac{\partial}{\partial\eta}\right|_x\left\{\eta\overline{vp}_0+\eta U\overline{uv}-\frac{\eta\nu\partial}{L_0\partial\eta}\bigg|_x\left(\frac{U^2}{2}+\frac{\overline{q}^2}{2}\right)\right\}=0\end{aligned} \tag{13}$$

$$\frac{1}{L_0\eta}\left.\frac{\partial}{\partial\eta}\right|_x(\eta V)+\left.\frac{\partial U}{x}\right|_\eta=0 \tag{14}$$

and the integral relation (7) is:

$$L_0^2\int_0^\eta \eta F(x,\eta)\,d\eta \tag{15}$$

Integrating equation (12) with respect to η and using (15),

$$\int_0^\eta \eta\left.\frac{\partial}{\partial x}\right|_y(U^2)\,d\eta+\frac{1}{L_0}\int_0^\eta\left.\frac{\partial}{\partial\eta}\right|_x(\eta UV)\,d\eta+\frac{1}{L_0}\int_0^\eta\left.\frac{\partial}{\partial\eta}\right|_x(\eta\overline{uv})\,d\eta=\int_0^\eta \eta U_1\frac{dU_1}{dx}\,d\eta$$

which becomes

$$\int_0^\eta \eta\left.\frac{\partial}{\partial x}\right|_y(U^2)\,d\eta+\frac{\eta}{L_0}(UV)_\eta+\frac{\eta}{L_0}\overline{uv}_\eta=\int_0^\eta \eta U_1\frac{dU_1}{dx}\,d\eta \tag{16}$$

Now using the integrated continuity equation

$$\frac{\eta}{L_0}V_\eta=\int_0^\eta \eta\frac{\partial U}{\partial x}d\eta \tag{14}$$

(16) becomes:

$$\int_0^\eta \eta\frac{\partial}{\partial x}(U^2)\,d\eta-U_\eta\int_0^\eta \eta\frac{\partial U}{\partial x}d\eta+\frac{\eta}{L_0}\overline{uv}_\eta=\int_0^\eta \eta U_1\frac{dU_1}{dx}d\eta \tag{17}$$

Now add to this the identity

$$-\int_0^\eta \eta\frac{\partial}{\partial x}(U_1U)\,d\eta+U_1\int_0^\eta \eta\frac{\partial U}{\partial x}d\eta=-\int_0^\eta \eta U\frac{dU_1}{dx}d\eta$$

and the result is:

$$\int_0^\eta \eta\frac{\partial}{\partial x}\bigg|_y[U(U-U_1)]\,d\eta-(U_\eta-U_1)\int_0^\eta \eta\frac{\partial U}{\partial x}\bigg|_y d\eta+\frac{dU_1}{dx}\int_0^\eta \eta(U-U_1)\,d\eta$$
$$=-\frac{\eta}{L_0}\,\overline{uv}_\eta \tag{18}$$

Before the energy equation can be integrated it must first be modified by having the continuity equation multiplied by $\frac{U^2-U_1{}^2}{2}+\frac{\overline{q^2}}{2}$ added to it. This is given by:

$$\frac{1}{L_0\eta}\left(\frac{U^2-U_1^2}{2}+\frac{\overline{q}^2}{2}\right)\frac{\partial}{\partial\eta}\bigg|_x(\eta V)+\left(\frac{U^2-U_1^2}{2}+\frac{\overline{q}^2}{2}\right)\frac{\partial U}{\partial x}\bigg|_y=0$$

With this addition (13) becomes:

$$\frac{\partial}{\partial x}\bigg|_y\left(U\frac{(U^2-U_1^2)}{2}+U\frac{\overline{q}^2}{2}\right)+\frac{1}{L_0\eta}\frac{\partial}{\partial\eta}\bigg|_x\left(\eta V\frac{(U^2-U_1^2)}{2}+\eta V\frac{\overline{q}^2}{2}\right)$$

$$+\frac{1}{L_0\eta}\frac{\partial}{\partial\eta}\bigg|_x[\eta\overline{vp}_0+\eta U\overline{uv}]-\eta\frac{\nu}{L_0}\frac{\partial}{\partial\eta}\bigg|_x[\frac{U^2}{2}+\frac{\overline{q}^2}{2}]+\varepsilon=0 \tag{19}$$

Applying (15) to this gives:

$$L_0\int_0^\eta \eta\frac{\partial}{\partial x}\bigg|_y\left(U\frac{(U^2-U_1^2)}{2}+\frac{\overline{q}^2}{2}U\right)d\eta+\eta V\ \frac{(U^2-U_1^2)}{2}+\eta V\ \frac{\overline{q}^2}{2}$$

$$+\eta(\overline{vp}_0)+\eta U\overline{uv}-\frac{\eta\nu\partial}{L_0\partial\eta}(\frac{U^2}{2}+\frac{\overline{q}^2}{2})+\int_0^\eta\eta\varepsilon d\eta=0 \tag{20}$$

For this work only the limit $\eta = \infty$ will be used for the integral energy equation, and the resulting relation is:

$$\frac{1}{L_0}\frac{\partial}{\partial x}\bigg|_y\left(L_0^2\int_0^\infty\left(\eta U\frac{(U^2-U_1^2)}{2}\ +\eta U\frac{\overline{q}^2}{2}\right)d\eta\right)+L_0\int_0^\infty\eta\varepsilon d\eta=0 \tag{21}$$

In order to proceed further with either the integral momentum or energy equation, a relation for the mean velocity profile is needed. Here use is made of the experimental fact that suitably non-dimensionalized mean velocity profiles of symmetric free jets and wakes are closely similar except near their origins (Halleen (1968)). Thus it has usually been assumed that:

$$U(x,\eta)=U_1(x)+U_0(x)f(\eta) \tag{22}$$

Introducing this into (18) results in:

$$\begin{aligned}&L_0'\left(2U_0U_1I_1(\eta)+2U_0^2I_2(\eta)-U_0U_1\eta^2f(\eta)-2U_0^2f(\eta)I_1(\eta)\right)\\&+L_0\frac{U_0'}{U_0}\left(U_0U_1I_1(\eta)+2U_0^2I_2(\eta)-U_0^2f(\eta)I_1(\eta)\right)\\&+L_0\frac{U_1'}{U_1}\left(2U_0U_1I_1(\eta)-U_0U_1\frac{\eta^2}{2}f(\eta)\right)=-\eta(\overline{uv})\end{aligned} \tag{23}$$

where

$$I_1(\eta)=\int_0^\eta \eta f(\eta)d\eta \tag{24}$$

and

$$I_2(\eta)=\int_0^\eta \eta f^2(\eta)d\eta \tag{25}$$

Now introduce a change in the dependent variable that will be useful when dealing with self-preserving flows.

$$G(x)=\frac{U_0}{U_1} \tag{26}$$

With this definition (23) becomes

$$\begin{aligned}&2L_0'\left[(1-Gf(\eta))I_1(\eta)+GI_2(\eta)-\frac{\eta^2}{2}f(\eta)\right]\\&+L_0\frac{U_0'}{U_0}\left[(3-Gf(\eta))I_1(\eta)+2GI_2(\eta)-\frac{\eta^2}{2}f(\eta)\right]\\&+L_0\frac{G'}{G}\left[\frac{\eta^2}{2}f(\eta)-2I_1(\eta)\right]=-\eta Gg(\eta,x)\end{aligned} \tag{27}$$

where

$$g(\eta,x)=\frac{\overline{uv}(\eta,x)}{U_0^2(x)} \tag{28}$$

Similarly, introducing (22) and (26) into (21) gives

$$\frac{1}{L_0|U_0^3|}\frac{\partial}{\partial x}\left\{\frac{L_0^2U_0^3}{2}\left(G^2I_3(\infty)+3GI_2(\infty)+2I_1(\infty)+GI_4(\infty,x)+G^2I_5(\infty,x)\right)\right\}+G^2I_6(\infty,x)=0 \tag{29}$$

where

$$E=\frac{L_0\varepsilon}{|U_0^3|} \tag{30}$$

$$h(\eta,x)H=\frac{\overline{q}^2(\eta,x)}{U_0^2} \qquad \left(H=\frac{\overline{q}_0^2}{U_0^2}\right) \tag{31}$$

$$I_3(\eta)=\int_0^\eta \eta f^3(\eta)\,d\eta \tag{32}$$

$$I_4(\eta,x)=\int_0^\eta \eta Hh(\eta,x)\,d\eta \tag{33}$$

$$I_5(\eta,x)=\int_0^\eta \eta f(\eta)Hh(\eta,x)\,d\eta \tag{34}$$

$$I_6(\eta,x)=\int_0^\eta \eta E(\eta,x)\,d\eta \tag{35}$$

These forms of the momentum and energy

integral equations, while still describing a general axisymmetric jet or wake, are readily modified to show the effects of the assumption of self-preservation.

2-1-2 Self-preservation

In the context of the incompressible jets and wakes studied here, the concept of self-preservation means that all flow characteristics scale with U_0 and L_0 (or some other velocity and length scale). This can only be true to the extent that the effect of Reynolds number can be ignored. Physically, this means that, while viscosity is directly involved in the turbulent transport of momentum and energy, and in the dissipation of turbulent energy, the flow is driven by the gross properties of the flow, and changes in viscosity affect only the very fine details of the turbulence.

Following Townsend (1956), a jet or wake is self-preserving if the integrals $I_1(\eta,x)$-$I_6(\eta,x)$, and the relations $g(\eta,x)$ and $f(\eta)$ are assumed to be independent of x. (This has already been assumed for f, I_1, and I_2). With these assumptions, (27) and (29) become,

$$[L_0'](2I_1-\eta^2 f)+[L_0'G](2I_2-2fI_1)+[L_0\frac{U_0'}{U_0}G](2I_2-fI_1)$$

$$+[L_0\frac{U_0'}{U_0}](3I_1-\frac{\eta^2}{2}f)+[L_0\frac{G'}{G}](2I_1-\frac{\eta^2}{2}f)+[G](\eta g_0)=0 \qquad (36)$$

and

$$[G^2L_0'+\frac{3}{2}G^2L_0\frac{U_0'}{U_0}](I_3+I_5)+[GL_0'+\frac{3}{2}GL_0\frac{U_0'}{U_0}](3I_2+I_4)$$

$$+[L_0'+\frac{3}{2}L_0\frac{U_0'}{U_0}](2I_1)-[L_0\frac{G'}{2}](3I_2+I_4) \qquad (37)$$

$$-[L_0\frac{G'}{G}](2I_1)+[|G|G](I_6)=0$$

This follows Newman's approach (1967). The terms in the square brackets are functions of x only, and the terms in the round brackets are functions of η only. Self-preservation thus requires that the ratios of the terms in the square brackets be constants for a particular flow. This leads directly to the requirement that,

$$G=\text{const.} \qquad (38)$$

$$L_0'=\text{const.} \qquad (39)$$

$$L_0\frac{U_0'}{U_0}=\text{const.} \qquad (40)$$

which in turn lead to,

$$L_0=C_0(x-x_0) \tag{41}$$

$$U_1=C_1(x-x_0)^m \tag{42}$$

where m is a constant for a particular flow.

Thus a self-preserving jet or wake grows linearly with distance from a virtual origin (x_0) with a growth parameter given by C_0; the ratio of the free stream velocity and the jet or wake scaling velocity remains constant; and both these velocities change at some power of the distance from the virtual origin of the flow.

The integral momentum equation for self-preserving flow is then,

$$\begin{aligned}&2C_0\left[(I_1(\eta)-\frac{\eta^2}{2}f(\eta))+G(I_2(\eta)-f(\eta)I_1(\eta))\right]\\&+C_0m\left[(3I_1(\eta)-\frac{\eta^2}{2}f(\eta))+G(2I_2(\eta)-f(\eta)I_1(\eta))\right]=-\eta Gg(\eta)\end{aligned} \tag{43}$$

and the energy integral equation is,

$$\begin{aligned}&C_0(1+\frac{3}{2}m)\left[2I_1(\infty)+G(3I_2(\infty)+I_4(\infty))+G^2(I_3(\infty)+I_5(\infty))\right]\\&+G|G|I_6(\infty)=0\end{aligned} \tag{44}$$

In order to calculate some of these constants an explicit expression for $f(\eta)$ is needed, and

$$f(\eta)=e^{-k\eta^2} \tag{45}$$

was chosen,

where $k = \ln(2) = .693$.

This has been used before by other researchers, and was chosen here as being mathematically simple, and, except near the edges of the flow, fitting the experimental data well.

For the integral momentum equation two limits will be used. One is $\eta = \infty$. This gives the overall momentum balance that must be obeyed by a self-preserving flow, and will be called the full integral momentum equation. The other limit is $\eta = 1$. The resulting relation here gives the momentum balance between the central part of the flow and the shear stress near its point of maximum (for a Gaussian profile), and will be called the half-integral momentum equation. For these limits f, I_1, I_2, and I_3 become

$$\begin{aligned}
&f(1)=e^{-k}=.5 && f(\infty)=0\\
&I_1(1)=\frac{1}{2k}(1-e^{-k})=.36 && I_1(\infty)=\frac{1}{2k}=.72\\
&I_2(1)=\frac{1}{4k}(1-e^{-2k})=.27 && I_2(\infty)=\frac{1}{4k}=.36\\
&I_3(1)=\frac{1}{6k}(1-e^{-3k})=.21 && I_3(\infty)=\frac{1}{6k}=.24
\end{aligned} \tag{46}$$

Using these constants the full integral equation reduces to,

$$m = \frac{-(2+G)}{(3+G)} \tag{47}$$

When this is introduced into (43), the half-integral momentum equation becomes

$$C_0 = \frac{G(3+G)g_0}{a_2G^2+a_1G+a_0} \tag{48}$$

where $$g_0 = g(\eta \doteq 1)$$

and

$$\begin{aligned} a_2 &= \frac{I_1(1)}{2} = .18 \\ a_1 &= 3I_1(1)-2I_2(1)+.25 = .79 \\ a_0 &= 1 \end{aligned} \tag{49}$$

Putting (47) into the integral energy equation gives another relation for C_0 as follows

$$C_0 = \frac{|G|(6+2G)I_6(\infty)}{G^2(I_3(\infty)+I_5(\infty))+G(3I_2(\infty)+I_4(\infty))+2I_1(\infty)} \tag{50}$$

This is essentially as far as these relations may be taken on safe grounds. Further progress depends upon developing expressions relating the shear stress, turbulent energy, and dissipation to the mean properties of the flow, and thus to G. As the basic energy and momentum equations have been 'used up', models must be developed which lead to plausible and tractable relations. Two methods of approach will be used, both using these integral equations.

2-2 The Large Eddy Equilibrium Model

2-2-1 Development of Model

This model was first proposed by Townsend (1956), and independently developed as a prediction method for two-dimensional wakes and jets by Gartshore (1964), (1965) and Bradbury (1967). Townsend postulated that the energy transfer from the mean flow to the bulk of the turbulent structure was a two step procedure. First the energy is transferred from the mean shear to large eddies with dimensions comparable to the width of the shear region. (These eddies are those that give the characteristic intermittent structure to the boundary of free shear flows). The energy is then transferred to the more nearly isotropic turbulence (that contains the bulk of the turbulent energy, or a constant proportion of the total turbulent energy) by turbulent transport processes describable by an eddy viscosity.

It was further postulated that during an appreciable part of the eddy's lifetime, the rate of input of energy from the mean shear was balanced by the energy loss rate to the bulk of the turbulence. This leads to a mixing length type of relation,

$$\frac{\tau}{\rho} \propto L^2 \left(\frac{\partial U}{\partial y}\right)^2 , \tag{51}$$

where L is a measure of the large eddy size rather than a measure of flow size.

To get a relation between L and some measure of the mean flow, Gartshore considered an eddy with a character consistent with the measurements of Grant (1958); this eddy being placed in a steady two-dimensional flow field such that

$$\frac{\partial U}{\partial x} = -\frac{\partial V}{\partial y} = B, \qquad \frac{\partial U}{\partial y} = A$$
$$\frac{\partial V}{\partial x} = 0, \qquad W = 0 \tag{52}$$

and further that

$$\frac{A}{B} >> 1$$

Energy is transferred to an eddy in this field by a process of stretching. The mean shear also rotates the eddy to an orientation where no more energy can be added; but energy transfer to smaller eddies continues, and the large eddy is destroyed by the mean shear. The time taken to rotate the eddy from 90° to the x-direction to 45° to the x-direction is A^{-1}, and consequently the eddy is assumed to have a lifetime

$$T = \beta/A$$

where β would be expected to have a value of 2 or 3.

Using these assumptions, the instantaneous vorticity equation was used to predict the growth of such an eddy, first with B non-zero, and then with B = 0. Assuming that the circulation remains constant through its lifetime, it is possible to calculate the ratio of the eddy sizes in the two cases. Gartshore obtained the relation

$$\frac{L^2}{L_1{}^2} = \frac{B/A}{\sinh(B/A)} \tag{53}$$

where L_1 refers to the large eddy size for B = 0.

Newman (1967) places an unspecified eddy in similar flow conditions, and uses the instantaneous and average vorticity equations to develop

$$\frac{L^2}{L_1{}^2} = 1 + (\text{const.})\left|\frac{B}{A}\right| \tag{54}$$

He also used independent dimensional arguments to show that

$$\frac{L^2}{L_1{}^2} = \text{Func.}\left(\left|\frac{B}{A}\right|\right)$$

which approximates to (54) for $B/A \ll 1$.

The next step is to consider these large eddies in the non-uniform shear flow of one half of a wake or jet. The assumption here is made that, while the effect of the mean flow on the large eddies is different for the two cases (B zero and non-zero) from that for the uniform flow, the relation given by (53) or (54) is unchanged. This assumes that the starting size of the eddies are the same in the two cases despite the fact that the flows are similar but not identical.

An expansion of (53) gives

$$\frac{L^2}{L_1{}^2} \simeq 1 + (\text{const.}) \left(\frac{B}{A}\right)^2 \tag{55}$$

although Gartshore actually used Equation (54) in his calculations. As will be seen later, the predictions using (54) and (55) differ by a negligible amount.

Using $R_T \propto \frac{1}{L^2}$ and Equation (53),

$$\frac{1}{R_T} = (\text{const.}) \left(1 + \beta \left|\frac{B}{A}\right|\right) \tag{56}$$

using (54), and

$$\frac{1}{R_T} = (\text{const.}) \left[1 + \beta_Q \left(\frac{B}{A}\right)^2\right] \tag{57}$$

using (53). The β for the two relations must obviously be different. This assumes some average R_T across the flow; however, for use in free shear flows it is more convenient to use R_T evaluated at some non-dimensional point in the flow. This seems a reasonable thing to do as R_T is usually fairly constant across the central regions of such a flow, and the point to be chosen (near the point of maximum $\partial U/\partial y$) should be near the centre of a large eddy.

The constant and β for two-dimensional flow were evaluated by considering two self-preserving flows: the small deficit wake in uniform flow, and the still air jet (the first of which has $B/A = 0$).

Relations (56) and (57) have here been adopted directly for use in describing axisymmetric flows (with, of course, different constants). This involves the obvious assumption that the concept is valid for such flows.

For the case of symmetric jets and wakes considered here, where the mean velocity profiles are self-preserving,

$$R_T = \frac{L_0 U_0}{\overline{uv}} \frac{\partial U}{\partial y}$$

can be replaced by

$$R_T = \frac{L_0 U_0}{|\overline{uv}|} (\text{const.}) \frac{U_0}{L_0} = (\text{const.}) \frac{U_0{}^2}{|\overline{uv}|} \propto \frac{1}{|g_0(x)|}$$

where $g(\eta,x)$ is defined in (28). Since this shear stress parameter is used throughout this work, (56) and (57) will be restated as,

$$|g_0| = \alpha(1-\beta|B/A|) \tag{58}$$

and

$$|g_0| = \alpha(1-\beta_Q(B/A)^2) \tag{59}$$

where g_0 is here less restrictive than as described in (49), as only local self-preservation is demanded. (This is the assumption that the energy transfer is affected only by the local B/A and not by what the eddies have experienced in the past. A criterion for it to be true is that B/A change relatively little in a time period of A^{-1}).

One of the consequences of the existence of large eddies is that these eddies will distort the boundary between vortical and non-vortical fluid at the edge of the flow. By measuring the size of these distortions it should be possible to get a measure of the size of the eddies. This was done in this experiment by measuring the mean and standard deviation of the intermittency as a function of the distance from the centreline of the flow. This will be assumed to be proportional to the size of the large eddies, and will be the only check performed on the large eddy equilibrium hypothesis other than comparing predicted results with experiment.

One of the unexpected rewards of the development of a closed form solution for the behaviour of self-preserving jets and wakes was the discovery of a problem in the concept of how B/A is evaluated. This affected both Gartshore and Bradbury in their calculations of the development of two-dimensional jets.

When predicted growth for the whole range of G from -1 to 0 (wakes) and 0 to $+\infty$ (jets) were calculated for two-dimensional and axisymmetric flows, anomalous behaviour was seen for medium strength jets. (See Figures 2-2 and 2-3). The predicted growth not only seems unlikely, but is wrong, as subsequent work by Fekete (1970) (two-dimensional jets) and the author (axisymmetric jets) show.

The cause of these unusual predictions and the approach adopted to deal with them are covered more thoroughly in earlier reports by the author (1968), (1969). Briefly, however, the equilibrium theory evolved by considering a flow field in which B is constant. When the concept is transferred to a turbulent jet or wake B obviously cannot be constant everywhere, but it would be expected that the character of B would be similar in some local region. For example, all the self-preserving two-dimensional and axisymmetric wakes and jets considered here have the $\partial U/\partial x$ of the external flow negative. Thus the eddies in the turbulent part of the flow should be experiencing a rising pressure and a longitudinal compression, which in turn should be reflected by a value for B which is negative.

The usual approach to evaluating B is as

$$B = \left.\frac{\partial U}{\partial x}\right|_y \tag{60}$$

which means the rate of change of U with x, holding y constant. Using

$$U = U_1 + U_0 f(\eta) \tag{22}$$

$$\left.\frac{\partial U}{\partial x}\right|_y = \underbrace{\left(\frac{dU_1}{dx} + f(\eta)\,\frac{dU_0}{dx}\right)}_{(1)} + \underbrace{\left(2k\eta^2 U_0 f(\eta)\,\frac{L_0'}{L_0}\right)}_{(2)} \tag{61}$$

An incremental movement in the x-direction, holding y constant, is thus seen to change the mean velocity in two ways. First, there is the decrease of mean velocity due to adverse pressure gradient. This is expressed by part (1) of (61). Second, because of the growth of the jet as the flow progresses, the movement is to a region that is non-dimensionally closer to the centre of the flow, and thus (for jets) a region of possibly higher velocity. Thus it is possible to get $B = 0$, or even $B > 0$ for flows where $\partial U_1/\partial x$ is negative, and in fact this is what happens when the calculations are carried out.

As well as the above physical and conceptual objections to evaluating B as in (60), there is an objection that the character of the flow prediction is critically dependent on the value of η chosen to evaluate B/A.

The way chosen here to overcome this problem was to redefine B as

$$B = \left.\frac{\partial U}{\partial x}\right|_{\eta} = \frac{dU_1}{dx} + f(\eta)\,\frac{dU_0}{dx} \tag{62}$$

(which will be recognized as term (1) of (61)), while leaving A as

$$A = \left.\frac{\partial U}{\partial y}\right|_{x} \tag{63}$$

This is the mathematical expression of the physical assumption that the path of the large eddy is such as to keep it non-dimensionally in the same place in the flow. This means that the eddy is not travelling along a mean velocity streamline, which for jets and part of the wake region have V negative at $y = L_0$. However, flow visualization experiments on boundary layer development would lead one to expect that during their active period that the large eddies do move outwards, and that the assumption given here about their paths may not be too bad a guess.

Two approaches were used to justify this choice. One was the use of cylindrical (for two-dimensional) or spherical (for axisymmetric) coordinates in which to calculate B/A. Using x and y along the coordinate direction plus use of the boundary layer approximations then leads to (62) and (63) for self-preserving flow. This is the approach adopted in Vogel (1968).

The other approach, from Vogel (1969), assumes that the position of the eddy remains fixed relative to the non-dimensional profile, and thus, to the boundary layer approximation, the longitudinal strain rate experienced by the eddy is given by (62).

The first approach is perhaps geometrically better justified, but is applicable only to self-preserving flows with their resultant linear growth. The second approach is physically more satisfying and more generally applicable. A way to justify it is to state that the original concept involved an eddy in a field, where the mean transverse and longitudinal rates of strain were everywhere constant. This cannot be true when the concept is transferred to a jet or wake, but it seems reasonable to evaluate these rates of strain along a line in the flow along which and around which they are constant. This means that $\partial U/\partial x$ should be evaluated along a line of constant η, and at the inflection point in the profile. (This should mean that η = .85. However, η = 1 is felt to be close enough). The rate of change of U in a direction at right angles to this line is (63), to the boundary layer approximation.

Using (63), (22) and (45)

$$A = -2k\frac{\eta}{L_0}\; U_0 e^{-k\eta^2} = -k\frac{U_0}{L_0} \qquad (64)$$

$$B = m\frac{U_0 C_0}{L_0}\;(1/G+e^{-k}) = m\frac{U_0 C_0}{L_0}\;(1/G+1/2) \qquad (65)$$

and, using (47)

$$\frac{B}{A} = \frac{C_0(2+G)^2}{2kG(3+G)} \tag{66}$$

For $G \geq -1$ (jets and wakes without back flow) $m < 0$, so

$$\left|\frac{B}{A}\right| = \frac{C_0(2+G)^2}{2k|G|(3+G)} \tag{67}$$

and putting this into

$$|g_0| = \alpha(1-\beta|B/A|) \tag{58}$$

it becomes

$$g_0 = (\text{sign } G)\left(1-\beta\frac{C_0(G+2)^2}{2k|G|(3+G)}\right)\alpha \tag{68}$$

combining this with (48) gives analytic relations for C_0 and g_0

$$C_0 = \frac{\alpha|G|(3+G)}{(a_2G^2+a_1G+a_0)+\frac{\alpha\beta}{2k}(2+G)^2} \tag{69}$$

$$g_0 = \frac{\alpha(a_2G^2+a_1G+a_0)(\text{sign } G)}{(a_2G^2+a_1G+a_0)+\frac{\alpha\beta}{2k}(2+G)^2} \tag{70}$$

using the other relation for g_0,

$$|g_0| = \alpha\left(1-\beta_Q (B/A)^2\right) \tag{59}$$

$$g_0 = (\text{sign } G)\alpha\left[1-\beta_Q\left(\frac{C_0^2(2+G)^4}{4k^2G^2(3+G)^2}\right)\right] \tag{71}$$

Combining this with (48) gives another set of analytical relations for C_0 and g_0

$$C_0 = \frac{2k|G|(3+G)}{\alpha\beta_Q(2+G)^4}\left[\{k^2(a_2G^2+a_1G+a_0)^2+\alpha^2\beta(2+G)^4\}^{\frac{1}{2}} - k(a_2G^2+a_1G+a_0)\right] \tag{72}$$

$$g_0 = \frac{2k(a_2G^2+a_1G+a_0)}{\alpha\beta_Q(2+G)^4}\left[\{k^2(a_2G^2+a_1G+a_0)^2+\alpha^2\beta(2+G)^4\}^{\frac{1}{2}} - k(a_2G^2+a_1G+a_0)\right](\text{sign } G) \tag{73}$$

2-2-2 Predicted Growth for Large Eddy Equilibrium Model

The next step is to obtain values for α and β so that numerical predictions for C_0 and g_0 can be obtained. Values for these are given in Table 2-1. Using these values,

$$C_0 = \frac{.0492|G|(3+G)}{.540G^2+2.232G+2.442} \tag{74}$$

$$|g_0| = \frac{.0492(.18G^2+.79G+1)}{.540G^2+2.232G+2.442} \tag{75}$$

and (72) and (73) become

$$C_o = \frac{.182|G|(3+G)}{(2+G)^4}\{P_1(G)\} \tag{76}$$

$$|\breve{g}_0| = \frac{.182(.18G^2+.79G+1)}{(2+G)^4}\{P_1(G)\} \tag{77}$$

where

$$P_1(G) = \{(.391G^4+3.136G^3+9.472G^2+12.758G+6.480)^{\frac{1}{2}} - (.125G^2+.548G+.693)\} \tag{78}$$

The predicted values from equations (74) and (76) are plotted on Fig. 2-4, and those from equations (75) and (77) on Fig. 2-5. As can be seen, the two methods of calculating g_0 ((58) and (59)) produce quite similar answers except perhaps for the strong wake region.

2-3 The Townsend Entrainment Model

An alternative theory may be developed by using the complete energy equation integrated across the flow, and, as a connection between this and the momentum integrals, a model connecting shear stress to turbulent energy.

Townsend (1966), (1970) argues that in the 'control loop' of turbulent shear flows, where entrainment provides energy to eddies that in turn determine the entrainment, the dominant element is the average total strain experienced by the large eddies of turbulent motion. He then argues that, for turbulent shear flows, the effect of this total strain on the Reynolds stresses is similar to that predicted by rapid distortion theory. In particular, Figure 3 in Townsend (1970) gives a prediction of how the ratio of $\frac{\overline{uv}}{\overline{q^2}}$ varies with α, the total strain. Over a limited range of α, this curve can be approximated by

$$\frac{\overline{uv}}{\overline{q^2}} \propto \alpha^{-n} \tag{80}$$

where n varies from near -1 (for $0 < \alpha < 1.5$), to 0 (for $1.5 < \alpha < 3.5$), and approaches a value somewhat less than 1 for α larger than 4. The assumption is made that this applies to non-uniform shear flows such as jets and wakes, and thus (80) may be restated as

$$\frac{\overline{uv}_{max}}{\overline{q^2}} \propto \alpha_{max}^{-n} \tag{81}$$

where $\overline{uv}_{max}$ is a representative value of shear stress near the position of maximum mean velocity gradient. α_{max} is similarly evaluated at a position across the flow where it is a maximum, and represents the average total strain experienced by a large eddy during its lifetime.

The equation describing the total strain following the mean motion (equation 5.1 in Townsend (1970)) involves an eddy diffusivity for effective strain. If this is taken to be universally proportional to the eddy viscosity, ν_T, it follows that for self-preserving flow

$$\alpha_{max} \propto \frac{U_0 L_0}{\nu_T} = R_T \qquad (82)$$

Experiments and comparisons with the two-dimensional small deficit wake, the two-dimensional still-air jet, the mixing layer and the boundary layer in zero pressure gradient tend to confirm this (see Table 3 in Townsend (1970)) and indicate that

$$\alpha_{max} \simeq \frac{1}{6} R_T$$

Thus the flow regime for the two-dimensional small deficit wake has $\alpha_{max} \simeq 2.5$ and equation (81) has $n = 0$, while for self-preserving jets and wakes $\alpha_{max} \simeq 6$ and $n \simeq .75$.

For flows with

$$U=U_1+U_0 f(y/L_0) \tag{22}$$

$$R_T=\frac{U_0 L_0}{\nu_T}=\frac{U_0 L_0}{\left(\overline{uv}/\frac{\partial U}{\partial y}\right)_{max}} \propto \frac{U_0^2}{\overline{uv}_{max}}$$

and using (81) and (82)

$$\frac{\overline{uv}_{max}}{\overline{q}_0^2} \propto \alpha^{-n} \propto (R_T)^{-n} \propto (U_0^2/\overline{uv}_{max})^{-n} \tag{83}$$

which leads to

$$\frac{\overline{uv}_{max}}{U_0^2}=\gamma\left(\frac{\overline{q}_0^2}{U_0^2}\right)^{\frac{1}{1-n}} \tag{84}$$

To calculate growth predictions for self-preserving axisymmetric jets and wakes, some further assumptions and numerical values are needed. Looking at relations (48) and (50) it is seen that the value of a number of integrals are needed. f, I_1, I_2, and I_3 have already been assumed to be constant for the full range of G (-1 to +∞) and values calculated assuming a Gaussian profile. The assumption is here made that the remaining integrals (I_4 - I_6) have universal shapes for these flows. Relations (33) - (35) can be restated as (using $\varepsilon_{avg}=\frac{\overline{q}_0^{2\,3/2}}{L_\varepsilon}$)

$$I_4=H\int_0^\infty \eta h(\eta)\,d\eta \tag{85}$$

$$I_5=H\int_0^\infty \eta h(\eta) f(\eta)\,d\eta \tag{86}$$

$$I_6=\int_0^\infty \eta E(\eta)\,d\eta=\int_0^\infty \eta \frac{L_0 \overline{q}_0^{2\,3/2}}{L_\varepsilon |U_0{}^3|}\,d\eta=\frac{L_0}{L_\varepsilon}H^{1.5}\int_0^\eta y_\eta\,d\eta=\frac{L_0}{L_\varepsilon}H^{1.5}\ \frac{\eta^2_{.5}}{2} \qquad (87)$$

where $h(\eta)$ is the shape factor for the distribution of turbulent energy across the flow, L_ε is the dissipation length scale for the flow and $\eta_{.5}$, the value of η for which the intermittency is ·5, defines the average width of the turbulent region.

The assumption is now made that $h(\eta)$, $\frac{L_0}{L_\varepsilon}$ and $\eta_{.5}$ are independent of the value of G, and thus values measured for the still-air jet will apply to all axisymmetric self-preserving flows. Thus all the experimentally determined constants in this theory are derived from measurements on just one flow, the jet in still air, and this flow is, furthermore, a member of the self-preserving family of axisymmetric jets and wakes. This is an obvious improvement over the large eddy equilibrium theory which requires, as well, measurements on the small-deficit axisymmetric wake in zero pressure gradient. This latter flow is a member of another possibly self-preserving group, and is one about which doubt exists whether it can ever be self-preserving.

From measurements by Rodi (1972) and from the present work (See Section 4-4-2),

$$H(\text{for still-air jet})=.124 \qquad (88)$$

and

$$I_4 = .701 \times H$$
$$I_5 = .387 \times H \qquad (89)$$
$$I_6 = .300 \times H^{1.5}$$

using these in (50) gives

$$C_0 = \frac{2|G|(3+G)(.300)H^{1.5}}{H(.387G^2+.701G)+(.24G^2+1.08G+1.44)} \qquad (90)$$

while replacing g_0 in (48) by (84) gives

$$C_0 = \frac{|G|(3+G)\gamma H^{\frac{1}{1-n}}}{.18G^2+.79G+1} \qquad (91)$$

where γ is calculated from (88) and the value of g_0 for the still air jet,

$$g_0(\text{still-air jet}) = .0164 \qquad (92)$$

using Rodi's(1972) correction to the measured growth.

Letting

$$e_1(G) = \frac{\gamma}{.18G^2+.79G+1} \qquad (93)$$

$$e_2 = 2 \times .300 = .600$$

$$e_3(G) = G(.387G+.701)$$

$$e_4(G) = (.24G^2+1.08G+1.44)$$

and equating (90) and (91) results in

$$H\left(e_1(G)e_3(G)\right)+e_1(G)e_4(G)=e_2H\left(\frac{1-3n}{2-2n}\right) \tag{94}$$

and this is, in general, soluble for given values of n and G. From the calculated H(G),

$$|g_0|=\gamma H\left(\frac{1}{1-n}\right) \tag{95}$$

and

$$C_0=\frac{G(3+G)g_0}{.18G^2+.79G+1} \tag{96}$$

Numerical solutions for C_0 and $|g_0|$ for n=.75 are presented in Figures 2-6 and 2-7. (On these and subsequent figures in this section experimental values from this thesis are plotted, and will be referred to in Section 4.)

There are some other models for the turbulent structure that can be formulated in terms of a value of n in equation (84). The concept of geometric similarity $\frac{\overline{uv}_{max}}{q_0^2}$ = constant for all flows) which was proposed by Townsend (1966) is equivalent to n=0. Predictions using this value of n are shown in Figures 2-8 and 2-9. Another model, used by Newman (1968) in predicting the growth of two-dimensional self-preserving flows, has $\overline{uv} \propto q_0U_0$. This is equivalent to n=-1 in equation (84). Predictions using this value of n are shown in Figures 2-10 and 2-11.

Finally the effect of assuming H = const. for the whole family of axisymmetric self-preserving flows could be considered. This is equivalent to n = 1 in equation (84). In this case only equation (90) is needed and (91) is not valid. Predictions using this value of n are shown in Figures 2-12 and 2-13.

An interesting sidelight came out of investigating a range of values for n. For $n = \frac{1}{3}$, equation (93) becomes

$$He_1(G)e_3(G)+e_1(G)e_4(G)=e_3$$

and thus

$$H=\frac{e_2-e_1e_4}{e_1e_3}=\frac{e_2/e_1-e_4}{e_3}=\frac{e_2}{\gamma}\,\frac{(.18G^2+.79G+1)-(.24G^2+1.08G+1.44)}{G(.387G+.701)} \quad (94)$$

For G = 0 this becomes

$$H=\frac{e_2}{\gamma}\left(\frac{1-1.44}{0}\right)=\infty$$

so H tends to ∞ as $|G|$ becomes small. In practice, numerical solutions to relation (94) tended to 'blow up' near $|G| = 0$ for $.25 \leq n \leq .4$. It is not clear what physical significance should be attached to this finding, as it is not known if this range of n is physically possible, or if the basic assumptions leading to (94) apply here.

2-4 The Small-Deficit Wake in Zero Pressure Gradient

For the axisymmetric wake where

$$\left|\frac{U_0}{U_1}\right| << 1$$

$$U_1 = \text{const.}$$

equation (27) becomes

$$\begin{aligned} & U_1 U_0 L_0' \; [2I_1(\eta) - \eta^2 f(\eta)] \\ + \; & L_0 U_1 U_0' \; I_1(\eta) + \eta U_0^2 g(\eta,x) = 0 \end{aligned} \tag{95}$$

This already assumes a self-preserving mean velocity profile. If it is further assumed that

$$g(\eta,x) = g(\eta)$$

then this leads to

$$\begin{aligned} L_0 &\propto (x-x_0)^{1/3} \\ U_0 &\propto (x-x_0)^{-2/3} \\ L_0^2 U_0 U_1 &= \text{const.} \end{aligned} \tag{96}$$

Thus (95) becomes

$$g(\eta) = \frac{U\, L_0'}{U_0}\,\eta\, f(\eta) \tag{97}$$

$$\left.\begin{aligned} &\text{For} \quad \eta = 1, \quad L_0' = \frac{L_0}{3(x-x_0)} \\ &g_0 = \frac{U_1 L_0'}{2U_0} = \frac{U_1 L_0}{6\, U_0 (x-x_0)} \end{aligned}\right\} \tag{98}$$

assuming a Gaussian velocity profile.

This value of g_0 is needed to calculate α and β in (58) and (59).

3. EXPERIMENTAL PROCEDURES

3-1 Wind Tunnel

The wind tunnel is of the open return type. The outlet diameter is 30 inches, and the velocity can be varied continuously from less than 1 ft./sec. to a maximum of 124 ft./sec. The variable speed system is described in Appendix B.

As hot-wire anemometers are to be used in this work, considerable care was taken in the design to have a low level of vibration and turbulence, and to remove atmospheric dust.

Pankhurst and Holder (1952), Pope (1954), and Bradshaw and Pankhurst (1964) were found helpful in the design of this tunnel. In particular, the report by Bradshaw and Pankhurst was used extensively. The design was also compared with the specifications and performance of an existing blower wind tunnel (Wygnanski and Gartshore (1963)).

A novel two-dimensional expansion was developed from the theory proposed by Hughes (1944). A large area-ratio expansion was needed in a limited space, and it was desired that this expansion have low turbulence and good spacial uniformity of flow at its exit even at the expense of no recovery in the static pressure. Appendix A gives the theory for this expansion in detail, how the theory was adapted for construction, and its performance.

A sketch of the tunnel is shown in Figure 3-1. With the exception of the fan unit the tunnel is almost entirely constructed of plywood.

3-1-1 Air Filter and Fan Unit

The tunnel is driven by a single stage centrifugal fan with backward curved blades (Buffalo No. 805 B.L., double inlet type). At the maximum operating speed of 900 RPM it delivers 37,000 CFM of air at a pressure differential of 4.6 inches of water. The fan is belt-driven through a 2:1 reduction from a 40 HP 110 Volt DC electric motor. The air velocity is controlled by varying the motor speed through a Ward-Leonard system. (See Appendix B). The speed controls are conveniently located on the tunnel just before the end of the contraction.

The fan and motor are mounted on a steel frame. This frame is in turn mounted on vibration isolators. To further isolate fan vibrations from the rest of the tunnel, the fan is connected to the transition section by a 6 inch wide rubber sleeve. This also allows for the small movement of the fan on the vibration isolators as the speed (and thus the pressure rise) varies.

The entire fan unit is enclosed by a 12 ft. x 12 ft. x 8 ft. high filter box. The upstream wall of this enclosure is occupied by 24-2 ft. x 2 ft. Dripak high efficiency air filters (American Air Filter Co., Type 2090), and their associated prefilters. These filters remove most dust particles down to .5 microns diameter. The pressure drop through the filters is appreciable, being .7 inches of water, but the use of filtered air greatly improves the performance of hot-wire anemometers. As a test of the filters, a hot-wire anemometer was operated for a 4-hour period. No measurable drift was noted, and later examination of the hot-wire probe under a microscope showed no accumulation of dust particles.

3-1-2 Transition and Two-Dimensional Expansion Sections

Following the fan there is a 48 inch long transition section. This section, which is of essentially constant area, has inlet dimensions of 55-3/4 inches wide by 43-1/4 inches high (to match the fan outlet), and outlet dimensions of 78-1/2 inches wide by 30 inches high (to match the inlet to the expansion section). This transition section also lowers the centre line of the flow by 5 inches to coincide with the centre line of the rest of the tunnel.

The expansion section has an inlet to outlet area ratio of 1:2.62, and is two-dimensional. The wall shape follows a free streamline theory first suggested by Hughes (1944) which permits the rational design of a rapid expansion. This is achieved without static pressure recovery in the expansion.

The length of the expansion is 80 inches, or 1.02 times the exit height. The inlet of the section matches that of the transition, while the outlet, which is 78-1/2 inches square, joins directly to the settling chamber. A curved screen stretches across the expansion at the section where there is an abrupt rise in pressure along the curved wall. The screen is designed to supress separation at that point. An optimum choice of screen pressure drop coefficient would have the expansion produce zero net static pressure rise. However, available screen material dictated the use of a perforated plate with a pressure drop coefficient 30% higher than optimum. By the usual definition of diffuser efficiency the expansion section has an efficiency of -30% instead of perhaps +90% that could be expected from a well designed diffuser with 5 degree cone angle. However, such a diffuser would have to be in excess of 32 feet long and available space prohibited such a choice. The difference amounts to about 6% of the total tunnel power.

Appendix A gives the theory for the design of the expansion.

3-1-3 Settling Chamber

The settling chamber is 80 inches long and 78-1/2 inches square at the inlet. It tapers along its length to a regular octagonal cross section at the outlet. As the sides which formed the square cross section at the inlet are kept parallel, the chamber has a 1.21:1 contraction ratio.

The settling chamber has four screens to reduce spatial variations of velocity and turbulence. These are equally spaced along the length of the section, and are approximately 2 ft. apart. The first screen is of steel, 18 mesh, 24 SWG wire, and has a pressure drop coefficient of about 4. The other three screens are bronze, 20 mesh, 30 SWG wire. Their pressure drop coefficient at the highest tunnel speed is 1.5 and they have an open area ratio of .56. This value was chosen as it appears that values of open area ratio less than this may produce spatial non-uniformities in the flow (Bradshaw (1963)). All the screens are mounted on wooden frames that can easily be slid out of the tunnel for cleaning. The steel screen was made up of two pieces carefully woven together, while each bronze screen is in one piece. All the screens were supplied by the Sankey Green Wire Weaving Co., Thelwall, England.

A honeycomb section is also included in the settling chamber. It too is mounted on a wooden frame for ease of removal and cleaning, and is positioned between the first two screens. The honeycomb is aluminum (Hexcell Manufacturing Co.), and is 1-1/2 inches thick, with 1/4 inch cell size. The biggest piece of honeycomb available was approximately 48 inches wide, so it was decided to join three pieces together. One 48 inch piece was placed in the centre of the frame and the space on either side filled with narrower pieces. The joints were made by gluing the pieces to a 1-1/2 inch side by 1/32 inch thick strip of aluminum placed between them. This method of construction was chosen to give a clear area of honeycomb in the centre of the tunnel.

3-1-4 Contraction Section

The contraction has an area ratio of 7.2:1, and is 90 inches long. The inlet shape is that of a regular octagon, which changes to a 32-sided shape at the outlet. The calculations for the contraction followed those of Cohen and Ritchie (1962). Extensive use of a digital computer was made in this design, first to calculate the shape of the theoretical axisymmetric contraction, and then to calculate the detailed shape of the frames and wall pieces. This allowed these complicated shapes to be precut to close tolerances, and very little fitting was required. It was built around a male jig.

3-1-5 Joining, Mounting, and Access

The sections of the tunnel, and the pieces that make up the sections, are all built with flanges, which form part of the framework. These pieces and sections are joined together with bolts. This was done to allow for the possible disassembly and relocation of the tunnel.

Each section of the tunnel is mounted on its own set of wooden legs, and was adjusted in position to maintain the tunnel centreline 56 inches from the floor.

Access to all parts of the tunnel is provided by a door and 4 hatches. A full size door allows entry into the filter box, and access to the back of the high efficiency filters and to the fan and motor assembly. A hatch in the bottom of the transition section permits access to the outlet end of the fan and to the expansion as far as the expansion screen. Another hatch in the downstream end of the expansion gives access to this area, while a hatch in the side of the settling chamber gives access to the region between the second and third screen. Partial removal of some of the screen frames makes the rest of the settling chamber accessible as well as the inlet to the contraction. Finally, a hatch in the bottom of the contraction section allows access to this region.

3-1-6 Total Pressure Investigation

Two total pressure surveys were made at the outlet of the tunnel. The first was made with no screens in the settling section, and allowed an assessment of the performance of the expansion section. The second survey was made with all screens and the honeycomb in place. In both cases the static pressure was found to be essentially constant across the outlet, and equal to atmospheric pressure. Both surveys were made by comparing the readings from a 1/16 inch diameter total head tube with a similar one mounted 2 inches out from the wall of the contraction and 4 feet upstream from the outlet, and were made at 115 ft./sec. outlet velocity. In the first survey measurements were made every inch in the horizontal direction, and every two inches vertically. The second survey was made every two inches in both directions. These measurements excluded the boundary layer region. Contour plots of these two surveys are given in Figures 3-2 and 3-3. The results are expressed relative to an average velocity, and assume constant static pressure across the exit plane.

The first survey shows that the fan plus the expansion section produce a high degree of uniformity in the outlet velocity, the total velocity variation over the working section being less than .5%. It would be expected that the two-dimensional expansion section might develop some secondary flows in the corners, as well as thicker boundary layers on the parallel (vertical) sides where the pressure gradient is adverse. This would perhaps explain the four regions of reduced velocity on the diagonals of the tunnel outlet and the generally reduced velocities on the sides indicated in Figure 3-2.

With the screens in position the outlet velocity shows less variation (.3%) and the pattern of variation is much simpler (Figure 3-3). The contours of constant velocity are approximately concentric circles, with the maximum velocity in the centre.

A static pressure tap was installed at the entrance to the contraction section 8 inches downstream from the last screen, and two others were installed 8 inches from the contraction section outlet and on opposite sides of the tunnel. The downstream static taps are connected together, and the pressure difference between them and the upstream tap is used to monitor tunnel speed. This pressure difference was not calibrated against tunnel speed as the vented working sections that would be attached to the tunnel would produce large static pressure variations across the tunnel outlet.

A boundary layer survey was made on the bottom of the tunnel outlet using a hot-wire anemometer. The test was made at a velocity of 85 ft./sec. The boundary layer was turbulent, with a thickness of .35 inches.

3-1-7 Tunnel Turbulence

A survey of the longitudinal component of turbulence was made, using a normal hot wire. Without the screens, the relative longitudinal turbulence intensity ($\sqrt{\overline{u^2}}/U$) varied from 1% in the centre of the outlet to about 1.5% near the walls (but outside the boundary layer). With all the screens in place, the relative intensity was .2% or less, and was essentially constant over the tunnel outlet. In both cases there seemed to be little variation with tunnel speed.

3-2 Jet Supply

The experiment required an axisymmetric source in the centre of the air flow from the tunnel. A preliminary experiment with an axisymmetric wake body suspended on piano wire was done. The tunnel working section was adjusted for an adverse pressure gradient similar to what was eventually used for the rest of the experiments. In this relatively strong adverse pressure gradient the originally small two-dimensional wakes from the supporting wires grew rapidly and soon swamped the wake from the axi-symmetric body. In retrospect this was not surprising, as the adverse pressure gradient needed for self-preserving growth of a two-dimensional wake is considerably less than that for an axisymmetric wake. It meant, however, that the jet producing apparatus should be truly axisymmetric and have no supporting struts or wires that could produce a wake.

The design evolved around a 2 inch diameter light-weight aluminum pipe extending the whole length of the tunnel, and supported on and cantilevered from the wind tunnel screens. Figure 3-4 gives the general arrangement of the jet supply. The feed into the longitudinal pipe was an aerofoil section just down-stream of the wind tunnel fan, and no evidence of any wake from it was found at the outlet of the tunnel contraction.

Halfway along the contraction the diameter of the pipe was smoothly reduced to 3/4 of an inch and there was a fitting to allow longitudinal adjustments of the jet pipe outlet. The fitting consisted of a sliding O-ring seal for air tightness, and part of a 3/4 of an inch lathe collet to lock the pipe into position. (See Figure 3-5). In some cases this 3/4 of an inch pipe was further reduced in diameter before the pipe outlet was reached.

The air supply came from a 15 H.P. air compressor used for the general building supply, and passed through a filter that removed oil and water droplets down to 2 micron size. The air compressor was run continuously to maintain a fairly steady pressure at the input to the pressure regulator. (This pressure was typically 100 to 110 p.s.i.). This was done by bleeding air off with a valve ahead of the filter until a stable condition was obtained. In practice this entailed 15 to 20 minutes of alternately adjusting the bleed valve and pressure regulator until a stable condition was achieved with the desired pressure in the pipe to the jet.

As hot-wire anemometers are sensitive to temperature as well as velocity, it was necessary to ensure the jet had the same temperature as the air flow from the tunnel. This turned out to be easy to do, as the long run of the 2 inch air pipe and the low velocity therein (5 to 10 ft./sec.) ensured that its temperature closely matched that of the room and tunnel. Since the temperature of the air after being throttled to room pressure and slowed to a low Mach number should be the same as the stagnation temperature before throttling (assuming adiabatic flow and C_p a function of temperature only), this appeared sufficient. Measurements of average temperature in the jet a few inches from the outlet showed no measurable temperature difference between that and the free stream (less than 0.5°C). As the jet downstream consisted mostly of entrained flow (volume flux 5 to 15 times larger than that emerging from the jet pipe), no further concern was felt in this area.

In all the cases used, the length/internal diameter ratio of the final jet pipe was 50, and essentially controlled the flow for a given setting of the pressure regulator.

Using a pipe R_e of 200,000 and standard curves for the smooth pipe friction factor (λ) gives $\lambda(\frac{L}{D}) = 1.$ with an L/D ~~of~~ 50. From the perfect gas relation for frictional adiabatic flow in a pipe

(Fanno Line) and assuming M = 1 at exit, M = .47 at the entrance to the pipe, and the static pressure ratio from the entrance to exit is

$$p/p^* = 2.28,$$

where p* is the pressure at the exit from the pipe where M = 1.

From the isentropic relations for a perfect gas, the ratio of the stagnation pressure to static pressure at M=.47 is

$$p_0/p = 1.163$$

and the overall pressure ratio is

$$p_0/p^* = 2.65$$

Thus to just achieve sonic velocity at the pipe exit it is necessary to have a supply pressure of at least 24.3 p.s.i.g. The supply pressures used for the three jet cases studied were 19, 20, and 30 p.s.i. gauges. Thus the jet using 30 p.s.i.g. was choked flow and

$$p^*/p_{atm} = 1.15$$

For the 20 p.s.i. jet the exit Mach number is

$$M_{exit} \simeq .91$$

and for the 19 p.s.i. jet,

$$M_{exit} \simeq .87$$

The total volume flow from the jet (at atmospheric pressure) is about .5 cu. ft./sec. and leads to a velocity in the 2 inch supply pipe (at 2 atm) of 10 to 15 ft./sec. With an effective pipe length/diameter ratio of 600 in the 2 inch supply pipe from the pressure gauge to the final small diameter jet pipe, the pressure drop in this pipe is very small ($\approx$ .03 p.s.i.), and may be ignored in these calculations.

3-3 Working Section

All self-preserving jets and wakes of practical interest require an adverse pressure gradient; consequently the working section of the tunnel must provide for an adjustable axisymmetric decrease in velocity down the working section. There are two basic ways to accomplish this - either with an adjustable cross-section or an adjustable air bleed (or some combination of both). As an adjustable cross-section seemed insurmountably complicated as well as requiring some form of boundary layer control to avoid separation, the latter approach was taken. Thus the working section was of uniform cross-section and it could be made up of identical short elements.

A system of air bleeds brings problems of its own, as the requirements of an axisymmetric air bleed are in conflict with the need for access to the working area, support for traversing gear, and general support for the structure.

It was decided to use a light-weight, low-blockage wooden support for a cylindrical working section made of high-porosity perforated sheet metal. The holes in the plate were 3/16 of an inch on 1/4 of an inch staggered centres. This sets an upper limit on the porosity, but in practice the desired porosity was much less than this maximum except right at the start of the working section.

The working section was made up of a number of identical elements, each 3 feet long and 30 inches in diameter. They were made as two half cylinders split horizontally and hinged on one side. The semi-cylinders of perforated plate were held by a 3/4 inch flange at each end and along the horizontal seam. There was also a 3/4 inch filler piece in the horizontal joint that could be removed and replaced by the supports for the traversing gear. See Figure 3-6.

The support for these 3 foot sections were two wooden rails to which the sections could be clamped. In use, the sections were held together with large

C-clamps.

There were ten positions in each section at which the traversing gear could be placed. For reference they were numbered 1 to 10 from the up-stream end. The working sections themselves were numbered from the tunnel outlet downstream. Thus the fifth traversing gear position in the second working section downstream from the tunnel is labelled (2 - 5). The zero for x was the leading face of the first working section, and Table 3-1 gives a list of the positions used and the resultant distance of the probe tip from the x = 0 position.

The blockage of the perforated plate to set the pressure gradient was done by covering some of the holes with masking tape. Considerable care was taken to ensure that the blockage produced was consistent, reproducible, and axially symmetric. Consequently the tape was placed on the inside of the sections, and the pattern was arranged so that each hole in the perforated plate was either completely open or completely covered. Thus there were no unadhered edges in the tape pattern to stretch or age and the flow was likely to be axisymmetric and invariant with time.

Where the ratio of closed holes to open holes did not exceed 12 or 14 to 1, the pattern was set up by leaving circumferential strips of holes uncovered by tape. This assured that the maximum distance between rows of open holes was 3.5 inches. For ratios larger than this the whole of the perforated plate was covered and the masking tape drilled out and neatly trimmed with a special cutter.

Ideally, the resultant porosity of the working section should vary smoothly in the axial direction and be constant around any circumference. Obviously, with say 14 rows of holes blocked and one open the porosity does not vary smoothly in the axial direction; and when the change is made to having individual holes open rather than complete circumferential strips, it is no longer circumferentially uniform either. The assumption is made that this is not important however, when the scale of these non-uniformities are small, relative to the distance from the edge of the jet to the wall, and when the change in U_1 is small. This was typically 8 to 10 inches at the point where a row of open holes was 3.5 inches from the preceeding row and where U_1 might be expected to decrease by 3% in this 3.5 inches. No calculations or measurements were made to check this but it was felt that the amount of non-uniformity in the variation of U_1 would not be serious.

Further downstream the maximum distance between holes varied as the square root of the open to total hole ratio, and the maximum distance at measured stations did not exceed 2 inches. Here flows were measured to within 4-1/2 inches of the wall, and U_1 varied by 1.5% over 2 inches in the x-direction.

The end of the working section was blocked by a flat piece of perforated plate of somewhat lower porosity than that forming the working section (1/8 inch holes on 3/16 inch centres). This provided the resistance that enabled the adverse pressure gradient to develop.

It is difficult to determine the pattern of tape which gives a desired velocity distribution, $U_1 = C(x-x_0)^m$. The outflow velocity must be largest near the jet origin, where unfortunately the pressure difference to drive it is smallest while the opposite is true far downstream. Thus the range of pressure drop coefficient from beginning to end of the working section must be large. In addition, the jet entrains the streaming flow U_1, and the amount of entrainment is strongly dependent on U_1, particularly near $x = 0$. As well, the elliptic character of the flow meant that changes in tape pattern at one station would affect the velocity gradient elsewhere in a manner that would be difficult to predict intuitively. When all this was considered along with the fact that a significant change in tape pattern and testing to measure its effect would take several days, it was felt that a "cut and try" approach would be retrogressive. Consequently analytic and semi-analytic methods were adopted.

The procedure used was first to predict the mean velocity field at the working section walls using a form of the continuity equation, and second, to use these velocities plus a simple theory for the pressure drop coefficient of a perforated plate to predict the ratio of open to closed holes as a function of x.

There were two assumptions used in predicting the behaviour of the flow through the perforated plate. First, that the pressure drop across a section of plate was a function of the perpendicular component of velocity only. (Taylor and Batchelor (1949)). Thus

$$2\,(P_0 - P_\infty) - (U^2 + V^2) = C_p\, V^2$$

where P_0 is the kinematic total pressure in the tunnel,

P_∞ is ambient kinematic static pressure outside the working section, U and V are evaluated at the working section walls

and C_p is a local pressure drop coefficient for the perforated plate.

The second assumption is that volume flow through a hole in the plate is a function only of the pressure drop across it, and is not affected by whether neighbouring holes are open or not. Then the effective local pressure drop coefficient is given by

$$C_p = N^2 C_{p_0}$$

where N is the ratio of total holes to open holes in any area, and C_{p_0} is the pressure drop coefficient for the completely open plate.

These assumptions are known to be inaccurate, as C_{p_0} is a function of Reynolds number and the amount of tangential flow, and blocking off some of the holes does affect those nearby. However, they did allow the prediction of a tape pattern with the right sort of character to use as a starting condition for the subsequent experimental iteration which was used to determine the required pattern.

Since the desired free stream velocity on the axis of the flow was specified by an analytic expression, $U_1 = C_1 x^m$, which has continuous derivatives of all orders, it seemed attractive to calculate the velocity field at the working section walls by using an expansion of the Stokes-Beltrami equation in powers of radius Y of the working section. (The Stokes-Beltrami equation is the axisymmetric equivalent of Laplace's equation in cylindrical polar coordinates). The mathematical procedure used by Cohen and Ritchie (1962) to predict the streamlines for an axisymmetric contraction was used. The attractive feature of this approach was the promise of more realistic values of U and V for x/Y small than would be obtained by assuming $U = U_1$ at the wall.

This procedure was used to set up the first tape pattern. While the resulting flow was used successfully as the starting point for the subsequent iterative approach to improving the flow, the hoped-for accuracy in flow prediction, particularly near the virtual origin of the flow, was not realized. Consequently the simpler approach assuming U = const. across the flow should have been used, especially as it also allows inclusion of the effects of jet entrainment.

This simpler approach was, however, used in the iterative procedure to predict improvements for the tape pattern in setting up all subsequent flows. The equation is

$$V_Y = -\frac{1}{2}\left(Y\frac{dU_1}{dx} + \frac{1}{kY}\frac{d}{dx}(U_0 L_0^2)\right)$$

where Y is the radius of the working section, the Gaussian form of jet or wake profile is assumed, and U_1 is assumed constant across the flow.

The velocity through the plane perforated plate at the end of the working section is assumed uniform across the plate, and given by

$$U_F = U_1 + \frac{(U_0 L_0^2)}{kY^2}$$

for values of U_1, U_0, and L_0 expected at this plate position. This satisfies volume flux requirements.

The iterative procedure made use of measured values of U_1, U_0, and L_0 to calculate values of $V_Y(x)$ and U_F, using this continuity equation. Then analytic relations for U_1, U_0, and L_0

$$U_1 = C_1(x-x_0)^m, \quad U_0 = G\,U_1, \quad L_0 = C_0(x-x_0)$$

were used to calculate the desired values of $V_Y(x)$ and U_F. Then these two sets of $V_Y(x)$'s and U_F's, along with tunnel total pressure, were used to predict the change in tape pattern needed to produce this flow, using the assumed behaviour of the perforated plate.

If measurements on the flow resulting from this new tape pattern were still unsatisfactory, these measured values became the input to a new iteration step. Approximate values of C_0 and G were selected and thus m calculated, and an approximate value of x_0 determined by extrapolating L_0 to zero. The rough approximations used in predicting the behaviour of the perforated plate worked, because the measured flow and existing tape pattern were used to calculate an effective local C_{p_0}, and a new value of N (the ratio of total to open holes) calculated for the desired flow using this C_{p_0}. Thus, as the measured and desired flows become closer, the more accurate should be the prediction of the tape pattern change.

As noted, the values measured for a flow pattern were used to calculate outflow velocities and wall pressure drop coefficients as they actually existed. This was done by interpolating the experimental values for U_1 and $(U_0L_0^2)$ to get intermediate values and derivatives. The process for doing this interpolation turned out to be crucial to the success of this method. Several reasonable choices, which might tempt a future experimenter, turned out to be unsatisfactory. Consequently it seems worthwhile to explain these methods and why they didn't work. It should be noted that all the methods used or considered produced satisfactory answers for the interpolated values of U_1, $(U_0L_0^2)$, and $\frac{d}{dx}(U_0L_0^2)$. It was the problem of obtaining the derivative of U_1 that created the difficulties.

The first and most obvious choice was to fit the n experimental points by a $(n-1)^{th}$ order polynomial in x. This would produce a smoothly varying derivative that is easily evaluated at any value of x, and standard programs and techniques are available to calculate the coefficients. This approach was, however, rejected at the outset, as a high order polynomial like this would be expected to show ripples about a 'smooth' line through a set of points that approximated an x^m relation (where m is negative). Thus the tape pattern corrections would show periodicities that had little to do with correcting the real flow that existed.

Initially a quadratic polynomial was fitted, through the four experimental points nearest the x-value of the point at which interpolated results were needed. A least-square error approach was used to fit the curve to the data. A quadratic polynomial seemed a simple curve that had the desired properties of a smoothly varying derivative and no inflection point, and again, standard programs and techniques are available to evaluate the coefficients. When this was tried a problem quickly showed up in that the predicted changes in hole pattern showed periodic large, abrupt jumps as the x_i value was changed. The wavelength was about that of the spacing between experimental points, and was caused by the changes in the set of the four experimental points used to evaluate the polynomial coefficients. Over a certain interval the interpolated derivatives would be determined by the fixed coefficients of a quadratic polynomial which were in turn determined by the values of the four experimental points near this region. Consequently, as the interpolation point was stepped along the derivative would vary in a smooth linear manner. But then a point would be reached where these four experimental points were no longer the closest, and the quadratic coefficients and thus the value of the derivative would change abruptly as one of the experimental points was dropped and a new one added to make up the set of four.

In the face of these difficulties modifications were made in the interpolation program to smooth the transition caused by the changing influence of the experimental points on the calculated derivative. The four-point procedure was to determine a_2-a_0 by solving

$$\frac{\partial}{\partial a_j}\left[\sum_{i=n-1}^{n+2}\left(F(x_i^{\circ})-(a_2x_i^2+a_1x_i+a_0)\right)^2\right]$$

where $j = \begin{Bmatrix} 0 \\ 1 \\ 2 \end{Bmatrix}$, and $F(x)$ was the experimental value of either $U_1(x)$ or $U_0L_0^2(x)$ at x_i and n is chosen so that the four experimental points are the closest available to the point at which interpolated values are desired. To eliminate the effect of changing the set of experimental points, this was changed to

$$\frac{\partial}{\partial a_j}\left\{\sum_{i=1}^{n_{max}}\left[\left(F(x_i)-(a_2x_i^2+a_1x_i+a_0)\right)^2\exp\left(\frac{-(x_i-x_p)^2}{\sigma^2}\right)\right]\right\}=0$$

where x_p is the x-value for the interpolated point. This used all the experimental points but weighted their importance so only those near x_p had much influence. The value of σ was chosen to be approximately one-half the distance between experimental points.

This relation gave a smoothly varying derivative, and the interpolated values of U_1 and $U_0L_0^2$ gave an excellent fit to a hand drawn curve through the experimental points.

This relation was used in the calculations for the pressure gradient for all the self-preserving jets. Two to three iterations seemed to be enough to set up a reasonable flow for these cases.

The jet with $G = .85$ (weakest jet) gave the most difficulty.

When this procedure was used for the self-preserving wake, it did not converge. After three iterations not much improvement had been achieved, and it was decided to re-examine the numerical aspects of the procedure. The apparently inconsistent finding was then made that while the interpolated values of U_1 fit the experimental data well, the value of the derivative was always too large in magnitude by a few percent. The discrepancy was not very big, but the resultant tape pattern consistently had too much blockage, and this caused an accumulated error between theory and reality.

The basic cause of the problem was that a quadratic polynomial was not a good function to use for fitting $U \approx C\,(x-x_0)^m$ where $-1/2 \geq m \geq -1$. A segment of such a velocity versus x curve will have its maximum curvature at the high velocity end. When a quadratic polynomial is fitted to such a curve the part of the parabola chosen will always have its maximum curvature at the low velocity end, and at the centre of the parabolic segment the magnitude of the gradient is always larger than that of the curve being fitted.

The solution to this problem was to use

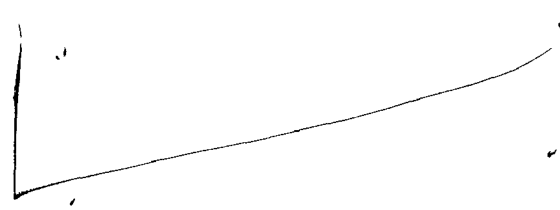

a more suitable function to fit the experimental points, and

$$U=a_1 e^{-a_2 x}+a_3$$

was chosen. (It might be noted here that in some similar earlier work an unsuccessful attempt had been made to use $U = a_1(x-a_2)^{a_3}$ as a fitting function. Although the problem may have been due to other causes than the choice of function, this experience led to using the exponential relation above). As before, the algorithm was to make

$$\frac{\partial}{\partial a_j}\left(\sum_{i=1}^{n_{max}}\left(\left(U_1(x_i)-(a_1 e^{-a_2 x}+a_3)\right)^2 \exp\left(-\left(\frac{x_i-x_p}{\sigma}\right)^2\right)\right)\right)=0$$

for j = 1, 2, 3.

Any suitable numerical routine can be used to find the value of the coefficients a_j; in this case a three-dimensional Newton-Raphson method was incorporated into the program for this purpose.

When this more suitable function was used to predict the tape pattern the first iteration produced a satisfactory flow. It is probable that it would also have been easier to set up the jet cases using this function.

3-4 Traversing Gear

The traversing gear used in this experiment was able to provide movement both horizontally and vertically. It consisted of a horizontal slide that extended the width of the tunnel and which was supported in the 3/4 inch slots available between the two halves of each working section segment. This slide in turn carried a shorter vertical slide on which was mounted the instrument probes. The traversing gear is shown in Figure 3-7.

Obviously there had to be some compromise in the design between obtaining maximum horizontal and vertical traversing distances as a long vertical slide would allow only limited horizontal movement. The choice made gave approximately 22 inches of travel horizontally and 15 inches of travel vertically. This gave sufficient vertical travel to allow checks of axisymmetry while allowing measurements to be made in the horizontal direction to within 4 inches of the working section walls. In practice the vertical slide was used primarily to find and position the probes at the centre of the jet or wake.

The horizontal slide consisted of two 18 inch segments of aluminum dovetail slide supported in a steel frame. The structure was 3/4 of an inch thick and 4 inches wide, with a wooden fairing to keep flow disturbances to a minimum. The vertical slide was also an aluminum dovetail unit, 18 inches high overall, 1/2 of an inch thick, and 2-1/2 inches wide, and it also had a wooden fairing. The slides were commercial Velmex Unislides. The probe tip was 13 inches ahead of the vertical slide and 16 inches ahead of the horizontal slide.

Blockage effects from the two slides were calculated by simple inviscid theory by replacing the slides by appropriate line sources. The total change in velocity at the probe was thus estimated at <2%. This was checked (for the part caused by the vertical slide), by comparing static pressures at the probe position (with a separate static probe) with and without the vertical slide in proximity, and this agreed with the calculated values. No corrections were applied and since all results are presented non-dimensionally, the only error is due to the change of interference due to the non-uniformity of the flow, an error which should be much less than 2%.

The probe holder mounted on the vertical slide had provision for carrying a hot-wire probe and two pressure measuring probes, positioned in a vertical row 1/2 of an inch apart. In practice either a static and total pressure probe were used together to measure mean velocity, or a total pressure probe and a hot wire were carried to measure mean and fluctuating velocity components. In this case the pressure probe was used only for hot-wire calibrations.

All definitive measurements of the flow were done with a hot-wire anemometer. Mean velocity and longitudinal turbulence were measured using a normal hot wire with the wire in the plane of the traverse. The other stress tensors were calculated using readings from a single slanting hot wire. For the slanting wire two readings were taken at each position of the traverse with the wire positioned in the plane of the traverse, rotating the wire 180° around the probe's longitudinal axis between readings. As well, a similar set of two readings were also taken at some positions with the plane of the wire vertical. Calculated values of Reynolds stresses that involve slanted hot-wire measurements were corrected for longitudinal cooling using measured values of wire angle and aspect ratio. (Champagne et al (1967), Patel (1968)). No higher order corrections were taken into account.

The hot-wire probes were mounted in a special holder that held them rigidly in alignment while allowing rotation of the probe around the longitudinal axis. Thus all slanting-wire measurements at a particular position could be made very close in time to each other. Indexing accuracy was not measured, but was estimated to be about one degree.

3-5 Instrumentation

Figure 3-8 is a block diagram of the instrumentation used in the measurements. A Disa constant-temperature hot-wire anemometer was used for mean flow and turbulence measurements. The output voltage was made linear with velocity by means of a Disa linearizer. This output was measured directly to obtain mean velocity, and fed to a Hewlett Packard true R.M.S. meter to measure the fluctuating components of velocity. This meter has a low frequency cutoff of 5 Hz.

Some mean flow measurements were also made with pressure probes, and these probes were also used in calibrating the hot wires. With the exception of the tunnel reference pressure, all pressure measurements were made with a single Statham 0.3 p.s.i. pressure transducer, which gave excellent linearity and repeatability. It in turn was calibrated against an Askania water manometer.

The technique for obtaining time averages is important when making accurate measurements in turbulent flow. For a few seconds average visual integration from a meter may be satisfactory, but for longer times it becomes tedious and inaccurate. The use of R-C analog circuitry to lengthen the response time of measuring instruments is useful, but beyond a time-constant of 10 to 20 seconds the problems of transient recovery and charge leakage become important.

The solution chosen here was to use a combination of analog and digital averaging, using a computer controlled multiplexer and analog-to-digital converter. Each voltage that was to be measured was first averaged, using an R-C time constant of 10 seconds. Then a measurement of each voltage was made every 5 seconds by the computer system, and ultimately averages were calculated and printed out. As well as solving the problems mentioned above, other benefits were realized from the use of this system. Because satisfactorily accurate measurements of the 'averaged' analog voltages took less than 20 milliseconds, it was reasonable to average both the mean and fluctuating component of velocity over the same time interval. With long total integration time (50 seconds), this cut the time for hot wire traverses almost in half. Secondly, having short term estimates of the voltages (set by the 10 second R-C time constants) enabled the computer program to compute a running estimate of the accuracy of the reading, using standard statistical techniques.

These estimates were used in two ways. The last estimate using all the data was printed out along with the data and gave a measure of the accuracy of the average. Secondly, if the estimate of the accuracy got better than a set amount before the maximum averaging time of 50 seconds, the program stopped taking readings and printed out the averages calculated for this shorter integration time. Typically one-quarter to one-third of the readings would take less than the maximum time.

This program was one of three used in data gathering, and, as noted, printed out for each position the values of mean and fluctuating voltages (taking into account the gain setting on the R.M.S. meter), and estimates of the accuracy of the readings.

The second program was used when mean velocity profiles were gathered using the pressure probes. The output of the pressure transducer was averaged, the zero voltage subtracted, and the velocity calculated using appropriate constants for the transducer calibration and air density. The voltage and velocity for each position was then printed out.

The third program was used to calibrate the hot-wire and set up the linearizer. It had previously been empirically determined that the performance of the hot-wire probes used could be adequately described by

$$(\text{Volts})^2 = A + B(\text{Vel.})^{.4}$$

Consequently the calibration program measured the pressure transducer voltage to obtain velocity along with output from the anemometer both before and after the linearizer. It then printed out the values of transducer voltage, calculated velocity, anemometor output voltage (unlinearized), linearizer output, $(\text{velocity})^{.4}$, $(\text{bridge voltage})^2$, and the value of transducer zero voltage used in the calculations. (In this and the previous program the transducer zero voltage to use could be updated at any time by taking a zero reading). This program was used both to set up the linearizer and to subsequently check the linearized output. Figures 3-9, 3-10, and 3-11 are examples of output from the three programs.

3-6 Experimental Procedures

The major aim of this research was to measure the growth and related parameters for self-preserving axisymmetric free shear flows covering the range from wakes to fairly strong jets. As well, some measurements were made on two other axisymmetric flows, the still-air jet and the small-deficit wake in zero pressure gradient.

3-6-1 Axial Symmetry

Axial symmetry was ensured in a number of ways. First of all, considerable care was taken to provide a symmetric environment. The jet or wake producing apparatus was cylindrical, had no support struts, and was carefully centred in the tunnel. The working sections were cylindrical and the hole pattern to control the flow was axially symmetric except at the division between the top and bottom halves of the sections. The 2-1/4 inch wide blockage here was compensated by extra openings on both sides of this blocked area.

When a satisfactory flow was achieved,

part of the information available was the centre position of the jet at each station. Any wandering of the flow would have indicated an asymmetry in the mean flow field. In practice the variation was in the order of $\pm.1$ inches, which is not much more than the absolute positioning accuracy of traversing gear from station ~~to station~~.

Another check was to make vertical mean velocity traverses and compare them with a horizontal one at the same station. In all cases the profiles were identical. As well, a contour plot of mean velocity at one station was generated and is shown in Figure 3-12. As the other indicators seemed favourable this was only done at one station for one self-preserving flow.

As a final check on one self-preserving flow, shear stress profiles were made in a vertical traverse at one station, and again the agreement with the horizontal traverses is excellent.

3-6-2 Setting Up the Flows

The procedure used to generate the appropriate pressure gradient has been described in the section on the working sections. In each case an approximately correct flow would be generated by changes in jet-pipe size and longitudinal position, and jet and tunnel working pressure. Mean velocity measurements were made of the streaming flow and the jet (or wake) profile at 8 to 10 stations in the flow that extended over approximately a 3:1 ratio of distance from the jet (or wake) source.

3-6-3 Self-preservation

In practice, the primary decision on whether a satisfactory flow had been achieved was based on G becoming nearly constant for a significant length of flow. Having L_0 varying linearly with x was also important, but this was always satisfactory when G became constant as G = constant seemed to be a much more sensitive indicator.

That U_0 and U_1 varied at the appropriate power of x was also checked, as was the self-preserving behaviour of the longitudinal component of turbulence. The value of m for $U_1 = C_1(x-x_0)^m$ agreed well with that predicted from the momentum equation.. The best fit of m for $U_0 = G \cdot C_1(x-x_0)^m$ did not seem to be in as good an agreement with the momentum equation prediction, but this disagreement was due to what were assumed to be acceptably small changes in G down the flow.

The longitudinal turbulence took longer to reach a self-preserving form, and was therefore a severer test of self-preservation.

3-6-4 Self-preserving Streaming Flow Cases

Four self-preserving axisymmetric flow cases were studied. Three were jets, with a G (= U_0/U_1) of .85, 1.83, and 3.00; the fourth was a wake with G = -.54. Details of the jet pipe positions and jet operating conditions are given in Table 3-2. The axisymmetric body used to produce the wake was one of the jet pipes with its exit blocked. The end 12 inches of this pipe was 1/4 inch outside diameter. Upstream from this was a smooth transition to the 3/4 inch diameter pipe that was in turn supported by the 2 inch jet supply pipe within the contraction section of the tunnel. This is described more fully in section 3-2.

In the process of setting up this wake several wake producing bodies were tried. All used the jet pipe apparatus as support. A bluff body (a 2 inch diameter disk), and a square-ended 3/4 inch rod were tried as well as the wake source ultimately used, and the aim was to produce as strong a wake as possible. The disk was unsatisfactory as the wake produced was broad and very shallow. The 3/4 inch rod was better, so the jet pipe with the 1/4 inch end section was tried and proved satisfactory. It appears that the strong eddies behind a bluff body are very effective at distributing momentum across the flow, and make for a wide, shallow wake. The wake from the slimmer pipe probably was largely composed of boundary layer from the 3/4 inch pipe upstream, with correspondingly lower turbulent intensity and scale than a separated flow. To further try and reduce the component of separated flow in the wake, and thus possibly making a deeper wake, a streamlined plug was added to the end of the 1/4 inch pipe. No change in the wake was noted, possibly because the boundary layer would not stay attached to the plug in the strong adverse pressure gradient existing at that point. In fact, this boundary layer may even have separated before the end of the pipe. No tests were conducted of the conditions near the end of the pipe.

As noted in Table 3-2, the end of the wake-producing apparatus was 17 inches further downstream than the jet outlet for any of the jet cases. This was necessary to enable the wake to be started in a strong adverse pressure gradient. When an attempt was made to start the wake further upstream it decayed too much before the pressure gradient became established.

For the three jet cases more detailed measurements were made at one or more stations. These stations were chosen to be ones at which measurements of longitudinal turbulence indicated that the turbulent structure had settled down to a self-preserving form. Measurements were made with a single slanting hot wire rotated about the x-axis to lie in the x-y and x-z planes. (More details are given in Section 3-4). These readings, combined with normal hot-wire measurements enabled $\overline{u^2}$, $\overline{v^2}$, $\overline{w^2}$, $\overline{uv}$, and $\overline{uw}$ to be calculated.

For the self-preserving wake only mean velocity and longitudinal turbulence measurements were made.

Intermittency profiles for the outer part of each jet flow were also measured at one station. At each traverse position 10 seconds of output was recorded on an F.M. tape recorder (Bruel and Kjaer, Type 7001). To emphasize the high frequencies and thus better distinguish rotational from irrotational flow the signal was differentiated with respect to time before recording, using an operational amplifier.

Subsequently the analog signal was digitized and recorded at 12,000 samples/second. This time series was then digitally filtered to remove the average value and the components with frequencies above 3000 Hz.

The intermittency was calculated by examining each sample to see if its magnitude was above a certain threshold. The intermittency at each position was calculated as the number of samples above this threshold divided by the total number of samples in this 10 second interval.

Clearly, sections of the record that are completely turbulent will have short intervals when the magnitude is less than the threshold as the signal crosses the zero axis from large values of one polarity to large values of the other. To take into account these zero crossings, samples which were below the threshold for a period of less than .4 milliseconds were counted as turbulent.

The threshold level and the above period of .4 milliseconds were determined empirically by examining a number of segments of the signal from a traverse position which was turbulent about 40% of the time. There was clearly a uniform background signal between segments that were turbulent, and the threshold was set to roughly 1.5 times the maximum of this background. Examination of a number of turbulent regions then suggested that .4 milliseconds would cover most of the zero crossings when the signal was below the threshold.

3-6-5 Measurements on Other Flows

Some measurements were also made on two related axisymmetric flows; a jet with still surroundings and a small deficit wake in zero pressure gradient.

For the still-air jet mean velocity and longitudinal turbulence was measured at a number of stations. The jet pipe was the same as that for the streaming flow cases, but the working section of the tunnel was removed so the jet exhausted directly into the room. The tunnel was of course not running.

Because of the unexpected value of the measured growth, other configurations were tested. Some measurements were made with the tunnel outlet blocked with a sheet of plywood to see if entrainment flow direction would influence the growth. Other tests were made using a jet source with a 'top-hat' velocity profile rather than the fully developed pipe flow of the main tests. The jet source consisted of a 1/2 inch thick orifice plate fastened directly to the end of an extension of the 2 inch jet supply pipe. This had a smooth contraction to a .218 inch hole in the centre of the plate. Two horizontal and one vertical traverses were made using this source.

The other flow measured was the small deficit axisymmetric wake in zero pressure gradient. This flow was produced by simply removing the perforated plate from the end of the working section. The wake-producing body was the pipe described in Section 3-6-4.

4. Results and Discussions

4-1 Results for Self-preserving Jets and Wakes in Streaming Flow

The data for these flows is presented in Figures 4-1 to 4-34, plus Tables 4-1 to 4-4. The data for the three jet flows are each presented in ten figures, and four more figures are used to present the data for the self-preserving wake.

The first three figures for each flow shows the development of the mean flow. The first figure shows values of G and L_0 as functions of downstream distance, with lines drawn to calculate an average value of G, the slope of the L_0 line, and x_0 (the virtual origin of the flow). In each case the value of G deviates no more than a few percent from the average value, and the L_0 values from the line $L_0=C_0(x-x_0)$ by 1% or less.

For each of the jet cases the virtual origin of the flow is upstream of the outlet of the jet pipe. Close to the pipe outlet the jet might be expected to grow with a larger rate, gradually reducing to the lower rate for the particular value of G for that flow. This would produce the observed effect on position of the virtual origin relative to the jet outlet, and the difference goes down with larger values of G as might be expected.

The second figure has experimental values of log (U_1) and log (U_0) plotted against log ($x-x_0$). Since $U_1 \propto (x-x_0)^m$ these points should lie on a straight line and the slope should be equal to the value of m predicted by equation (47). Best lines are drawn through the experimental points and the slope indicated. For the log (U_1) data a dashed line with the slope given by equation (47) is drawn for comparison. Generally the fit to the log (U_1) points is very good, while that of the log (U_0) is not as good. Since, if U_0/U_1 = constant and $U_1 \propto (x-x_0)^m$, then $U_0 \propto (x-x_0)^m$, then $U_0 \propto (x-x_0)^m$ also. So the variation of log (U_0) values from the expected slope must be due to the small variations in G and should be acceptable.

One table for each flow collects the data from these figures, and presents measured values of U_1, U_0, G, L_0, and Re for each station.

The next figure in each set presents the normalized mean velocity profiles plotted non-dimensionally. It is seen that for each flow they all collapse satisfactorily onto one curve, and, as was assumed in the theoretical development, the curves are identical for each flow. Also drawn on each of these figures is the assumed Gaussian profile used in the theory. It is seen to be in close agreement over most of the width of the flow, but over-estimates the amplitude in the outer part.

The next five figures of each set present the measured Reynolds stress profiles of each flow. These are suitably non-dimensionalized with U_0 and L_0. Presented are $\overline{u^2}/U_0{}^2$, $\overline{uv}/U_0{}^2$, $\overline{v^2}/U_0{}^2$, $\overline{u^2}/U_0{}^2$, and $\overline{uw}/U_0{}^2$. (For the wake only $\overline{u^2}/U_0{}^2$ data is presented as no slanted-wire measurements were made in that flow). Longitudinal turbulence measurements were made at each station that mean flow measurements were made, and were used as a measure of how well the turbulent structure was self-preserving.

The figures showing radial shear stress ($\overline{uv}/U_0{}^2$) have drawn on them a line of shear stress profile predicted using the momentum equation and the measured growth. It is calculated assuming self-preservation and the Gaussian velocity profile. For the flows with $G = .85$ and $G = 1.83$ the agreement between the data prints and this line is very good out to the value of η at which the measured mean velocity and the Gaussian profile start to differ. For the flow with $G = 3.00$ the agreement between the predicted and measured shear stress is not as good as for the other two jet flows; the measured values being ~ 10% lower than the calculated curve. It is possible that this is an effect of high turbulence intensity; the larger value of G for this flow means that the ratio of turbulent velocities to mean flow velocity can be relatively high. Looking at the term $\frac{\sqrt{\overline{u^2}}}{U}$ across the flow indicates that it reaches a maximum of ~30% for $\eta \simeq 1.4$ and 22% at the point where $\overline{uv}/U_0{}^2$ is maximum. This can be compared with values of 22% and 20% for the flow with G = 1.83.

For the flows with G = .85 and G = 3.00 shear stress measurements are made at a number of stations, and the fact that the measurements collapse onto one curve can be taken as another indication that the flows are self-preserving in the stress tensor term. For these flows the other two normal stress terms ($\overline{v^2}/U_0{}^2$ and $\overline{w^2}/U_0{}^2$) are also measured. There is considerably more scatter in the data than for the $\overline{u^2}/U_0{}^2$ values, and, for the flow with G = .85 a trend towards increasing values down the flow.

The three normal stress terms are collected together and plotted as twice the turbulent kinetic energy ($\overline{q^2}/U_0{}^2$) in Figures 4-9, 4-19, and 4-29.

The last of the measured Reynolds stress profiles ($\overline{uw}/U_0{}^2$) are plotted in Figures 4-8, 4-18, and 4-28. From symmetry considerations these measured values should be zero, and this seems to be the case for all the measured flows.

For each of the jet cases the intermittency in the outer part of the flow was measured, and profiles for the three jet flows are presented in Figures 4-10, 4-20, and 4-30. Values of $y_{.5}/L_0$ and σ/L_0 are calculated by fitting a curve of $\mathrm{erf}(\frac{y-y_0}{\sigma})$ to the data points, and the calculated values are included with the figure.

In the Tables 4-1 to 4-4 where information for each of the flows is collected the values of $(x-x_0)/b$ (where b is the jet outlet diameter or wake body diameter) are listed for each station. The choice of a value of b for the wake is not obvious, as the wake is probably made up to a considerable extent of boundary layer that has built up over the 3/4 inch diameter pipe that supported the final 12 inches of the 1/4 inch diameter pipe at the end of the wake body. The value of b was chosen as 1/4 of an inch, but the values of $(x-x_0)/b$ at the measured station should be considered in light of the above information.

4-2 Results for Jet with Still Surroundings

Mean velocity and longitudinal turbulence measurements were made at six stations for this jet. The range of x/b was 43 to 290.

Figure 4-35 gives the values of L_0 at each station. The growth of the jet is linear, with $C_0 = .0964$, and the virtual origin is 0.7 inches downstream from the jet source. This distance was unaffected by whether the jet source was a fully developed turbulent pipe flow from the jet pipe or a top-hat profile from the orifice-plate source. The growth rate measured also was not affected by the change in jet source, and, at the one station measured, L_0 from a vertical traverse was the same as for the horizontal traverse.

Although not noted in Figure 4-35, a traverse at one station was also made to determine if the growth rate was affected by a change of entrainment conditions. To test this, a 4 foot square board with a hole in the centre for the jet was fitted over the tunnel outlet perpendicular to the flow axis and plane with the end of the jet pipe. No difference in the measured L_0 was noted with and without this board.

Figure 4-36 shows how the centreline

velocity of the jet varies with x. The value of $1/U_0$ is seen to vary linearly with x ($m = -1$ for $G = \infty$), and the virtual origin defined by the values of U_0 is very close to that defined by L_0.

Figure 4-37 is a plot of the non-dimensionalized mean velocity profiles, and they are seen to be fairly well self-preserving. The self-preserving shape is, however, distinctly different in the outer part of the flow from that of the jets and wake with external flow. This is likely to be a measurement error due to the extremely high intensity turbulence in this region.

The longitudinal turbulence profiles are presented in Figure 4-38. As noted earlier, rather hurried measurements were made of the jet in still surroundings using a source that gave a non-turbulent 'top-hat' profile at the jet exit. Figure 4-43 shows the longitudinal turbulence at one station for both a horizontal and a vertical traverse. These were measured at the x = 58 inch station, and can be compared with the measurements from that station in Figure 4-38. At the time it was only intended that L_0 be measured for this different jet source, so the hot wire was not calibrated (the output was, however, linear with velocity). Consequently U_0 is not known directly, but calculations from the jet condition would indicate that U_0 at each station was 1.0 - 1.2 times its value for the flow using the jet pipe.

These profiles do not seem to reach a self-preserving form, there being large differences in the last two stations. This is most likely a feature of the instrumentation, as the R.M.S. meter used (see Section 3-5) had a low frequency cutoff of 5 Hz and the work by Wygnanski and Fiedler (1969) indicated that the longitudinal turbulence of the still-air jet has a significant portion of its energy at low wave numbers. Using their spectrum of $\overline{u^2}$ and assuming that the measured frequency for a particular value of $(k\ L_0)$ in the spectrum varies as U_0/L_0, the 5 Hz cutoff for the R.M.S. meter would be expected to give answers that are ~20% too low. This is assuming that the shape of the spectrum of the Reynolds stresses scale with L_0 in wave number space. Then it should be possible to say that the relation between the cutoff frequency of a measuring instrument and a specific point in the non-dimensionalized spectrum of a Reynolds stress term is

$$F_{cutoff} \propto \frac{U}{L_0}$$

where U is the velocity with which the fluid is being transported past the measuring probe and F cutoff is, say, the frequency at which a specified percentage of the measured quantity will be lost by the measuring instrument. If U is defined as $U_1 + \frac{U_0}{2}$ it also allows comparison between the jet with still surroundings and the other self-preserving flows with finite values of G. Table 4-8 gives values of this frequency for the first acceptably self-preserving station and the last measured station for each of the flows, and includes the station from Wygnanski and Fiedler (1969) where the spectrum measurements were made. Indications from their work and the present measurements on the jet in still surroundings would indicate that as long as the measuring instrument cutoff frequency was below 1 - 1.5 times the values given in the table that the loss of signal will be <3%. From this it is seen that perhaps the last station measured for the self-preserving wake might turn out to be low in value at the centre of the flow.

4-3 Small-Deficit Wake in Zero Pressure Gradient

From equations (96), the growth of the wake (for $\left|\frac{U_0}{U_1}\right| << 1$) should be such that

$$L_0{}^3 \propto (x-x_0)$$

$$\frac{1}{U_0{}^{1.5}} \propto (x-x_0)$$

The experimental values of L_0 are plotted on Figure 4-39, and those for U_0 on Figure 4-40. Both $L_0{}^3$ and $U_0{}^{-3/2}$ exhibit satisfactorily linear variation with x when U_0/U_1 becomes small, and the virtual origins calculated by extrapolating best lines through these points are in fair agreement. Also, the momentum flux, expressed as $U_0U_1L_0{}^2$, is (for the last six stations) constant, ±1.3%.

Table 4-7 gives the growth information for this flow and the measured mean flow values at each station. The calculated g_0's for each station vary from the average by +2.5%, - 1.2%.

The normalized mean velocity profiles are given in Figure 4-41. Except for the first station they collapse satisfactorily onto one curve.

Thus mean velocity measurements all indicate that this wake is self-preserving when U_0/U_1 become reasonably small. When the longitudinal turbulence measurements (Figure 4-42) are examined, however, the evidence contradicts this assumption. The values of $\overline{u^2}/U_0{}^2$ do not reach a self-preserving form and do not even seem to be tending towards a stable value. Clearly, then, this flow is not completely self-preserving for turbulence. Since U_0, L_0 and $f(\eta)$ satisfied the self-preserving relation, the $\overline{uv}/U_0{}^2$ profiles must have been invariant also. No direct measurements were made of this quantity, but calculations from the measured mean quantities should be accurate. Thus this is a situation where one component of the stress tensor, $\overline{uv}/U_0{}^2$ remains essentially constant while another component, $\overline{u^2}/U_0{}^2$ increases by over 65%.

These results should be considered in the light of recent work on both the small-deficit wake and small-increment jet. Bukreev et al (1973) have measured the wakes from two different axisymmetric bodies, a slender streamlined body and a sphere. They found that the mean and turbulent structure reached a self-preserving form in each flow, but that the growth for the two cases was very different. For example, the calculated shear stresses, as expressed by R_T, the turbulent Reynolds number, are

$$R_T = 20.4 \text{ for the slender body}$$
$$R_T = 3.2 \text{ for the sphere}$$

(The calculated and measured values of $\overline{uv}$ are in good agreement), and

$$\frac{\overline{u^2}_{max}}{U_0{}^2} = .086 \text{ for the slender body}$$
$$\frac{\overline{u^2}_{max}}{U_0{}^2} = .488 \text{ for the sphere}$$

Rodi (1972) has surveyed experiments involving axisymmetric small-deficit wakes, and he too finds that there are large variations in the rates of growth and the non-dimensionalized Reynolds stresses from one flow to the other in spite of the apparent self-preservation of the individual flows.

In another related experiment Antonia and Bilger (1973) studied two jets in uniform streaming flow, following their development from close to the jet source (where $U_0/U_1 > 1$) to far downstream (where $U_0/U_1 \ll 1$). They studied two jet flows, and found that although the mean velocity measurements appeared reasonably self-preserving when U_0/U_1 became small, the growth rates were different for the two flows and were generally quite a lot lower than investigators have found for small-deficit wakes. (The present work is an exception to this).

All the evidence of these investigations point to the conclusion that the universally self-preserving axisymmetric wake in uniform flow does not develop, at least not in the length of flows studied so far, despite the presence of the necessary condition as provided by the momentum and energy boundary layer equation. It is still possible that there is a universally self-preserving form for this flow that is being approached very slowly, but the Reynolds number for these flows is generally fairly low and, from the variation of U_0 and L_0, is continuing to fall in the downstream direction. Consequently there can only be at best a limited region of self-preservation. It is interesting to note that Townsend (1970) predicts from a study of the mechanism of entrainment in shear flow that the small deficit wake in zero pressure gradient can never become self-preserving.

This leaves the problem of choosing a value of g_0 for this flow to use to evaluate α and β in equations (58) and (59). Since the present measurements indicate that the flow is not self-preserving and the value of R_T calculated is much higher than other small deficit wake measurements, a median value from the literature was chosen for g_0, as shown in Table 2-1.

4-4 General Review and Comparison with Theory

In this work five flows have been studied, all belonging to the family of exactly self-preserving axisymmetric jets and wakes. These extended from a fairly strong wake through three jets with streaming flow to the jet with still surroundings.

The questions that need to be answered about these flows fall into three areas; are the flows self-preserving, what are the mean and turbulent parameters of the flow and how do they compare with each other, and is there an adequate theory to predict their behaviour? These will be dealt with in turn.

4-4-1 Self-Preservation

This subject has already been covered to some extent in Section 3-6-3. The theory predicts that if $U_1 \alpha (x-x_0)^m$ then G = constant down the flow, L_0 varies linearly with x, and the non-dimensionalized velocity profiles are the same at all stations. These conditions seem to be met satisfactorily for all the flows studied, as described in Section 4-1.

The non-dimensionalized profiles of all the terms in the Reynolds stress tensor should also be invariant down the flow when the flow is self-preserving. The longitudinal turbulence $(\overline{u^2}/U_0{}^2)$ was taken as a measure of this, and again for all the flows it reached a self-preserving form, although, as might be expected, it took further to reach this state than the mean flow, particularly when $|G|$ was small. For two of the jet flows the other two normal stress terms were also measured at more than one station, and here the similarity of the profiles at the different stations is not as good, especially for the jet with $G = .85$.

The radial shear stress term $(\overline{uv}/U_0{}^2)$ of the stress tensor was also measured at the same stations as the previous two normal stress terms;

the profiles were self-preserving, and except for the jet with $G = 3.00$, were in excellent agreement with the profiles calculated from the momentum equation. This should probably not be considered evidence of self-preservation apart from that of the mean flow, as the connection between the mean flow growth and the shear stress through the momentum equation, as expressed by equation (27)', is well established theoretically and it would be surprising if there was much difference. This is different from the situation for two-dimensional flows where relatively small departures from two-dimensionality can produce sizeable disagreements between measured and calculated shear stress.

For the jet with still surroundings ($G = \infty$), the requirement that the longitudinal turbulence be self-preserving appeared to be violated. However, as explained in Section 4-2, this is believed to be due to lack of low frequency response in the R.M.S. meter. Certainly there is plenty of evidence from other research that this particular flow is self-preserving for the values of $(x-x_0)/b$ measured in this work.

As can be seen from Figures 4-31, 4-32, and 4-34 the self-preserving wake took longer to reach self-preservation than the jet flows. It was also much more difficult to set up than the others. Part of this may be due to the fact that the wake body was further downstream than the normal position for the jet pipe and that there was no easy, independent way of adjusting wake strength as there is for the jet.

It may also be, however, that the self-preserving wake is inherently less stable than the jet. A self-preserving jet involves a jet in a co-flowing stream with an adverse pressure gradient adjusted to give the external flow a specified longitudinal variation. Since the velocity in the jet is higher than the external stream, then, if there were no shearing stresses Bernoulli's equation would apply, and the jet would be less affected by the pressure gradient. Thus the jet-to-free-stream velocity ratio would continuously increase. The effect of the turbulent shear is to counteract this by 'holding back' the jet, and self-preservation is achieved when these two effects balance and U_0/U_1 is a constant. A similar pattern describes the self-preserving wake, with the slower wake being 'pulled along' by the external flow and the turbulent shear stress.

When the pressure gradient is not exactly that called for by the value of G, the jet and wake are seen to behave differently, if the shearing stress is assumed to be unaffected by the perturbation. If the pressure gradient is too strong for the local value of G, the effect will be to slow the external flow more than the jet and $G(= U_0/U_1)$ will rise. By equation (47) a larger G demands a larger value of m and thus a steeper pressure gradient for self-preservation. Thus the flow tends to the value of G appropriate to the new pressure distribution and is 'stable'.

For a wake the situation is different. Here a stronger pressure gradient than required also increases the magnitude of the ratio U_0/U_1 but now by slowing the wake more than the free stream. This, however, produces a more negative value of G and thus the m calculated from equation (47) is smaller in magnitude. This means that deviation from self-preserving conditions tends to produce a flow that is even farther from self-preservation and the flow is now 'unstable'.

It is not implied that the wake is impossible to set up in practice because changes of shear stress will occur to counteract the changes of G. The present argument, however, helps to explain why the wake was a more difficult flow to stabilize.

4-4-2 Comparison Between the Flows

Table 4-5 collects together some of the parameters for the five self-preserving flows studied. The growth rate (as expressed by C_0) obviously increases with $|G|$. The value of $g_0 = \frac{\overline{uv}}{U_0^2}$ (as calculated from C_0 and G using equation (48) or from direct turbulence measurements) show remarkably little variation over the range of G from a strong wake to the jet with still surroundings. For the Gaussian profile R_T (the turbulent Reynolds number at $y = L_0$) is related to g_0 by $R_T = \frac{k}{g_0}$. In this range g_0 varies by $\sim$10%-15%.

Leaving out for the moment consideration of the jet with still surroundings ($G = \infty$), this lack of variation of turbulent structure extends to the other components of the stress tensor. For the three self-preserving jets the variation of the normal stresses are again $\sim$10%, using values for the centre of the flow. The $\overline{u^2}/U_0^2$ values for the self-preserving wake are considerably lower, although the value in the table exaggerates this trend as the profile of $\overline{u^2}/U_0$ for the wake shows a much more pronounced dip in the centre than the jets. It might be noted here that there does seem to be a trend in the profile of $\overline{u}^2/U_0{}^2$ from a pronounced central dip for the wake to a barely noticeable one for the jet in still surroundings.

All this seems to indicate that the turbulent structure of the flows are remarkably unaffected by the strength of the external flow relative to the jet or wake. The external flow merely convects the turbulence along and this is the principal reason for the variation of C_0 with G.

The measurements of intermittency at the edge of the turbulent flow also indicate little difference between the three jet flows studied. The value of $y_{.5}/L_0$ is 1.8 to the accuracy of the measurements, and this is the value found for the jet in still surroundings by Wygnanski and Fiedler (1969). The value of σ/L_0 for the three jet flows studied was essentially constant at $\sim .27$, but this is in disagreement with Wygnanski and Fiedler who measure $\sigma/L_0 = .36$ for the still-air jet. Their interpretation of signals may have been different, however.

The constancy of $y_{.5}/L_0$ for the measured flow and the agreement with the value for the still-air jet is good support for the assumption in Section 2-3 that it is constant for the full range of G. The constancy (to the accuracy of the measurements) of σ/L_0 for the three measured jet flows, for which g_0 is fairly close to constant, is in agreement with the measurements of Gartshore (1965) for two-dimensional flows. Gartshore predicts that g_0 and $(\sigma/L_0)^2$ should be proportional on the basis of the large eddy equilibrium hypothesis. This hypothesis is now somewhat suspect, as expounded by Townsend (1966), but in the same paper he also shows that the mechanism of entrainment based on a quasi-elastic behaviour of the turbulent eddies is still consistent with g_0 being proportional to $(\sigma/L_0)^2$. This is considered in more detail in the introduction.

The measurements on the jet in still surroundings ($G = \infty$) were intended to confirm that the growth rate (C_0) for this flow was the generally accepted value of .085 (see values collected by Newman (1967) and measurements by Wygnanski and Fiedler (1969)). However, the value of C_0 measured (over a range of x/b from 43-290) was .0964. This was unaffected by the presence or not of a back wall and whether or not the jet source was an orifice producing a 'top-hat' profile or a pipe providing fully developed pipe flow.

Subsequent work by Tjio (1971) and Rodi (1972) and an investigation and reassessment of the literature have indicated that this value of C_0 is reasonable, and furthermore, that the question of universality of the turbulent structure of the flow for the jet in still surroundings is still an open question. Table 4-9 lists information from a representative sample of the experiments with the jet in still surroundings.

With regard to growth rate, results fall into two groups. First there are the experiments with $C_0\,(=\frac{dL_0}{dx})$ very close to .095, and secondly a group with values of $0.8 \leq C_0 \leq .092$. For the following reasons the results by Rodi (1972) have been recalculated to give C_0=.0956 instead of .090. From the reported results it appears that mean velocity profiles were taken only at an x/b of 68 and 75, which are probably not enough to accurately define the virtual origin of the jet. Measurements of centerline velocity in the same flow over $50 \leq x/b \leq 75$ indicate that $x_0/b=4$. When this value of x_0/b is used instead of the value 0 used by Rodi, C_0=.0956 instead of .090.

This concern about the value of x_0 is one that has affected the work of most experimenters. From the work of Albertson et al (1948) and Wygnanski and Fiedler (1969) is is apparent that only points with an x/b beyond ~ 30 should be used to define x_0 and dL_0/dx. This is most apparent in plots of U_{jet}/U_0.

If it is arbitrarily assumed that only values of C_0 for flows where measurements of L_0 were made beyond a value of x/b of 50 will be recognized, the only value of C_0 that differs appreciably from .095 is that of Wygnanski and Fiedler. For their jet the growth rate defined by the longitudinal variation of L_0 between an x/b of 30 and 97.5 is .086, and has the virtual origin at the jet exit. However, the longitudinal variation of U_0 defines a virtual origin having $x/b = 7$. This sort of difference in x_0 is equivalent to about a 10% difference in C_0 (using a median value of 70 for x/b). For their jet, $U_0 \propto \left(\frac{x-x_0}{b}\right)^{-1}$, and $L_0 \propto \frac{x}{b}$, so that $(U_0L_0)^2 \propto \left(\frac{x}{x-x_0}\right)^2$, and this varies by 23% between $x/b = 40$ and $x/b = 97$. But $(U_0L_0)^2$ is proportional to the momentum flux for a self-preserving profile, and should be constant down the flow. Thus there is a question about the growth rate for this flow.

Table 4-9 notes if the experimental set-up used a back wall (a plane surface perpendicular to the jet axis and placed at the jet outlet). This was of concern because experiments on the two-dimensional jet in still surroundings indicate that the presence or absence of a back wall causes a difference in the growth rate of ~10%. (See Fekete (1970) and Smith (1970)). The evidence from the table indicates that this is not the case for the axisymmetric jet. The following argument lends support to this finding.

For a jet issuing from a hole in a wall the induced entrainment of velocity will be radially inwards. If there is no wall, however, there should be some longitudinal component of velocity and thus $G(= U_0/U_1)$ will not be infinite. Using equation (48) and assuming that g_0 is constant for large G leads to the result that a 10% reduction in C_0 can be induced by changing G from ∞ to $\simeq 12$.

Assuming a Gaussian profile, $U_0 \propto x^{-1}$, and $L_0 = C_0 x$, the volume entrainment rate is constant and is given by

$$\frac{dQ}{dx} = -\pi \, \frac{U_0 L_0 C_0}{k}$$

Thus to calculate the mean flow outside the jet, the jet may be replaced by a line sink of that strength extending from $0 \le x \le \infty$.

The flow field induced by this line sink has

$$U = \frac{U_0 L_0 C_0}{4k(x^2+y^2)^{\frac{1}{2}}}$$

and the velocity of U just outside the jet is

$$U_1 = \frac{U_0 L_0 C_0}{4k|x|(1+A^2 C_0{}^2)^{\frac{1}{2}}} \simeq \frac{U_0 L_0 C_0}{4k|x|}$$

(assuming $A \simeq 2$-3 and $C_0 = .095$).

Since $L = C_0 x$, then

$$\hat{U}_1 \simeq \frac{U_0 \, C_0{}^2}{4k},$$

and $G \simeq 340$.

Thus the mean longitudinal entrainment velocity is not nearly enough to cause the observed variation in growth rate.

When measurements of the turbulent energy (using the longitudinal turbulence as a measure) are examined, a great variation is found in published work; values of $\overline{u_0{}^2}/U_0{}^2$ (the centre-line turbulence) varying from .042 to .082. The values from Corrsin (1943) of .068 and Corrsin and Uberoi (1949) of .042 might be ignored as they were made at an x/b of only 20. This leaves the measurements of Wygnanski and Fiedler (1969) and of Rodi (1972) with values of $\overline{u_0{}^2}/U_0{}^2$ in the range of .075 - .082, and those of Tjio and the present work with values of .058 and .055 respectively. Rodi used a very similar experimental setup to Wygnanski and Fiedler and the jet in both cases had a low-turbulence 'top-hat' profile. Tjio and the present work, on the other hand, used a jet source that gave turbulent pipe flow. However, as noted earlier, some measurements were made by the author with a jet source having a top-hat profile and the turbulence profiles were essentially similar in the two cases. (See Figures 4-38 and 4-43).

The explanation given by Wygnanski and Fiedler that the scatter in the turbulence measurements is due to lack of low frequency response in the measuring instruments does not seem to be valid. As explained earlier, the effect of a particular cutoff frequency of a measuring instrument is a function of the ratio of this frequency to a 'flow frequency' defined as $\frac{U_0}{2L_0}$. This varies as x^{-2}, and thus profiles which are affected should show a rapid change with longitudinal station.

In the present work the profiles of $\overline{u^2}/U_0{}^2$ do show a distinctive change for the last two stations, while the stations further upstream do not seem to be affected. This is in agreement with the calculations (based on the work of Wygnanski and Fiedler) that measurements will be relatively unaffected if the ratio of 'flow frequency' to instrument cutoff frequency is above 1 - 1.5.

For the experiments by Tjio (which were on a water jet) the velocity and length scales were much different, but the 'flow frequencies' were similar and calculation indicates that only the measurements at the last two stations should be affected by instrument cutoff; the profiles presented seem to bear this out.

The predictions for the Townsend entrainment model use information from the jet in still surroundings to evaluate constants in the theory. The question is, what values to use? For the growth rate it was relatively easy to choose the .096 value. However, Rodi has shown that the effect of the high turbulence intensity is to make the estimates of L_0, and thus C_0 too high. Since the theory is going to be used to predict the growth of the self-preserving jets and wake in streaming flow where the effect of this high intensity correction to C_0 will be small, it was decided not to use his linearized readings but instead to use those for which the response was made proportional to the square of the velocity so that corrections for high intensity turbulence became more accurate. These results give a rate of growth $C_0 = .091$.

Getting a value for H ($= \frac{\overline{q_0{}^2}}{U_0{}^2}$ at the centre of the flow) and the constants for the integral $I_4 - I_6$ in (89) was more difficult as no measurements were made of $\frac{\overline{v^2}}{U_0{}^2}$ and $\frac{\overline{w^2}}{U_0{}^2}$ for the jet in still surroundings. The choice was to assume that the shape and amplitude relative to $u^2/U_0{}^2$ were the same as measured by Rodi (1972). Thus the numerical values of I_4 and I_5 can be calculated. H for this flow is then assumed to equal $\overline{q_0{}^2}/U_0{}^2$ for Rodi's measurements multiplied by the ratio of $\overline{u_0{}^2}/U_0{}^2$ from the present work to $\overline{u_0{}^2}/U_0{}^2$ from Rodi's jet. This sets H = .124 for the jet in still surroundings.

It is unfortunate that the other two normal stress terms were not measured, but at the time the measurements were made only the theory based on the large eddy equilibrium hypothesis was available, and that only required knowing the growth rates for two specific self-preserving flows.

4-4-3 Comparison with Theory

The predicted values of growth and shear stress parameter for each theory and their variants are shown in Figures 2-2 to 2-13. For comparison the experimentally measured values are plotted on each figure.

As noted in Section 2-2, using the x-axis as the direction along which to evaluate the longitudinal rate of strain produced growth predictions that appeared unlikely. Figures 2-2 and 2-3 compare these predictions with the measured values, and the results are clearly in disagreement with this theory. Using the line of $y=L_0$ along which to evaluate this longitudinal rate of strain gives a much more resonable prediction, as shown in Figures 2-4 and 2-5. There is not much difference shown between the predictions of the linear and quadratic relations for B/A, and as the former is mathematically simpler it clearly is to be preferred.

As noted earlier, the constants in this theory depend on the growth rate of the small-deficit wake in zero pressure gradient and a wide range of values have been measured for this growth rate. Consequently better agreement between theory and experiment could probably be achieved by using a different value from that given in Table 2-1. However, since the basis of this theory is now being questioned and the second theory gives better results nothing more was done in this direction.

Predictions using the integral energy equation are shown in Figures 2-6 to 2-13. Four different variants are shown, each representing a different relation between the shear stress parameter and the non-dimensional turbulent kinetic energy, and are characterized by a particular value of n in equation (83). Townsend's(1970) work indicates that for the range of R_T in these axi-symmetric flows n should be ≃.75. Figures 2-6 and 2-7 show results using this prediction. The results are reasonable, but the agreement with experiment is not much better than for the large eddy equilibrium theory. Using n=1, which is equivalent to assuming that $\frac{\overline{q_0^2}}{U_0^2}$ is the same for all flows in this family, gives a little better prediction of the growth rates as shown in Figures 2-12 and 2-13.

The assumption of geometric similarity given by n=0 leads to a rather poor agreement with experiment. This comparison is shown in Figures 2-8 and 2-9.

The best fit to the experimental data, however, is achieved with n=-1. This is one of the relations used by Newman(1968) for two-dimensional flows, and assumes that the stress to intensity ratio is directly proportional to R_T. This prediction is compared with experiment in Figures 2-10 and 2-11.

As an empirical prediction method the assumption that g_0 (and thus R_T) is constant for all flows and equal to the value for the jet in still surroundings produces predicted values for growth that are in as good an agreement with experiment as using n=-1 in the integral energy equation. This lends support to the work by Hill(1967) who used the assumption of constant R_T to obtain predictions for axisymmetric jet mixing in a converging-diverging duct.

5. Conclusions

5-1 Major Conclusions

Axisymmetric jets and wakes have been set up according to the constraints of the mean momentum and turbulence energy equations for self-similar flow. The measurements indicated that each of the five flows were satisfactorily self-preserving in both mean velocity and turbulence.

Probably the dominant character of these axisymmetric flows is that the turbulent structure is relatively independent of the value of $\frac{U_0}{U_1}$. This is illustrated by the fact that the shear stress parameter $g_0 (= \frac{\overline{uv}}{U_0^2}$ at $y=L_0)$ varies from a minimum of .0155 to a maximum of .0170, a range of less than 10%. Since g_0 is inversely proportional to R_T, this means that R_T varied from 40.7 to 44.7.

The turbulent kinetic energy shows little variation between flows for the three jets in which this was measured. Measurements of the longitudinal turbulence in the wake would lead one to expect the turbulent kinetic energy of this flow is somewhat less than that of the jets.

Two methods of prediction have been developed. Both are integral methods and assume a Gaussian shape for the mean velocity profile. The first is based on Townsend's original large-eddy equilibrium hypothesis in which the transfer of energy down the scale of eddies is assumed to occur in a quasi-viscous manner and the turbulence is also assumed to be structurally similar in all flows. When combined with an equation which relates the large eddy size to the rates of strain in the mean flow (assumed to be homogeneous) a solution is obtained. Two empirical constants are required, and are determined from the measured growth of the jet in still surroundings and the small-deficit wake in zero pressure gradient. The latter flow is not well established and indeed is not strictly universal; nevertheless it is shown that if a slanting axis system is used in which the longitudinal axis corresponds to the locus of $y=L_0$ along which the rates of strain are more nearly homogeneous, the rate of growth is reasonably well predicted.

The second theory is based on Townsend's later work in which the integral form of the complete energy equation is used, $\frac{L_\epsilon}{L_0}$ is assumed constant, and the unknown shearing stress, $\overline{uv}$, is assumed to be a constant proportion of the average turbulent energy, $\frac{\overline{q_0^2}}{2}$, which depends on the strain which the flow has experienced. Good predictions are made when $\frac{\overline{uv}}{\overline{q_0^2}}$ is assumed to be directly proportional to the average total strain.

An equally good empirical prediction method is to assume that the turbulent Reynolds number of the flow is the same for all values of $\frac{U_0}{U_1}$ and equal to that for the jet in still surroundings.

5-2 Minor Conclusions

A satisfactory method has been developed for setting a prescribed adverse pressure gradient which involves an approximate one-dimensional theory used iteratively with experimental measurements. Two or three iterations are usually sufficient to give an adequate distribution of porosity for the ventilated working section.

The rate of growth of the jet in still surroundings seems to be well established ($\pm$1%), although there are some measurements that disagree with this universal growth rate. The turbulence, which is more difficult to measure, is much less universal.

In agreement with recent work of others, it is concluded that the self-preserving small-deficit wake in zero pressure gradient is not universal, but always depends on the turbulence introduced by the body which produced the wake.

Intermittency measurements indicate that the non-dimensional standard deviation, $\frac{\sigma}{L_0}$, for the position of the surface separating the turbulent rotational from the outer irrotational flow is the same for all the self-preserving flows. This is consistent with R_T being effectively the same since both theories show that $\frac{\sigma}{L_0}$ is a function of R_T.

5-3 Suggestions for Further Work

A self-preserving wake with larger $\left|\frac{U_0}{U_1}\right|$ should be measured, since it would provide a more stringent test of the theories.

The present results should be compared with differential methods of prediction in which the turbulence energy and the individual components of the Reynolds stress tensor are modelled.

The rate of dissipation of turbulence energy should be measured for these flows.

REFERENCES

Albertson, M.L., Dai, Y.B., Jensen, R.A., Rouse, H. Diffusion of submerged jets; Proc. ASCE, 74, Separate No. 10 (1948)

Antonia, R.A., Bilger, R.W. An experimental investigation of an axisymmetric jet in a co-flowing air stream; J. Fluid Mech., 61, part 4 (1973)

Baldwin L.V., Sandborn, V.A. Intermittencey of far wake turbulence; AIAA Jour., 66 (1968)

Bilger, R.W. The turbulent plane jet-wake; Conference on Hydraulics and Fluid Mechanics, The Institution of Engineers, Australia (1968)

Bilger R.W. Turbulent energy equilibrium in free turbulent flows; Dept. Mech. Eng., Univ. of Sydney, Charles Kolling Res. Lab. Tech. Note F-3 (1969)

Bradbury, L.J.S. The structure of a self-preserving turbulent plane jet; J. Fluid Mech., 23 (1965)

Bradbury, L.J.S., Riley, J. The spread of a turbulent plane jet issuing into a parallel moving airstream; J. Fluid Mech., 27 (1967)

Bradshaw, P.	The effect of wind tunnel screens on 'two-dimensional' boundary layers; N.P.L. Aero. Rept. 1085, A.R.C. 25402 (1963)
Bradshaw, P. Pankhurst, R.C.	The design of low-speed wind tunnels; Prog. Aero. Sci., 5 (1964)
Bradshaw, P. Ferriss, D.H. Atwell, N.P.	Calculation of boundary layer development using the turbulent energy equation; J. Fluid Mech., 28 (1967)
Bradshaw, P.	The strategy of calculation methods for complex turbulent flows; Imperial College, Dept. of Aeronautics, Rept. 73-05 (1973)
Bukreev, V.I. Vasil'ev, O.F. Lytkin, Yu.M.	Influences of the shape of a body on the characteristics of a self-similar wake; Soviet Physics-Doklady, Fluid Mechanics, 17-12, (1973)
Champagne, F.H. Sleicher, C.A. Wehrmann, O.H.	Turbulence measurements with inclined hot-wires, part 1&2; J. Fluid Mech., 28 (1967)
Cohen, M.J. Richie, N.J.B.	Low-speed three-dimensional contraction design; J. Royal Aero. Soc., 66 (1962)

Donaldson, C.duP. Calculation of turbulent shear flow for atmospheric and vortex motion; AIAA Jour., 10, 4 (1972)

Fekete, G.I. Two-dimensional, self-preserving turbulent jets in streaming flow; Mech. Eng. Res. Lab. Rept. 70-11, McGill Univ. (1970)

Gartshore, I.S. Jets and wall jets in uniform streaming flow; Mech. Eng. Res. Lab. Rept. 64-4, McGill Univ. (1964)

Gartshore, I.S. The streamwise development of two-dimensional turbulent shear flows; Ph.D. Thesis, McGill Univ. (1965)

Gartshore, I.S. An experimental examination of the large-eddy equilibrium hypothesis; J. Fluid Mech., 24 (1966)

Gartshore, I.S. Two-dimensional turbulent wakes; J. Fluid Mech., 30,3 (1967)

Gartshore, I.S. Newman, B.G. Small-perturbation jets and wakes which are approximately self-preserving in a pressure gradient; CASI Trans., 2,2 (1969)

Gibson, C.H.
Chen, C.C.
Lin, S.C. — Measurements of turbulent velocity and temperature fluctuations in the wake of a sphere; AIAA Jour., 6,4 (1968)

Gibson, M.M. — The design and performance of a streamline diffuser with a rapid expansion; A.R.C. 21,126, F.M. 2843 (1959)

Glusko, G.S. — Turbulent boundary layer on a flat plate in an incompressible fluid; NASA TT F-10,080, translation from Isvestia Akademii Nauk SSSR, Seriya Mekanika, 4 (1965)

Grant, H.L. — The large eddies of turbulent motion; J. Fluid Mech., 4,2 (1958)

Halleen, R.M. — A literature review on subsonic free turbulent shear flow; Mech. Eng. Rept. MD-11, Stanford Univ. (1964)

Harsha, P.T. — Free turbulent mixing: a critical evaluation of theory and experiment; Arnold Engineering Development Center, Air Force Systems Command, AEDC-TR-71-36 (1971)

Herring, H.I.
Mellor, G.I. — A method of calculating turbulent boundary layers; NASA Contractors Report No. 1144 (1968)

Hill, P.G. — Incompressible jet mixing in converging-diverging axisymmetric ducts; ASME Trans., J. Basic Eng, 89 (1967)

Hughes, N.J.S. — Stream expansion with discontinuity in velocity on the boundary; A.R.C. R. and M. 1978 (1944)

Kruka, V.
Eskinazi, S. — The wall jet in a moving stream; Syracuse Univ., Mech. Eng. Dept., Rept. No. ME-937-6309F (1963)

Launder, B.E.
Reece, G.J.
Rodi, W. — Progress in the development of a Reynolds stress turbulence closure; Inperial College, Mech. Eng. Dept., HTS/73/31 (1973)

NASA, Langley — Free turbulent shear flows; Vol. I, Conference Proceedings, NASA SP-321 (1973)

Newman, B.G. — The growth of self-preserving turbulent jets and wakes; Mech. Eng. Res. Lab. Rept. 68-10, McGill Univ. (1968)

Newman, B.G. Turbulent jets and wakes in a pressure gradient; Fluid Mechanics of Internal Flow, pp. 170-209, Ed. by Gino Sovran; Elsevier (1967)

Pankhurst, R.C.
Holder, D.W. Wind tunnel technique; Pitman (1952)

Patankar, S.V.
Spalding, D.B. Heat and mass transfer in boundary layers; Intertext, London (1970)

Patel, R.P.
Newman, B.G. Self-preserving, two-dimensional turbulent jets and wall jets in a moving stream; Mech. Eng. Rept. No. Ae. 5, McGill Univ. (1961)

Patel, R.P. Reynolds stresses in fully developed turbulent flow down a circular pipe; Mech. Eng. Res. Lab. Rept. 68-7, McGill Univ. (1968)

Patel, R.P. A study of two-dimensional symmetric and asymmetric turbulent shear flows; Ph.D. Thesis, Mech. Eng. Dept., McGill Univ. (1970)

Pope, A. Wind tunnel testing; Wiley and Sons (1954)

Reynolds, A.J. Observations on distorted turbulent wakes; J. Fluid Mech., 13 (1962)

Rodi, W. — The prediction of free turbulent boundary layers by the use of a two-equation model of turbulence; Ph.D. Thesis, Mech. Eng. Dept., Imperial College (1972)

Smith, P.A. — The curved free jet; M. Eng. Thesis, Mech. Eng. Dept., McGill Univ. (1970)

Squire, H.B., Trouncer, J. — Round jets in a general stream; A.R.C. R. and M. No. 1974 (1944)

Squire, H.B., Hogg, H. — Diffuser resistance combinations in relation to wind tunnel design; A.R.C. 7628 - T.P. 34 (1944)

Taylor, G.I., Batchelor, G.K. — The effect of a wire gauze on small disturbances in a uniform stream; Quart. J. Mech. & Appl. Math., 2 (1949)

Tjio, H.K. — Three-dimensional turbulent axisymmetric wall and surface jets originating from circular orifices; M. Eng. Thesis, Civil Eng. Dept., McGill Univ. (1971)

Townsend, A.A. — The structure of turbulent shear flow; Cambridge Univ. Press (1956)

Townsend, A.A. The mechanism of entrainment in free turbulent flows; J. Fluid Mech., 26 (1966)

Townsend, A.A. Entrainment and the structure of turbulent flow; J. Fluid Mech., 41,1 (1970)

Vogel, W.M. Exact solution of growth parameters for two-dimensional and axisymmetric self-preserving turbulent jets and wakes; Mech. Eng. Res. Lab. Rept. 68-5, McGill Univ. (1968)

Vogel, W.M. An analytic solution for flow development of symmetric self-preseving jets and wakes, using an integral method; CASI. Trans., 2,2 (1969)

Wygnanski, I. Gartshore, I.S. General description and calibration of the McGill 17 in. x 30 in. blower cascade wind tunnel; Mech. Eng. Res. Lab. T.N. 63-7, McGill Univ. (1963)

Wygnanski, I. Fiedler, H. Some measurements in the self-preserving jet; J. Fluid Mech., 38 (1969)

Values of g_0 and B/A from Measured Flow and the Resultant Values of α and β.

	Still-air Round Jet Rodi (1972); present work (with Rodi's high intensity correction)	Small-Deficit Round Wake Rodi (1972) (collected values)
$\lvert g_0 \rvert$	.0164	.0492
B/A	.0656	0
α	.0492	
β	10.16	
β_Q	154.9	

Table 2 - 1

Longitudinal Probe Positions for Traversing Gear Stations

Station	x(in.)	Station	x(in.)	Station	x(in.)
(2-1)	23.18	(3-1)	59.25	(4-1)	95.37
(2-5)	32.06	(3-5)	68.13	(4-5)	104.25
(2-6)	39.44	(3-6)	75.51		
(2-10)	48.18	(3-10)	84.26		

Table 3-1

Jet Working Conditions for Self-preserving Streaming-flow Cases

G	Pipe inside diameter (in.)	Working pressure (psig.)	Longitudinal position (in.)
.85	.178	19	-2.12
1.83	.303	20	-7.88
3.00	.303	30	-6.00

Table 3-2

Table 4-1

Growth Information for Self-preserving Jet, G = 0.85

Diameter of jet outlet (b)	= .178
Jet pressure (at pipe inlet)	= 19 p.s.i.g.
$x_{jet}-x_0$	= +10.1 in.
x_0 (virtual origin)	= -12.3 in.
m (best fit to $U_1 \propto (x-x_0)^m$)	= -.732
m (best fit to $U_0 \propto (x-x_0)^m$)	= -.719
m (calculated for G = .85)	= -.740
C_0 ($L_0 = C_0(x-x_0)$)	= .0311

Values at Measured Stations

station	$x-x_0$ (in.)	$\frac{x-x_0}{b}$	U_1 (ft/sec)	U_0 (ft/sec)	G	L_0 (in.)	Re (U_0L_0/ν) ($\times 10^4$)
(2-1)	35.4	199	57.49	49.11	.854	1.10	2.81
(2-5)	44.3	249	49.53	41.43	.836	1.38	2.98
(2-6)	51.7	290	44.49	37.03	.832	1.61	3.10
(2-10)	60.4	339	39.01	33.45	.857	1.88	3.28
(3-1)	71.5	402	35.14	29.93	.852	2.21	3.45
(3-5)	81.4	457	31.31	27.08	.865	2.50	3.53
(3-6)	87.8	493	29.86	25.59	.857	2.75	3.67
(3-10)	96.5	542	27.78	23.73	.854	3.01	3.72
(4-1)	107.6	604	25.56	23.31	.873	3.35	4.07
(4-5)	116.5	654	25.04	20.44	.816	3.61	3.84

Table 4-2

Growth Information for Self-preserving Jet, G = 1.83

Diameter of jet outlet (b)	= .303 in.
Jet pressure (at pipe inlet)	= 20 p.s.i.g.
$x_{jet} - x_0$	= +3.6 in.
x_0 (virtual origin)	= -11.5 in.
m (best fit to $U_1 \propto (x-x_0)^m$)	= -.777
m (best fit to $U_0 \propto (x-x_0)^m$)	= -.836
m (calculated for G = 1.83)	= -.793
C_0 ($L_0 = C_0(x-x_0)$)	= .0452

Values at Measured Stations

station	$x-x_0$ (in.)	$\frac{x-x_0}{b}$	U_1 (ft/sec)	U_0 (ft/sec)	G	L_0 (in.)	Re (U_0L_0/ν) ($\times 10^4$)
(2-1)	34.7	115	54.1	97.1	1.79	1.56	7.89
(2-5)	43.6	144	43.2	81.2	1.88	1.98	8.37
(2-6)	50.9	168	38.8	70.8	1.82	2.32	8.56
(2-10)	59.7	197	33.6	63.0	1.87	2.69	8.83
(3-1)	70.8	234	29.5	54.3	1.84	3.23	9.13
(3-5)	79.6	263	27.0	49.0	1.81	3.56	9.09
(3-6)	87.0	287	25.3	45.7	1.81	3.91	9.31
(3-10)	95.8	316	23.4	41.8	1.79	4.37	9.51

Table 4-3

Growth Information for Self-preserving Jet, G = 3.00

Diameter of jet outlet (b)	=	.303 in.
Jet pressure (at pipe inlet)	=	30 p.s.i.g.
$x_{jet}-x_0$	=	+0.5 in.
x_0 (virtual origin)	=	-6.5 in.
m (best fit to $U_1 \propto (x-x_0)^m$)	=	-.837
m (best fit to $U_0 \propto (x-x_0)^m$)	=	-.852
m (calculated for G = 3.00)	=	-.833
C_0 ($L_0 = C_0(x-x_0)$)	=	.0570

Values at Measured Stations

station	$x-x_0$ (in.)	$\frac{x-x_0}{b}$	U_1 (ft/sec)	U_0 (ft/sec)	G	L_0 (in.)	Re (U_0L_0/ν) ($\times 10^5$)
*(2-1)	*29.7	98	41.6	124.4	2.99	1.70	1.10
(2-5)	38.6	127	33.0	98.4	2.98	2.21	1.13
(2-6)	45.9	151	29.6	88.7	3.00	2.61	1.21
(2-10)	54.7	181	24.7	74.4	3.01	3.13	1.21
(3-1)	65.8	217	21.3	63.9	3.00	3.72	1.24
(3-5)	74.7	246	19.3	56.6	2.93	4.26	1.26
(3-6)	82.0	271	17.9	52.9	2.96	4.65	1.28
*(3-10)	*90.8	300	16.2	47.8	2.95	5.20	1.29

*from pressure profiles

Table 4-4

Growth Information for Self-preserving Wake, $G = -.54$

Diameter of wake body (b)	= .25 in.
$x_{body} - x_0$	= +3.7 in.
x_0 (virtual origin)	= 11.1 in.
m (best fit to $U_1 \propto (x-x_0)^m$)	= −.600
m (best fit to $U_0 \propto (x-x_0)^m$)	= −.630
m (calculated for G = −.54)	= −.593
C_0 ($L_0 = C_0(x-x_0)$)	= .0358

Values at Measured Stations

station	$x-x_0$ (in.)	$\frac{x-x_0}{b}$	U_1 (ft/sec)	U_0 (ft/sec)	G	L_0 (in.)	Re(U_0L_0/ν) ($\times 10^4$)
(2-6)	28.3	113	45.90	−28.70	−.625	1.09	1.63
(2-10)	37.1	148	40.77	−24.27	−.595	1.34	1.69
(3-1)	48.2	193	35.85	−19.90	−.555	1.72	1.78
(3-5)	57.0	228	32.50	−17.70	−.545	2.03	1.87
(3-6)	64.4	258	30.30	−16.40	−.542	2.31	1.97
(3-10)	73.2	293	28.04	−15.12	−.540	2.63	2.07
(4-1)	84.3	337	25.68	−14.10	−.549	3.05	2.24
(4-5)	93.2	373	24.15	−13.00	−.538	3.32	2.25

Average Values of Normal Stresses at Center of Flows

G	$\overline{u^2}/U_0^2$	$\overline{v^2}/U_0^2$	$\overline{w^2}/U_0^2$	$\overline{q^2}/U_0^2$
.85	.0412	.0397	.0393	.1202
1.83	.0454	.0380	.0390	.1224
3.00	.0404	.0374	.0368	.1146
−.54	.0321			
∞	.0546			

Measured Constants

G	C_0	$g_0\left(\frac{\overline{uv}}{U_0^2}\text{ at }\eta=1\right)$ calc. from C_0 and G	from meas. turbulence	Intermittency $\frac{Y_{.5}}{L_0}$	$\frac{\sigma}{L_0}$
.85	.0311	.0170	.0170	1.79	.265
1.83	.0452	.0155	.0154	1.86	.264
3.00	.0570	.0158	.0145	1.77	.280
−.54	.0358	.0168	—	—	—
∞	.0910	.0164			

Average Values of Mean and Turbulent Quantities for Self-preserving Flows

Table 4.5

Table 4-6

Growth Information for Still-Air Jet

for jet pipe source

Diameter of jet outlet (b) = .178 in.
Jet pressure (at pipe inlet) = 20 p.s.i.g.
$x_{jet}-x_0$ = -0.7 in.
x_0 (virtual origin) = 18.4 in.
C_0 ($L_0 = C_0(x-x_0)$) = .0964

for square profile source

Diameter of orifice = .218 in.
Jet pressure (upstream of orifice) = 9 p.s.i.g.
$x_{jet}-x_0$ = -0.7 in.
x_0 (virtual origin) = 18.4 in.
C_0 ($L_0 = C_0(x-x_0)$) = .0964

Values at Measured Stations

$x-x_0$ (in.)	$\frac{x-x_0}{b}$	U_0 (ft/sec)	L_0 (in.)	Re (U_0L_0/ν) ($\times 10^4$)	Details	
7.6	43	132.8	.73	5.05	Jet pipe source	
11.6	65	87.1	1.12	5.08		
15.6	88	63.3	1.53	5.04		
19.6	110	50.8	1.88	4.97		
39.6	222	24.9	3.82	4.95		
51.6	290	18.6	5.10	4.94		
39.6	222	--	3.85	--	Horiz. traverse	Square profile source
51.6	290	--	5.00	--		
39.6	222	--	3.83	--	Vert. traverse	

Growth Information for Small-deficit Wake in Zero Pressure Gradient

Diameter of wake body		= .25 in.
$x_{body}-x_0$ †		= +3.5 in.
x_0	(calculated by fitting $L_0{}^3 \propto (x-x_0)$)*	= 14.1 in.
x_0	(calculated by fitting $U_0{}^{-1.5}$ $(x-x_0)$)*	= 16.0 in.
x_0	(average of above two)	= 15.0 in.
g_0	(calculated from $g_0=U_1L_0/6U_0(x-x_0)$)*	= .0221
R_T	(calculated from $R_T=k/g_0$)*	= 31.3

Values at Measured Stations (using average x_0)

$x-x_0$ (in.)	U_1 (ft/sec)	U_0 (ft/sec)	L_0 (in.)	$\frac{L_0U_1}{U_0(x-x_0)}$	Re (U_0L_0/ν) ($\times 10^3$)
8.2	103.2	-31.50	.288	.115	4.73
17.1	102.4	-19.08	.445	.140	4.42
*24.4	101.8	-15.48	.505	.136	4.07
*33.2	101.7	-12.96	.555	.131	3.75
*44.3	101.5	-10.64	.610	.131	3.38
*53.1	101.3	-9.28	.646	.133	3.12
*60.5	100.9	-8.51	.676	.132	3.00
*69.3	101.0	-7.74	.708	.133	2.85

*Using values from stations marked with (*)

†Using average x_0

Table 4-7

Self-preserving Flow	Frequency $\frac{U_0/2 + U_1}{L_0}$ first self-preserving station	last station
G = .85	74.6	9.7
G = 1.83	42.3	10.1
G = 3.00	37.2	7.7
G = -.54 (wake)	15.1	5.3
G = ∞	90.9	1.9
G = ∞ (Wygnanski and Fiedler (1969) x/b = 90)	.61	

Relative Frequency of Spectrum of Longitudinal Turbulence

Table 4-8

Table 4-9

Measurements of Jet with Still Surroundings

Experimenter(s)	Re_{jet} (× 10^4)	Jet Size	Jet Profile	Back Wall?	Measuring Instrument	Range x/D	$\frac{dL_u}{dx}$	$\frac{\overline{U_1'^2}}{U_c^2}$	Remarks
Corrsin (1943)	1.7	~ 1 in.	'top-hat'	Yes	hot wire	10-40	.082	.068 (x/D = 20)	momentum not constant, heated jet (10°C rise)
Albertson et al (1948)	2.2 4.4 8.8	.25 in. .5 in. 1 in.	'top-hat'	4'x 4' plate	pressure	12-65	.0953	----	centreline velocity measured to x/D = 250
Corrsin and Uberoi (1949)	3.4-6	1 in.	'top-hat'	18' dia. disk	hot-wire	12-25	.092	≈.042 (x/b = 20)	heated jet (15°C rise)
Hinze and van der Hegge Zijnen (1949)	7	2.5 cm	---	---	pressure	3-20	.080	----	quoted from Hinze (1959)
Corrsin and Kistler (1954)	7.8	.5 in.	'top-hat'	no	pressure	20-35	.0951	----	
Wygnanski and Fiedler (1969)	9	1.04 in.	'top-hat'	see note	hot wire	30-100	.086	.082 (x/b = 50-100)	back wall, but jet nozzle possibly extended outwards
Tjio (1971)	1	.2 cm	pipe-flow	no	hot film	75-200	.095	.058 (x/b = 75-175)	jet in water, tank 1 m. x 1 m. x ~ 10 m.
Rodi (1972)	8.7	1.29 cm	'top-hat'	yes	hot wire	50-80	.0956	.075 (x/b=62-75)	value of dL_u/dx different from author's
present work	~8	.178 in.	pipe flow and 'top-hat'	yes, no	hot wire	43-290	.0964	.055 (x/b = 200)	

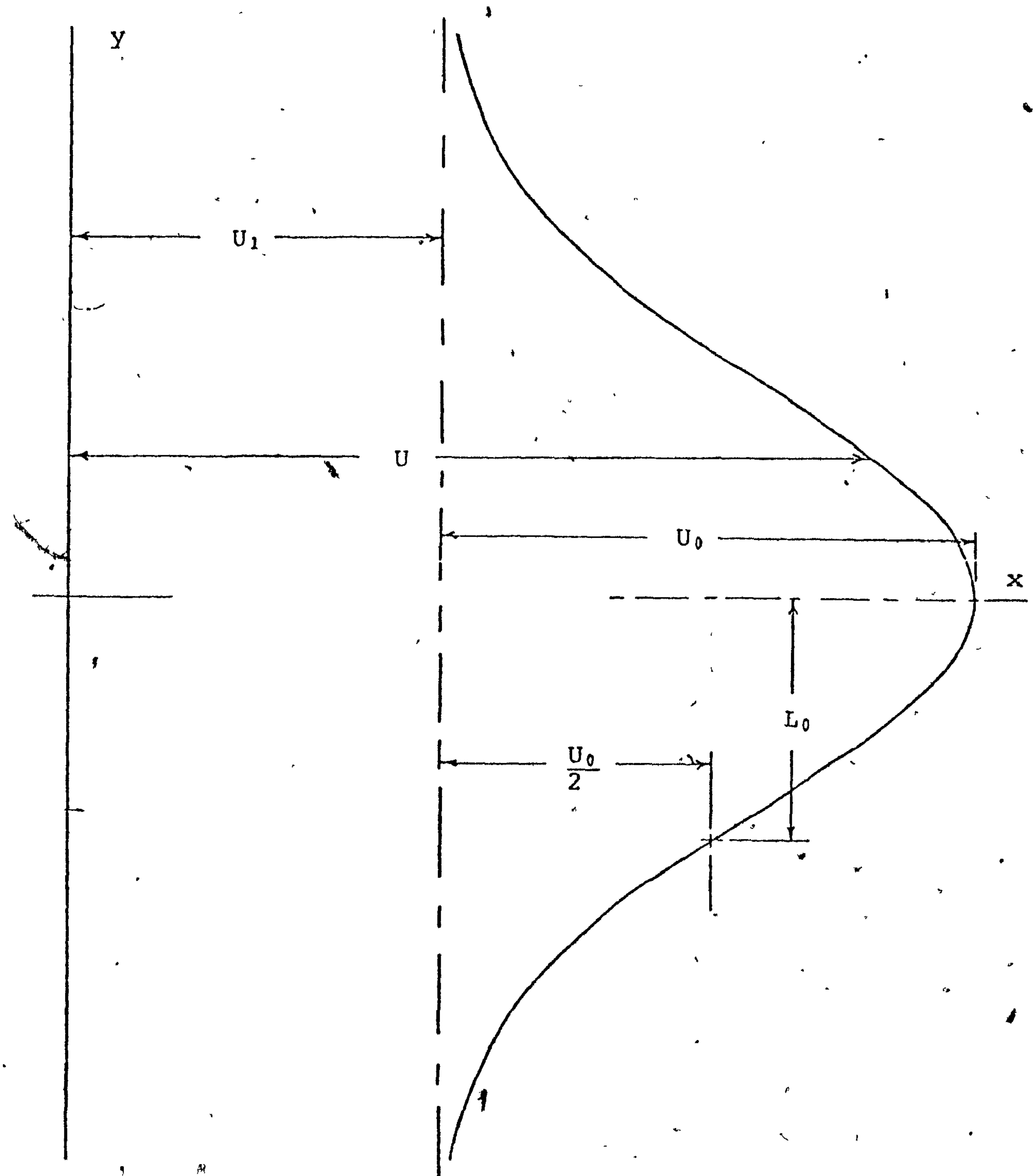

Axis System for Jets and Wakes

Fig. 2-1

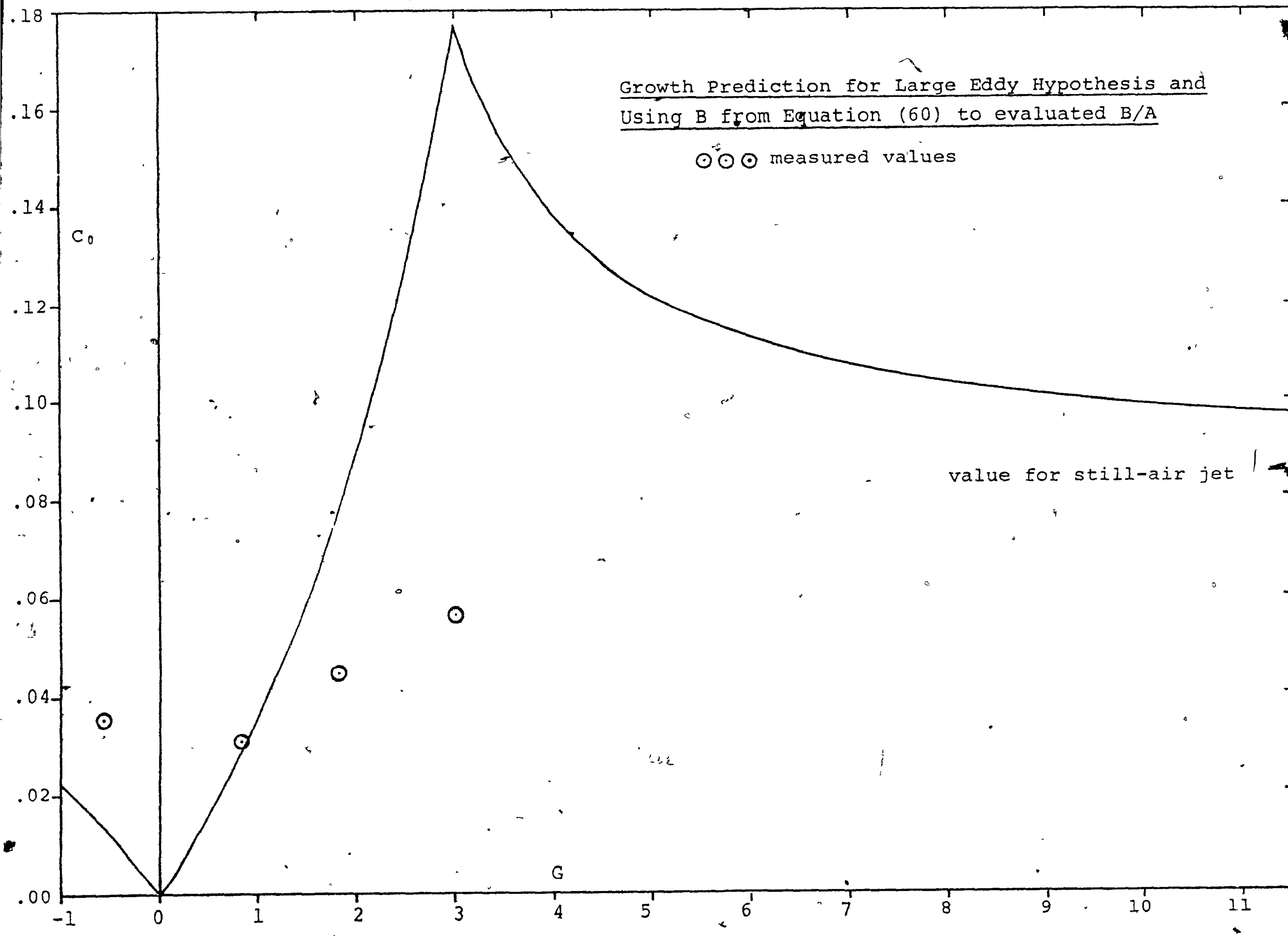
Growth Prediction for Large Eddy Hypothesis and
Using B from Equation (60) to evaluated B/A
measured values
value for still-air jet
C_0
G
.18
.16
.14
.12
.10
.08
.06
.04
.02
.00
-1
0
1
2
3
4
5
6
7
8
9
10
11

Fig. 2-2

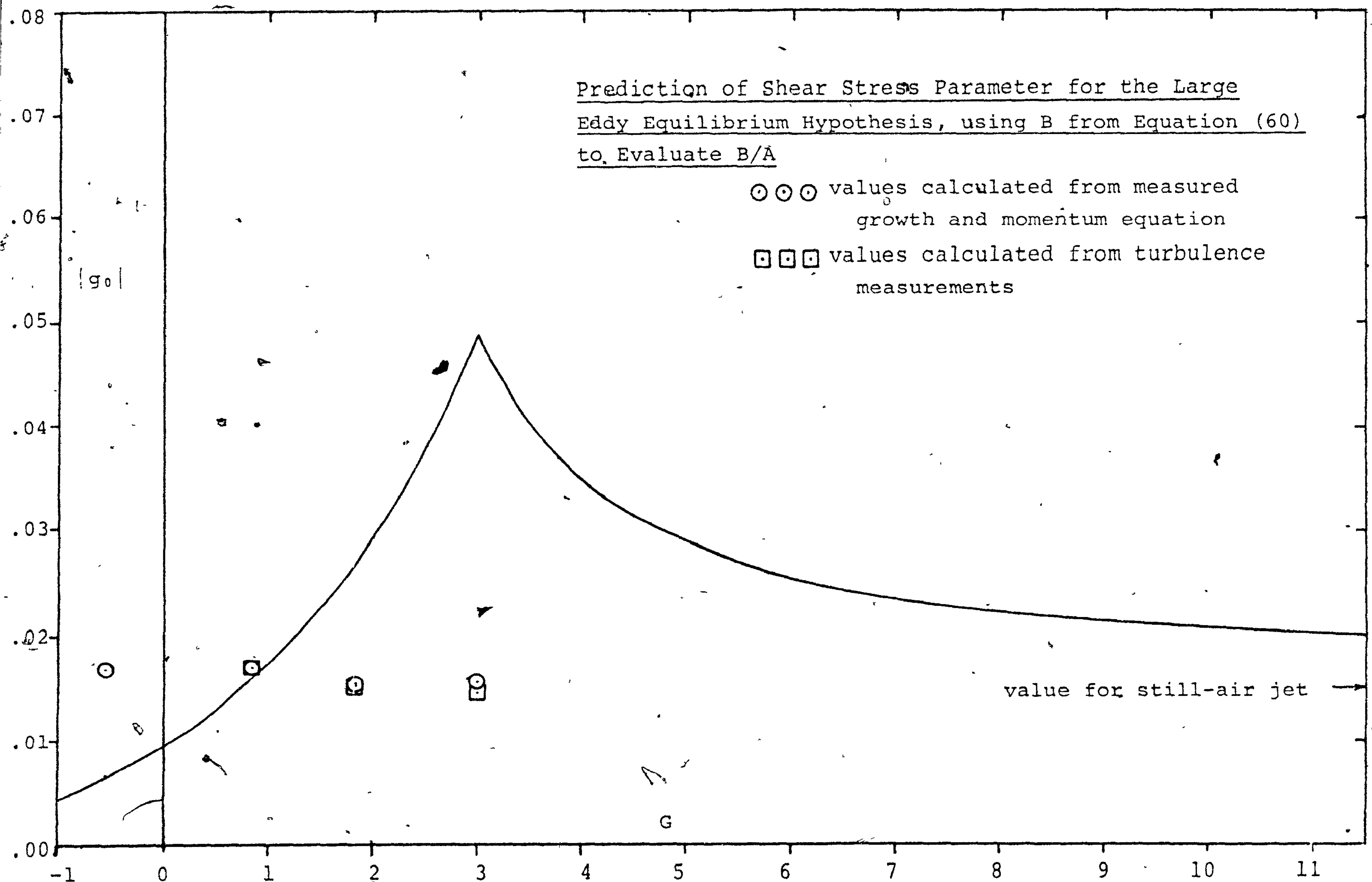
Prediction of Shear Stress Parameter for the Large
Eddy Equilibrium Hypothesis, using B from Equation (60)
to Evaluate B/A
values calculated from measured growth and momentum equation
values calculated from turbulence measurements
value for still-air jet
|g0|
G
.08
.07
.06
.05
.04
.03
.02
.01
.00
-1
0
1
2
3
4
5
6
7
8
9
10
11

Fig. 2-3

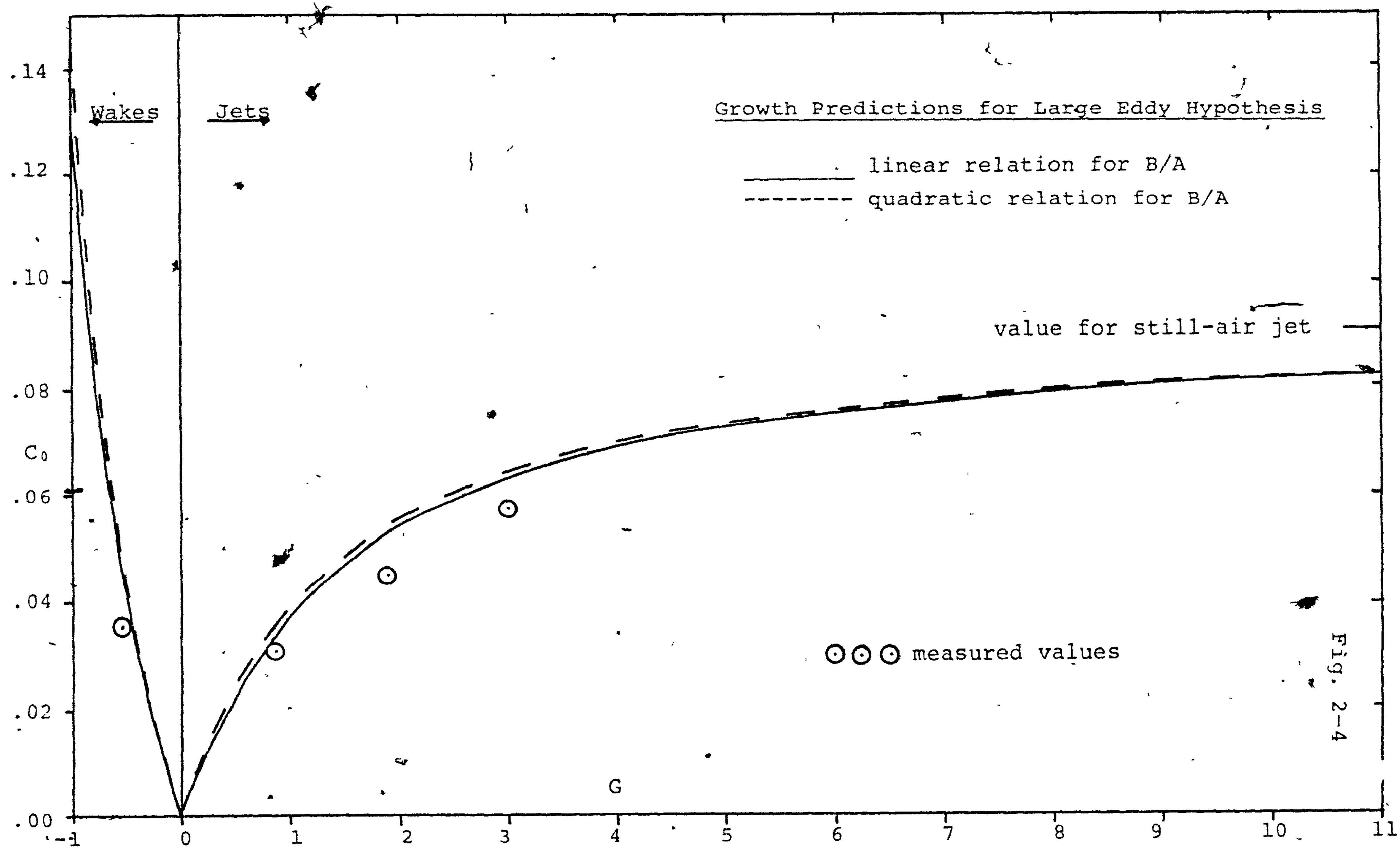
Growth Predictions for Large Eddy Hypothesis
linear relation for B/A
quadratic relation for B/A
value for still-air jet
measured values
Wakes
Jets
C_0
G
.14
.12
.10
.08
.06
.04
.02
.00
-1
0
1
2
3
4
5
6
7
8
9
10
11

Fig. 2-4

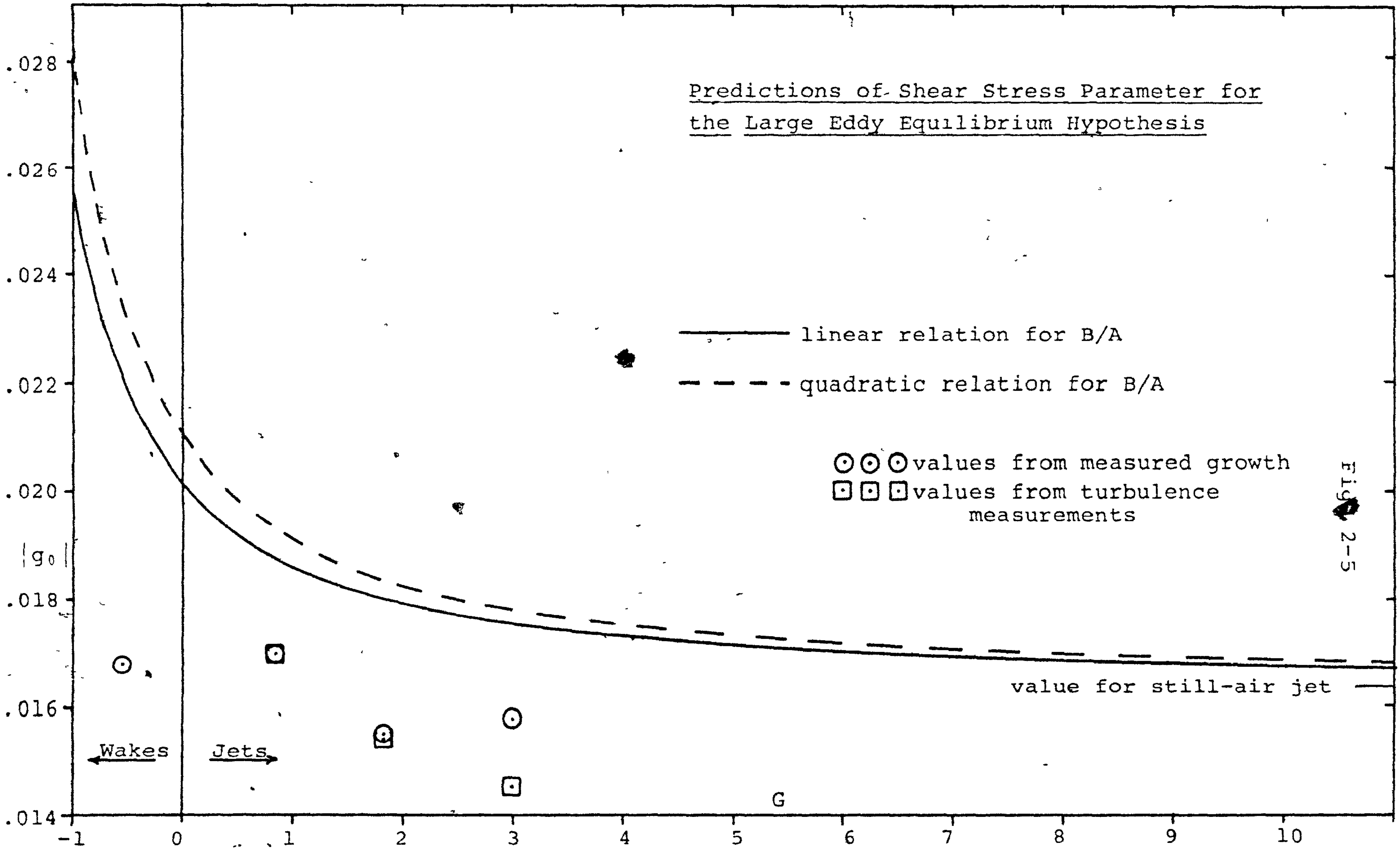
Predictions of Shear Stress Parameter for the Large Eddy Equilibrium Hypothesis
linear relation for B/A
quadratic relation for B/A
values from measured growth
values from turbulence measurements
value for still-air jet
Wakes
Jets
|g₀|
G
.028
.026
.024
.022
.020
.018
.016
.014
-1
0
1
2
3
4
5
6
7
8
9
10

Fig. 2-5

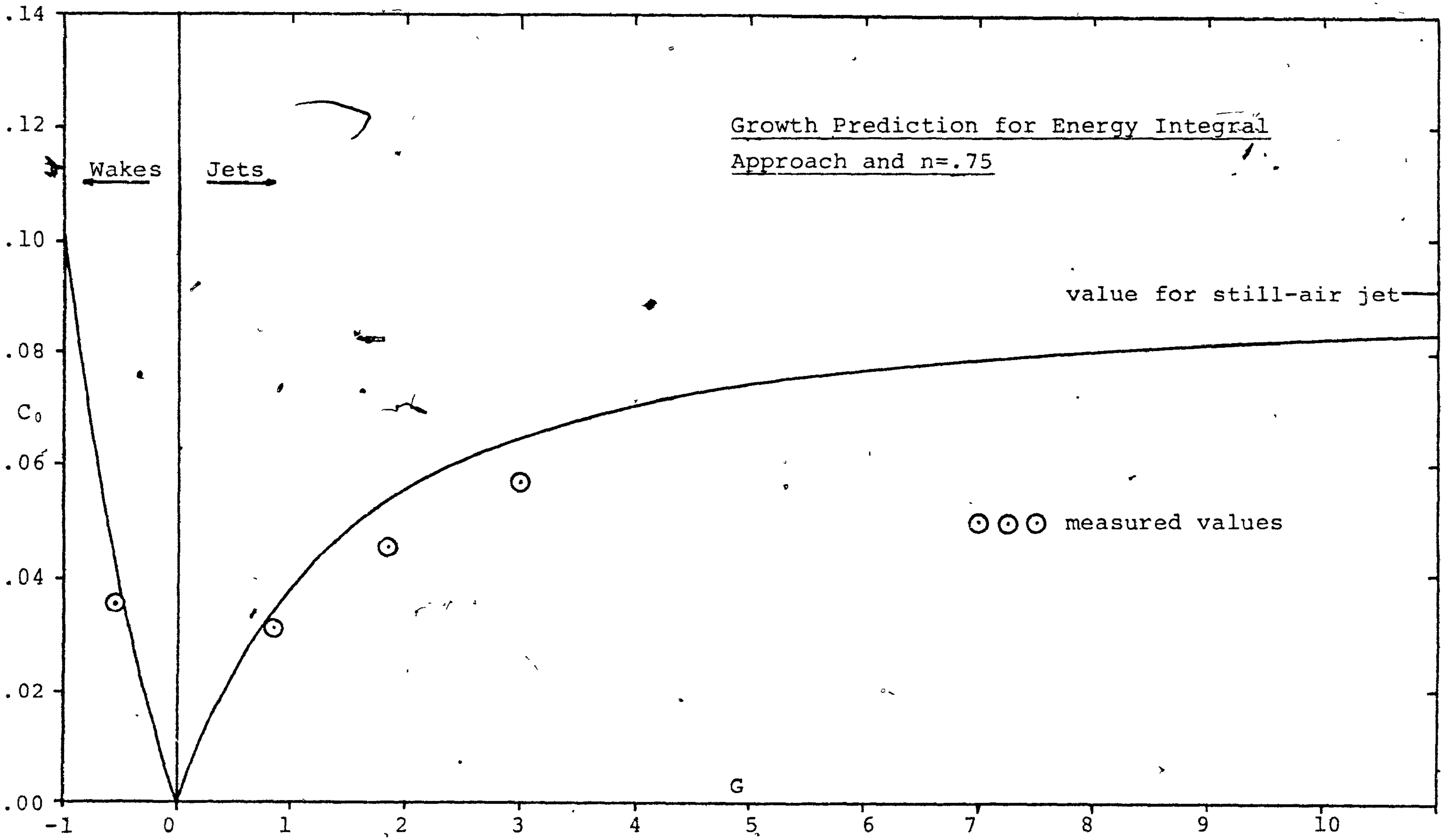
Growth Prediction for Energy Integral
Approach and n=.75
Wakes
Jets
value for still-air jet
measured values
C_0
G
.14
.12
.10
.08
.06
.04
.02
.00
-1
0
1
2
3
4
5
6
7
8
9
10

Fig. 2-6

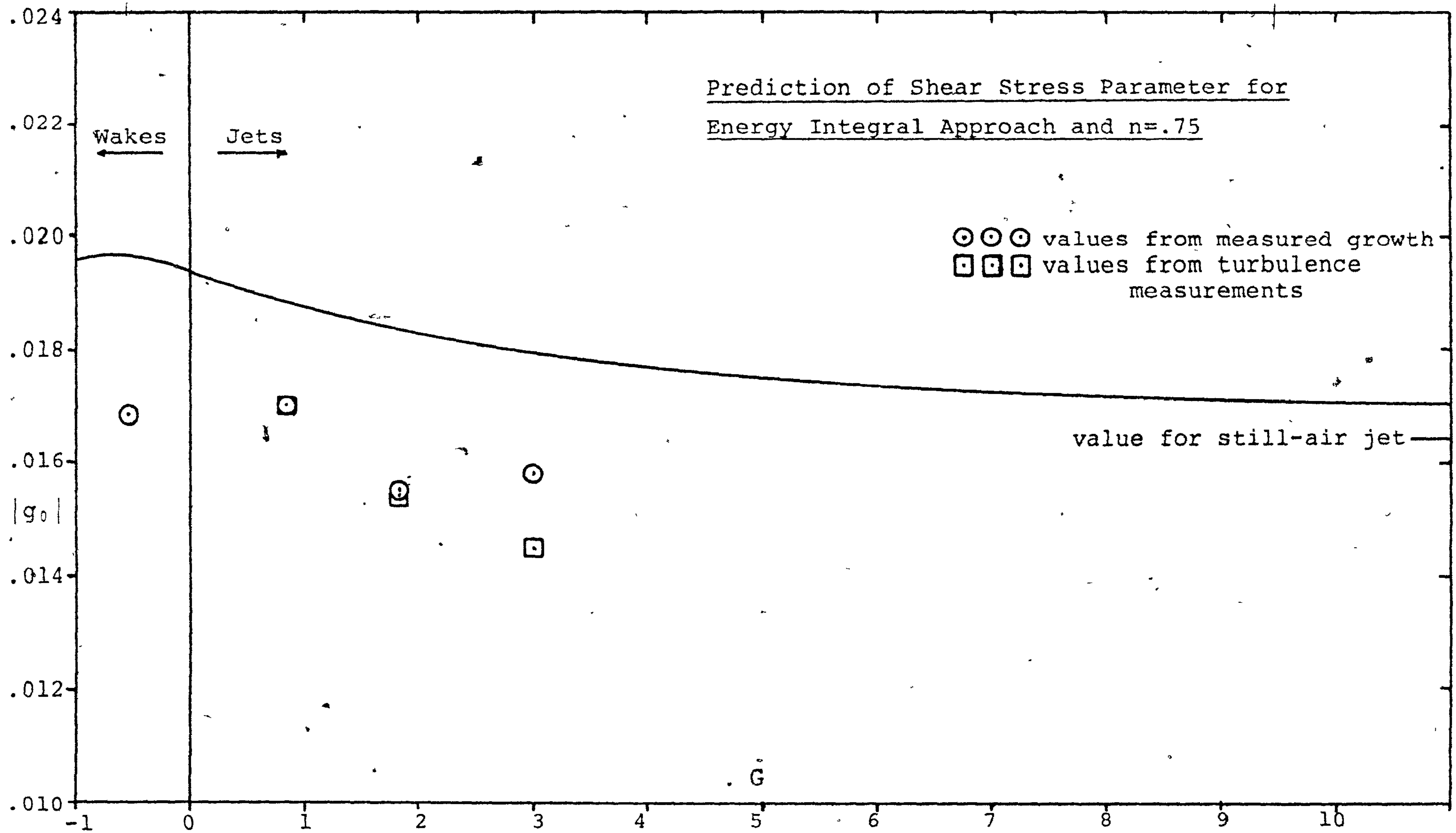

.024
.022
.020
.018
.016
.014
.012
.010
$|g_0|$
-1
0
1
2
3
4
5
6
7
8
9
10
Wakes
Jets
Prediction of Shear Stress Parameter for
Energy Integral Approach and n=.75
values from measured growth
values from turbulence measurements
value for still-air jet
G

Fig. 2-7

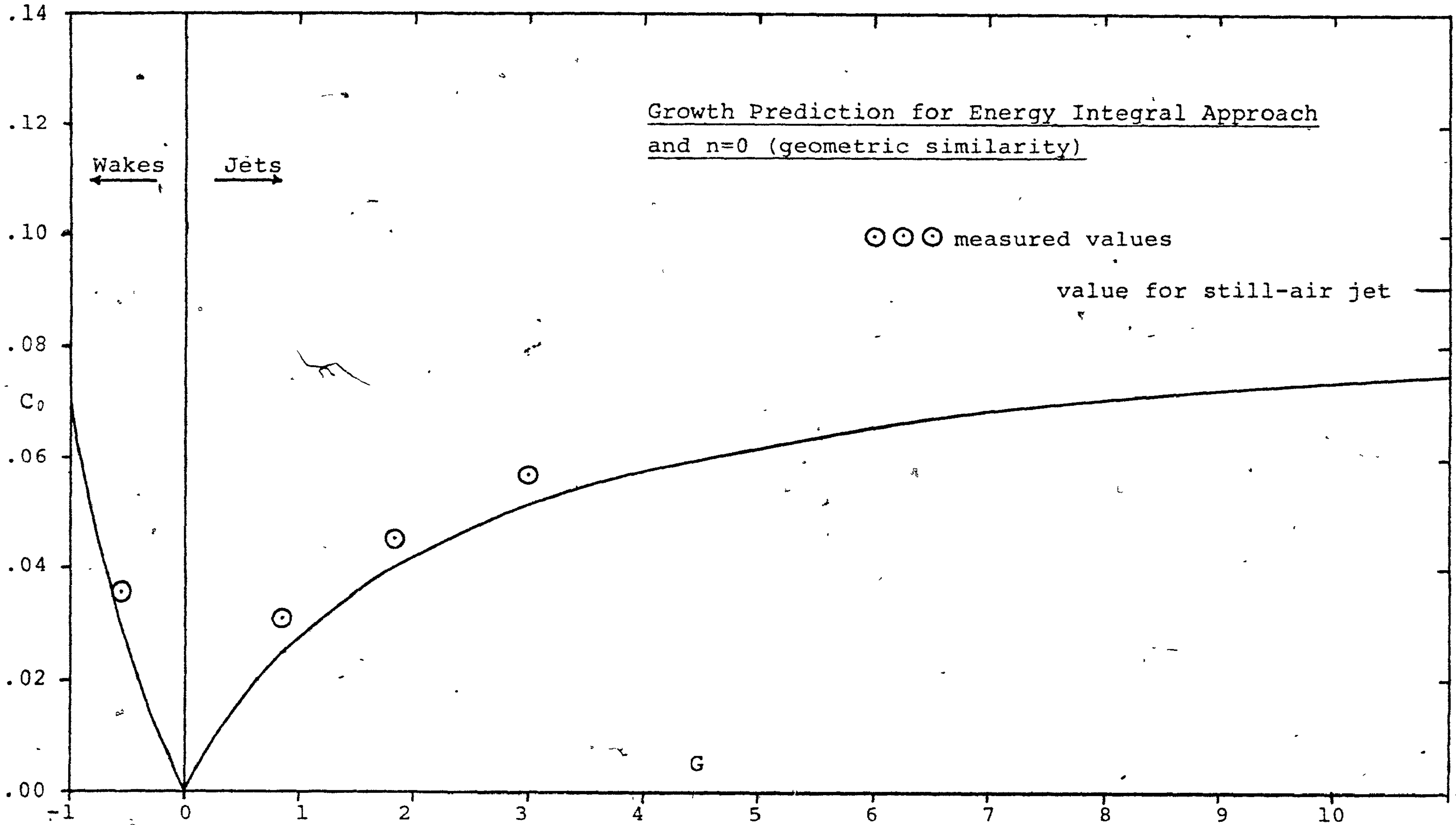

Growth Prediction for Energy Integral Approach
and n=0 (geometric similarity)
Wakes
Jets
measured values
value for still-air jet
C0
G
.14
.12
.10
.08
.06
.04
.02
.00
-1
0
1
2
3
4
5
6
7
8
9
10

Fig. 2-8

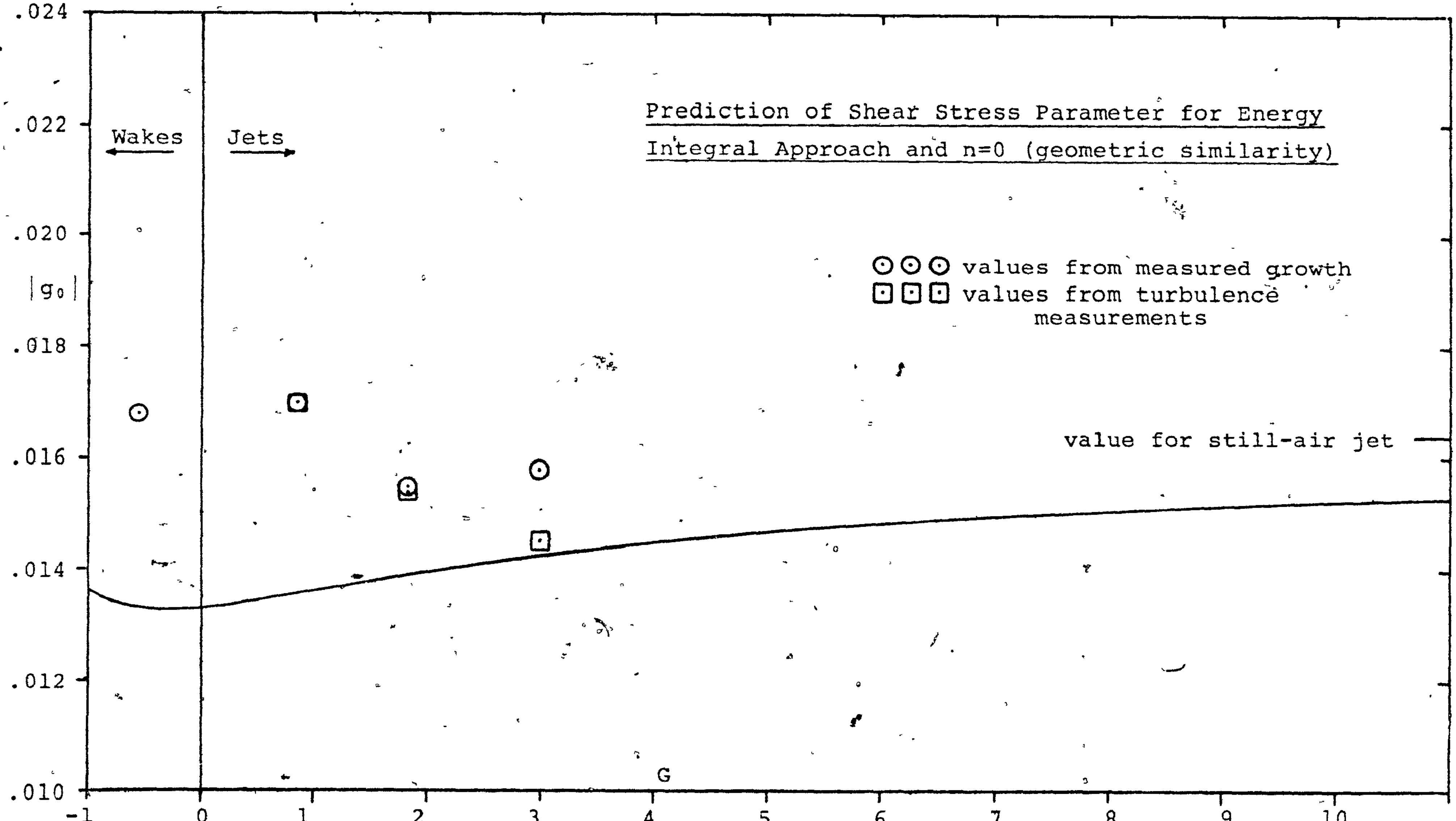

Prediction of Shear Stress Parameter for Energy Integral Approach and n=0 (geometric similarity)
Wakes
Jets
values from measured growth
values from turbulence measurements
value for still-air jet
|g₀|
.024
.022
.020
.018
.016
.014
.012
.010
G
-1
0
1
2
3
4
5
6
7
8
9
10

Fig. 2-9

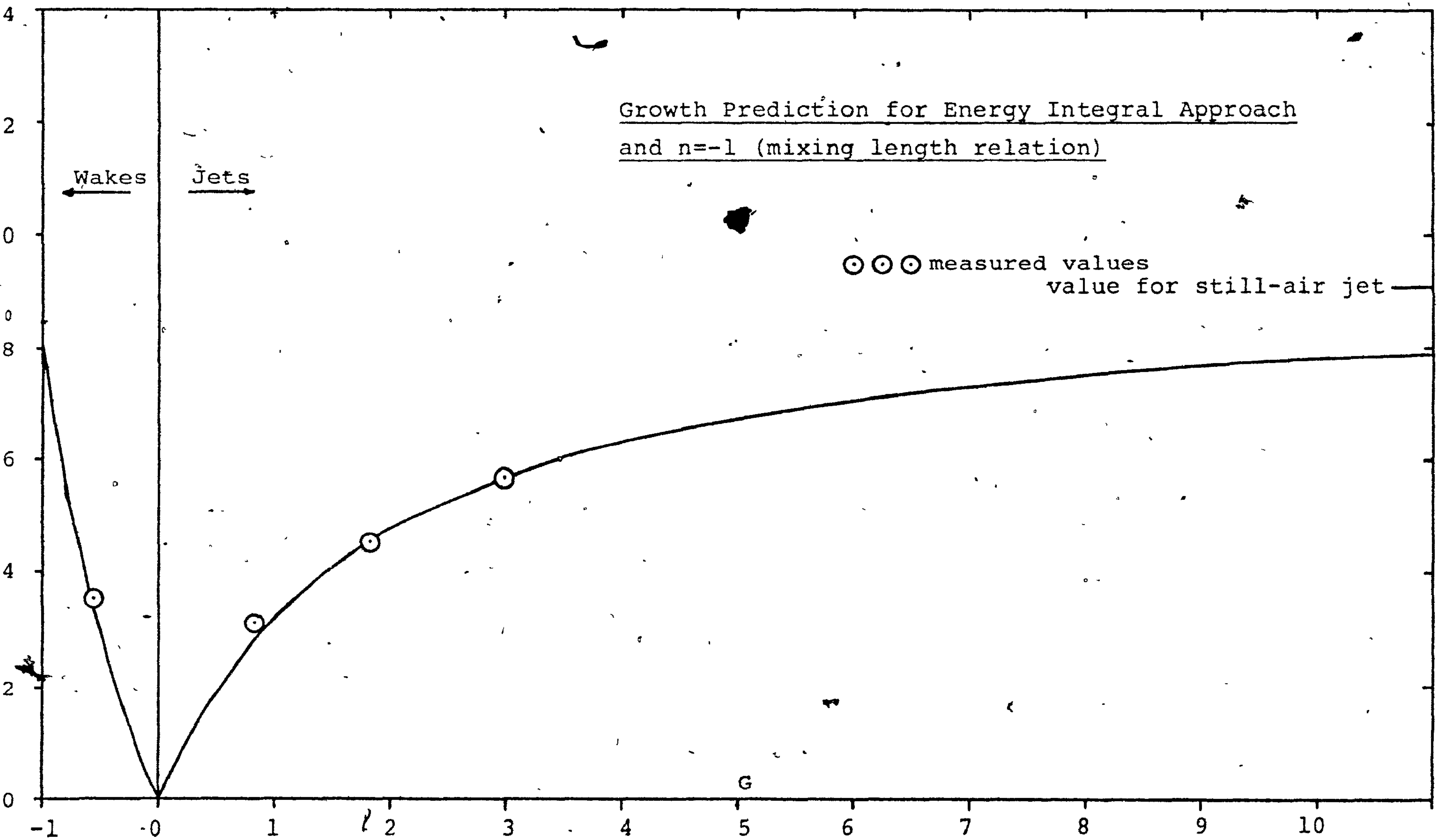
Growth Prediction for Energy Integral Approach
and n=-1 (mixing length relation)
Wakes
Jets
measured values
value for still-air jet
C_0
G
.14
.12
.10
.08
.06
.04
.02
.00
-1
0
1
2
3
4
5
6
7
8
9
10

Fig. 2-10

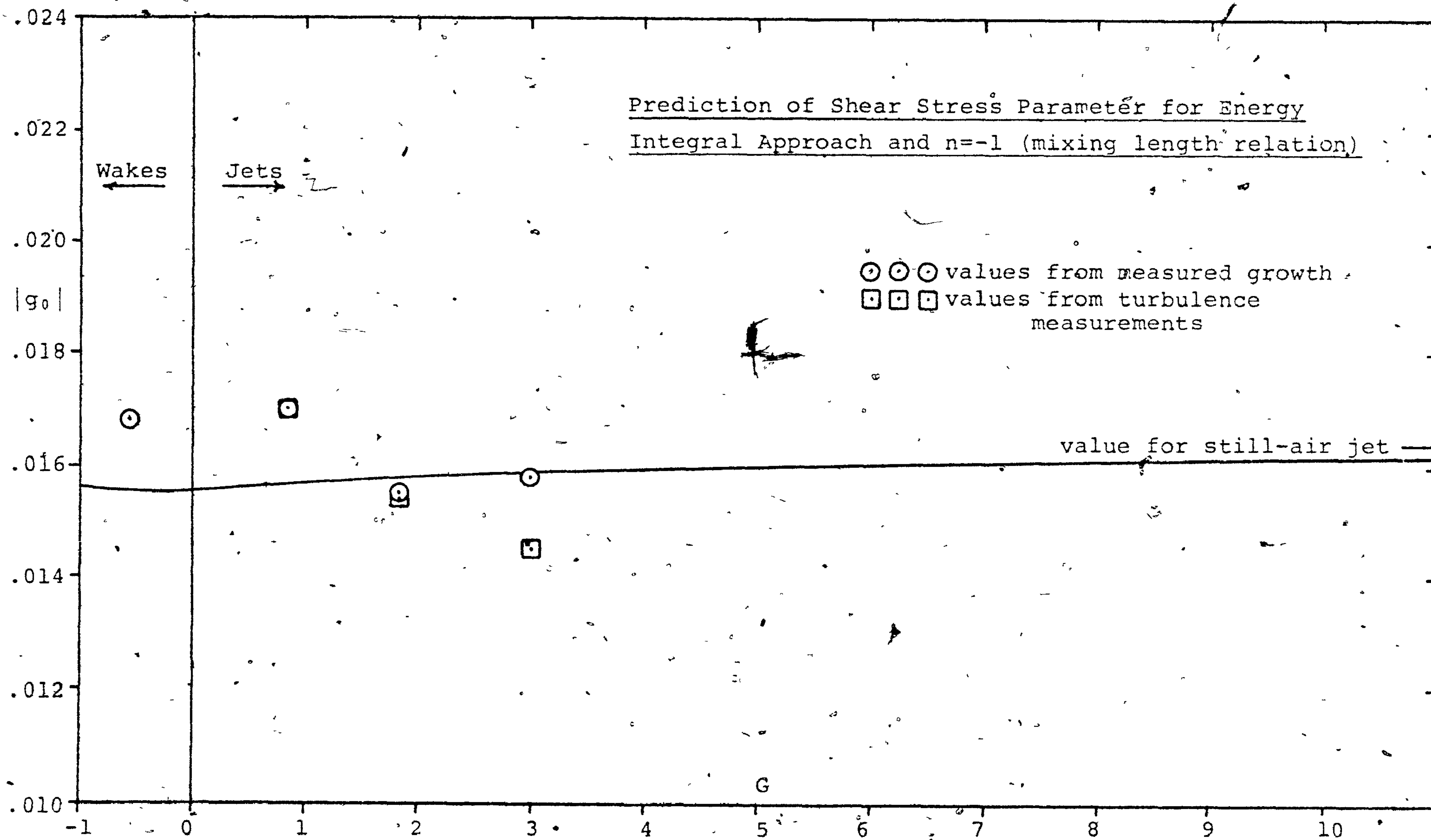
Prediction of Shear Stress Parameter for Energy Integral Approach and n=-1 (mixing length relation)
Wakes
Jets
values from measured growth
values from turbulence measurements
value for still-air jet
.024
.022
.020
.018
.016
.014
.012
.010
$|g_0|$
-1
0
1
2
3
4
5
6
7
8
9
10
G

Fig. 2-11

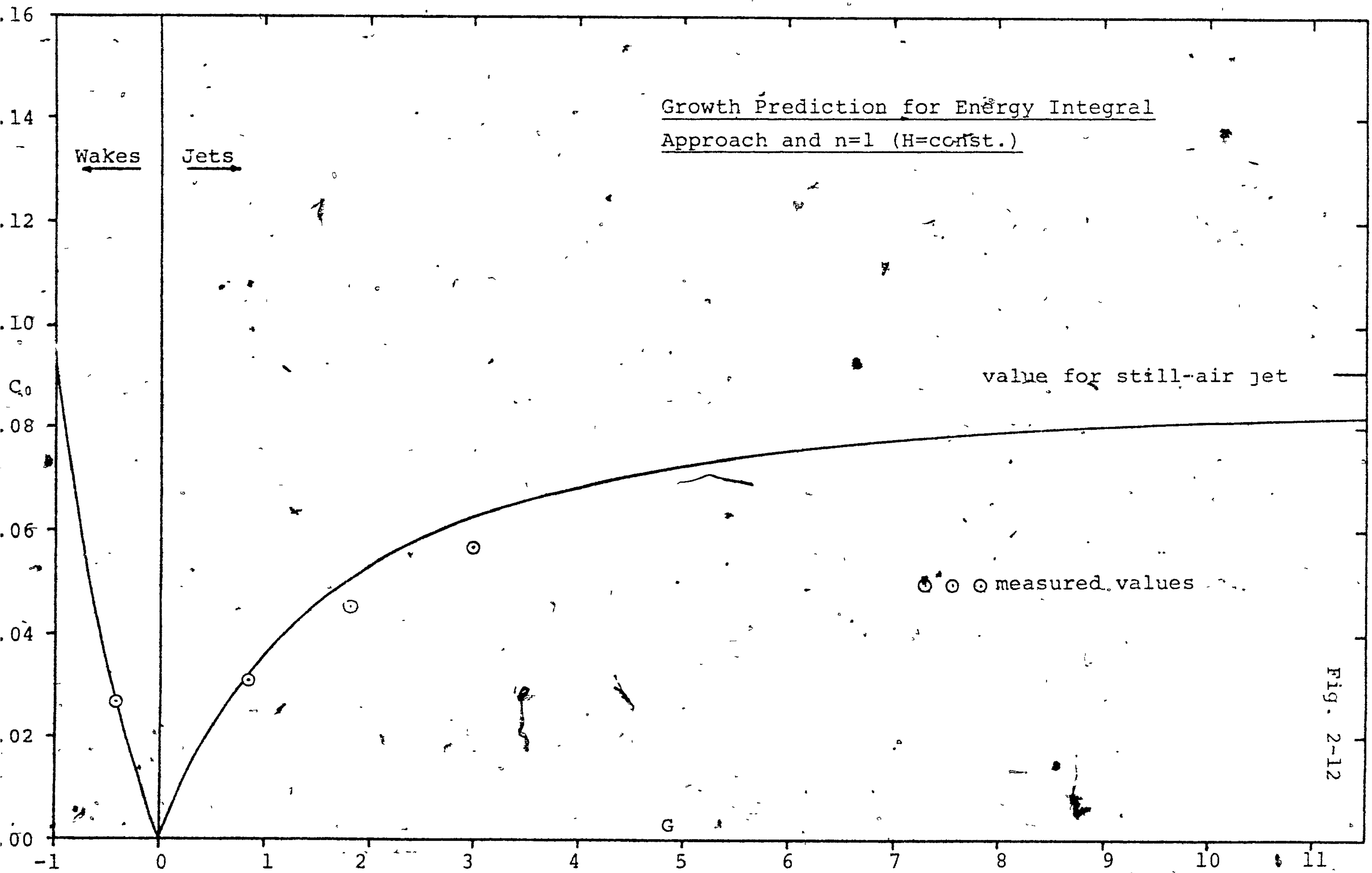
Growth Prediction for Energy Integral
Approach and n=1 (H=const.)
Wakes
Jets
value for still-air jet
measured values
C_0
G
.16
.14
.12
.10
.08
.06
.04
.02
.00
-1
0
1
2
3
4
5
6
7
8
9
10
11

Fig. 2-12

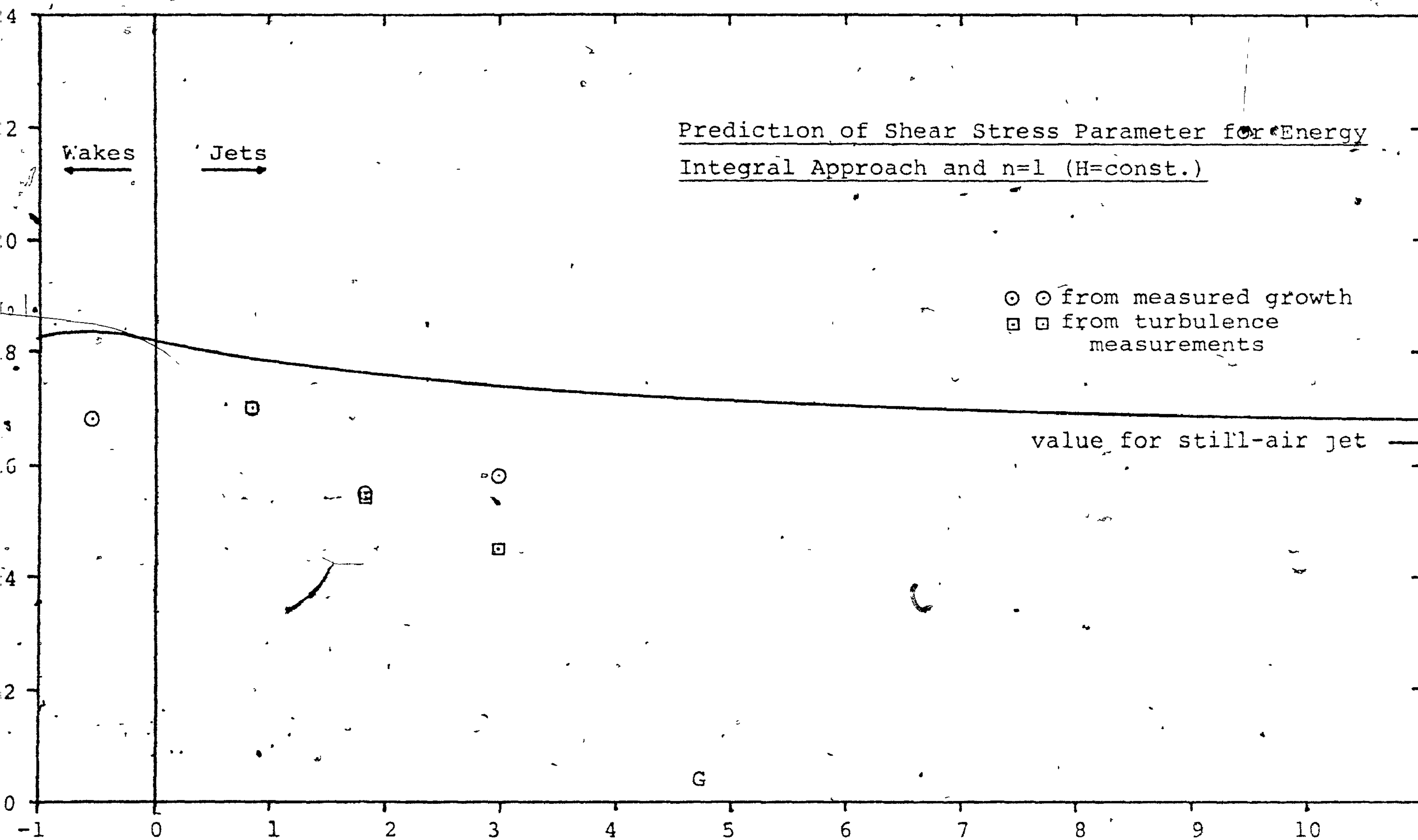
Prediction of Shear Stress Parameter for Energy Integral Approach and n=1 (H=const.)
Wakes
Jets
from measured growth
from turbulence measurements
value for still-air jet
G
-1
0
1
2
3
4
5
6
7
8
9
10

Fig. 2-13

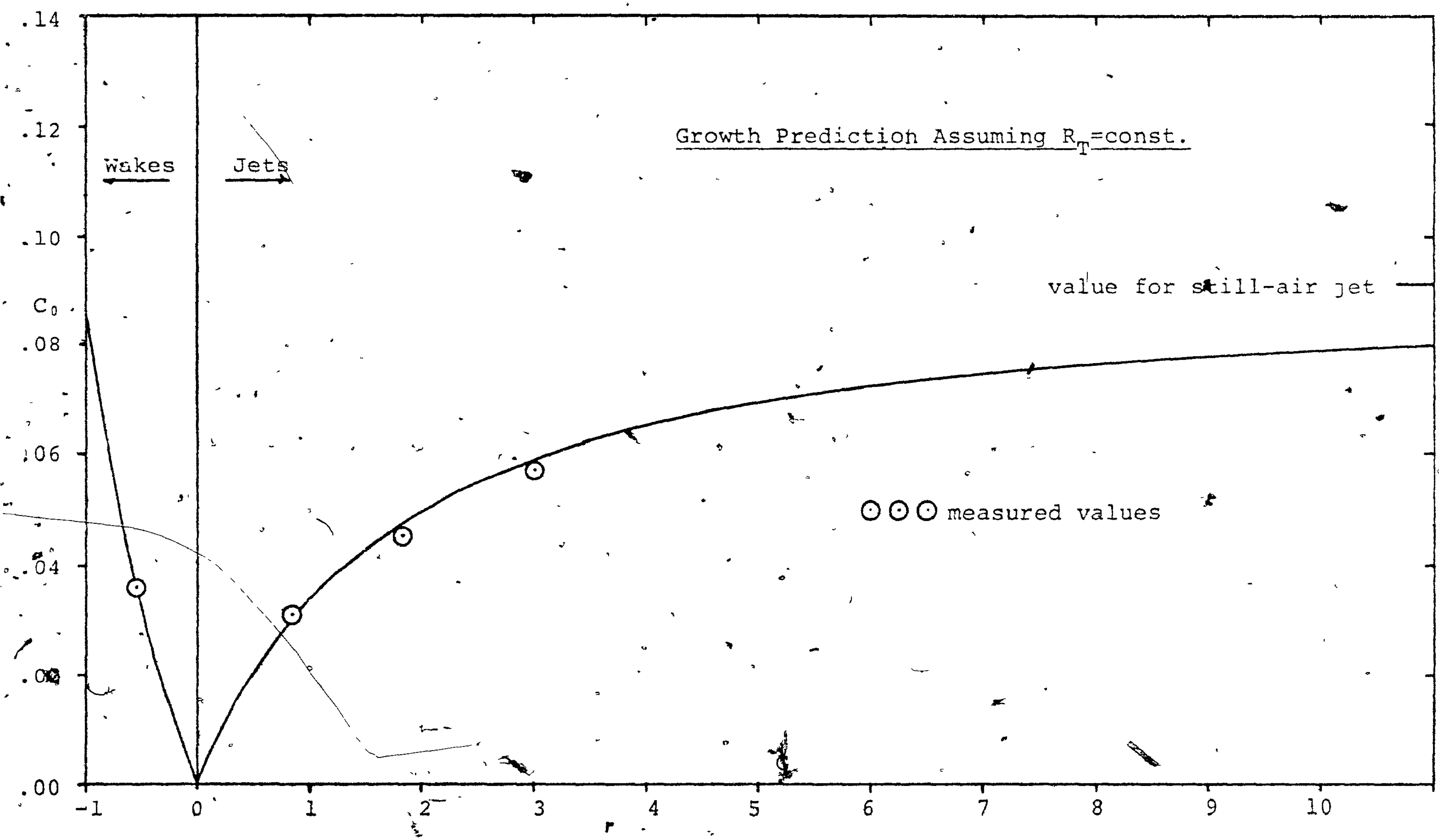
.14
.12
.10
C_0
.08
.06
.04
.02
.00
Wakes
Jets
Growth Prediction Assuming R_T=const.
value for still-air jet
measured values
-1
0
1
2
3
4
5
6
7
8
9
10
r

Fig. 2-14

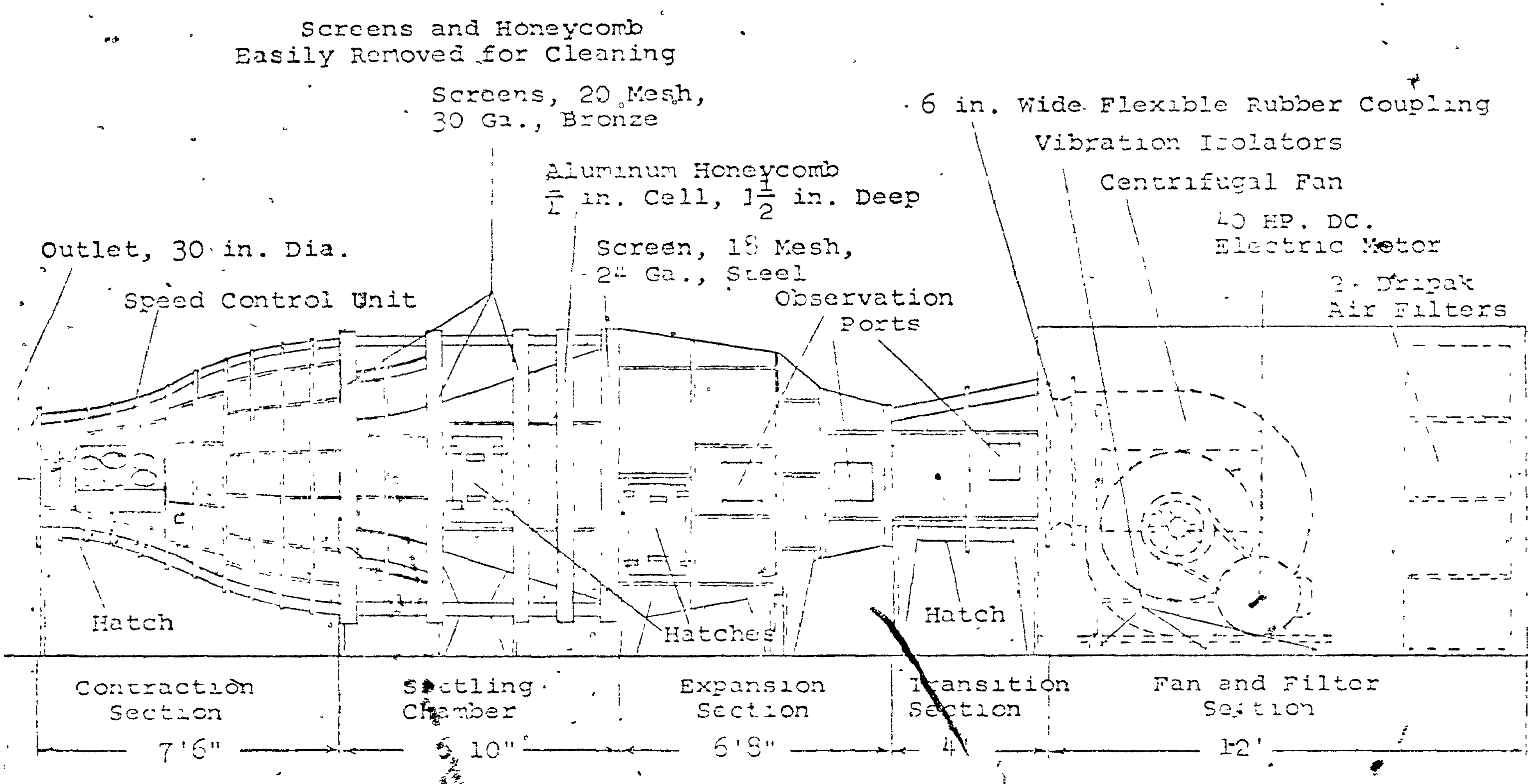

Screens and Honeycomb
Easily Removed for Cleaning
Screens, 20 Mesh,
30 Ga., Bronze
Aluminum Honeycomb
in. Cell, 1 1/2 in. Deep
Outlet, 30 in. Dia.
Screen, 18 Mesh,
24 Ga., Steel
Speed Control Unit
Observation
Ports
6 in. Wide Flexible Rubber Coupling
Vibration Isolators
Centrifugal Fan
40 HP. DC.
Electric Motor
Air Filters
Hatch
Hatches
Hatch
Contraction
Section
Settling
Chamber
Expansion
Section
Transition
Section
Fan and Filter
Section
7'6"
10"
6'8"
4'
12'

Fig. 3-1

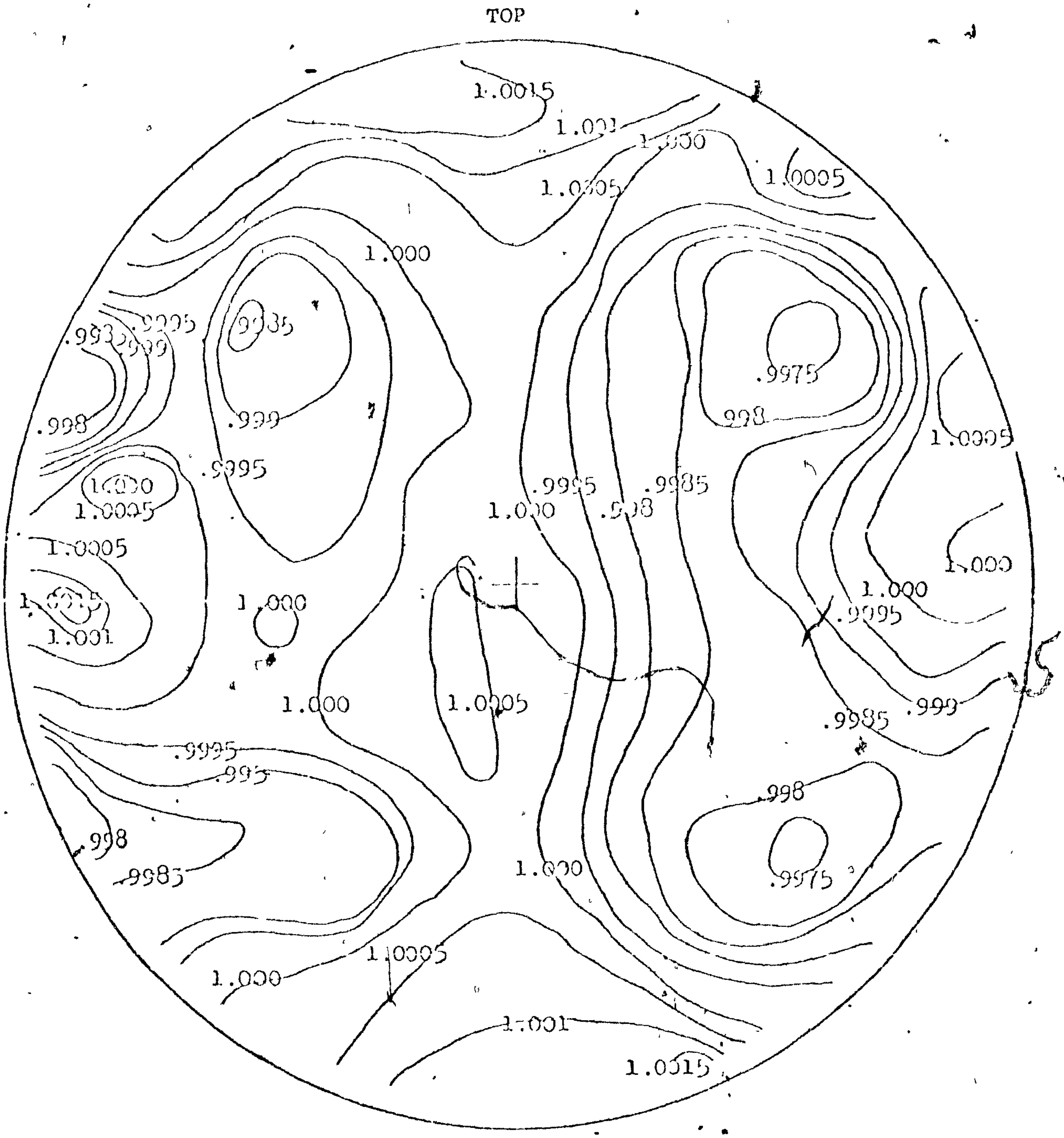

Velocity Contours at Tunnel Outlet,
No Screens or Honeycomb, $(V/V_{ref.})$

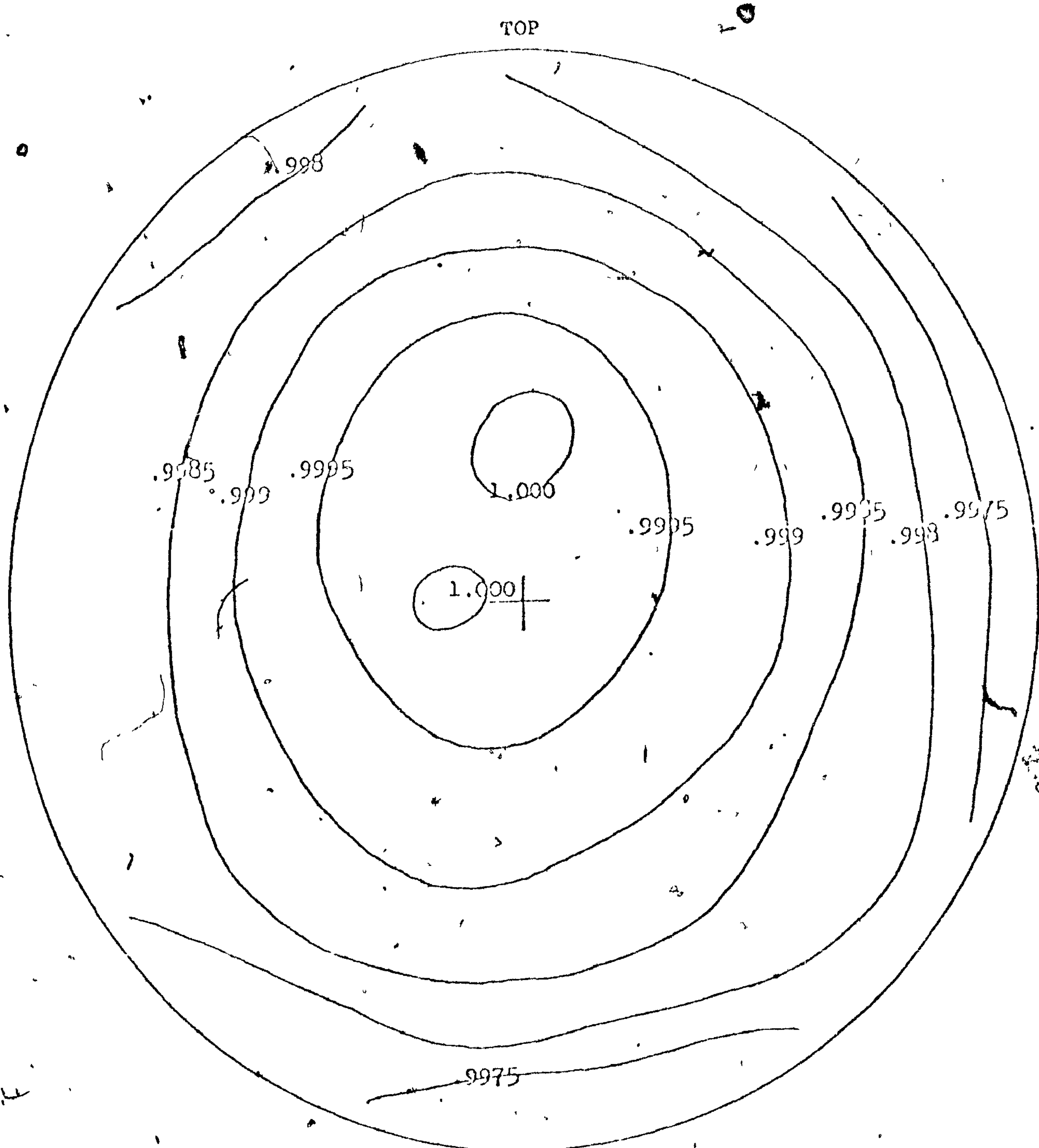

Velocity Contours at Tunnel Outlet, with Screens and Honeycomb, ($V/V_{ref.}$)

JET SUPPLY

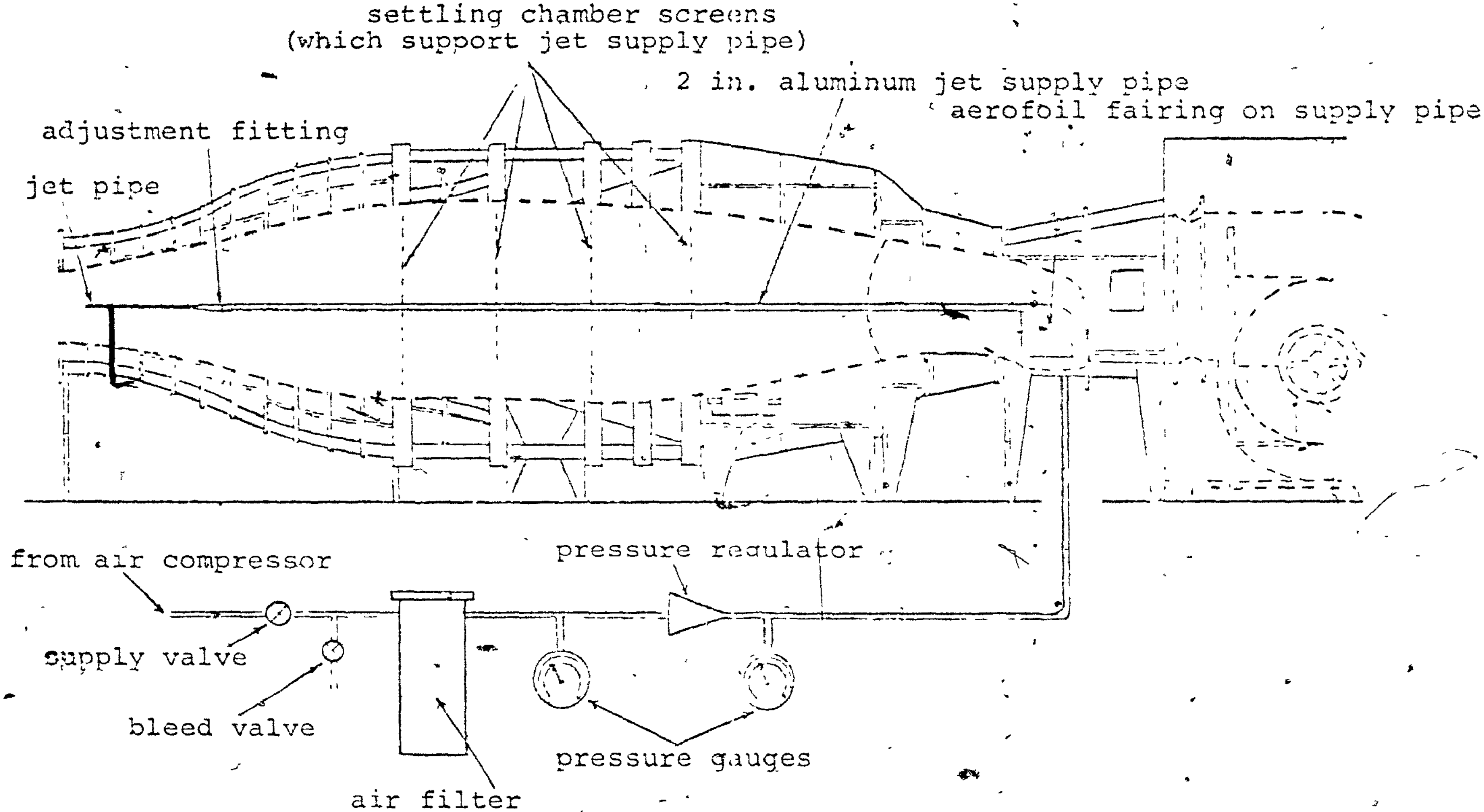

Fig. 3-4

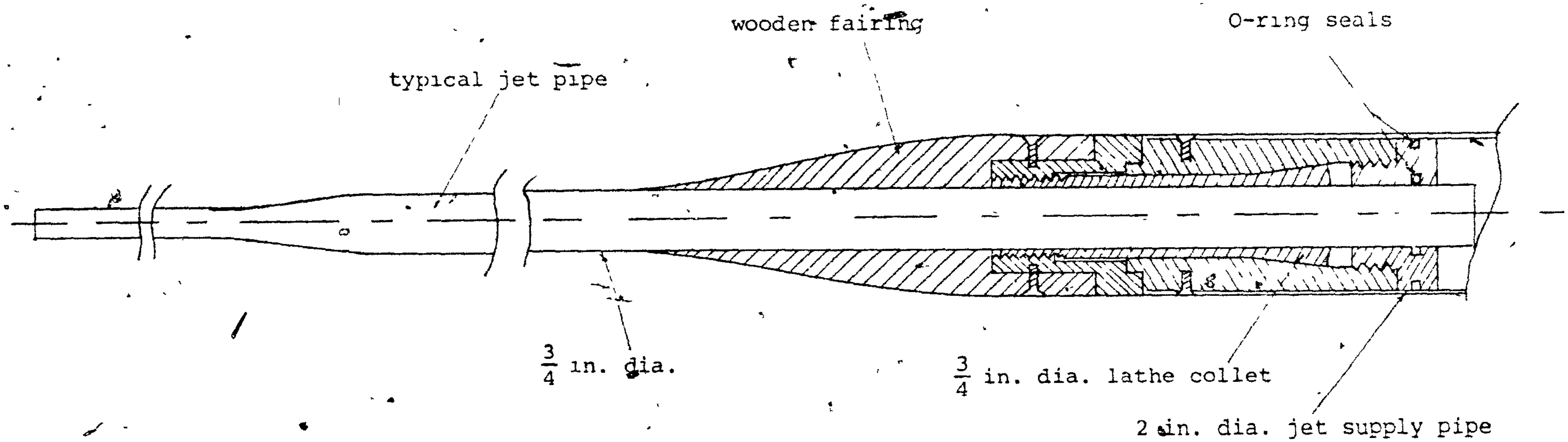

Jet Pipe Support and Adjustment Fitting

Fig. 3-5

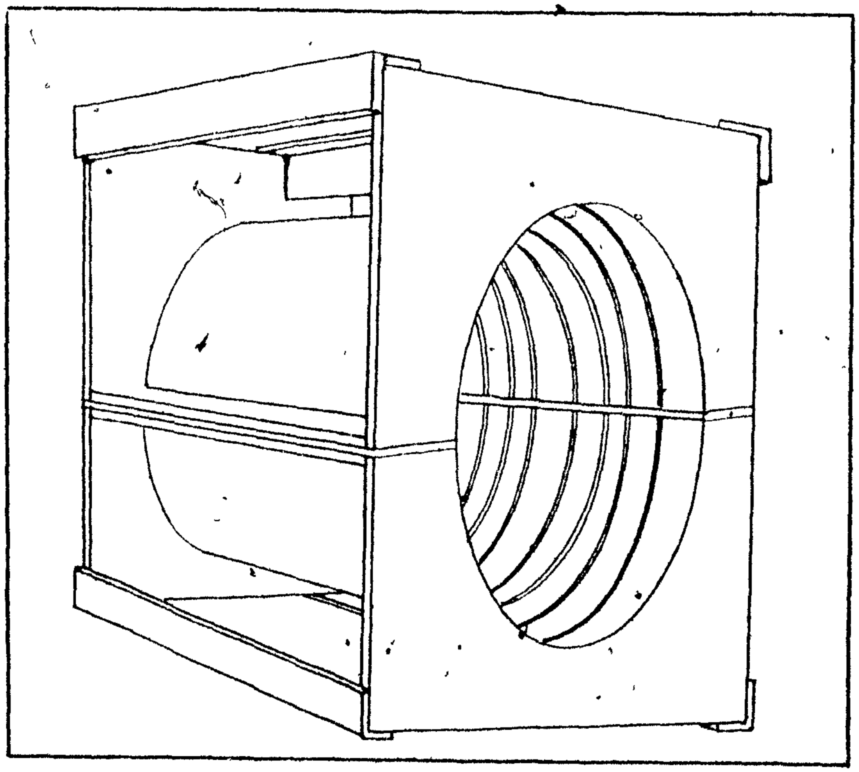

Fig. 3-6 Working Section

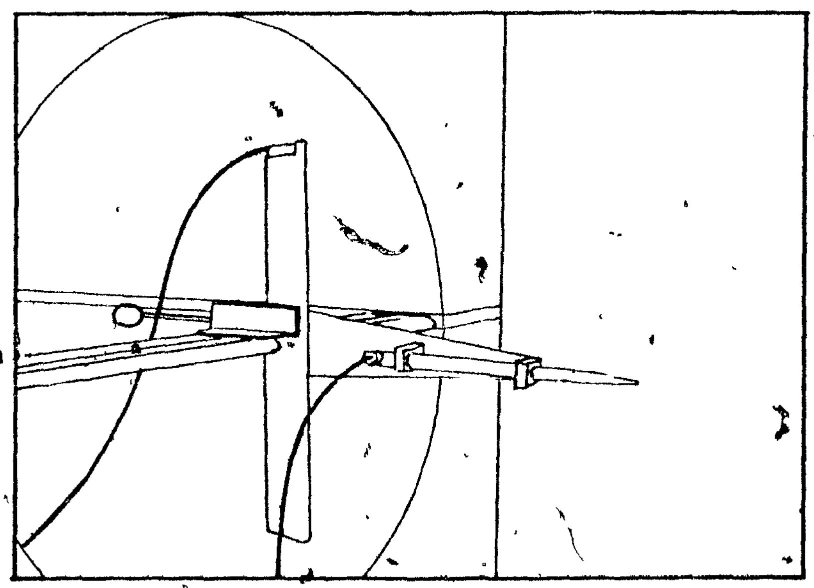

Fig. 3-7 Traversing Gear

Instrumentation

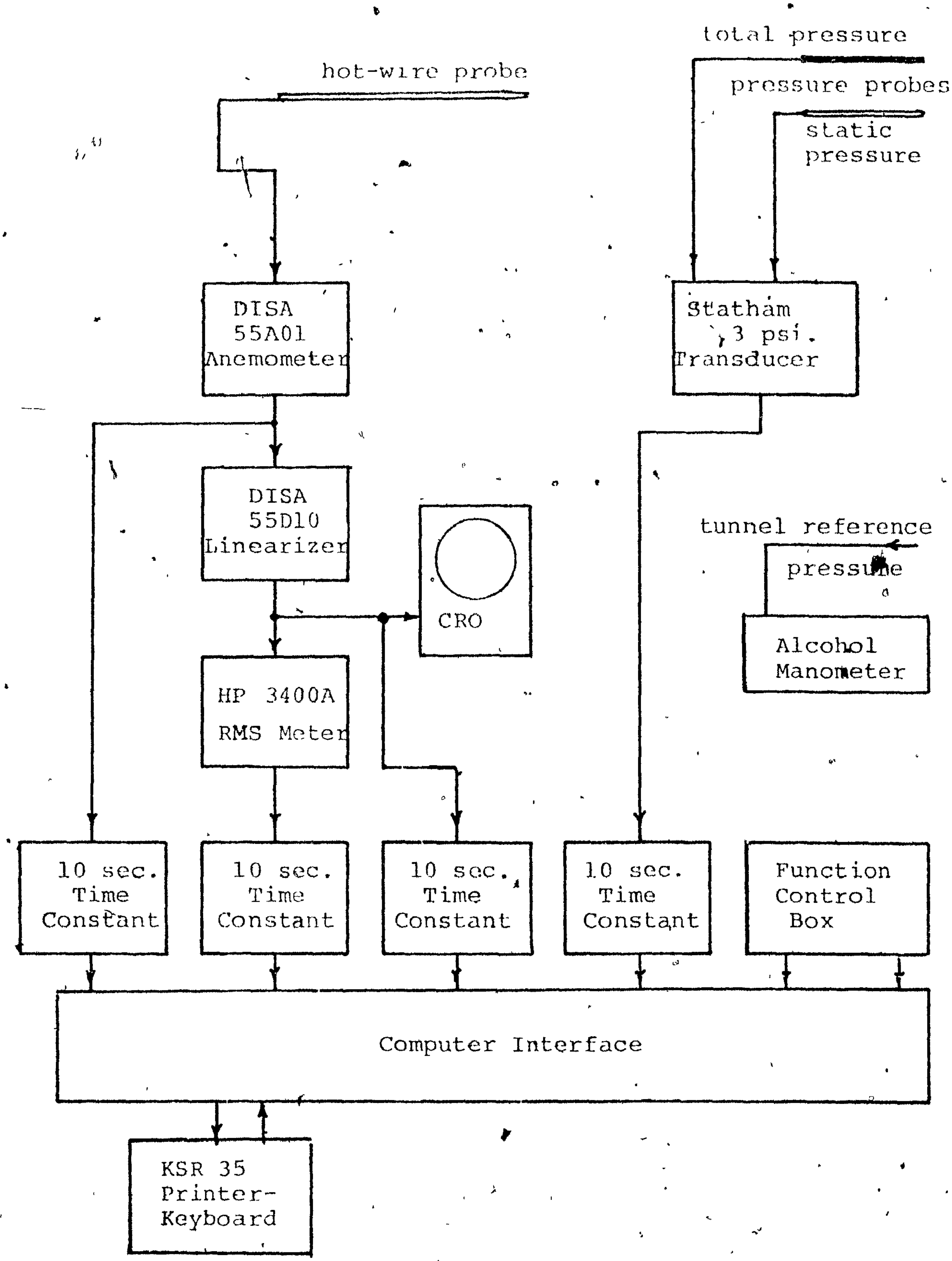

Fig. 3-9

Example of Hot-wire Data Program Output

STATION 2-5, 0126, 12/11/69, WIRE AS ABOVE.

J	EM	EF	EF**2	VAR1	VAR2	ITR
15.5	3.4290	-0.0220	0.4825E-03	[illegible]E-01	-0.3186E-02	10
16.	3.4332	-0.0355	0.1259E-02	0.3043E-01	-0.1452E-01	10
16.5	3.4405	-0.0773	0.59[illegible]E-02	0.3956E-01	-0.2801E-01	10
17.	3.5381	-0.2326	0.5411E-01	0.2163E 00	-0.7360E 00	10
17.5	3.9104	-0.4791	0.2295E 00	0.3006E 00	-0.9783E 00	18
17.75	4.2358	-0.5721	0.3273E 00	0.3695E 00	-0.9914E 00	28
18.	4.5799	-0.6223	0.3872E 00	0.3849E 00	-0.9[illegible]E 00	25
18.25	4.9541	-0.6583	0.4340E 00	0.2994E 00	-0.9924E 00	24
18.5	5.2793	-0.6640	0.4409E 00	0.2500E 00	-0.9934E 00	28
18.75	5.6467	-0.6609	0.4368E 00	0.1731E 00	-0.9953E 00	36
19.	5.9053	-0.6451	0.4161E 00	0.1839E 00	-0.9957E 00	26
19.25	6.1633	-0.6163	0.3799E 00	0.1673E 00	-0.9704E 00	31
19.5	6.2871	-0.5878	0.3455E 00	0.3162E 00	-0.9833E 00	17
19.75	6.2634	-0.5956	0.3547E 00	0.2298E 00	-0.9509E 00	21
20.	6.0997	-0.6173	0.3811E 00	0.2309E 00	-0.9868E 00	16
20.25	5.8533	-0.6437	0.4143E 00	0.1920E 00	-0.9583E 00	18
20.5	5.5444	-0.6521	0.4252E 00	0.1775E 00	-0.9921E 00	37
20.75	5.1839	-0.6564	0.4309E 00	0.2151E 00	-0.9808E 00	31
21.	4.8439	-0.6343	0.4023E 00	0.2012E 00	-0.9823E 00	31
21.25	4.5000	-0.5998	0.3598E 00	0.2542E 00	-0.9797E 00	33
21.5	4.1791	-0.5423	0.2941E 00	0.2177E 00	-0.9895E 00	24
21.75	3.9057	-0.4584	0.2101E 00	0.1898E 00	-0.9951E 00	15
22.	3.6864	-0.3420	0.1170E 00	0.2459E 00	-0.9883E 00	23
22.5	3.4969	-0.1179	0.1390E-01	0.6478E-01	-0.2070E 00	10
23.	3.4818	-0.0478	0.2283E-02	0.1630E-01	-0.3624E-01	10
23.5	3.4762	-0.0259	0.6696E-03	0.4210E-01	-0.1167E-01	10
24.	3.4746	-0.0180	0.3244E-03	0.3366E-01	-0.2659E-02	10

Fig. 3-10

Example of Hot-wire Calibration Program Output

P(MM)	VEL	EB	EL	V**.4	EB**2	ZERO
0.150	8.42	3.676	0.617	2.345	13.51	0.061
0.743	18.82	4.039	1.365	3.235	16.31	0.061
2.112	31.63	4.316	2.263	3.982	18.63	0.056
3.577	41.17	4.473	2.931	4.424	20.01	0.056
5.213	49.71	4.593	3.526	4.770	21.10	0.056
7.055	57.82	4.693	4.083	5.063	22.02	0.056
10.513	70.59	4.828	4.943	5.499	23.31	0.056
13.889	81.13	4.926	5.654	5.803	24.27	0.056
17.354	90.69	5.008	6.284	6.067	25.08	0.056
20.197	97.34	5.064	6.756	6.254	25.64	0.056
23.765	106.13	5.124	7.261	6.461	26.25	0.056
26.621	112.32	5.167	7.675	6.609	26.69	0.056

Example of Pressure-probe Data Program Output

```
STATION 2-6, 112>, 6/1/70

ZERO=  0.20 MM.H20 EQUIV.
P(REF)-P(S)= 11.66 MM.H20
14.5   P(0)-P(S)= 11.57 MM.H20          VELOCITY= 45.07 FT/SEC
15.    P(0)-P(S)= 11.58 MM.H20          VELOCITY= 45.10 FT/SEC
15.5   P(0)-P(S)= 11.56 MM.H20          VELOCITY= 45.06 FT/SEC
16.    P(0)-P(S)= 11.52 MM.H20          VELOCITY= 44.97 FT/SEC
16.5   P(0)-P(S)= 11.42 MM.H20          VELOCITY= 44.78 FT/SEC
17.    P(0)-P(S)= 10.59 MM.H20          VELOCITY= 43.12 FT/SEC
17.5   P(0)-P(S)=  8.59 MM.H20          VELOCITY= 39.83 FT/SEC
18.    P(0)-P(S)=  6.25 MM.H20          VELOCITY= 33.11 FT/SEC
18.5   P(0)-P(S)=  4.09 MM.H20          VELOCITY= 26.81 FT/SEC
19.    P(0)-P(S)=  2.71 MM.H20          VELOCITY= 21.92 FT/SEC
19.25  P(0)-P(S)=  2.04 MM.H20          VELOCITY= 18.95 FT/SEC
19.5   P(0)-P(S)=  1.65 MM.H20          VELOCITY= 17.02 FT/SEC
19.75  P(0)-P(S)=  1.41 MM.H20          VELOCITY= 15.97 FT/SEC
20.    P(0)-P(S)=  1.42 MM.H20          VELOCITY= 15.77 FT/SEC
ZERO=  0.19 MM.H20 EQUIV.
P(REF)-P(S)= 11.59 MM.H20
20.    P(0)-P(S)=  1.41 MM.H20          VELOCITY= 15.72 FT/SEC
20.25  P(0)-P(S)=  1.55 MM.H20          VELOCITY= 16.40 FT/SEC
20.5   P(0)-P(S)=  1.65 MM.H20          VELOCITY= 18.02 FT/SEC
20.75  P(0)-P(S)=  2.38 MM.H20          VELOCITY= 20.45 FT/SEC
21.    P(0)-P(S)=  3.08 MM.H20          VELOCITY= 2[illegible].24 FT/SEC
21.5   P(0)-P(S)=  4.99 MM.H20          VELOCITY= 29.59 FT/SEC
22.    P(0)-P(S)=  7.23 MM.H20          VELOCITY= 35.64 FT/SEC
22.5   P(0)-P(S)=  9.53 MM.H20          VELOCITY= 41.02 FT/SEC
23.    P(0)-P(S)= 11.06 MM.H20          VELOCITY= 44.07 FT/SEC
23.5   P(0)-P(S)= 11.50 MM.H20          VELOCITY= 44.92 FT/SEC
24.    P(0)-P(S)= 11.53 MM.H20          VELOCITY= 44.95 FT/SEC
24.5   P(0)-P(S)= 11.52 MM.H20          VELOCITY= 44.97 FT/SEC
25.    P(0)-P(S)= 11.52 MM.H20          VELOCITY= 44.97 FT/SEC
25.5   P(0)-P(S)= 11.53 MM.H20          VELOCITY= 44.98 FT/SEC
```

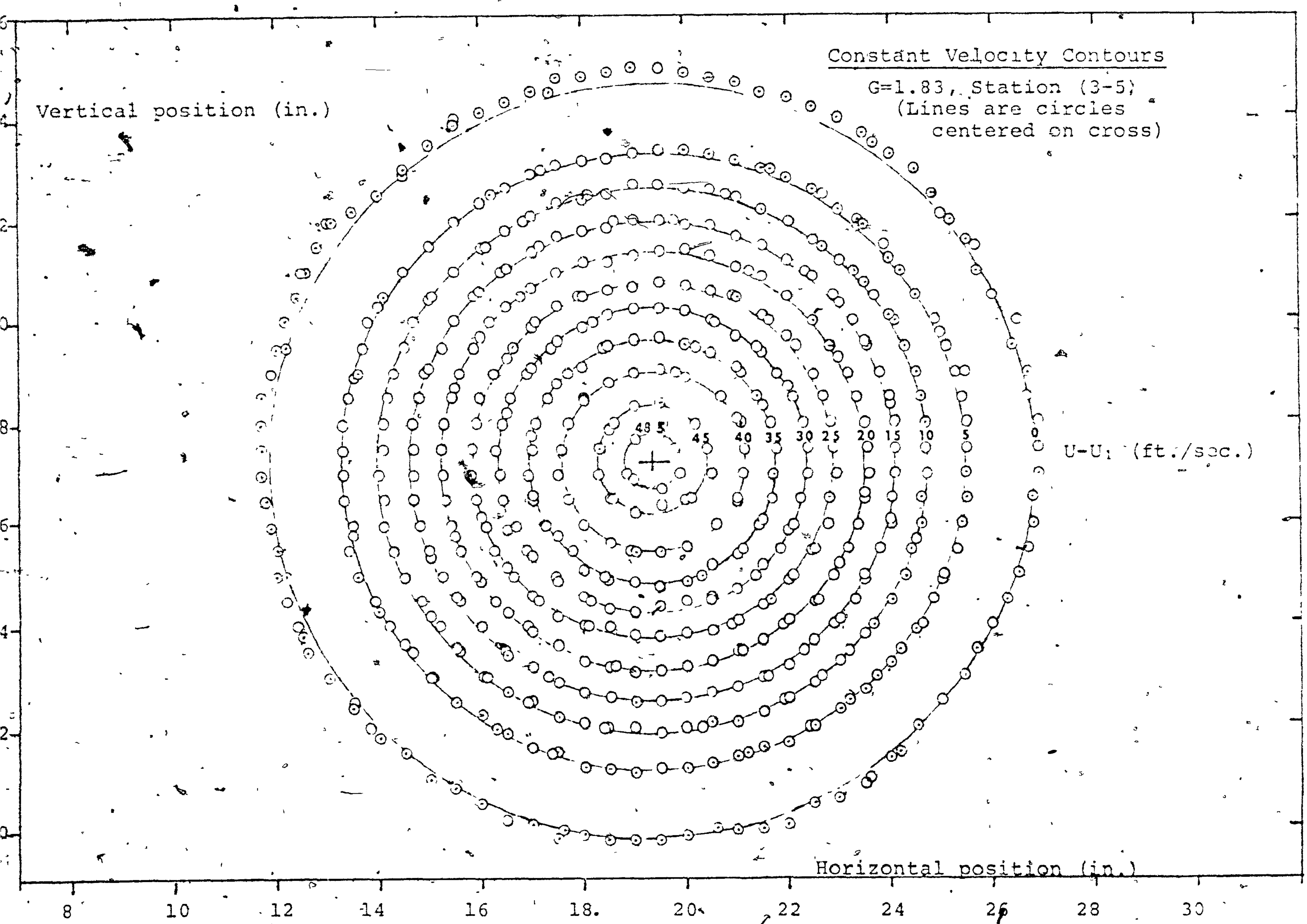
Constant Velocity Contours
G=1.83, Station (3-5)
(Lines are circles
centered on cross)
Vertical position (in.)
Horizontal position (in.)
U-U₁ (ft./sec.)
48 5
45
40
35
30
25
20
15
10
5
0
8
10
12
14
16
18.
20
22
24
26
28
30

Fig. 3-12

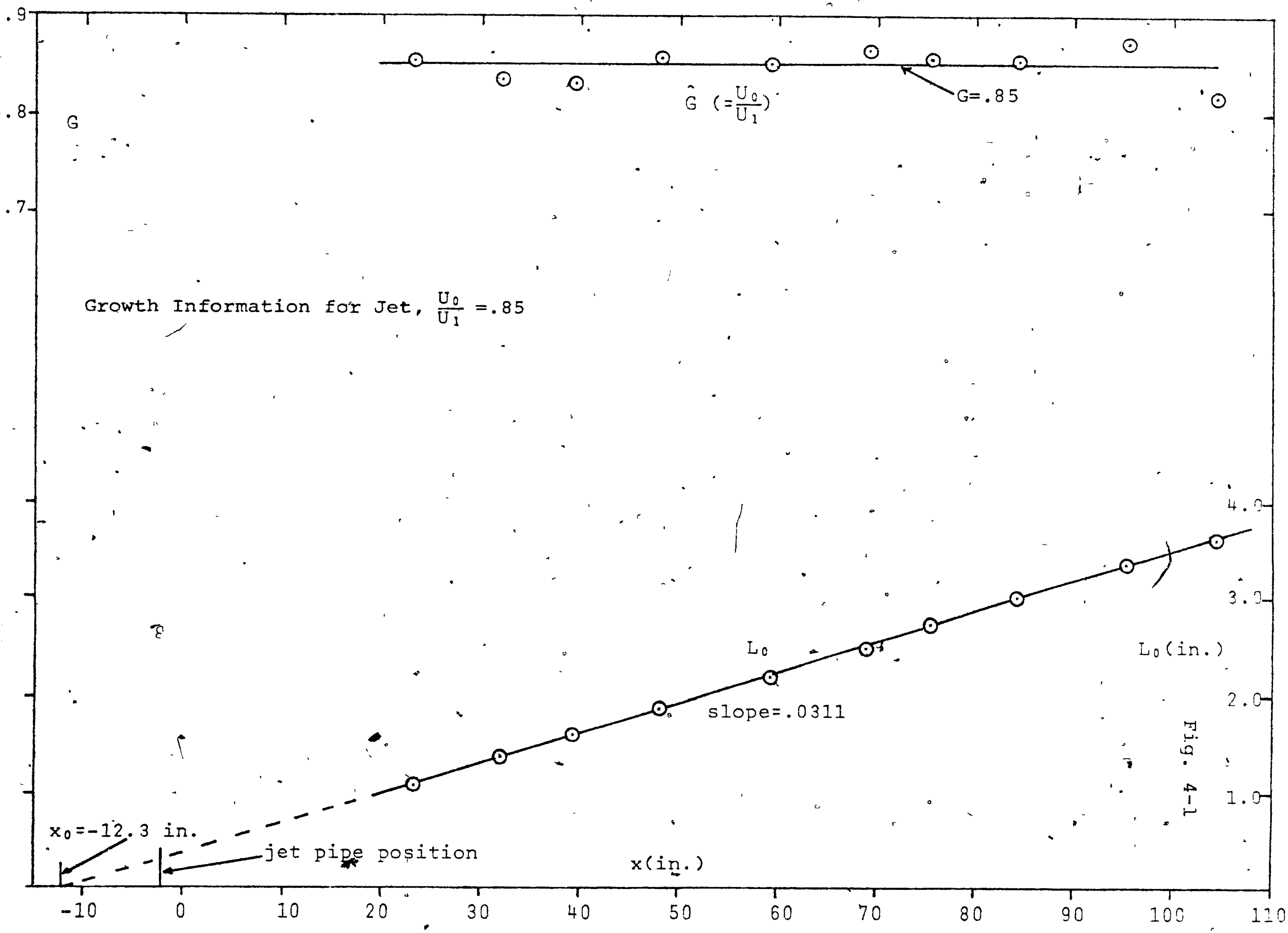

.9
.8
.7
G
$\hat{G}$ $(=\frac{U_0}{U_1})$
G=.85
Growth Information for Jet, $\frac{U_0}{U_1}$ =.85
4.0
3.0
2.0
1.0
L_0
L_0(in.)
slope=.0311
x_0=-12.3 in.
jet pipe position
x(in.)
-10
0
10
20
30
40
50
60
70
80
90
100
110

Fig. 4-1

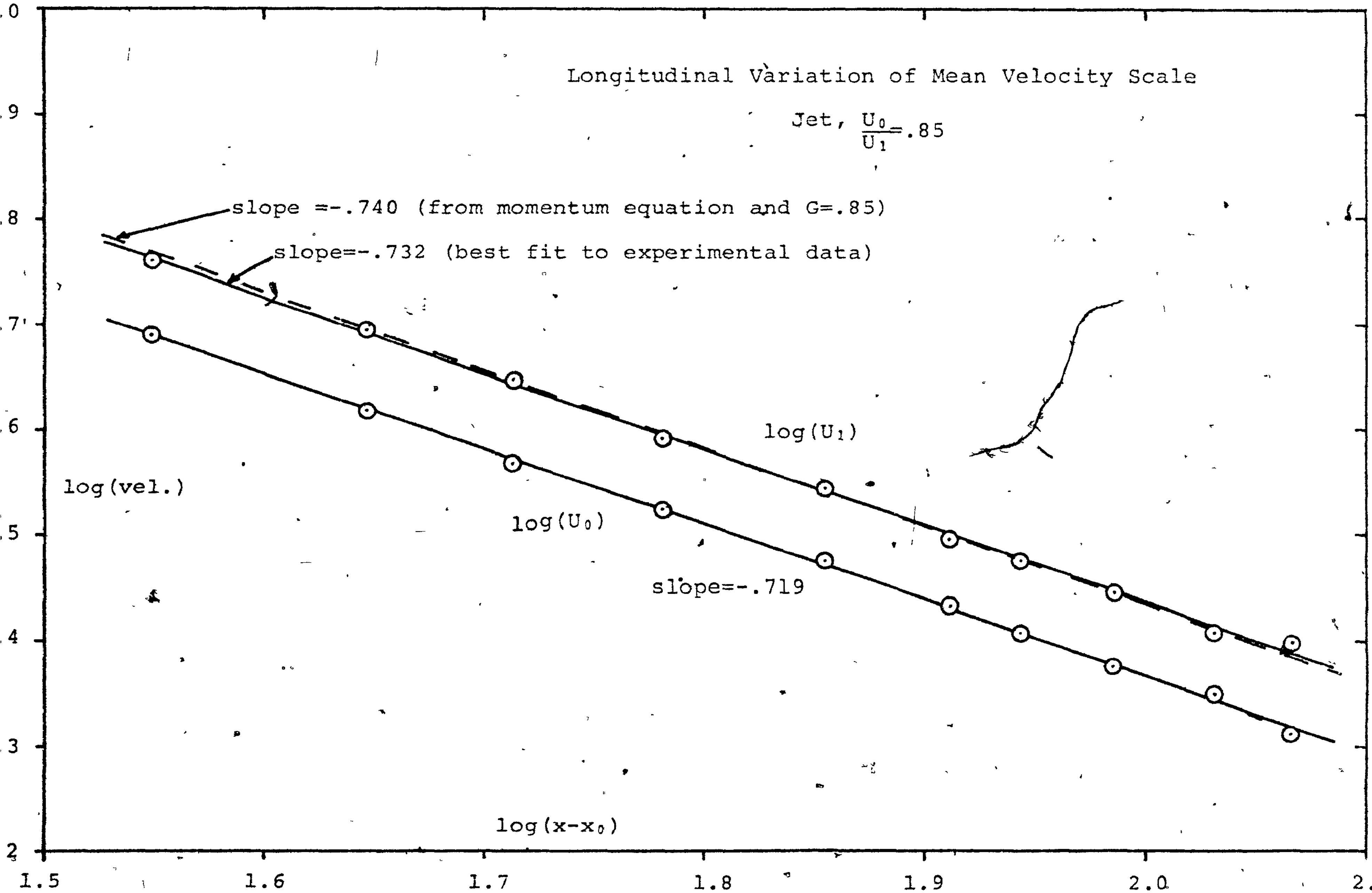

Longitudinal Variation of Mean Velocity Scale
Jet, $\frac{U_0}{U_1}$=.85
slope =-.740 (from momentum equation and G=.85)
slope=-.732 (best fit to experimental data)
log(U_1)
log(vel.)
log(U_0)
slope=-.719
log($x-x_0$)
.0
.9
.8
.7
.6
.5
.4
.3
.2
1.5
1.6
1.7
1.8
1.9
2.0
2.1

Fig. 4-2

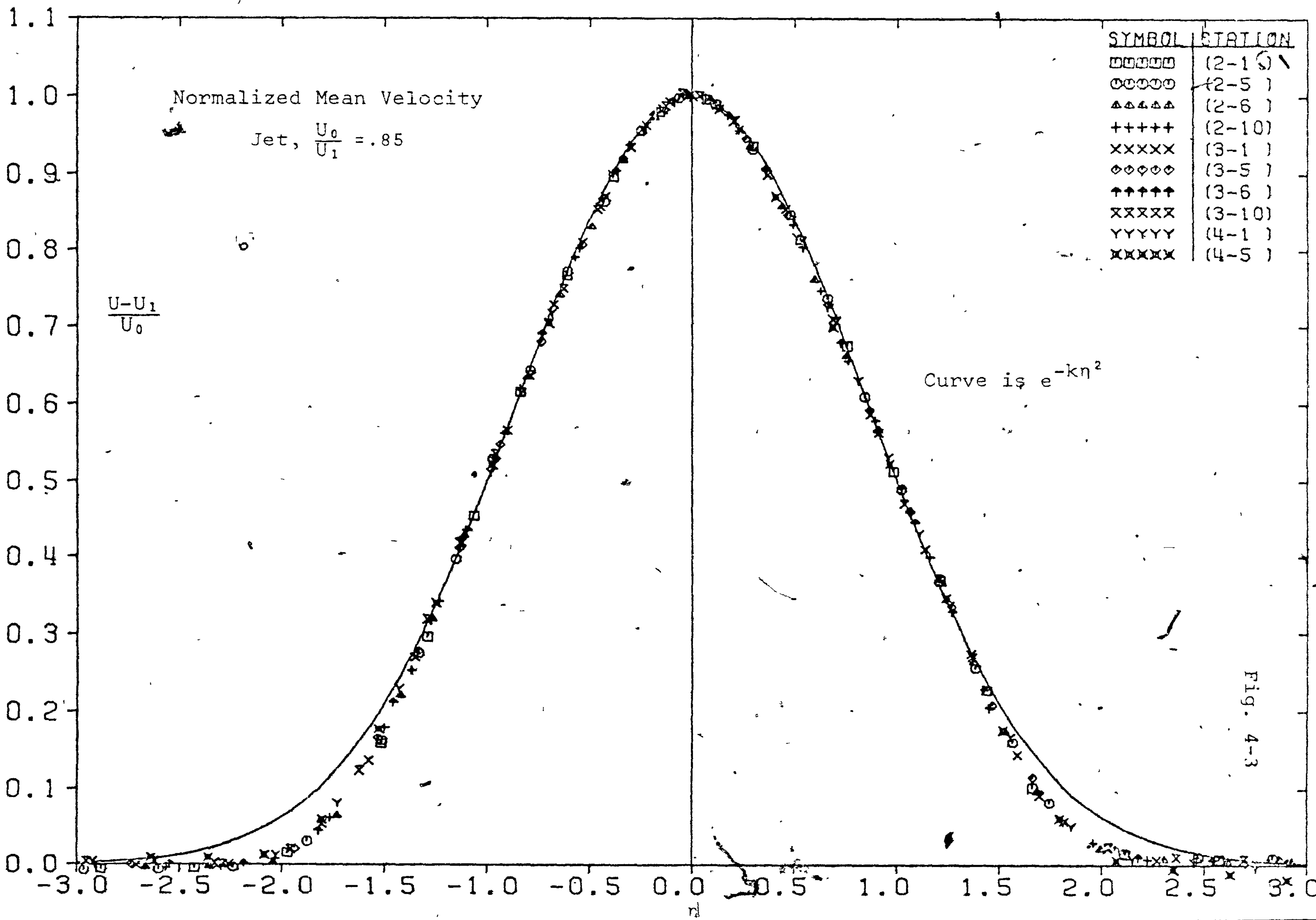

Normalized Mean Velocity
Jet, $\frac{U_0}{U_1}$ = .85
$\frac{U-U_1}{U_0}$
Curve is $e^{-k\eta^2}$
SYMBOL | STATION
(2-1)
(2-5)
(2-6)
(2-10)
(3-1)
(3-5)
(3-6)
(3-10)
(4-1)
(4-5)
η

Fig. 4-3

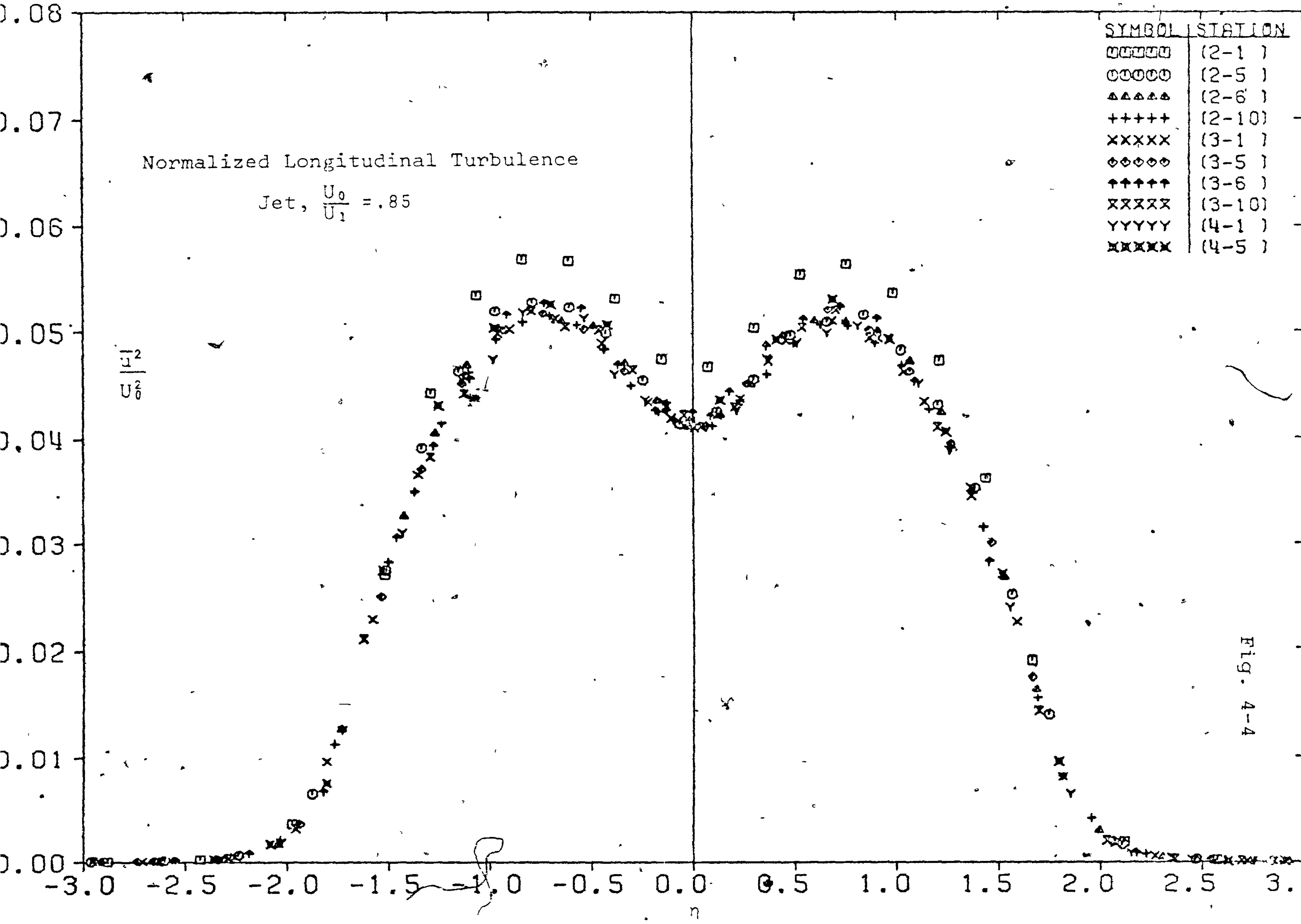

Normalized Longitudinal Turbulence
Jet, $\frac{U_0}{U_1}$ = .85
$\frac{\overline{u^2}}{U_0^2}$
η
SYMBOL | STATION
(2-1)
(2-5)
(2-6)
(2-10)
(3-1)
(3-5)
(3-6)
(3-10)
(4-1)
(4-5)
0.08
0.07
0.06
0.05
0.04
0.03
0.02
0.01
0.00
-3.0
-2.5
-2.0
-1.5
-1.0
-0.5
0.0
0.5
1.0
1.5
2.0
2.5
3.0

Fig. 4-4

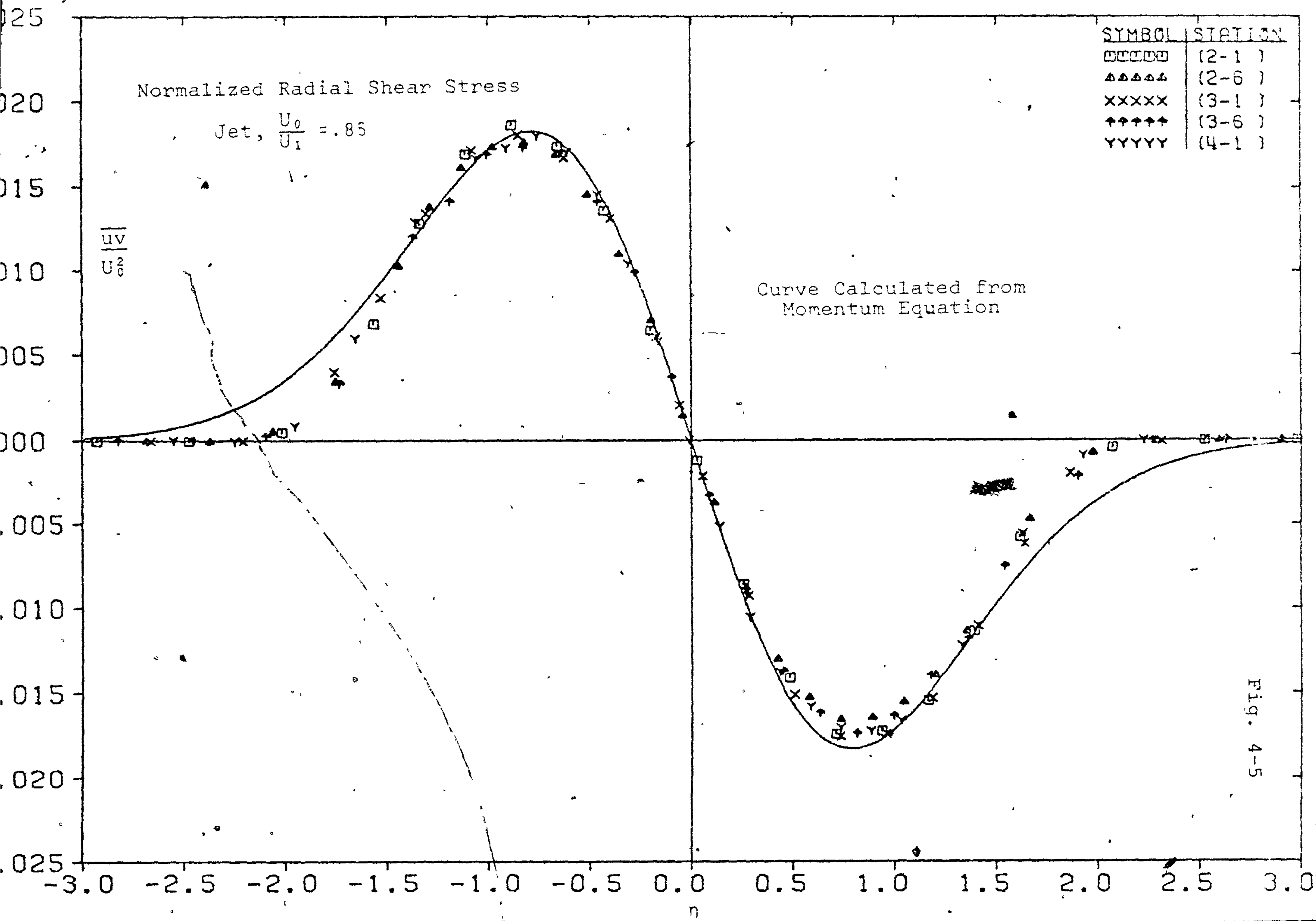

Normalized Radial Shear Stress
Jet, $\frac{U_0}{U_1}$ =.85
$\frac{\overline{uv}}{U_0^2}$
Curve Calculated from Momentum Equation
SYMBOL | STATION
(2-1)
(2-6)
(3-1)
(3-6)
(4-1)
.025
.020
.015
.010
.005
.000
-.005
-.010
-.015
-.020
-.025
-3.0 -2.5 -2.0 -1.5 -1.0 -0.5 0.0 0.5 1.0 1.5 2.0 2.5 3.0
η

Fig. 4-5

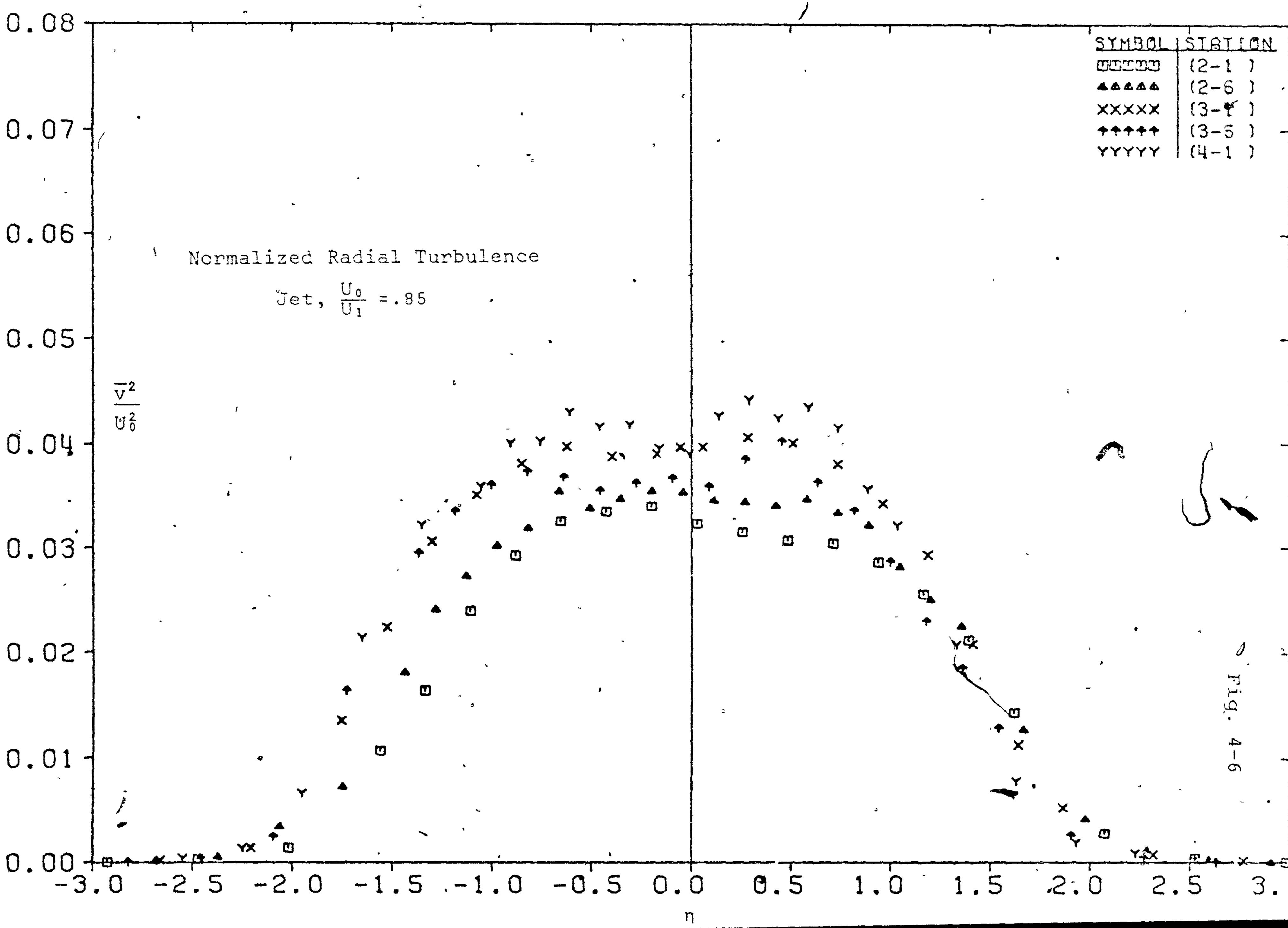

Normalized Radial Turbulence
Jet, $\frac{U_0}{U_1}$ =.85
SYMBOL | STATION
(2-1)
(2-6)
(3-1)
(3-6)
(4-1)
$\frac{\overline{v^2}}{U_0^2}$
0.08
0.07
0.06
0.05
0.04
0.03
0.02
0.01
0.00
-3.0 -2.5 -2.0 -1.5 -1.0 -0.5 0.0 0.5 1.0 1.5 2.0 2.5 3.0
η

Fig. 4-6

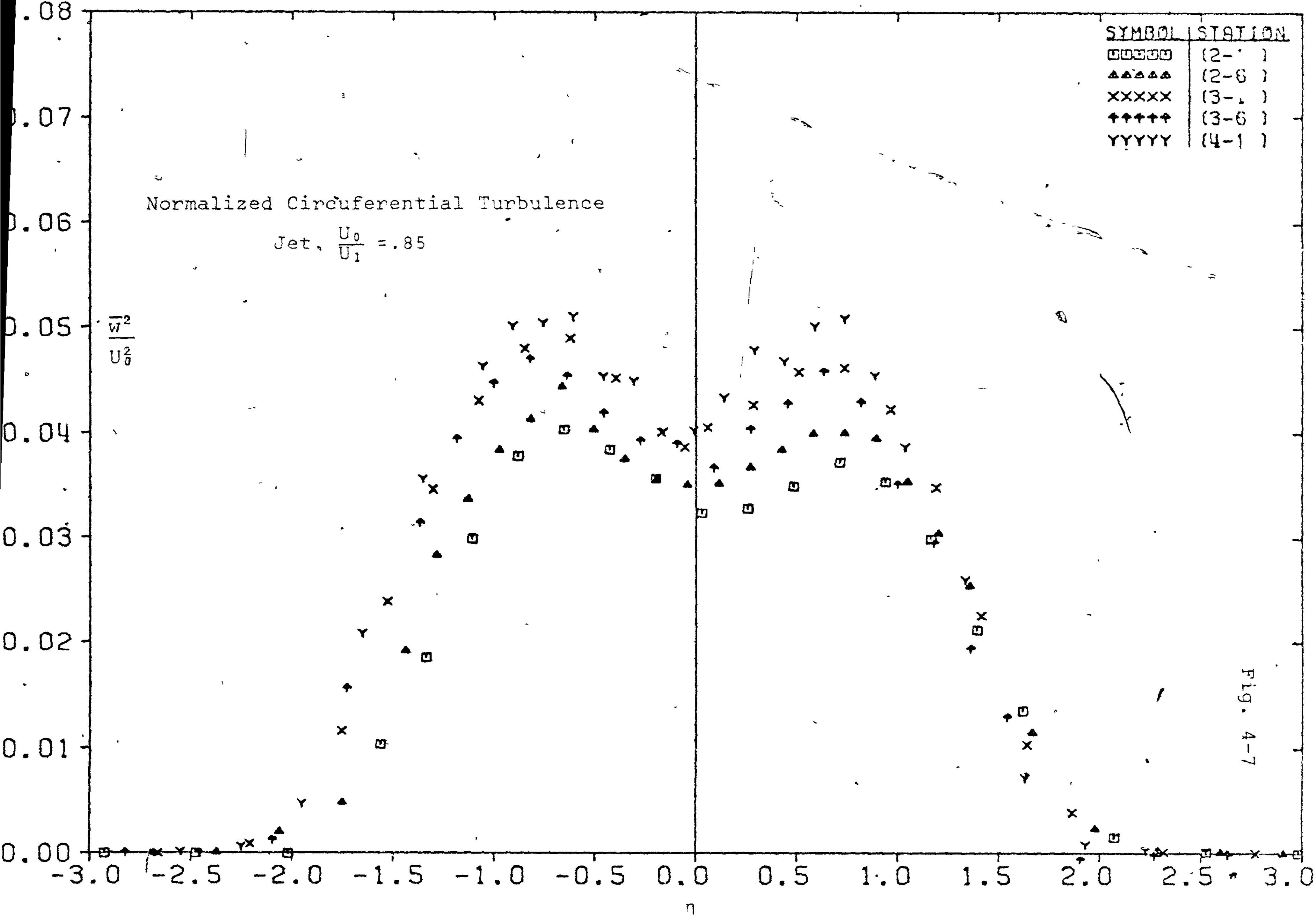

Normalized Circuferential Turbulence
Jet, $\frac{U_0}{U_1}$ =.85
SYMBOL | STATION
(2-')
(2-6)
(3-1)
(3-6)
(4-1)
$\frac{\overline{w^2}}{U_0^2}$
.08
0.07
0.06
0.05
0.04
0.03
0.02
0.01
0.00
-3.0 -2.5 -2.0 -1.5 -1.0 -0.5 0.0 0.5 1.0 1.5 2.0 2.5 3.0
η

Fig. 4-7

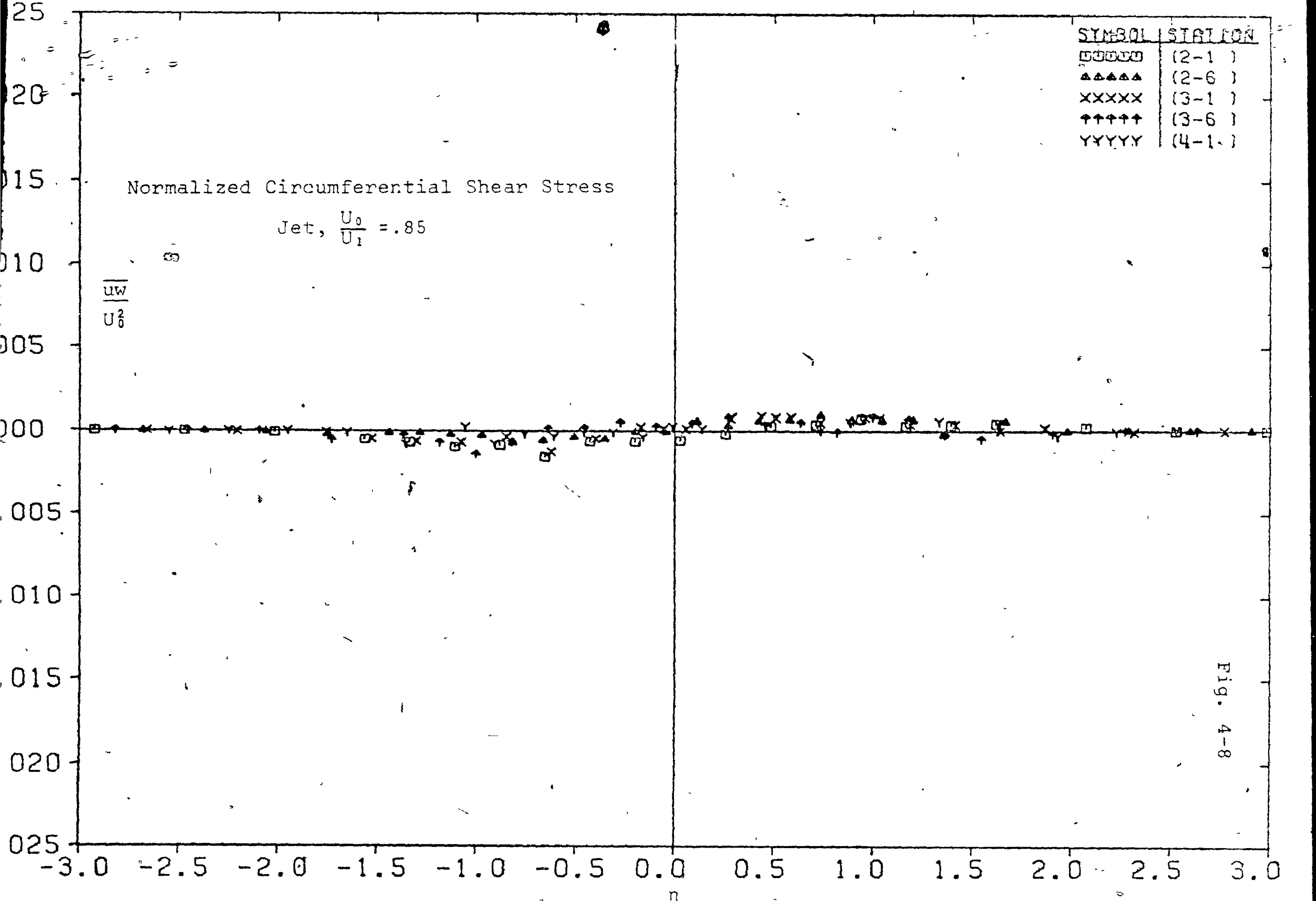
Normalized Circumferential Shear Stress
Jet, $\frac{U_0}{U_1}$ = .85
$\frac{\overline{uw}}{U_0^2}$
SYMBOL | STATION
(2-1)
(2-6)
(3-1)
(3-6)
(4-1)
η
Fig. 4-8

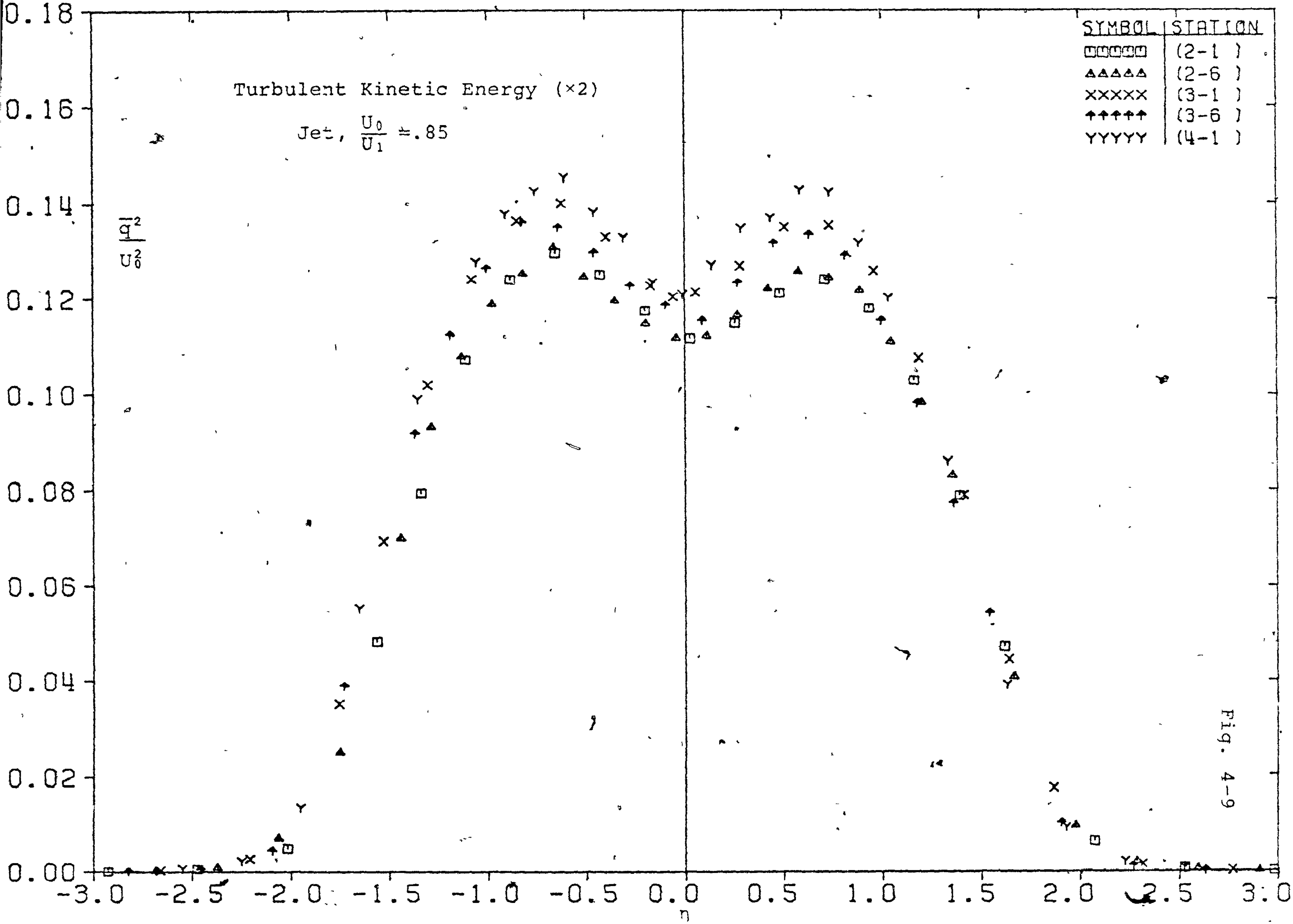
Turbulent Kinetic Energy (×2)
Jet, $\frac{U_0}{U_1} \doteq .85$
$\frac{\overline{q^2}}{U_0^2}$
SYMBOL | STATION
□□□□□ (2-1)
△△△△△ (2-6)
XXXXX (3-1)
↑↑↑↑↑ (3-6)
YYYYY (4-1)
0.18
0.16
0.14
0.12
0.10
0.08
0.06
0.04
0.02
0.00
-3.0 -2.5 -2.0 -1.5 -1.0 -0.5 0.0 0.5 1.0 1.5 2.0 2.5 3.0
η
Fig. 4-9

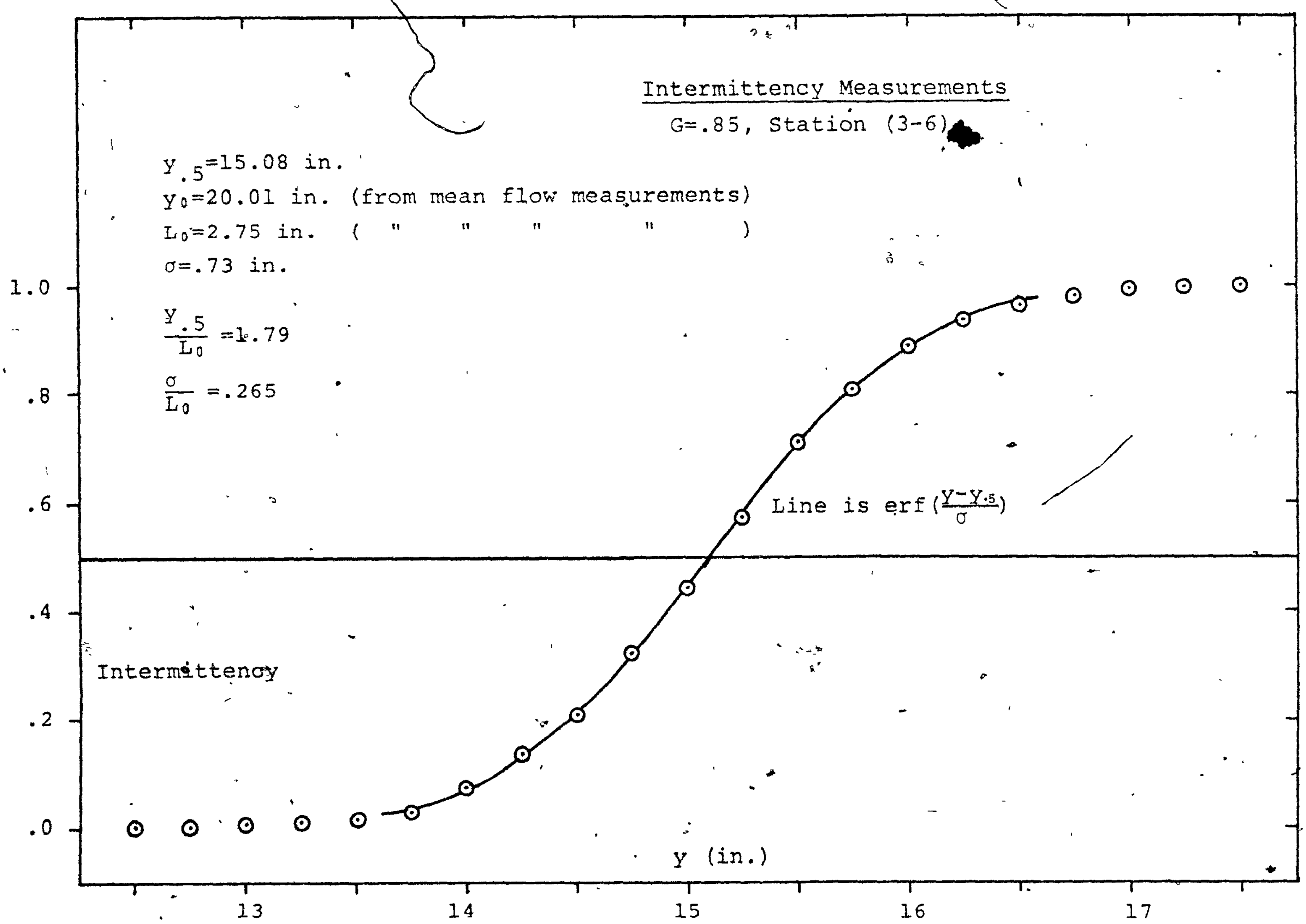
Intermittency Measurements
G=.85, Station (3-6)
y.5=15.08 in.
y0=20.01 in. (from mean flow measurements)
L0=2.75 in. (" " " ")
σ=.73 in.
y.5/L0 =1.79
σ/L0 =.265
Line is erf((y-y.5)/σ)
Intermittency
y (in.)
1.0
.8
.6
.4
.2
.0
13
14
15
16
17

Fig. 4-10

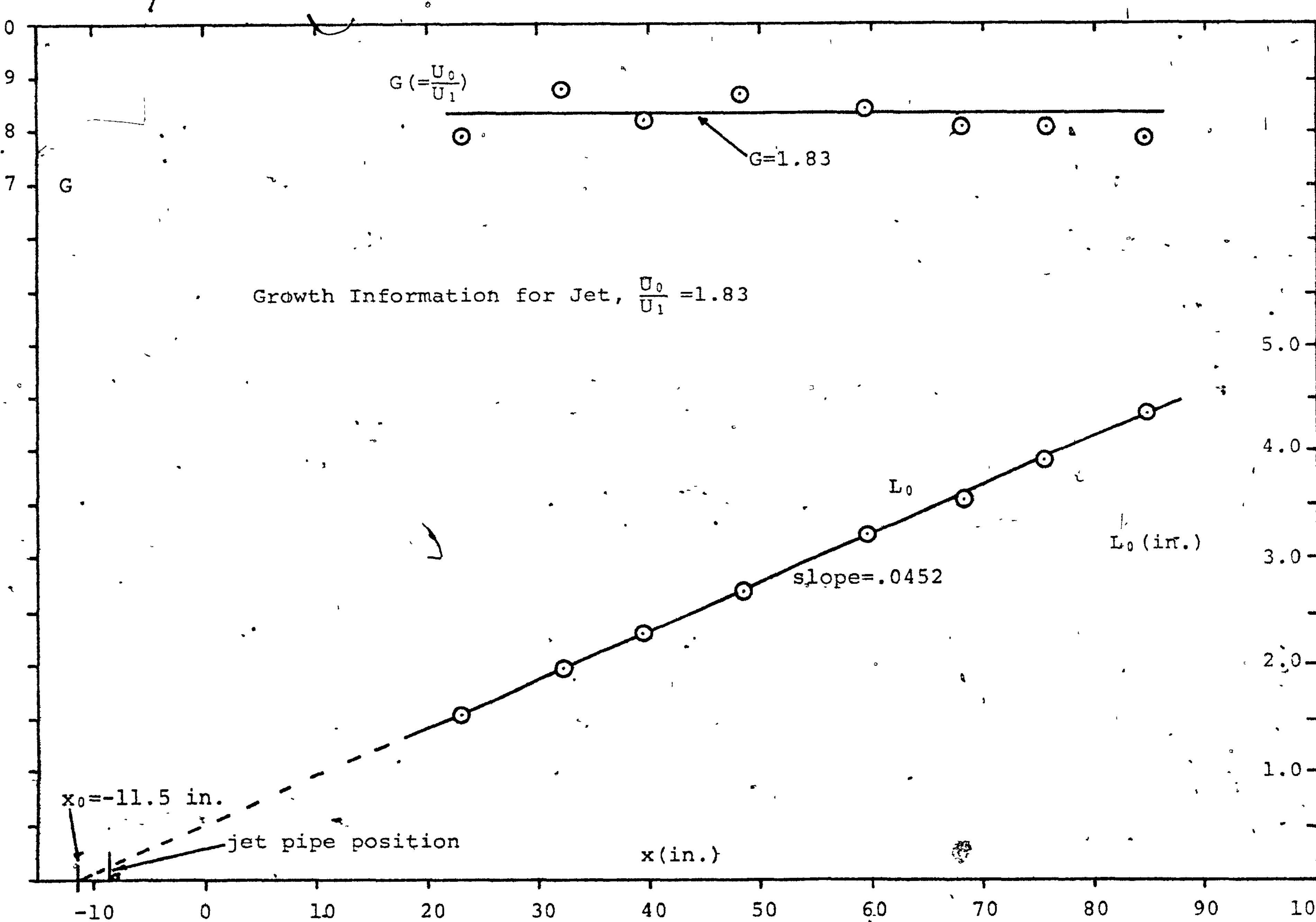

Growth Information for Jet, $\frac{U_0}{U_1}$ =1.83
$G(=\frac{U_0}{U_1})$
G=1.83
G
0
9
8
7
L_0
slope=.0452
L_0 (in.)
5.0
4.0
3.0
2.0
1.0
x_0=-11.5 in.
jet pipe position
x(in.)
-10
0
10
20
30
40
50
60
70
80
90
100

Fig. 4-11

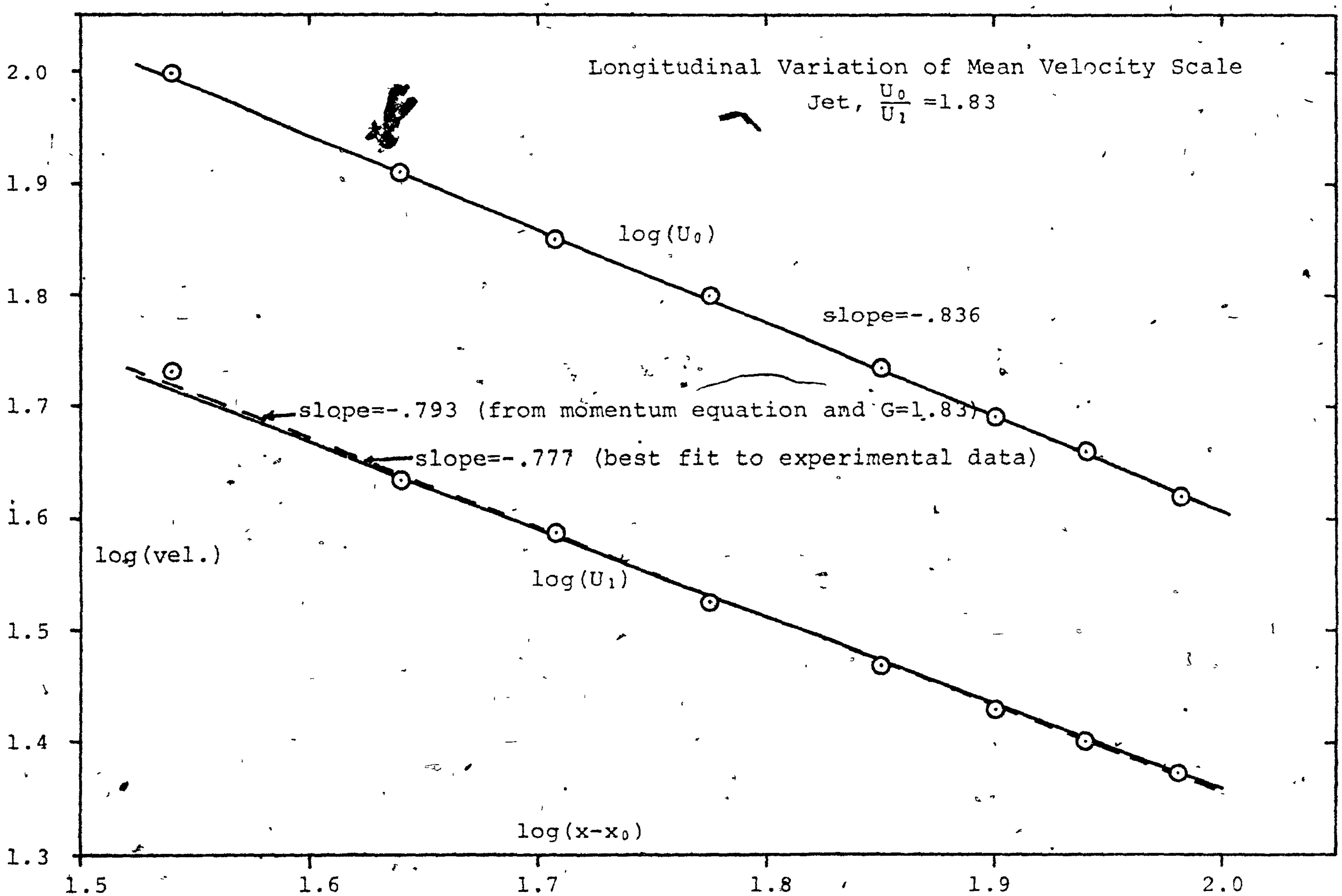

Longitudinal Variation of Mean Velocity Scale
Jet, $\frac{U_0}{U_1}$ =1.83
log(U_0)
slope=-.836
slope=-.793 (from momentum equation and G=1.83)
slope=-.777 (best fit to experimental data)
log(vel.)
log(U_1)
log($x-x_0$)
2.0
1.9
1.8
1.7
1.6
1.5
1.4
1.3
1.5
1.6
1.7
1.8
1.9
2.0

Fig. 4-12

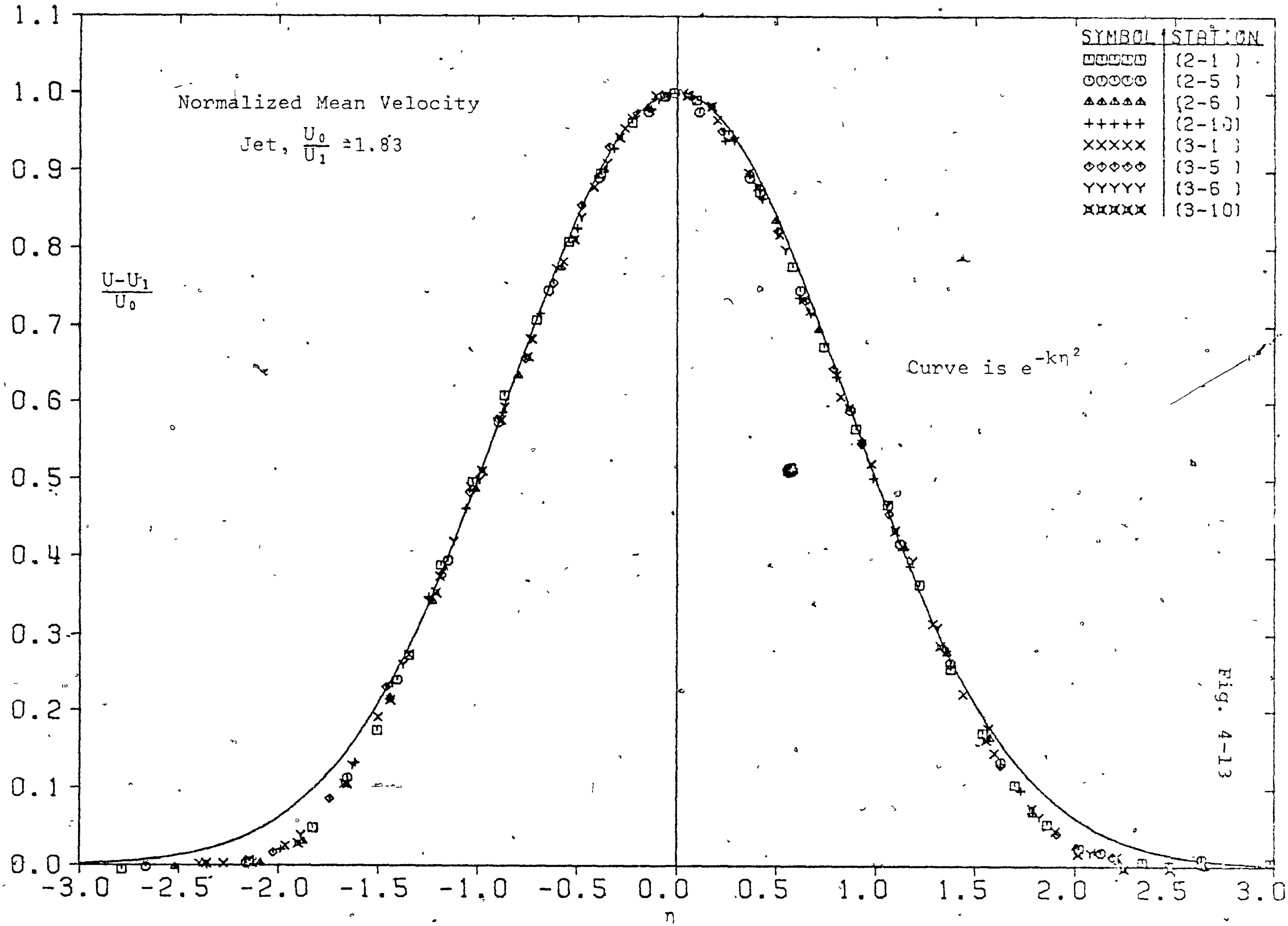
Normalized Mean Velocity
Jet, $\frac{U_0}{U_1} \doteq 1.83$
$\frac{U-U_1}{U_0}$
Curve is $e^{-k\eta^2}$
SYMBOL | STATION
(2-1)
(2-5)
(2-6)
(2-10)
(3-1)
(3-5)
(3-6)
(3-10)
η

Fig. 4-13

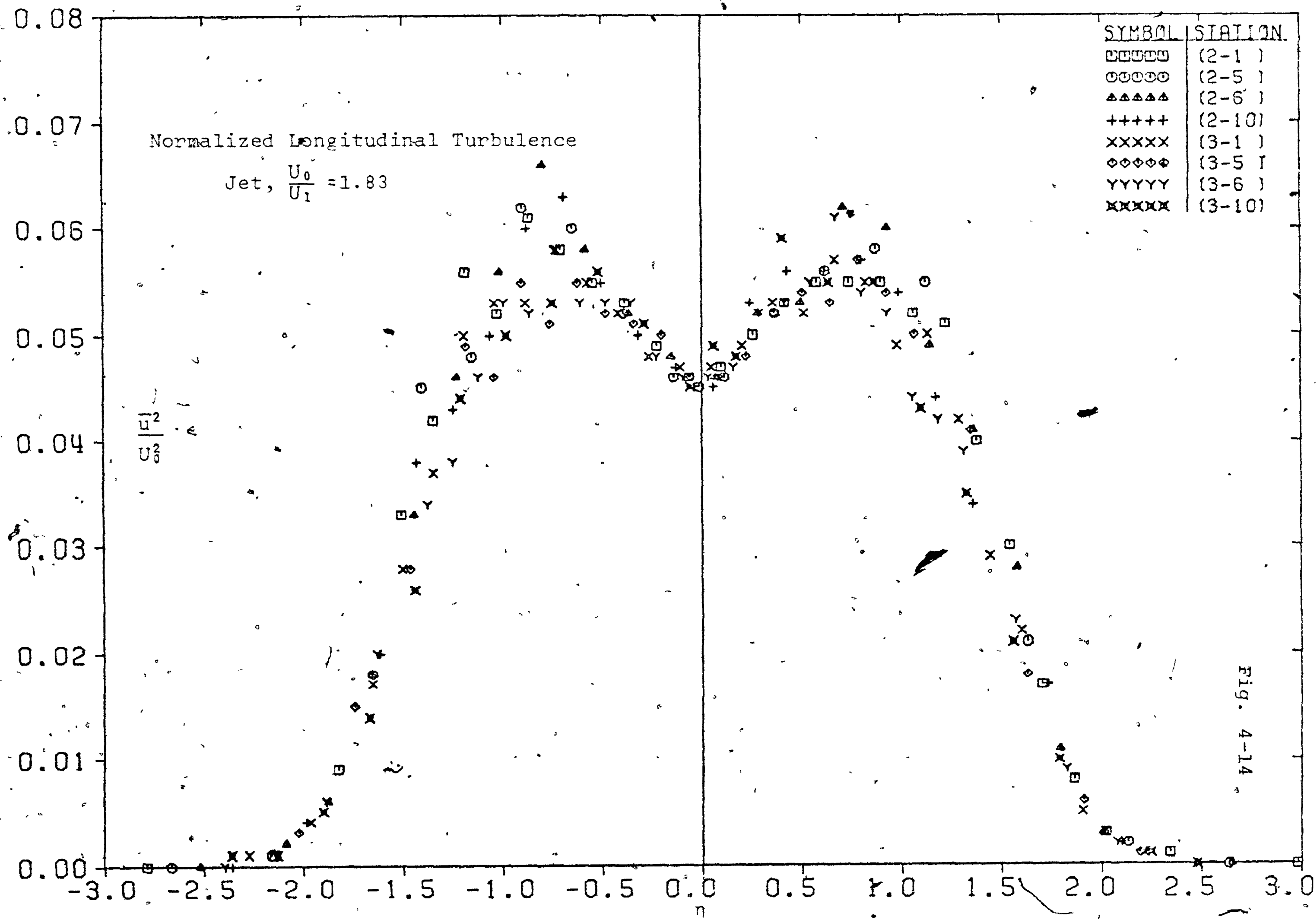

Normalized Longitudinal Turbulence
Jet, $\frac{U_0}{U_1}$ =1.83
SYMBOL | STATION
(2-1)
(2-5)
(2-6)
(2-10)
(3-1)
(3-5)
(3-6)
(3-10)
$\frac{\overline{u^2}}{U_0^2}$
η
0.00
0.01
0.02
0.03
0.04
0.05
0.06
0.07
0.08
-3.0 -2.5 -2.0 -1.5 -1.0 -0.5 0.0 0.5 1.0 1.5 2.0 2.5 3.0

Fig. 4-14

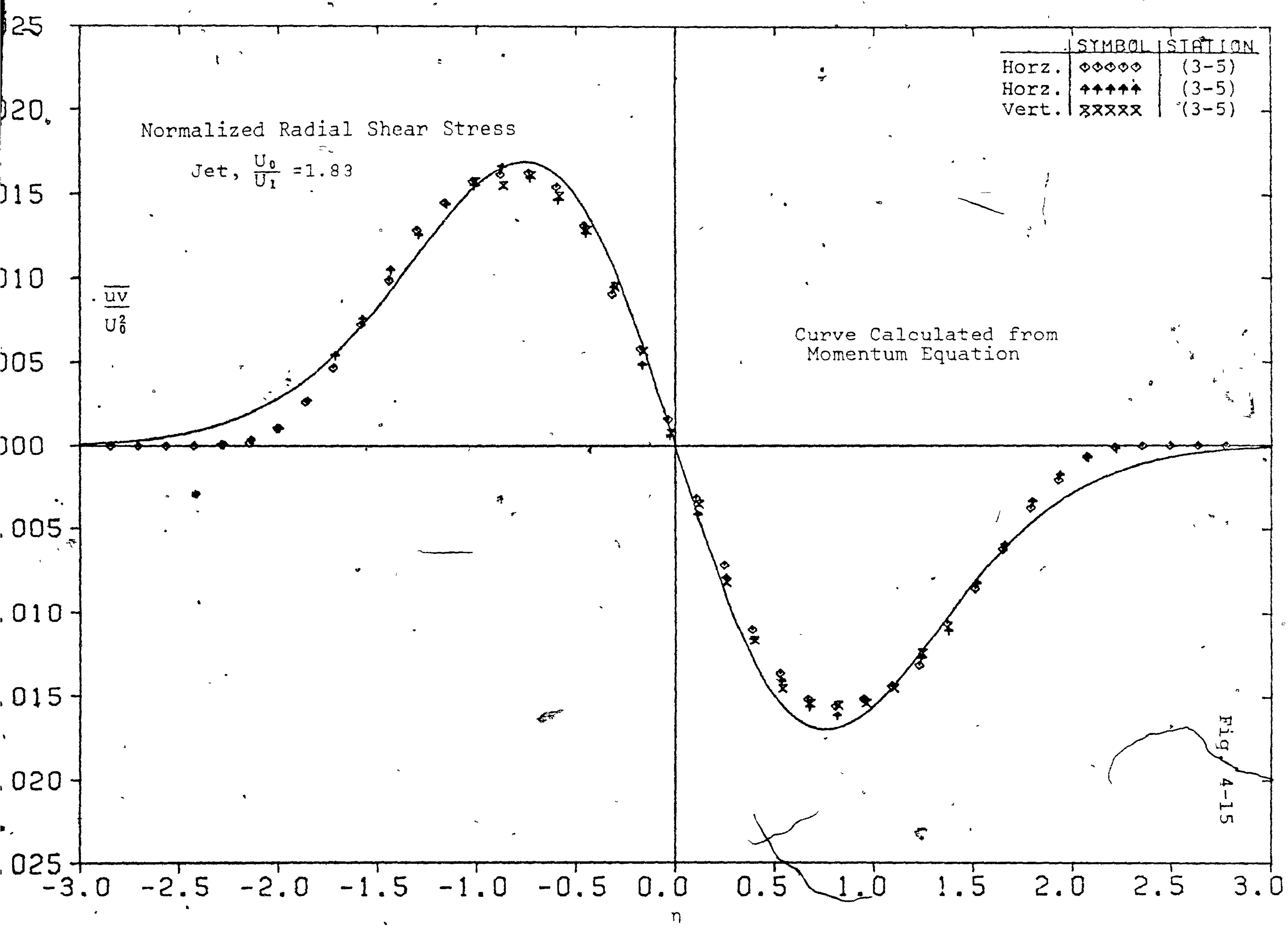

Normalized Radial Shear Stress
Jet, $\frac{U_0}{U_1}$ =1.83
SYMBOL | STATION
Horz. ◇◇◇◇◇ (3-5)
Horz. ✦✦✦✦✦ (3-5)
Vert. XXXXX (3-5)
$\frac{\overline{uv}}{U_0^2}$
Curve Calculated from Momentum Equation
.025 .020 .015 .010 .005 .000 -.005 -.010 -.015 -.020 -.025
-3.0 -2.5 -2.0 -1.5 -1.0 -0.5 0.0 0.5 1.0 1.5 2.0 2.5 3.0
η

Fig. 4-15

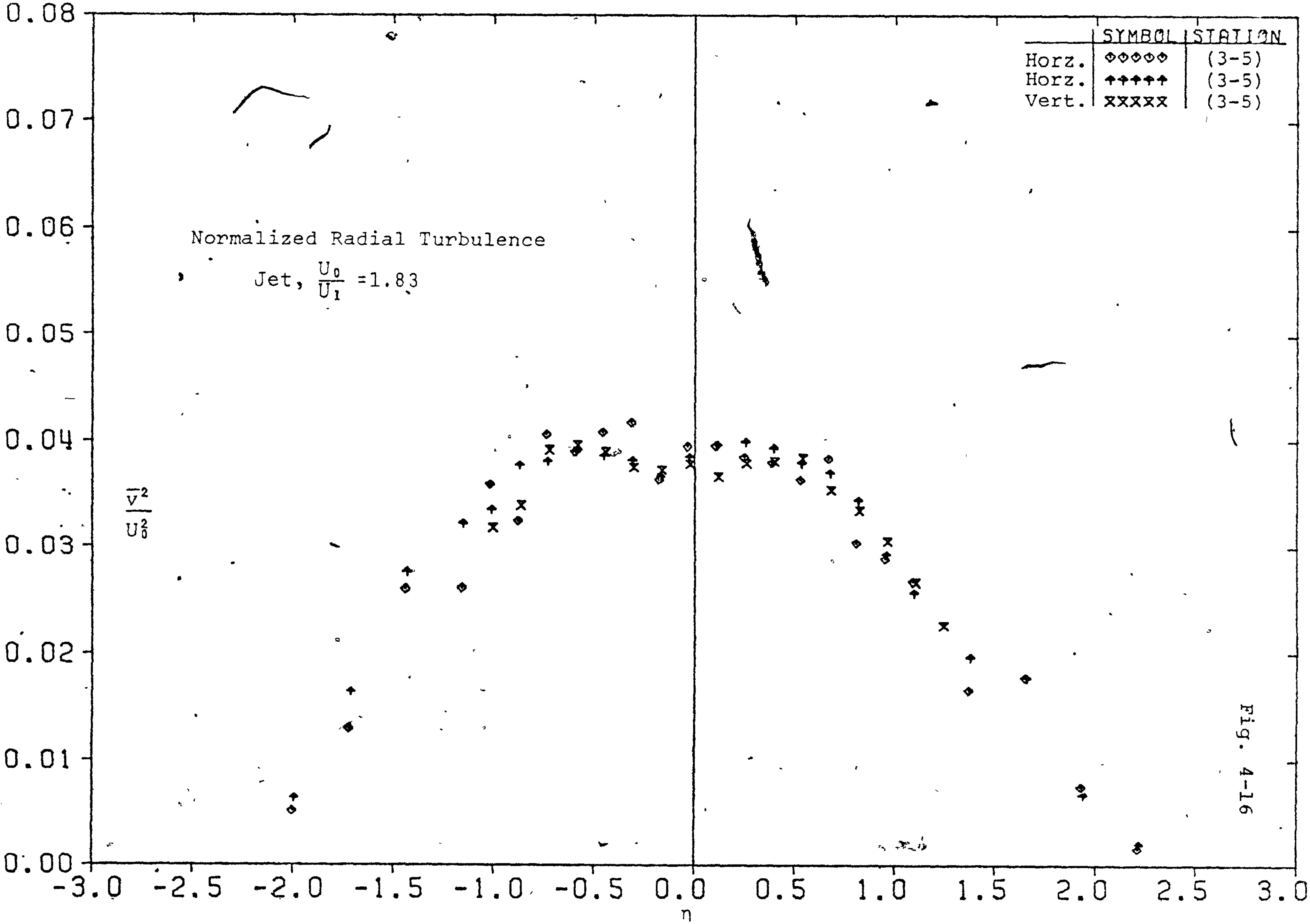
Normalized Radial Turbulence
Jet, $\frac{U_0}{U_1}$ =1.83
SYMBOL STATION
Horz. ◇◇◇◇◇ (3-5)
Horz. +++++ (3-5)
Vert. XXXXX (3-5)
$\frac{\overline{v^2}}{U_0^2}$
η
0.08
0.07
0.06
0.05
0.04
0.03
0.02
0.01
0.00
-3.0 -2.5 -2.0 -1.5 -1.0 -0.5 0.0 0.5 1.0 1.5 2.0 2.5 3.0

Fig. 4-16

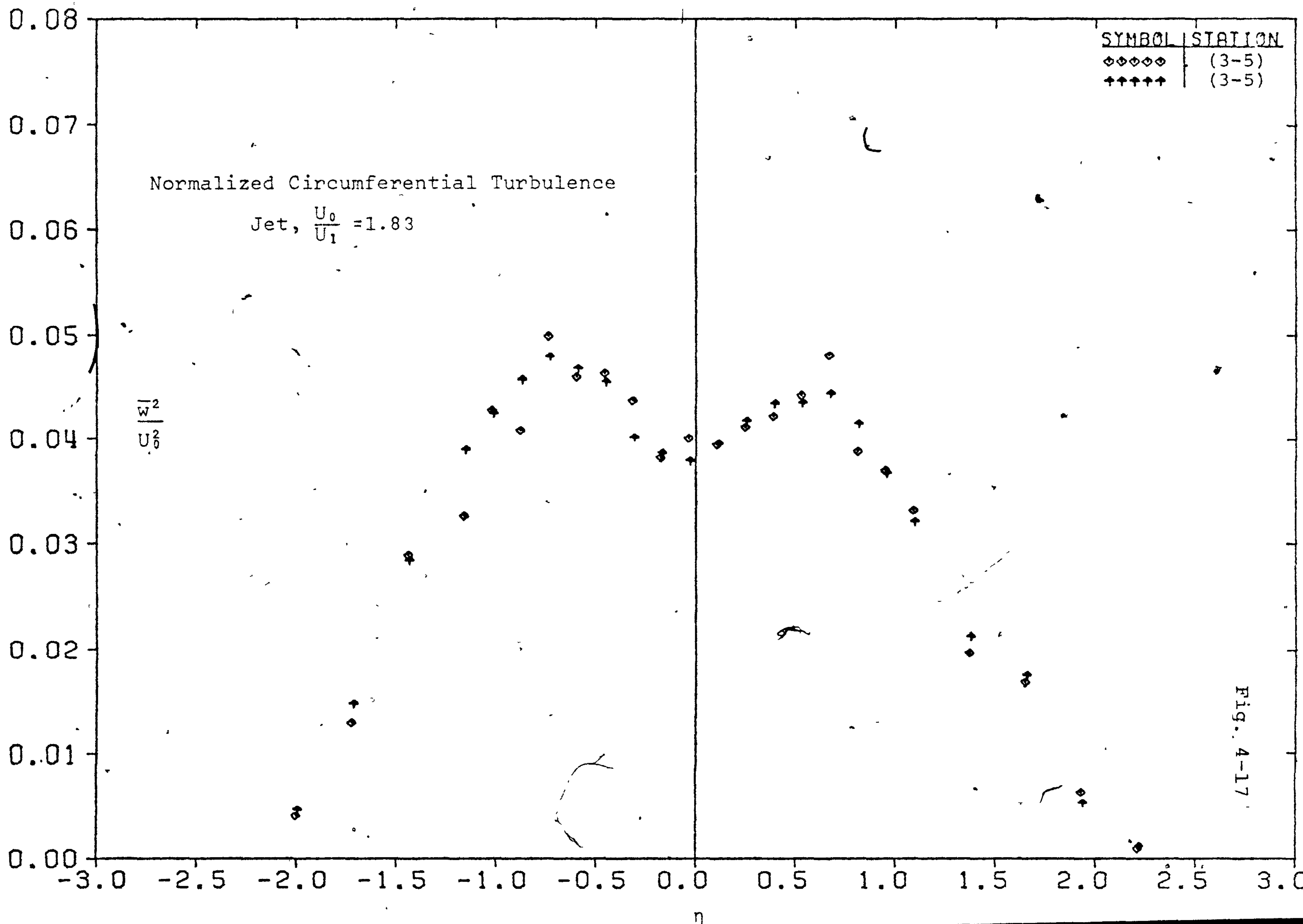

Normalized Circumferential Turbulence
Jet, $\frac{U_0}{U_1}$ =1.83
SYMBOL | STATION
◇◇◇◇◇ | (3-5)
+++++ | (3-5)
$\frac{\overline{w^2}}{U_0^2}$
0.08
0.07
0.06
0.05
0.04
0.03
0.02
0.01
0.00
-3.0 -2.5 -2.0 -1.5 -1.0 -0.5 0.0 0.5 1.0 1.5 2.0 2.5 3.0
η

Fig. 4-17

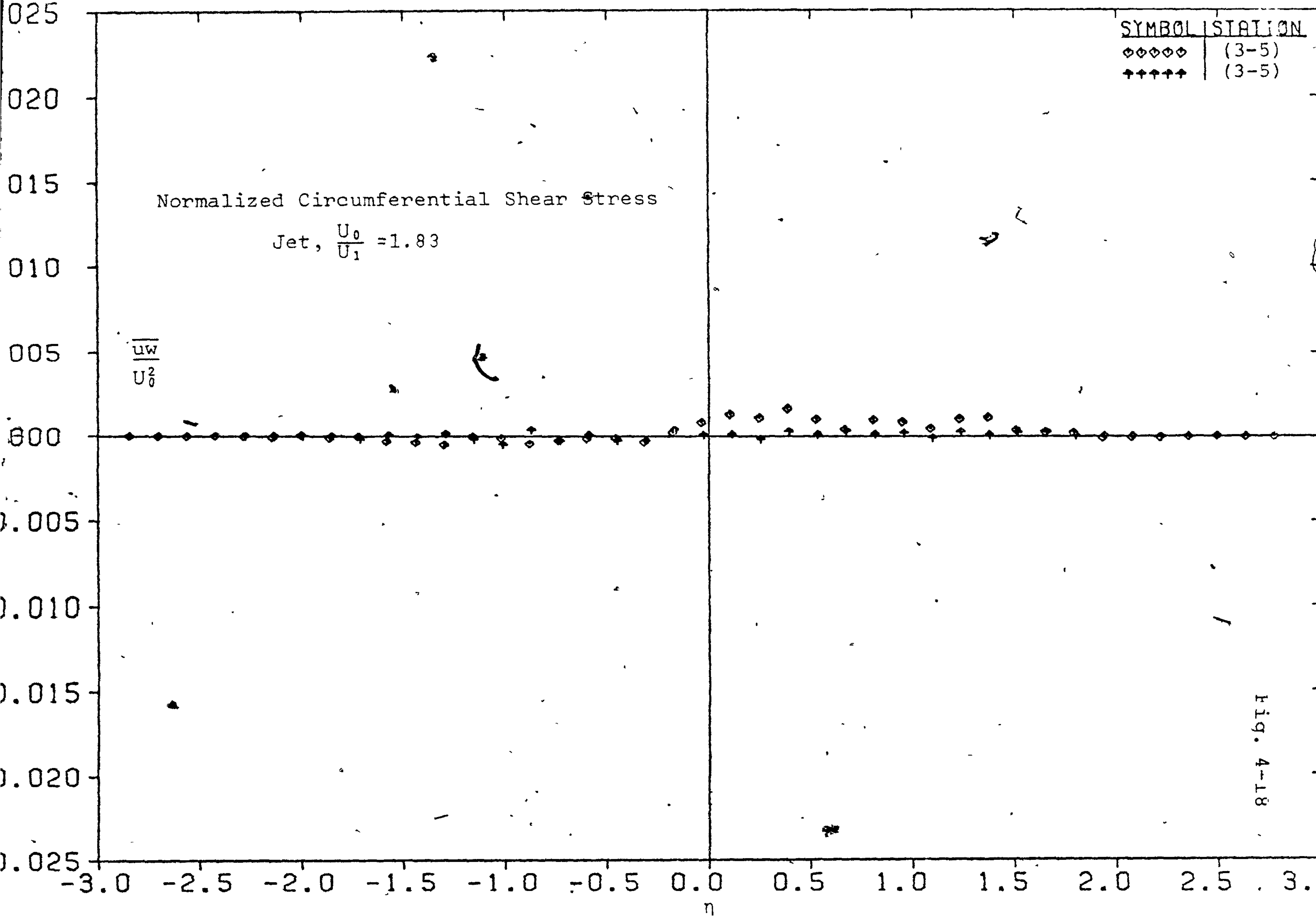

Normalized Circumferential Shear Stress
Jet, $\frac{U_0}{U_1}$ =1.83
SYMBOL | STATION
◇◇◇◇◇ (3-5)
+++++ (3-5)
$\frac{\overline{uw}}{U_0^2}$
.025
.020
.015
.010
.005
.000
-.005
-.010
-.015
-.020
-.025
-3.0 -2.5 -2.0 -1.5 -1.0 -0.5 0.0 0.5 1.0 1.5 2.0 2.5 3.0
η

Fig. 4-18

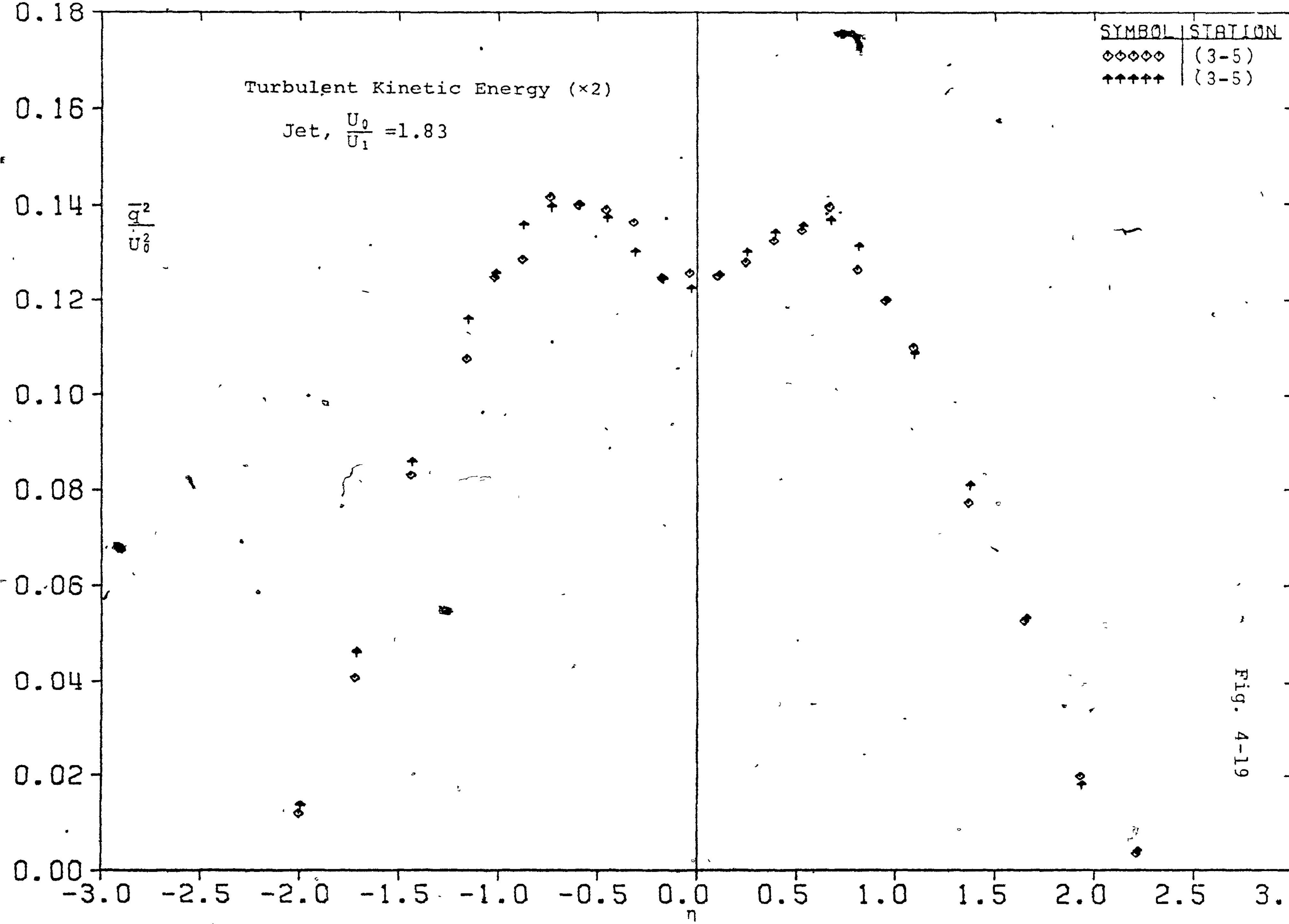

Turbulent Kinetic Energy (×2)
Jet, $\frac{U_0}{U_1}$ =1.83
SYMBOL STATION
◇◇◇◇◇ (3-5)
✦✦✦✦✦ (3-5)
$\frac{\overline{q^2}}{U_0^2}$
0.18
0.16
0.14
0.12
0.10
0.08
0.06
0.04
0.02
0.00
-3.0 -2.5 -2.0 -1.5 -1.0 -0.5 0.0 0.5 1.0 1.5 2.0 2.5 3.0
η

Fig. 4-19

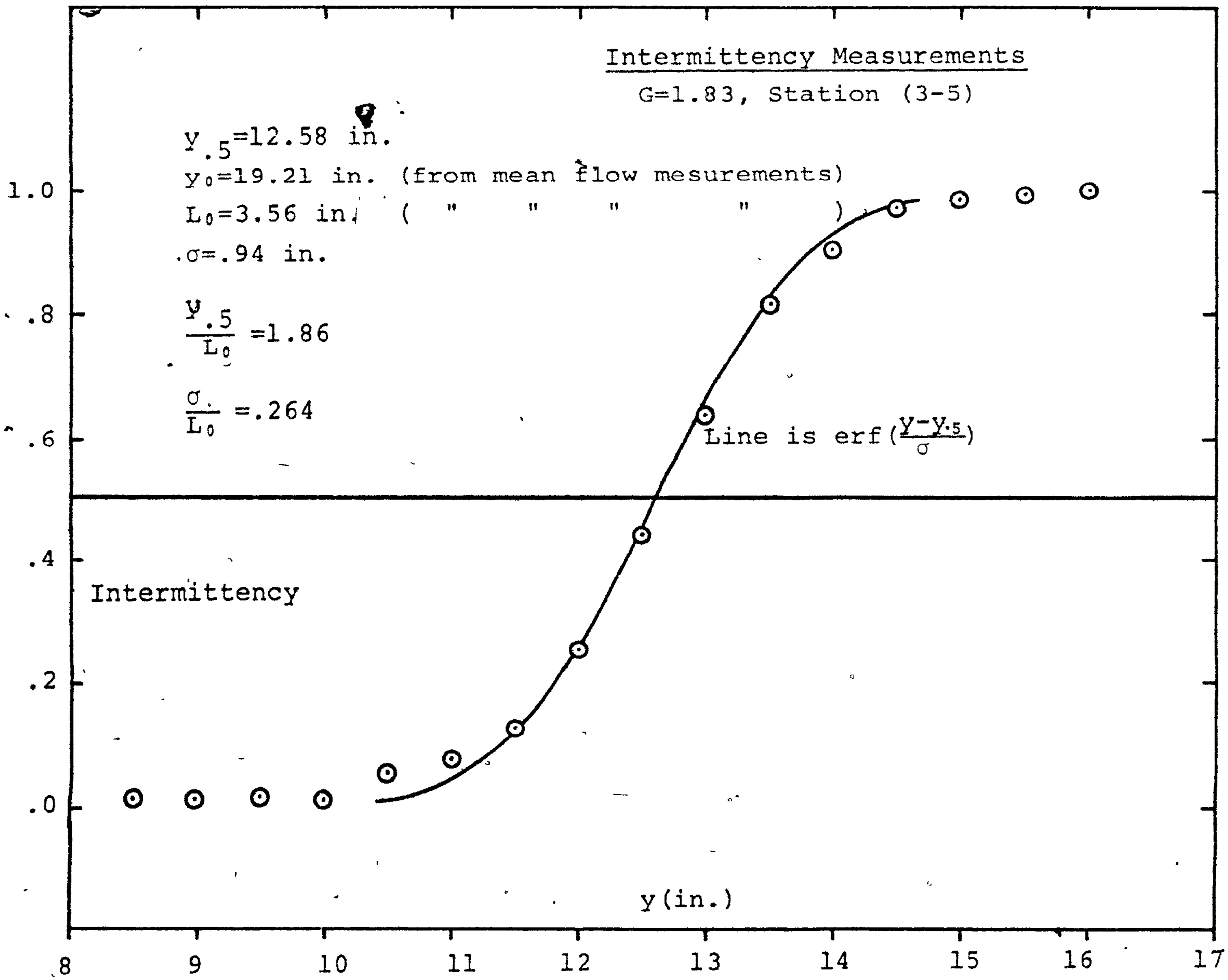
Intermittency Measurements
G=1.83, Station (3-5)
y.5=12.58 in.
y0=19.21 in. (from mean flow mesurements)
L0=3.56 in. (" " " ")
σ=.94 in.
y.5/L0 =1.86
σ/L0 =.264
Line is erf((y-y.5)/σ)
Intermittency
y(in.)
1.0
.8
.6
.4
.2
.0
8
9
10
11
12
13
14
15
16
17

Fig. 4-20

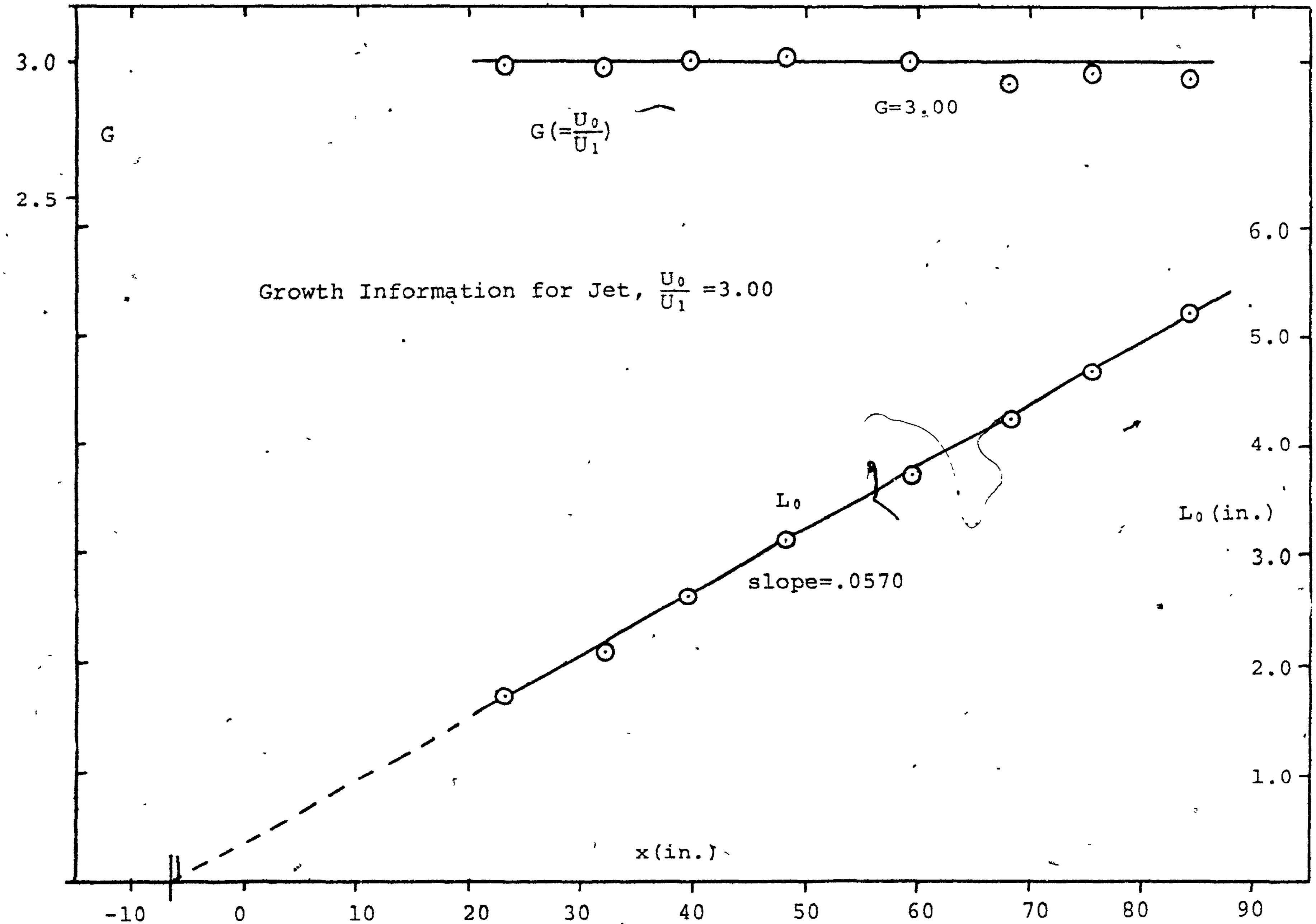

3.0
2.5
G
$G(=\frac{U_0}{U_1})$
G=3.00
Growth Information for Jet, $\frac{U_0}{U_1}$ =3.00
6.0
5.0
4.0
3.0
2.0
1.0
L_0
L_0 (in.)
slope=.0570
x(in.)
-10
0
10
20
30
40
50
60
70
80
90

Fig. 4-21

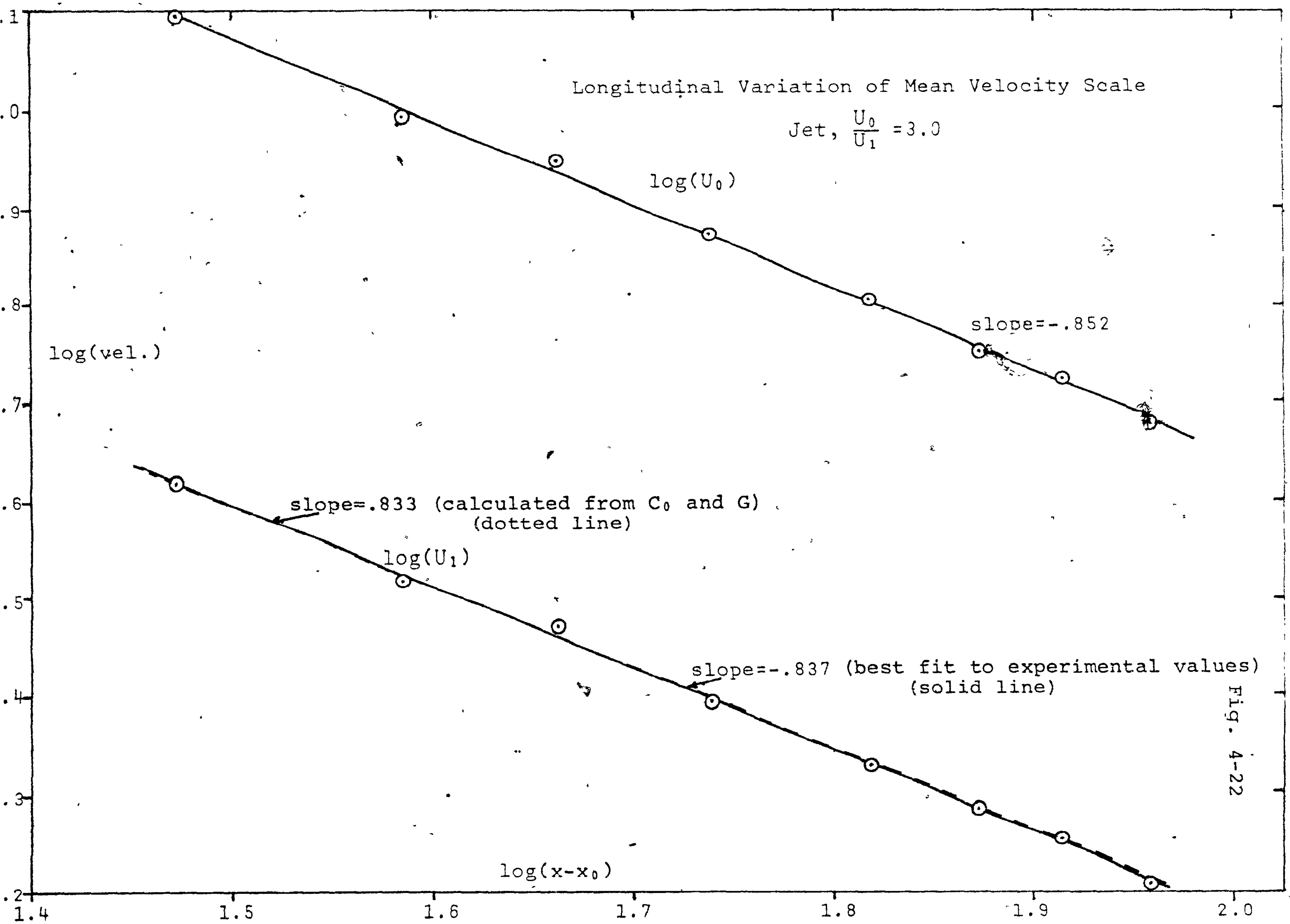
Longitudinal Variation of Mean Velocity Scale
Jet, $\frac{U_0}{U_1}$ =3.0
log(U_0)
slope=-.852
log(vel.)
slope=.833 (calculated from C_0 and G)
(dotted line)
log(U_1)
slope=-.837 (best fit to experimental values)
(solid line)
log($x-x_0$)
.1
.0
.9
.8
.7
.6
.5
.4
.3
.2
1.4
1.5
1.6
1.7
1.8
1.9
2.0

Fig. 4-22

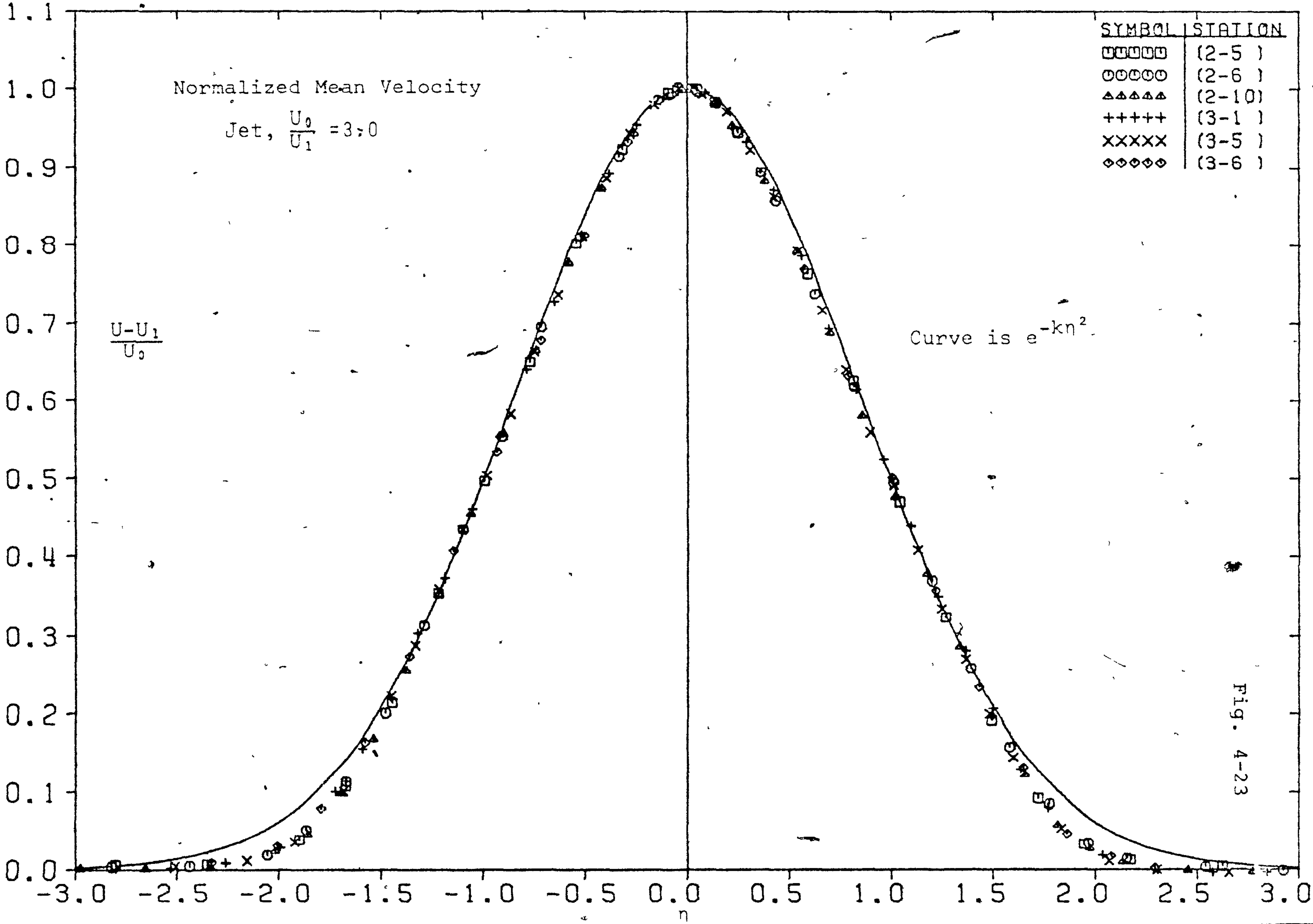
Normalized Mean Velocity
Jet, $\frac{U_0}{U_1}$ = 3.0
$\frac{U-U_1}{U_0}$
SYMBOL | STATION
(2-5)
(2-6)
(2-10)
(3-1)
(3-5)
(3-6)
Curve is $e^{-k\eta^2}$
η
1.1
1.0
0.9
0.8
0.7
0.6
0.5
0.4
0.3
0.2
0.1
0.0
-3.0 -2.5 -2.0 -1.5 -1.0 -0.5 0.0 0.5 1.0 1.5 2.0 2.5 3.0

Fig. 4-23

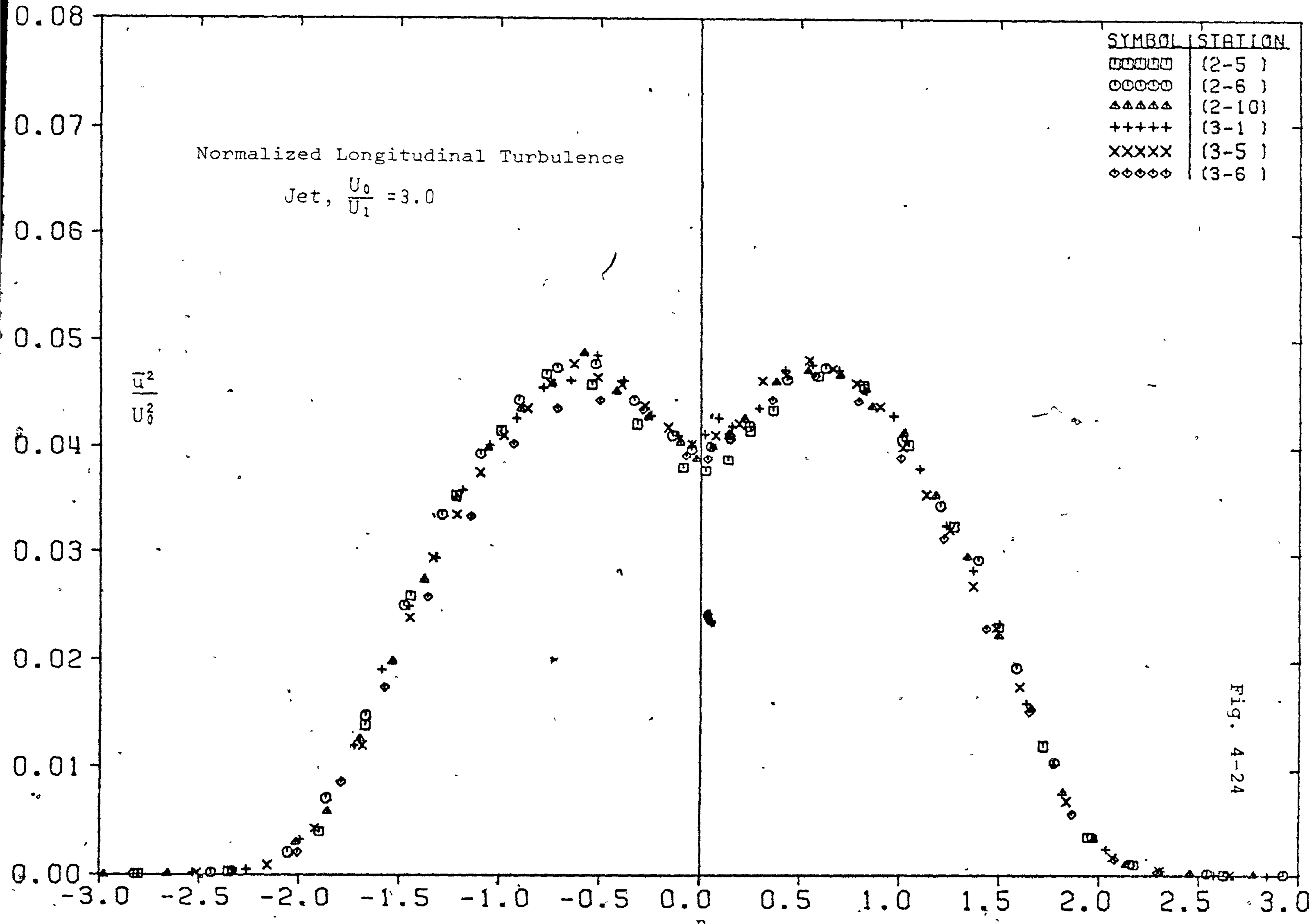
0.08
0.07
0.06
0.05
0.04
0.03
0.02
0.01
0.00
-3.0
-2.5
-2.0
-1.5
-1.0
-0.5
0.0
0.5
1.0
1.5
2.0
2.5
3.0
η
SYMBOL STATION
(2-5)
(2-6)
(2-10)
(3-1)
(3-5)
(3-6)
Normalized Longitudinal Turbulence
Jet, $\frac{U_0}{U_1}$ =3.0
$\frac{\overline{u^2}}{U_0^2}$

Fig. 4-24

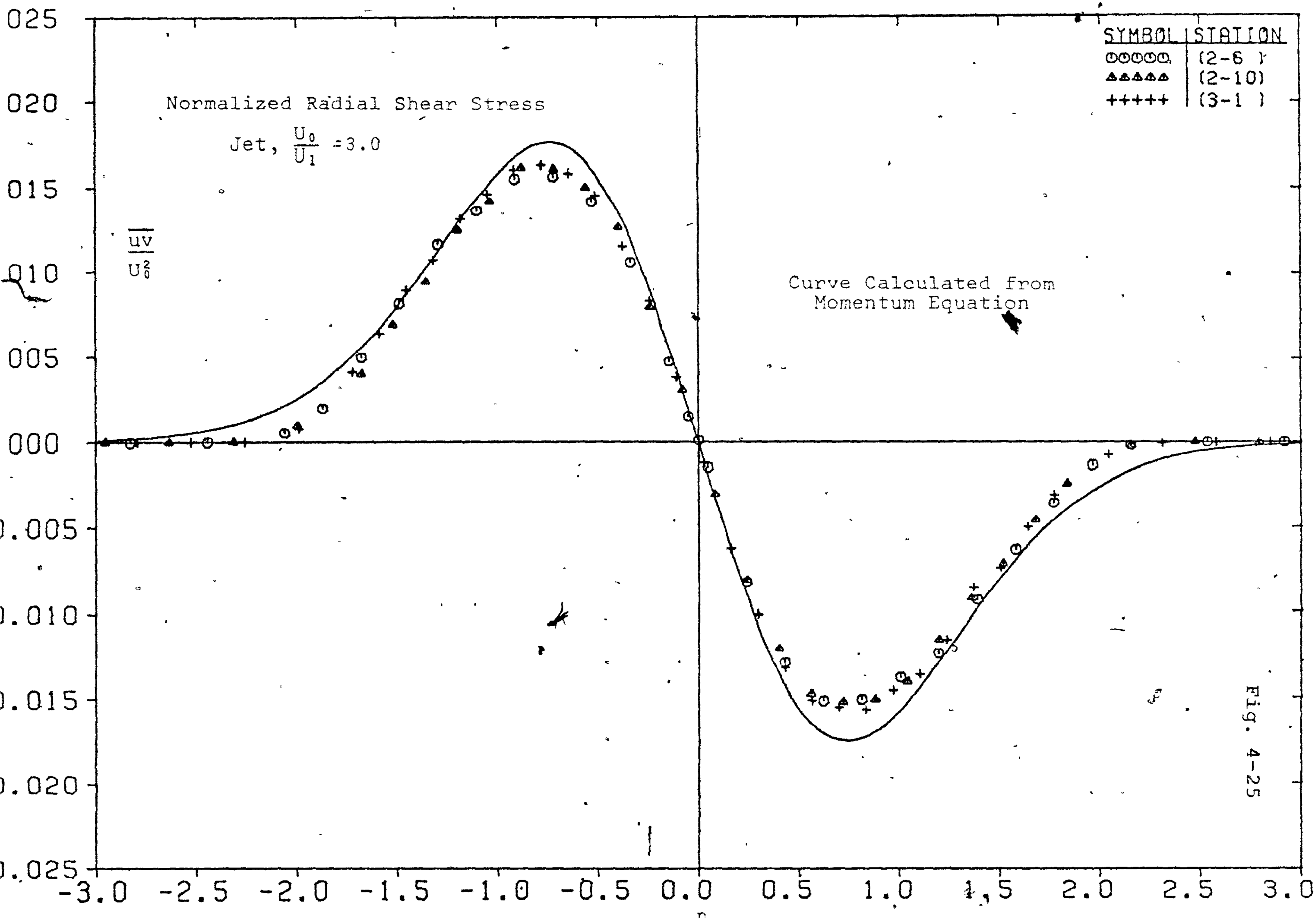

Normalized Radial Shear Stress
Jet, $\frac{U_0}{U_1}$ =3.0
$\frac{\overline{uv}}{U_0^2}$
SYMBOL | STATION
(2-6)
(2-10)
(3-1)
Curve Calculated from Momentum Equation
025
020
015
010
005
000
.005
.010
.015
.020
.025
-3.0 -2.5 -2.0 -1.5 -1.0 -0.5 0.0 0.5 1.0 1.5 2.0 2.5 3.0

Fig. 4-25

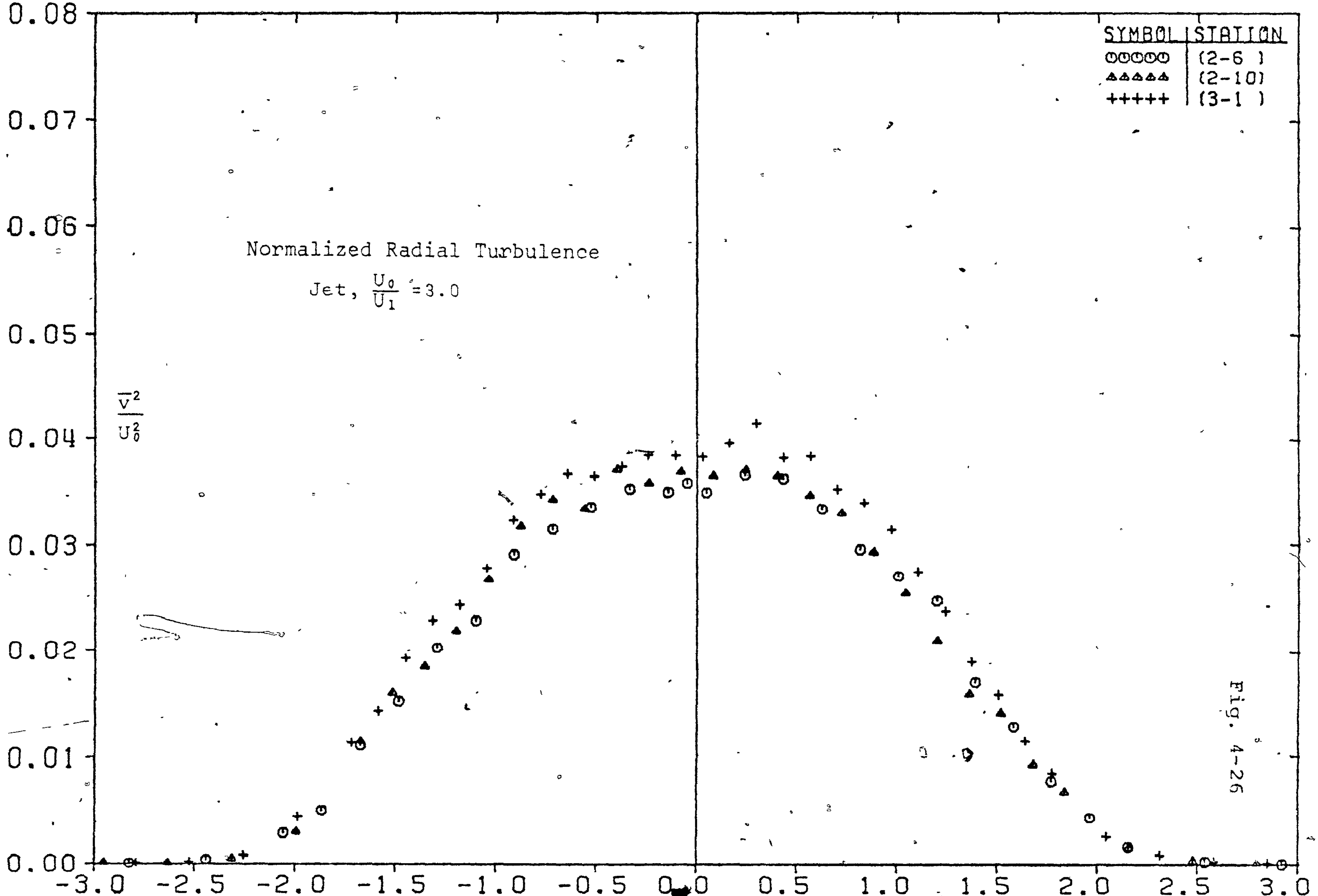
SYMBOL | STATION
(2-6)
(2-10)
(3-1)
Normalized Radial Turbulence
Jet, $\frac{U_0}{U_1} = 3.0$
$\frac{\overline{v^2}}{U_0^2}$
0.08
0.07
0.06
0.05
0.04
0.03
0.02
0.01
0.00
-3.0
-2.5
-2.0
-1.5
-1.0
-0.5
0.0
0.5
1.0
1.5
2.0
2.5
3.0
Fig. 4-26

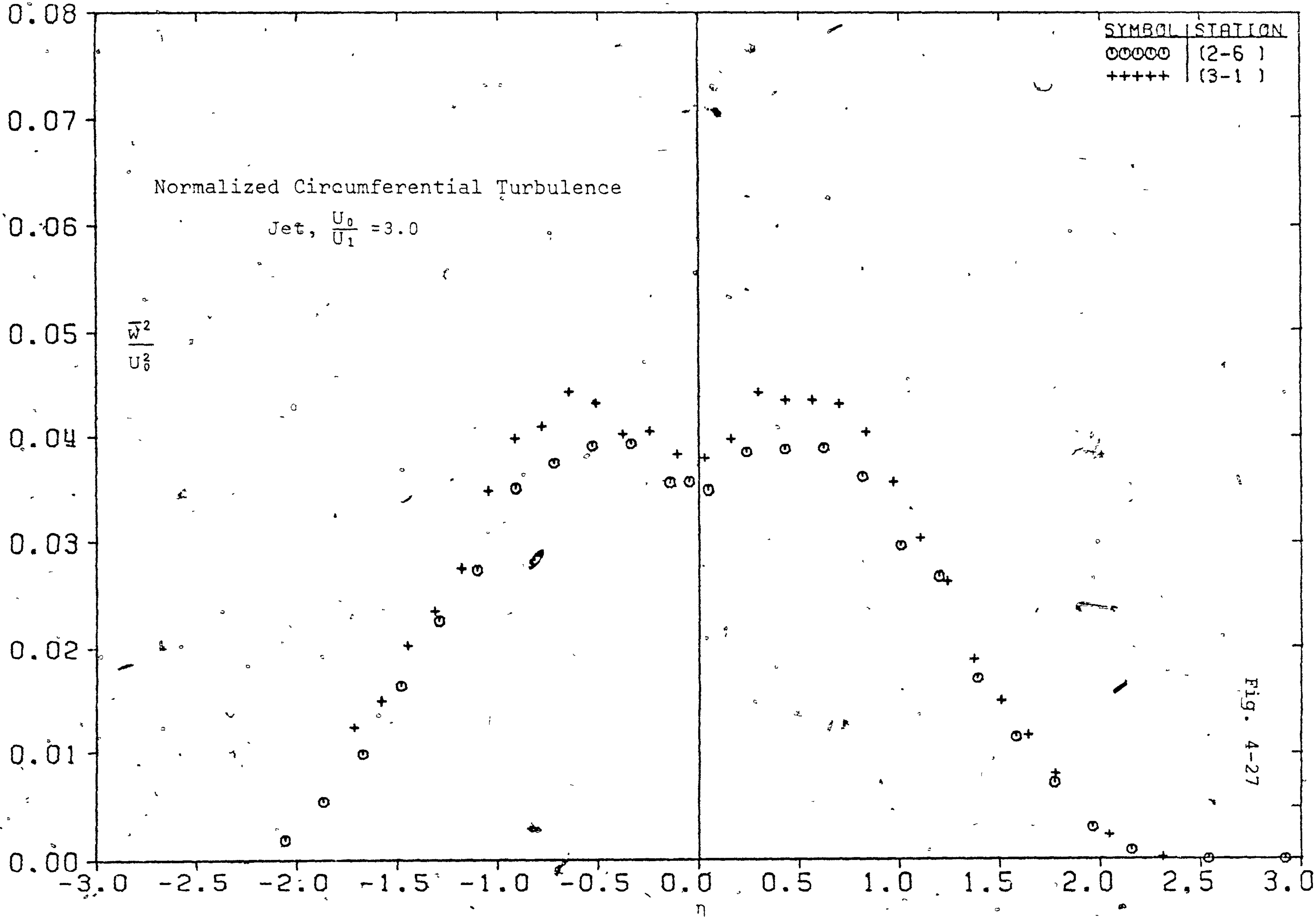

Normalized Circumferential Turbulence
Jet, $\frac{U_0}{U_1}$ =3.0
SYMBOL | STATION
ΘΘΘΘΘ | (2-6)
+++++ | (3-1)
$\frac{\overline{w}^2}{U_0^2}$
0.08
0.07
0.06
0.05
0.04
0.03
0.02
0.01
0.00
-3.0 -2.5 -2.0 -1.5 -1.0 -0.5 0.0 0.5 1.0 1.5 2.0 2.5 3.0
η

Fig. 4-27

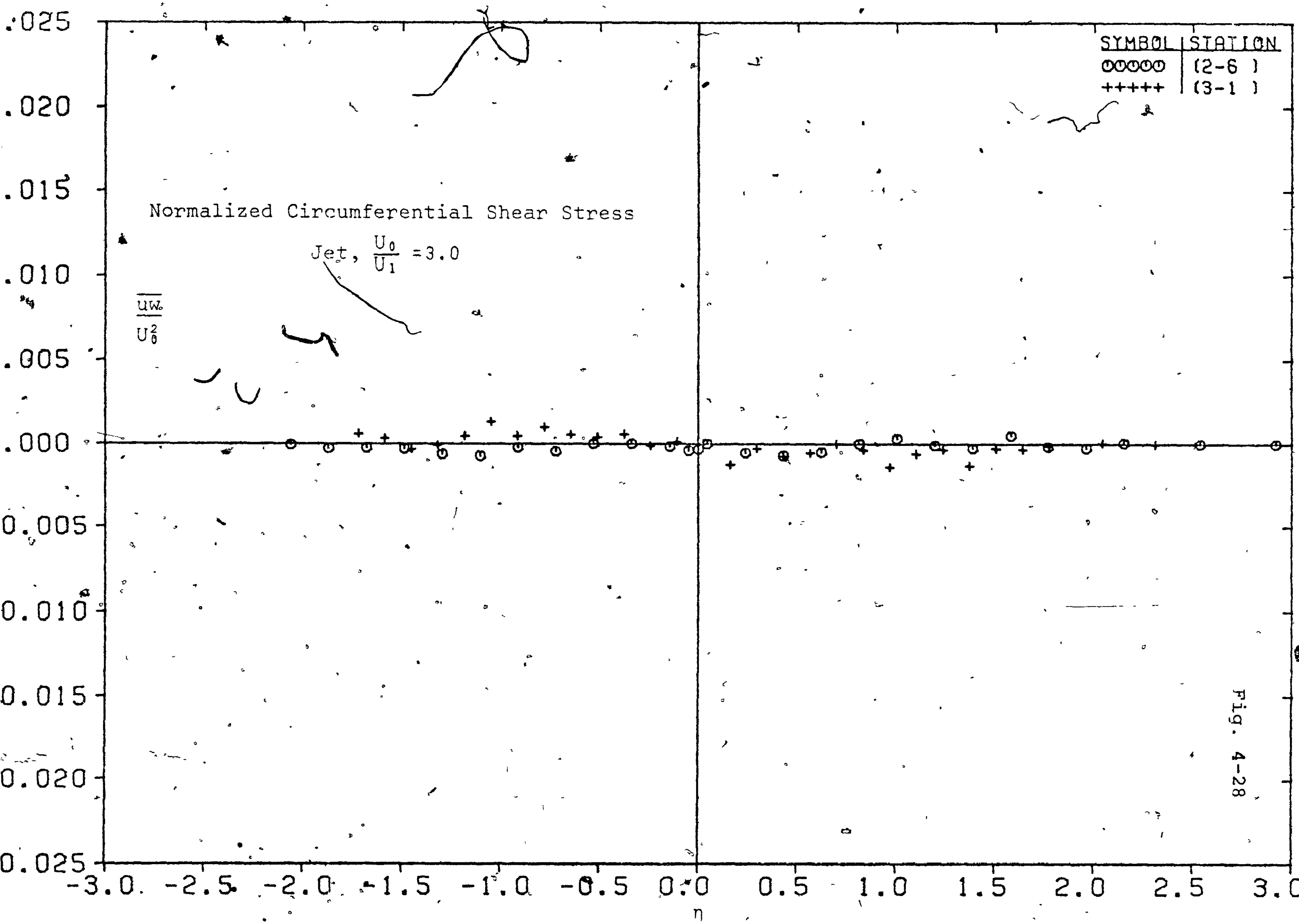
Normalized Circumferential Shear Stress
Jet, $\frac{U_0}{U_1}$ =3.0
SYMBOL | STATION
ooooo | (2-6)
+++++ | (3-1)
$\frac{\overline{uw_o}}{U_0^2}$
.025
.020
.015
.010
.005
.000
0.005
0.010
0.015
0.020
0.025
-3.0 -2.5 -2.0 -1.5 -1.0 -0.5 0.0 0.5 1.0 1.5 2.0 2.5 3.0
η
Fig. 4-28

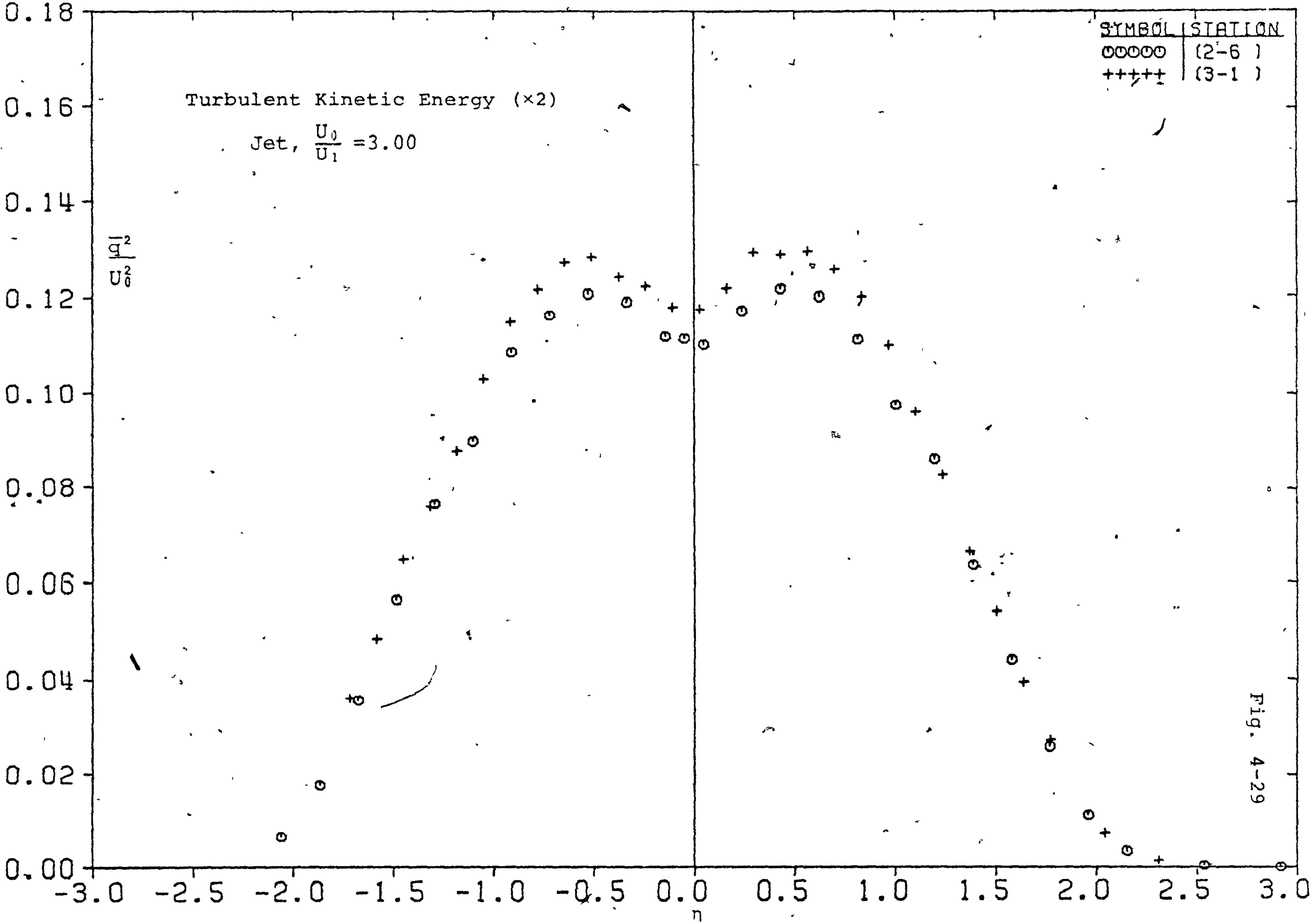
SYMBOL | STATION
OOOOO (2-6)
+++++ (3-1)
Turbulent Kinetic Energy (×2)
Jet, $\frac{U_0}{U_1}$ =3.00
$\frac{\overline{q^2}}{U_0^2}$
0.18
0.16
0.14
0.12
0.10
0.08
0.06
0.04
0.02
0.00
-3.0 -2.5 -2.0 -1.5 -1.0 -0.5 0.0 0.5 1.0 1.5 2.0 2.5 3.0
η

Fig. 4-29

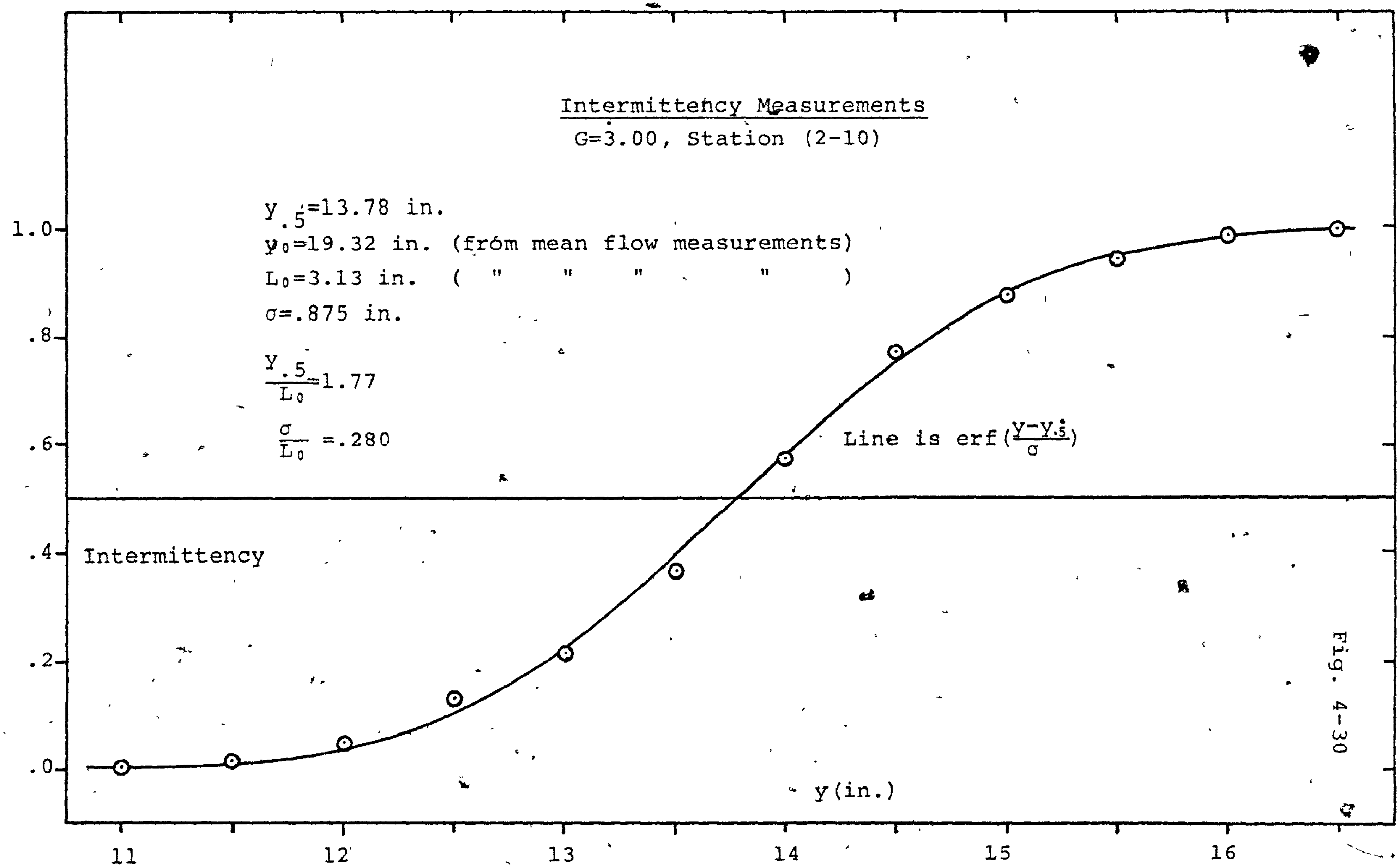
Intermittency Measurements
G=3.00, Station (2-10)
$y_{.5}$=13.78 in.
y_0=19.32 in. (from mean flow measurements)
L_0=3.13 in. (" " " ")
σ=.875 in.
$\frac{y_{.5}}{L_0}$=1.77
$\frac{\sigma}{L_0}$ =.280
Line is erf$\left(\frac{y-y_{.5}}{\sigma}\right)$
Intermittency
y(in.)
1.0
.8
.6
.4
.2
.0
11
12
13
14
15
16

Fig. 4-30

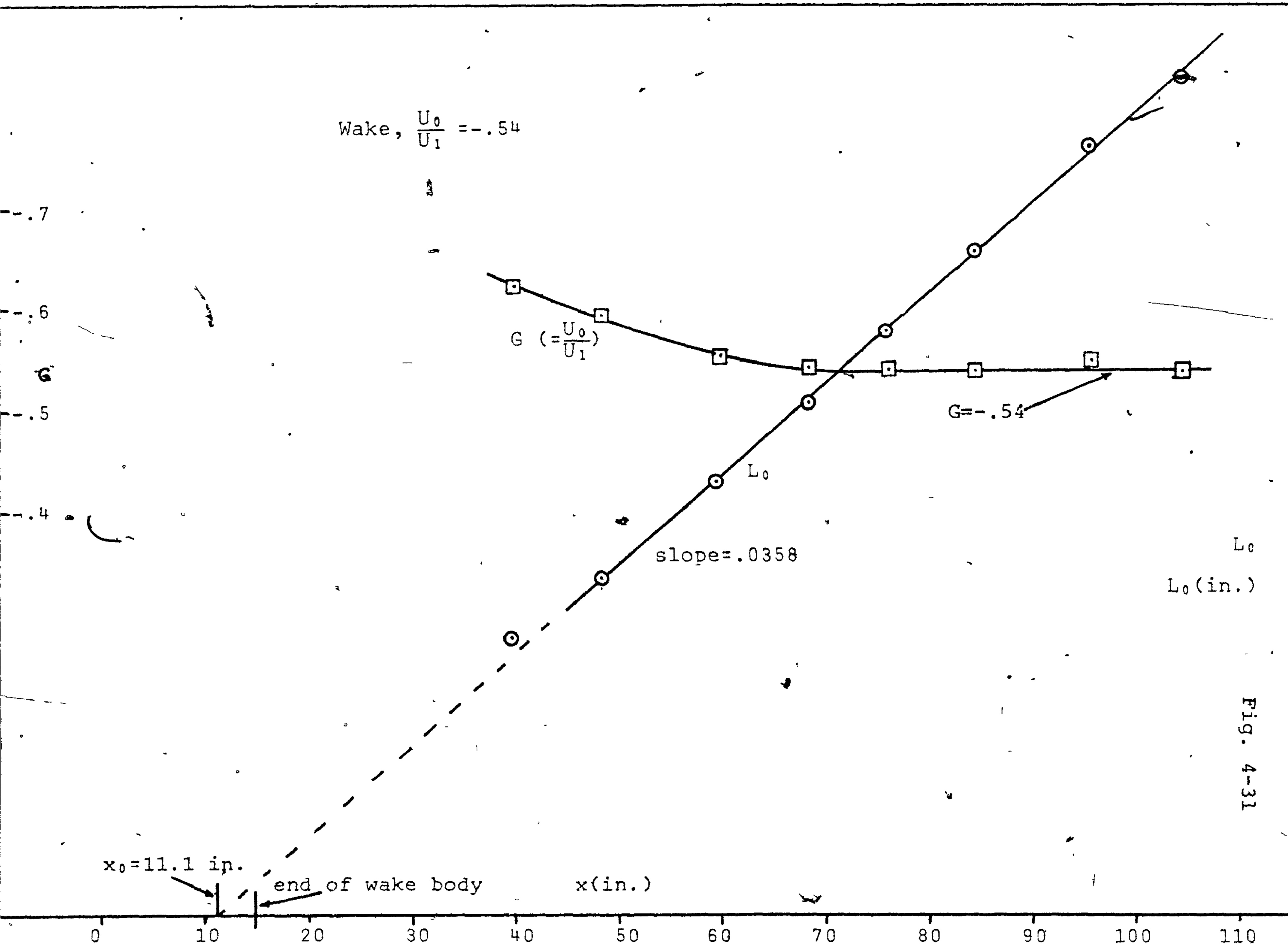
Wake, $\frac{U_0}{U_1}$ =-.54
G
.7
.6
.5
.4
G $(=\frac{U_0}{U_1})$
G=-.54
L_0
slope=.0358
L_0
L_0(in.)
3.5
3.0
2.5
2.0
1.5
1.0
0.5
x_0=11.1 in.
end of wake body
x(in.)
0
10
20
30
40
50
60
70
80
90
100
110

Fig. 4-31

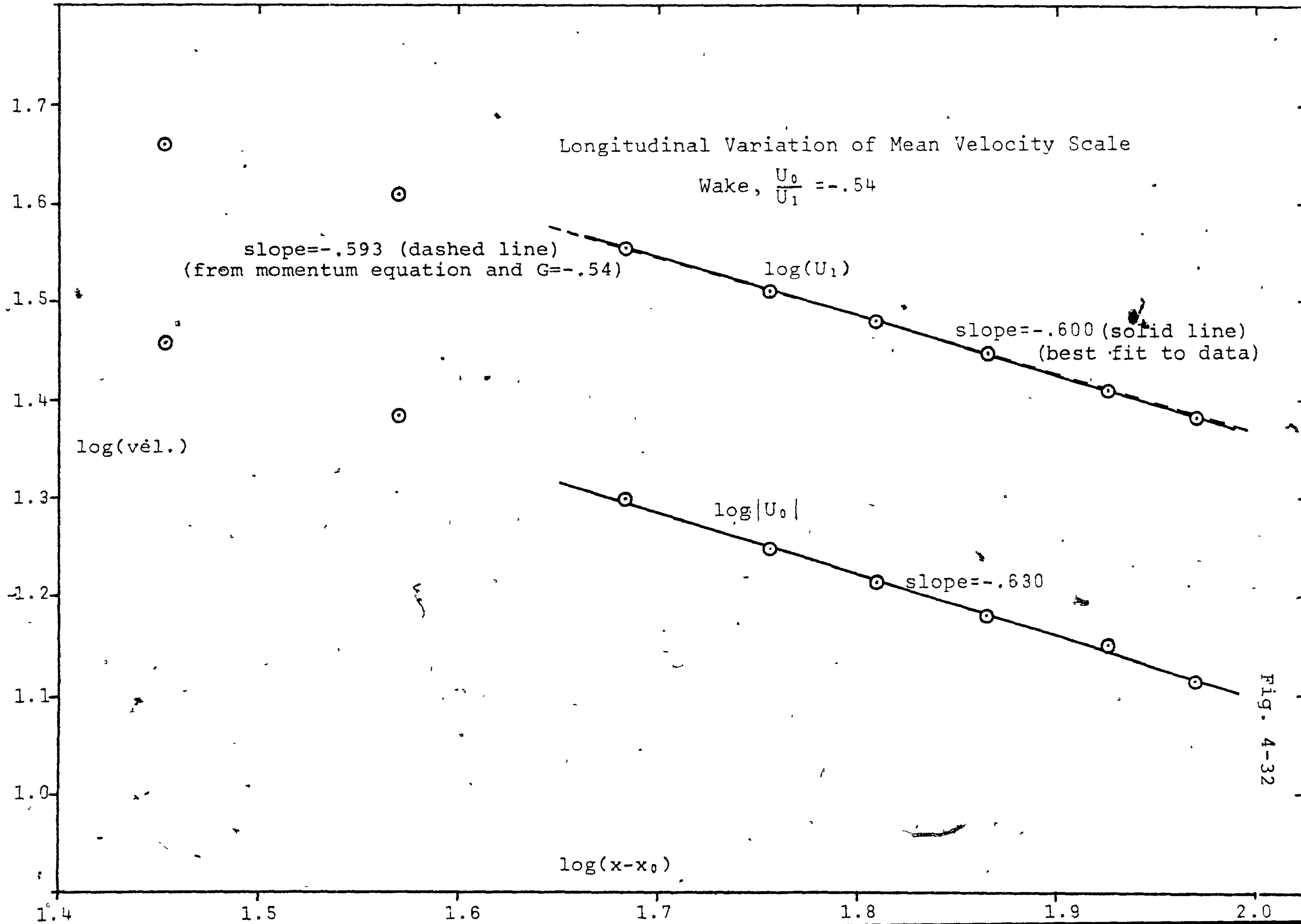

Longitudinal Variation of Mean Velocity Scale
Wake, $\frac{U_0}{U_1}$ =-.54
slope=-.593 (dashed line)
(from momentum equation and G=-.54)
log(U_1)
slope=-.600 (solid line)
(best fit to data)
log|U_0|
slope=-.630
log(vel.)
log(x-x_0)
1.7
1.6
1.5
1.4
1.3
1.2
1.1
1.0
1.4
1.5
1.6
1.7
1.8
1.9
2.0

Fig. 4-32

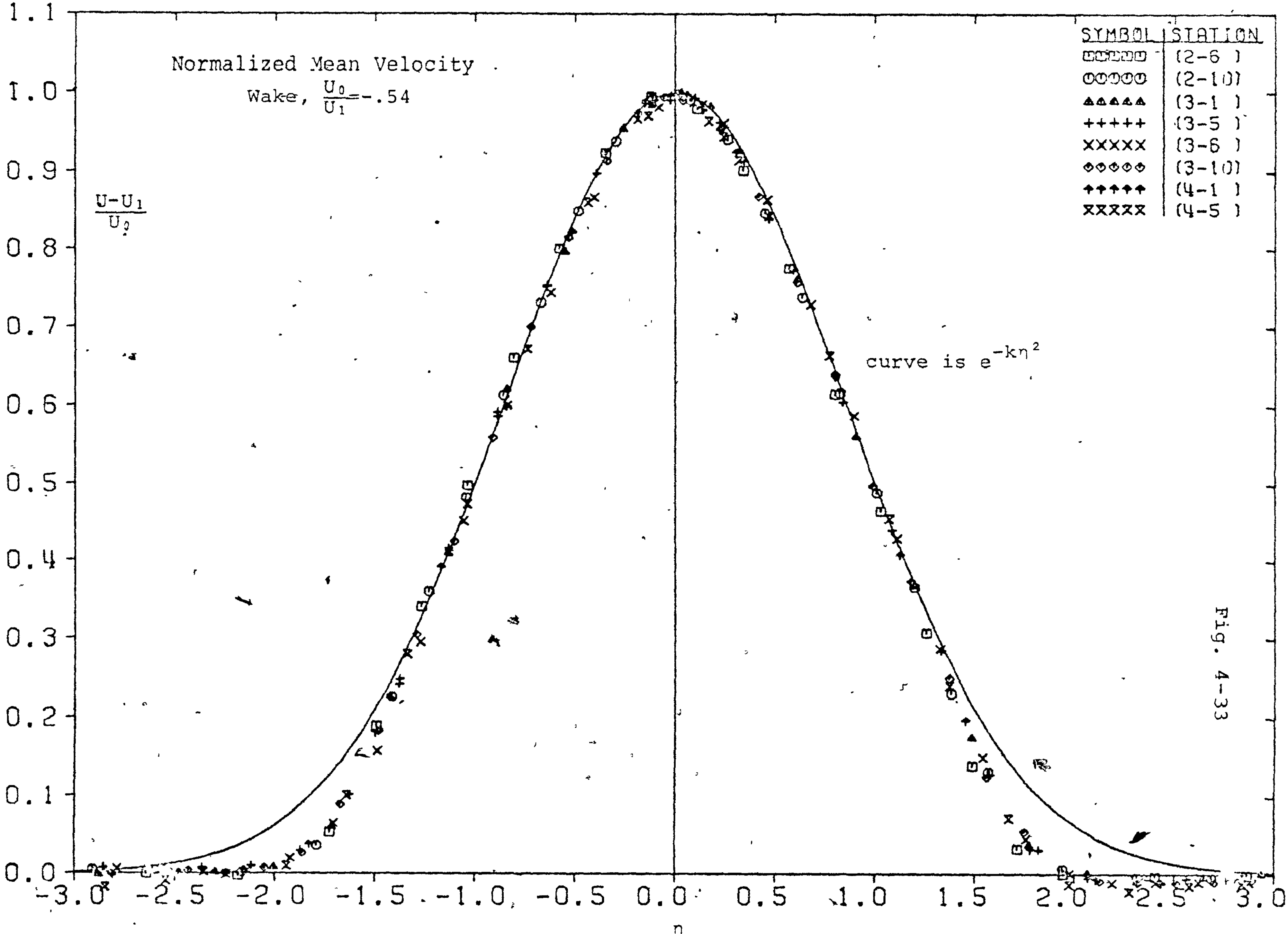
Normalized Mean Velocity
Wake, $\frac{U_0}{U_1} = -.54$
$\frac{U-U_1}{U_0}$
SYMBOL | STATION
(2-6)
(2-10)
(3-1)
(3-5)
(3-6)
(3-10)
(4-1)
(4-5)
curve is $e^{-k\eta^2}$
1.1
1.0
0.9
0.8
0.7
0.6
0.5
0.4
0.3
0.2
0.1
0.0
-3.0
-2.5
-2.0
-1.5
-1.0
-0.5
0.0
0.5
1.0
1.5
2.0
2.5
3.0
η

Fig. 4-33

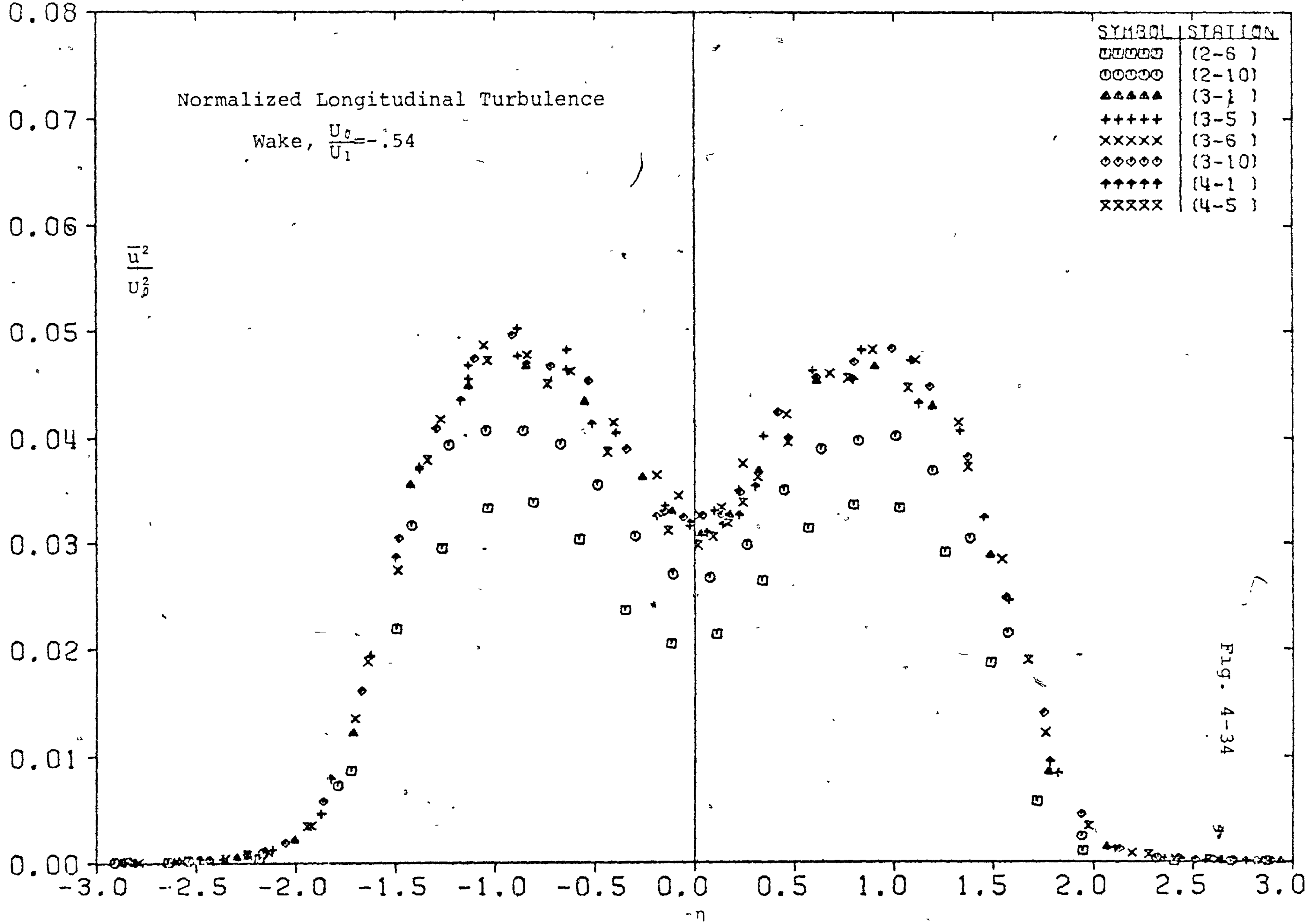
Normalized Longitudinal Turbulence
Wake, $\frac{U_0}{U_1}$=-.54
$\frac{\overline{u^2}}{U_0^2}$
SYMBOL | STATION
(2-6)
(2-10)
(3-1)
(3-5)
(3-6)
(3-10)
(4-1)
(4-5)
0.08
0.07
0.06
0.05
0.04
0.03
0.02
0.01
0.00
-3.0
-2.5
-2.0
-1.5
-1.0
-0.5
0.0
0.5
1.0
1.5
2.0
2.5
3.0
-η

Fig. 4-34

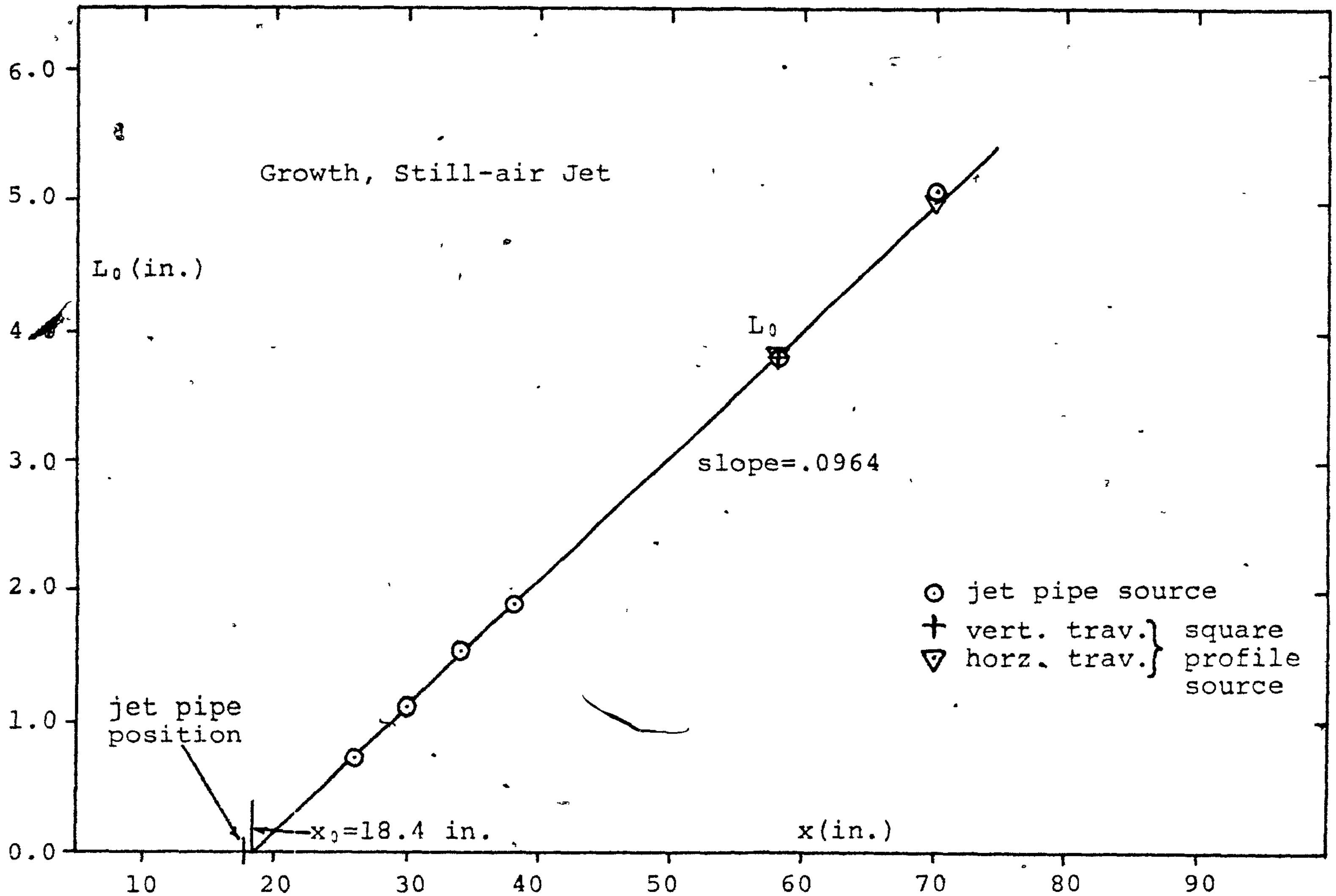
Growth, Still-air Jet
L_0 (in.)
L_0
slope=.0964
jet pipe source
vert. trav.
horz. trav.
square profile source
jet pipe position
x_0=18.4 in.
x(in.)
6.0
5.0
4
3.0
2.0
1.0
0.0
10
20
30
40
50
60
70
80
90

Fig. 4-35

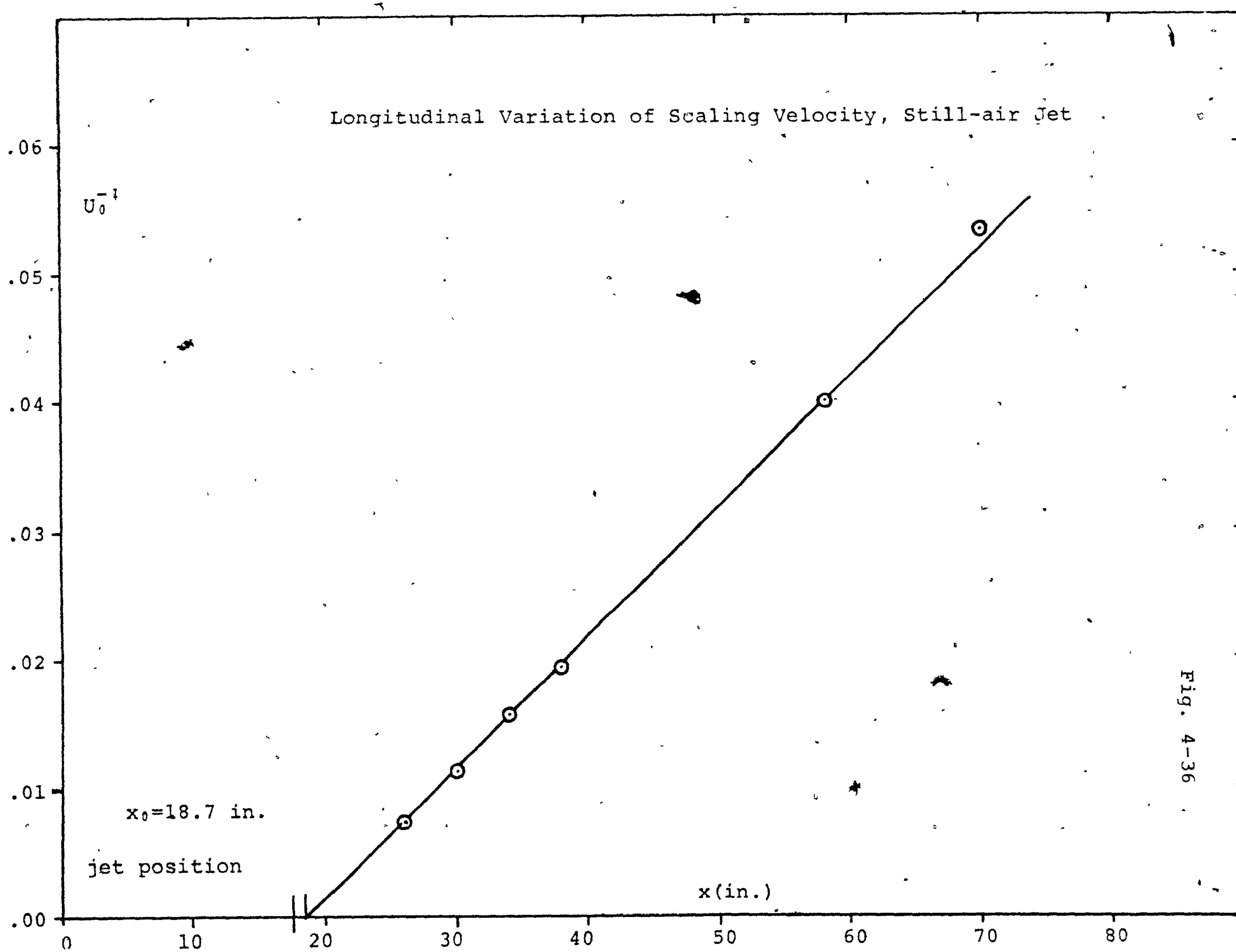

Longitudinal Variation of Scaling Velocity, Still-air Jet
U_0^{-1}
.06
.05
.04
.03
.02
.01
.00
x_0=18.7 in.
jet position
x(in.)
0
10
20
30
40
50
60
70
80

Fig. 4-36

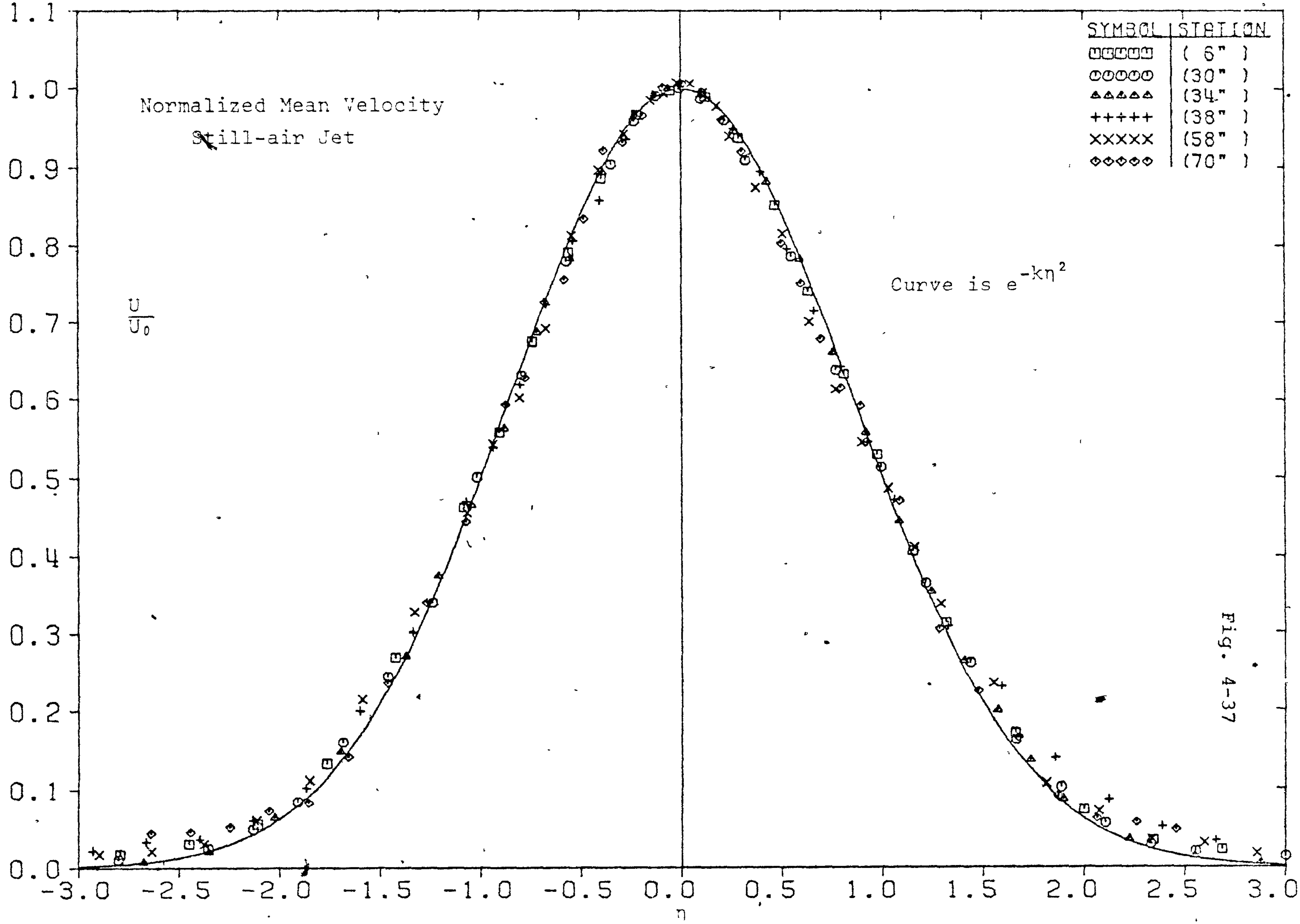

Normalized Mean Velocity
Still-air Jet
$\frac{U}{U_0}$
Curve is $e^{-k\eta^2}$
SYMBOL | STATION
(6")
(30")
(34")
(38")
(58")
(70")
1.1
1.0
0.9
0.8
0.7
0.6
0.5
0.4
0.3
0.2
0.1
0.0
-3.0
-2.5
-2.0
-1.5
-1.0
-0.5
0.0
0.5
1.0
1.5
2.0
2.5
3.0
η

Fig. 4-37

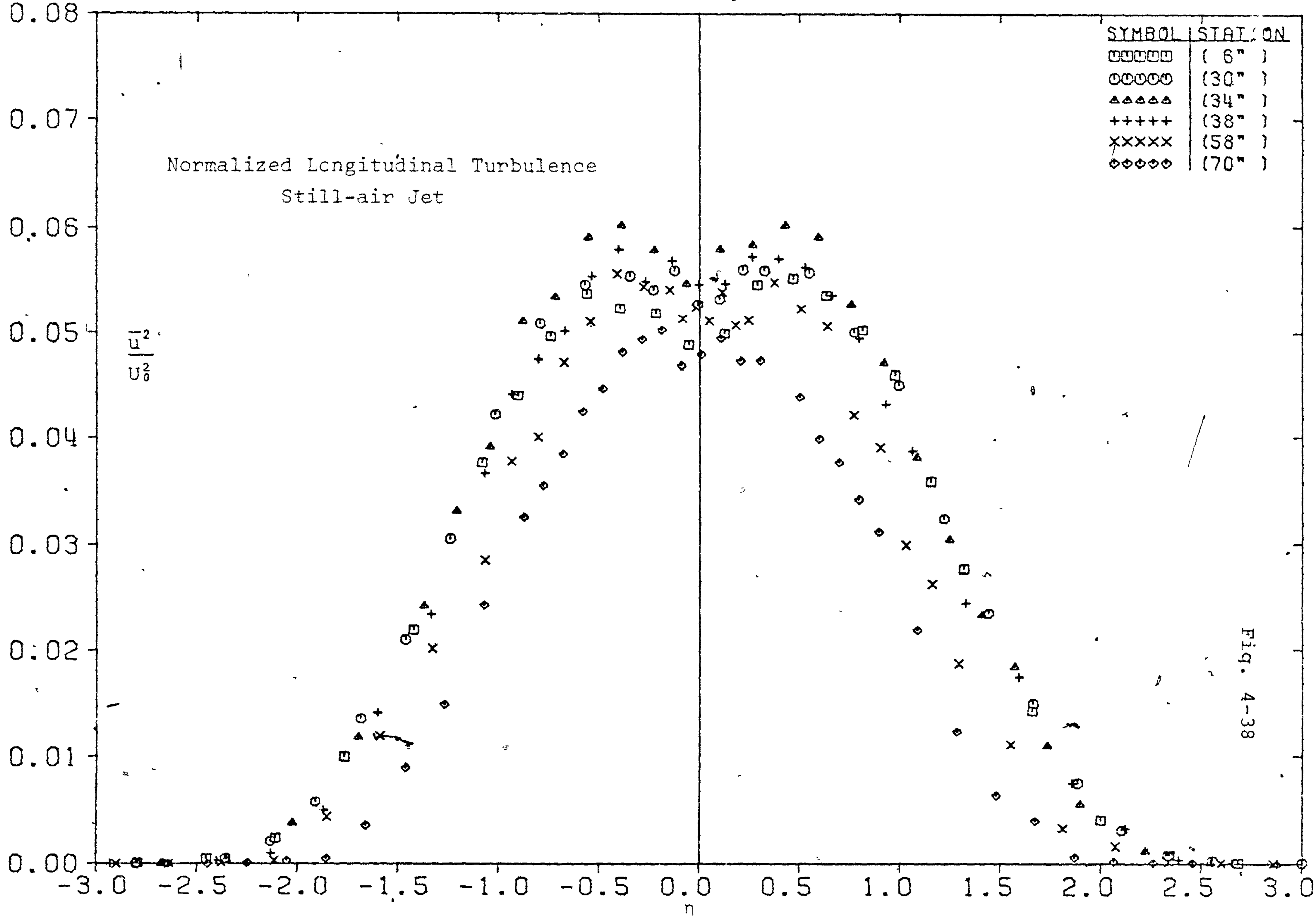

SYMBOL | STATION
(6")
(30")
(34")
(38")
(58")
(70")
Normalized Longitudinal Turbulence
Still-air Jet
$\overline{u^2}/U_0^2$
0.08
0.07
0.06
0.05
0.04
0.03
0.02
0.01
0.00
-3.0
-2.5
-2.0
-1.5
-1.0
-0.5
0.0
0.5
1.0
1.5
2.0
2.5
3.0
η

Fig. 4-38

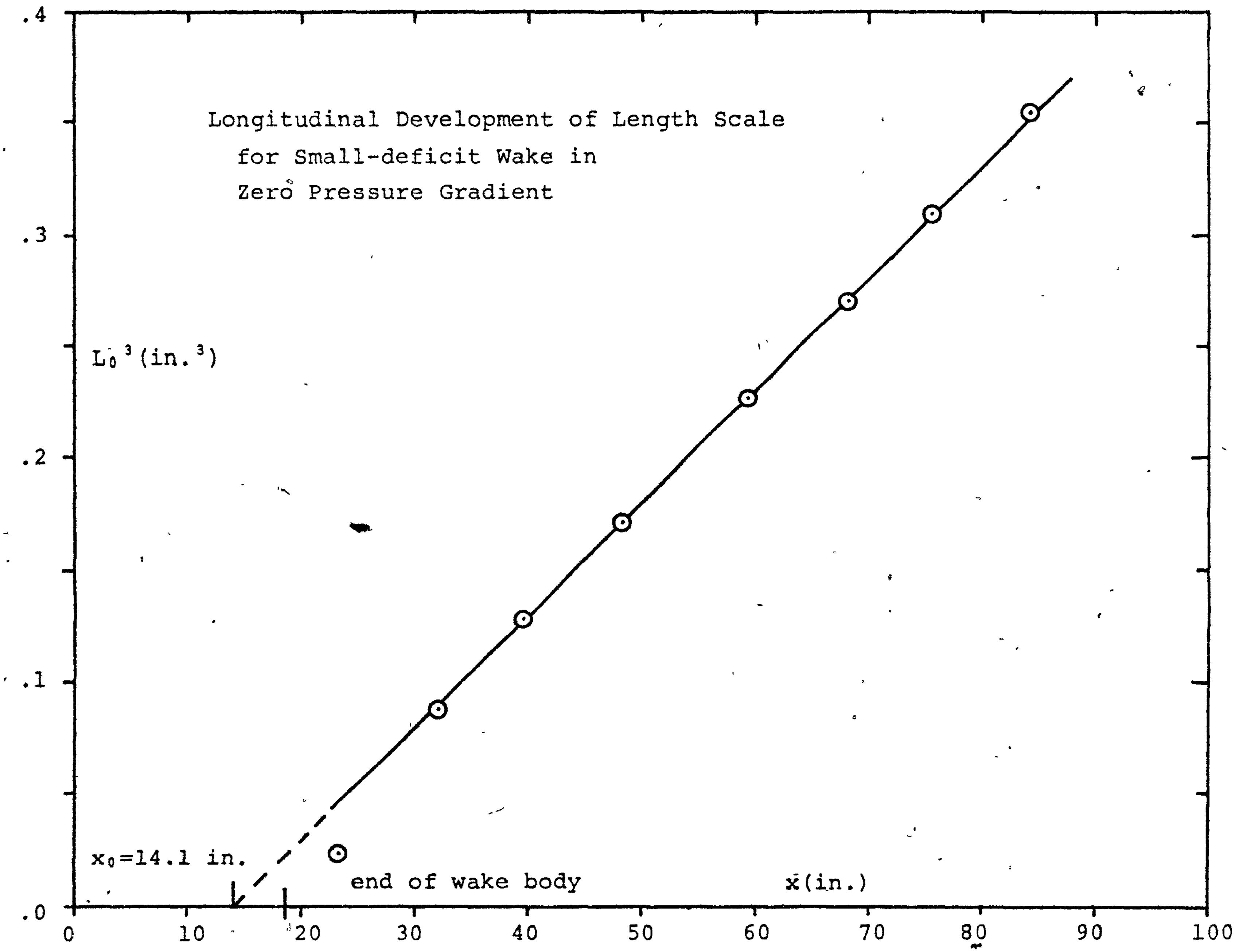

Longitudinal Development of Length Scale
for Small-deficit Wake in
Zero Pressure Gradient
$L_0{}^3$(in.^{3})
x_0=14.1 in.
end of wake body
x(in.)
.4
.3
.2
.1
.0
0
10
20
30
40
50
60
70
80
90
100

Fig. 4-39

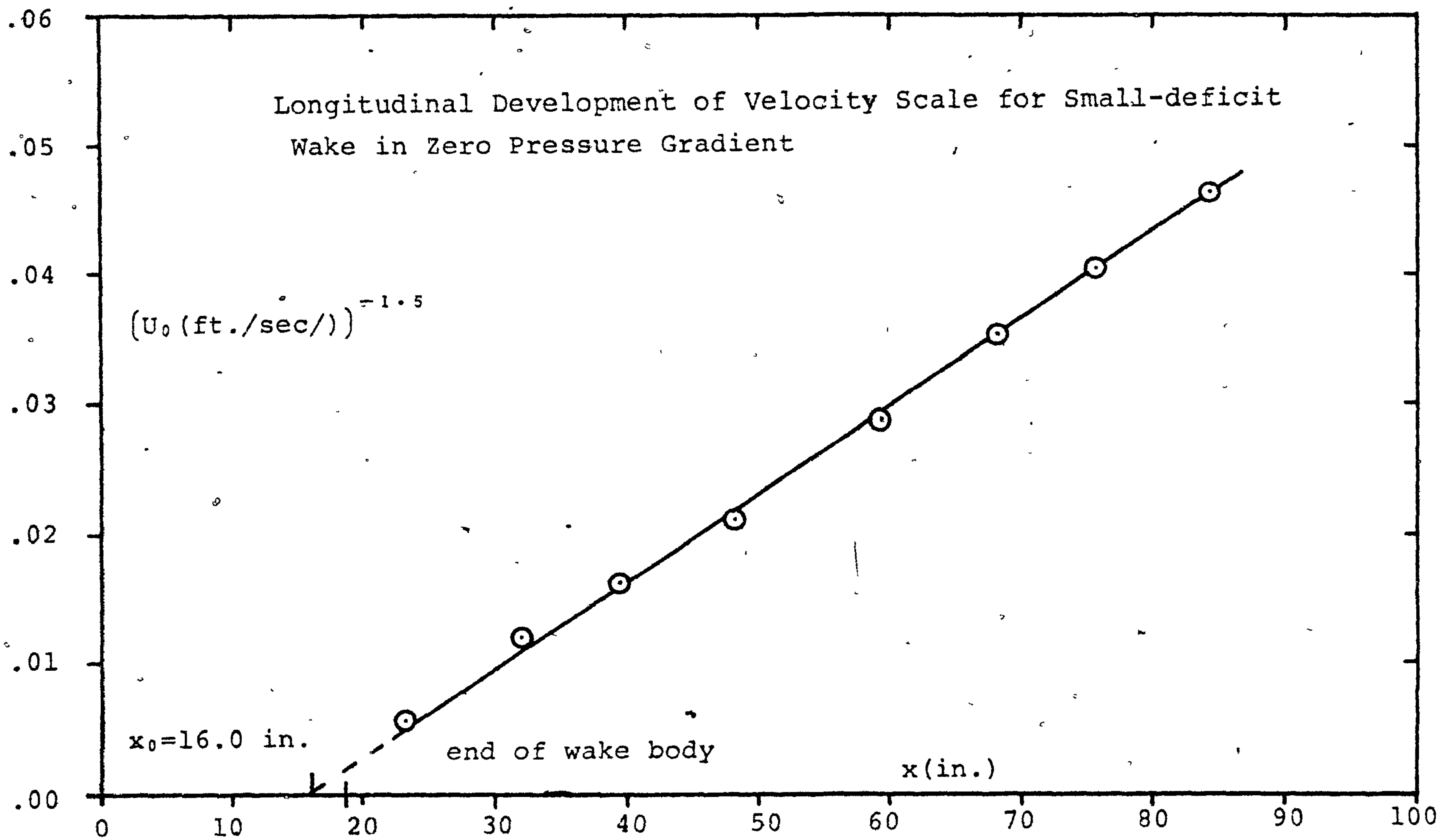
Longitudinal Development of Velocity Scale for Small-deficit Wake in Zero Pressure Gradient
(U0 (ft./sec/))-1.5
x0=16.0 in.
end of wake body
x(in.)
.06
.05
.04
.03
.02
.01
.00
0
10
20
30
40
50
60
70
80
90
100

Fig. 4-40

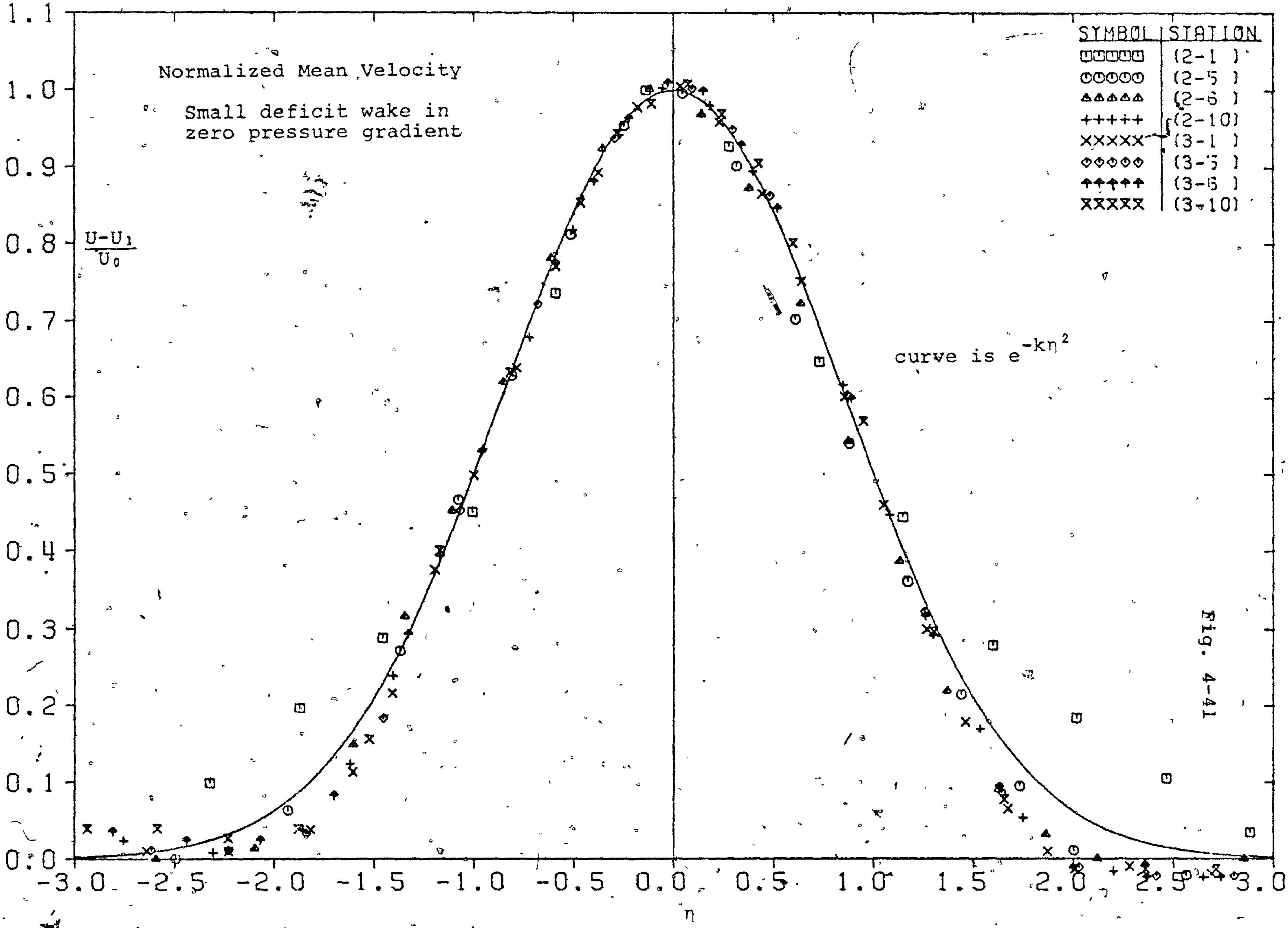

Normalized Mean Velocity
Small deficit wake in zero pressure gradient
SYMBOL | STATION
(2-1)
(2-5)
(2-6)
(2-10)
(3-1)
(3-5)
(3-6)
(3-10)
curve is $e^{-k\eta^2}$
$\frac{U-U_1}{U_0}$
η
1.1
1.0
0.9
0.8
0.7
0.6
0.5
0.4
0.3
0.2
0.1
0.0
-3.0
-2.5
-2.0
-1.5
-1.0
-0.5
0.0
0.5
1.0
1.5
2.0
2.5
3.0

Fig. 4-41

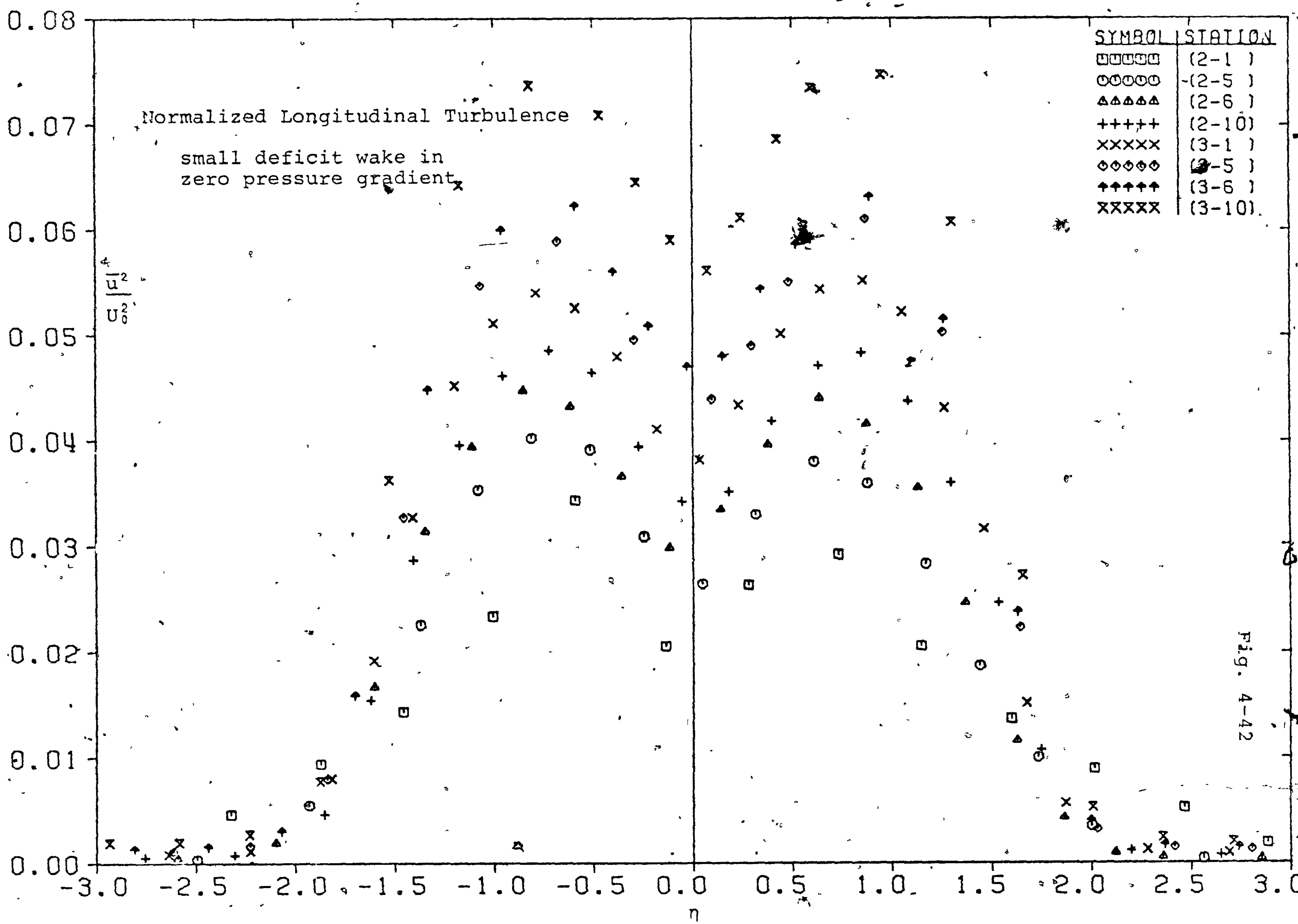
Normalized Longitudinal Turbulence
small deficit wake in
zero pressure gradient
SYMBOL STATION
(2-1)
(2-5)
(2-6)
(2-10)
(3-1)
(3-5)
(3-6)
(3-10)
$\overline{u^2}/U_0^2$
η
0.00
0.01
0.02
0.03
0.04
0.05
0.06
0.07
0.08
-3.0
-2.5
-2.0
-1.5
-1.0
-0.5
0.0
0.5
1.0
1.5
2.0
2.5
3.0

Fig. 4-42

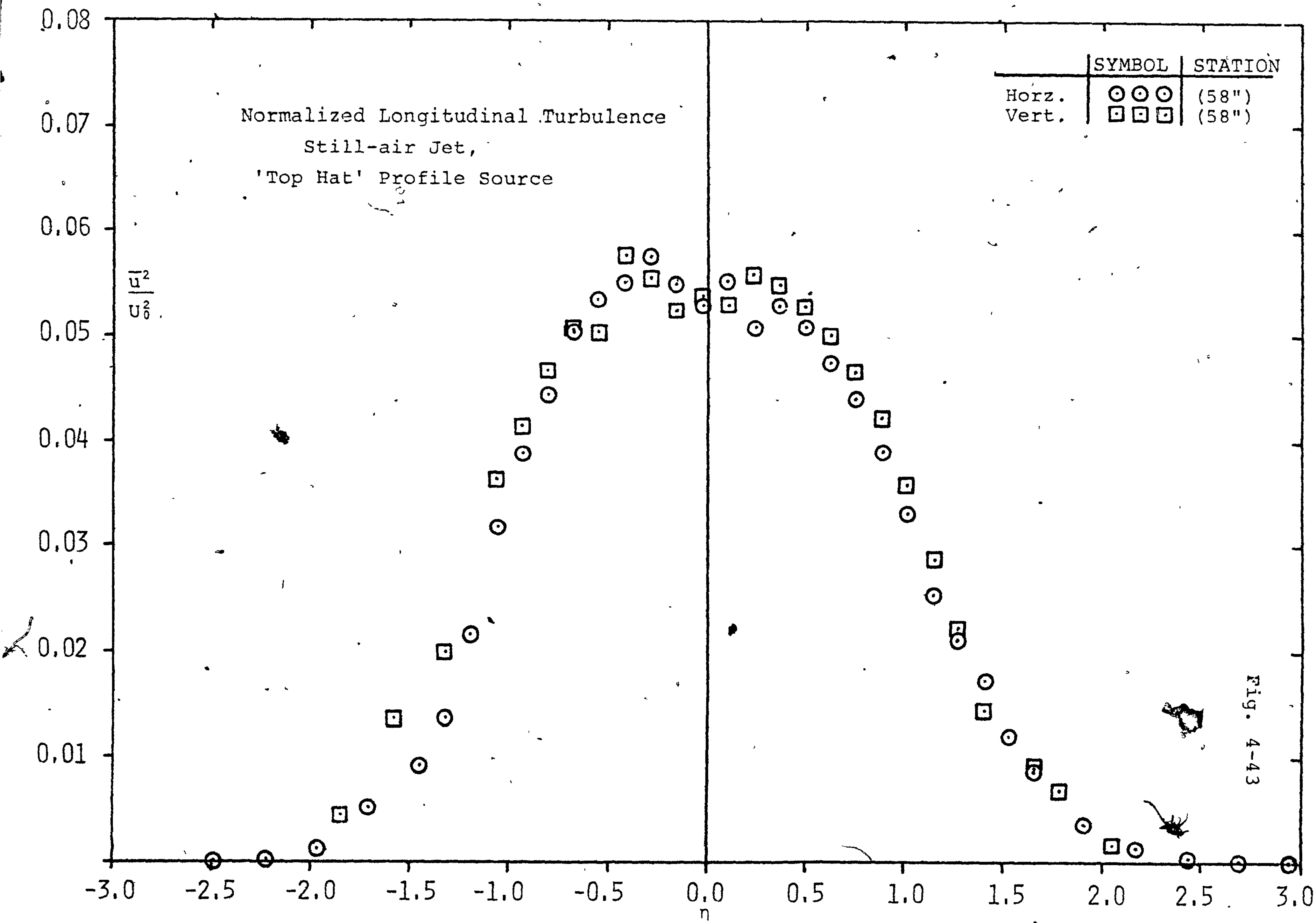

Normalized Longitudinal Turbulence
Still-air Jet,
'Top Hat' Profile Source
SYMBOL
STATION
Horz.
(58")
Vert.
(58")
$\frac{\overline{u^2}}{U_0^2}$
0.08
0.07
0.06
0.05
0.04
0.03
0.02
0.01
-3.0
-2.5
-2.0
-1.5
-1.0
-0.5
0.0
0.5
1.0
1.5
2.0
2.5
3.0
η

Fig. 4-43

Appendix A

TWO-DIMENSIONAL EXPANSION

Most wide-angle expansions are built with straight sided walls, and sufficient screens are added to eliminate or reduce unsteadiness associated with flow separation. As the number, placement and pressure drop coefficient of the screens are usually determined by a combination of guesswork and experiment, such an expansion is often wasteful of power and may still have regions of high turbulence due to local separation and reattachment.

The more rational approach used in the present expansion was first suggested by Hughes (1944) and Squire and Hogg (1944). Hughes developed the theory and pointed out the salient features of the design. His numerical solution made use of a series expansion. The present availability of digital computers now makes direct integration the more logical approach.

Gibson (1959) described the design and building of such an expansion for a wind tunnel, and his theoretical approach is followed, although the calculations are described in more detail. The expansion described by Gibson was rendered axisymmetric by making its area at each station the same as an appropriate two-dimensional expansion of the same length. There is, however, an ambiguity in such a conversion, as the length to diameter ratio, and thus the wall slope, of such an axisymmetric expansion depends on the width of the two-dimensional expansion, and there appears to be no rational way of choosing this width. Although not stated, it appears that Gibson chose the width of the two-dimensional expansion to be the same as the inlet height.

This problem plus the relative ease of construction, led us to build a two-dimensional expansion.

THEORY

A desirable wide-angle diffuser would have the velocity on the walls constant everywhere except at one point. The separation induced by the large adverse pressure gradient at that point may then be controlled by a screen or by blowing or suction*. The theory should give the wall profile and indicate the amount of boundary layer control needed at the discontinuity. Half such a proposed symmetrical diffuser is sketched in Figure A1.

For the purposes of calculation the flow is considered ideal and irrotational. The diffuser has an expansion ratio of λ. The outlet velocity is assumed to be 1, and the outlet half-width to be π. On the curved walls the velocity is to be constant, and equal to λ and 1, upstream and downstream of the discontinuity, respectively. This problem is best solved using complex variables. In this representation position is represented by a complex variable $Z = x + iy$, and the flow is represented by a complex potential, $W = \phi + i\psi$, where ϕ and ψ are the potential and stream functions of the velocity field, respectively. Letters A-F identify points in this complex plane.

---

*If a screen is used, there will probably be no pressure recovery, and 'expansion' would be a better description than 'diffuser'. However, to avoid confusion, the word diffuser will be used.

Solution of the problem involves operating on the complex variable Z with an analytic transformation, or transformations, that convert the boundaries of the flow into ones that have a recognizable solution. For this problem, the first transformation is to the hodograph plane defined by

$$H = - \ln\left(\frac{dw}{dz}\right) = \ln\left(\frac{1}{V}\right) + i\theta \qquad \text{(A1)}$$

which transforms the problem to that of flow in a semi-infinite channel with a source and sink of strength π in the corners, as shown in Figure A2. Letters A-F identify points that correspond to those in Figure A1. V is the magnitude of the flow, and θ is the angle of the flow direction, both measured in the physical Z-plane.

As originally postulated, there is a discontinuity at the point where the flow changes speed abruptly, and there is a spiral boundary there, as the flow angle must go to infinity as the discontinuity is approached.

The problem in the H-plane is now transformed to that of a source and sink on a semi-infinite plane, the T-plane, by means of the Schwarz-Cristoffel transformation

$$H = \frac{i}{\pi} \ln(\lambda) \cosh^{-1} (T) \qquad \text{(A2)}$$

This plane is shown in Figure A3, and again the characteristic points are denoted by the letters A-F. It is easily seen that this is the upper half of the problem with a source and sink strength 2π located on the real axis -1 and +1, respectively, and with no boundaries. The solution to this is well-known, and is

$$W = \ln \frac{T+1}{T-1} \tag{A3}$$

when the real part of T is zero or infinite $\phi = 0$ from expression (A3). Then points F, E_1, and E_2 are points where $\phi = 0$ and are also shown in the physical Z-plane (Fig. A1). Similarly, $\psi = -\pi$ from A,D to B,C, and equals 0 from E_1 to A,D, and from B,C to E_2.

Solving (A3) for T gives

$$T = \frac{e^W + 1}{e^W - 1} = \coth\left(\frac{W}{2}\right) \tag{A4}$$

then

$$H = \frac{i}{\pi} \ln(\lambda) \cosh^{-1}\left[\coth\left(\frac{W}{2}\right)\right] \tag{A5}$$

but

$$dZ = e^H \, dW \tag{A6}$$

and thus

$$dZ = \exp\left[i\ M \cosh^{-1}\left[\coth\left(\frac{W}{2}\right)\right]\right] dW \tag{A7}$$

where

$$M = \frac{\ln(\lambda)}{\pi} \tag{A8}$$

Now

$$\cosh^{-1}(x) = \ln\left[x + \sqrt{x^2 - 1}\right]$$

and thus

$$\cosh^{-1}\left[\coth\left(\frac{W}{2}\right)\right] = \ln\left[\frac{2\cosh\left(\frac{W}{4}\right)}{2\sinh\left(\frac{W}{4}\right)}\right] = \ln\left[\coth\left(\frac{W}{4}\right)\right] \tag{A9}$$

so that

$$dz = \exp\left[i\, M \ln\left[\coth\left(\frac{W}{4}\right)\right]\right] dW \tag{A10}$$

This cannot be integrated in closed form and was therefore solved numerically on a digital computer. A program could have been written to integrate the general complex equation, but only the values of x and y when $\psi = 0$ (for the walls) and for $\phi = 0$ (for the screen position) are required. The choice of the $\phi = 0$ line as the position for the screen was made for two reasons. Firstly, the $\phi = 0$ line goes through the discontinuity where boundary layer control is needed; and secondly, the line, like all constant ϕ lines, is at right angles to the local streamlines and, as will be shown in relation (A21), the flow speed across this line is the same at all points on the line. Thus the drop in total pressure across the screen is the same for all streamlines, and therefore the ideal flow pattern is not affected by the presence of the screen, and at the diffuser outlet the flow will have uniform velocity.

When $\psi = 0$

$$dZ = \left[\exp i\ M \ln\left[\coth\left(\frac{\phi}{4}\right)\right]\right] d\phi \tag{A11}$$

but

$$\coth\left(\frac{\phi}{4}\right) = \left[e^{i\pi}\right]^n \coth\left|\frac{\phi}{4}\right| \tag{A12}$$

where

$$\begin{cases} n = 0 \text{ when } \phi \geq 0 \\ n = 1 \text{ when } \phi < 0 \end{cases}$$

Thus

$$\ln\left[\coth\left(\frac{\phi}{4}\right)\right] = ni\pi + \ln\left[\coth\left|\frac{\phi}{4}\right|\right] \tag{A13}$$

and

$$e^{iM(ni\pi)} = e^{-\ln(\lambda^n)} = \frac{1}{\lambda^n}, \text{ from (A8)} \tag{A14}$$

Using (A13) and (A14) in (A11) and separating Z into its real and imaginary parts gives

$$dx = \frac{\cos\left[M \ln\left[\coth\left|\frac{\phi}{4}\right|\right]\right] d\phi}{\lambda^n} \tag{A15}$$

$$dy = \frac{\sin\left[M \ln\left[\coth \left|\frac{\phi}{4}\right|\right]\right] d\phi}{\lambda^n} \tag{A16}$$

For the other case of interest, where

$\phi = 0, -\pi \leq \psi \leq 0$

$$\coth\left(\frac{W}{4}\right) = \coth\left(-i\left|\frac{\psi}{4}\right|\right) = -i \cot\left|\frac{\psi}{4}\right|$$

and

$$dW = i d\psi$$

then

$$dZ = \frac{i}{\sqrt{\lambda}} \exp\left[i M \ln\left[\cot\left|\frac{\psi}{4}\right|\right]\right] d\psi \tag{A17}$$

and

$$dx = \frac{-\sin\left[M \ln\left[\cot\left|\frac{\psi}{4}\right|\right]\right] d\psi}{\sqrt{\lambda}} \tag{A18}$$

$$dy = \frac{\cos\left[M \ln\left[\cot\left|\frac{\psi}{4}\right|\right]\right] d\psi}{\sqrt{\lambda}} \tag{A19}$$

In general, the speed of the flow is given by

$$V = \sqrt{\left(\frac{dW}{dZ}\right) \left(\frac{dW}{dZ}\right)^*} \tag{A20}$$

and for $\phi = 0$ this becomes

$$V = \left[\frac{\sqrt{\lambda}}{\exp\left[i\, M \ln \left[\cot \left| \frac{\pi}{4} \right| \right] \right]} \cdot \frac{\sqrt{\lambda}}{\exp\left[-i M \ln \left[\cot \left| \frac{\pi}{4} \right| \right] \right]} \right]^{\frac{1}{2}} = \sqrt{\lambda} \qquad \text{(A21)}$$

Thus the speed of fluid across the $\phi = 0$ line is constant across the width of the diffuser and is equal to the geometric mean of the inlet and outlet speeds. This is different from that predicted by the one-dimensional actuator disk theory which predicts this speed to be the arithmetic mean of the inlet and outlet speeds. Gibson apparently was not aware of this relation when he designed his diffuser as he used Squire and Hogg's one-dimensional theory (7) to determine the screen pressure drop coefficient that would maintain constant wall pressure. This one-dimensional theory predicts that the pressure coefficient for such a screen should be

$$K_{1-D} = \frac{4(\lambda-1)}{\lambda+1} \qquad \text{(A22)}$$

whereas the above two-dimensional theory predicts that

$$K_{2-D} = \frac{\lambda^2 - 1}{\lambda} \qquad \text{(A23)}$$

These become significantly different as λ increases.

When (A15), (A16), (A18), and (A19) are integrated numerically a difficulty arises, as both coth and cot become infinite as their arguments tend to zero. However, for small values of the argument coth $\frac{\psi}{4}$ and cot $\frac{\phi}{4}$ may be approximated by $\frac{4}{\psi}$ and $\frac{4}{\phi}$, respectively, and then the equation is integrable in closed form. If these equations are integrated between the limits of 0 and ϕ, and 0 and ψ, respectively, the following equations result.

When $\psi = 0$,

$$x = \frac{\phi}{(M^2+1)\lambda^n}\left[\cos\left[M \ln\left|\frac{4}{\phi}\right|\right] - M \sin\left[M \ln\left|\frac{4}{\phi}\right|\right]\right] \quad \text{(A24)}$$

$$y = \frac{\phi}{(M^2+1)\lambda^n}\left[\sin\left[M \ln\left|\frac{4}{\phi}\right|\right] + M \cos\left[M \ln\left|\frac{4}{\phi}\right|\right]\right] \quad \text{(A25)}$$

for small ϕ (it is noted that these relations differ from those given by Gibson (6)).

When $\phi = 0$, $0 \geq \psi \geq -\pi$

$$x = \frac{-\psi}{(M^2+1)\sqrt{\lambda}}\left[\sin\left[M \ln\left|\frac{4}{\psi}\right|\right] + M \cos\left[M \ln\left|\frac{4}{\psi}\right|\right]\right] \quad \text{(A26)}$$

$$y = \frac{\psi}{(M^2+1)\sqrt{\lambda}}\left[\cos\left[M \ln\left|\frac{4}{\psi}\right|\right] - M \sin\left[M \ln\left|\frac{4}{\psi}\right|\right]\right] \quad \text{(A27)}$$

for small ψ.

This allows a choice of finite starting value of dx and dy for the numerical integration with the starting values of x and y determined by equations (A24) - (A27).

Some trials had to be made to determine a satisfactory matching point between the approximate analytic solution and the solution using numerical integration. Further, it was found that the step size for the numerical integration had to be very small near the discontinuity and therefore had to be increased further out in order to maintain reasonable computation times.

DESIGN AND CONSTRUCTION

The previous theory gives the wall shape for an infinitely long diffuser with an expansion ratio λ. This theoretical design must be truncated to an acceptable length, the choice being set by λ, the acceptable discontinuity in wall slope at the inlet and outlet, and the available room. This in turn means that the actual expansion ratio will be somewhat less than λ. A few trial calculations are usually needed to achieve a satisfactory compromise. A second problem with the theoretical design is that the walls and the screen approaching the discontinuity form a tight logarithmic spiral around the discontinuity, and must be suitably faired.

For the proposed 'diffuser', an overall expansion ratio of 1:2.62 was needed, and a 'diffuser' with a theoretical expansion ratio of 1:2.9, suitably truncated, was chosen. The degree of truncation was based on Gibson's tests. Figure A4 shows the profile of half of this 'diffuser'. The dotted lines near the discontinuity are the faired positions for the walls and the screen that were used in the actual 'diffuser'.

Before the prototype was constructed tests were made on a 1/20 scale model. A piece of square mesh wire screen of appropriate pressure drop coefficient was used to control separation. Tufts were placed on all the walls to find any regions of separation, and none were found. As both the turbulence level and Reynolds number for the model were lower than for the prototype, this gave confidence that the design was sound.

PERFORMANCE TESTS

As noted in the main section of this report a total pressure survey was made at the tunnel outlet before the screens and honeycomb were installed in the settling chamber. No unsteadiness was noted and the variation of mean velocity over the outlet (outside of the boundary layer) was less than .5%. As well, tufts were fastened to all the walls and the screen inside the diffuser to see if there were any regions of separation, especially in the corners just upstream and downstream of the screen. Observation at several speeds showed no evidence of separation or any significant secondary flows.

APPENDIX NOTATION

A, B, C, D, E, F_1, F_2	-	points on the complex physical plane, and on the transform planes.
H	-	complex number, position on hodograph plane
K_{1-D}	-	pressure drop coefficient for one-dimensional expansion theory
K_{2-D}	-	pressure drop coefficient for two-dimensional expansion theory
M	-	constant in two-dimensional expansion theory, $= \ln(\lambda)/\pi$
T	-	complex number, position on a transform plane in complex flow theory
u	-	mean flow velocity in x-direction
v	-	flow speed in Z-plane
W	-	complex potential, $= \phi + i\psi$
x	-	real part of Z
y	-	imaginary part of Z
Z	-	complex number, position on physical plane
η	-	imaginary component in T-plane
θ	-	direction of flow in Z-plane
λ	-	theoretical expansion ratio for streamline diffuser
ξ	-	real component in T-plane
ϕ	-	velocity potential function, real part of W
ψ	-	velocity stream function, imaginary part of W

Fig. A1

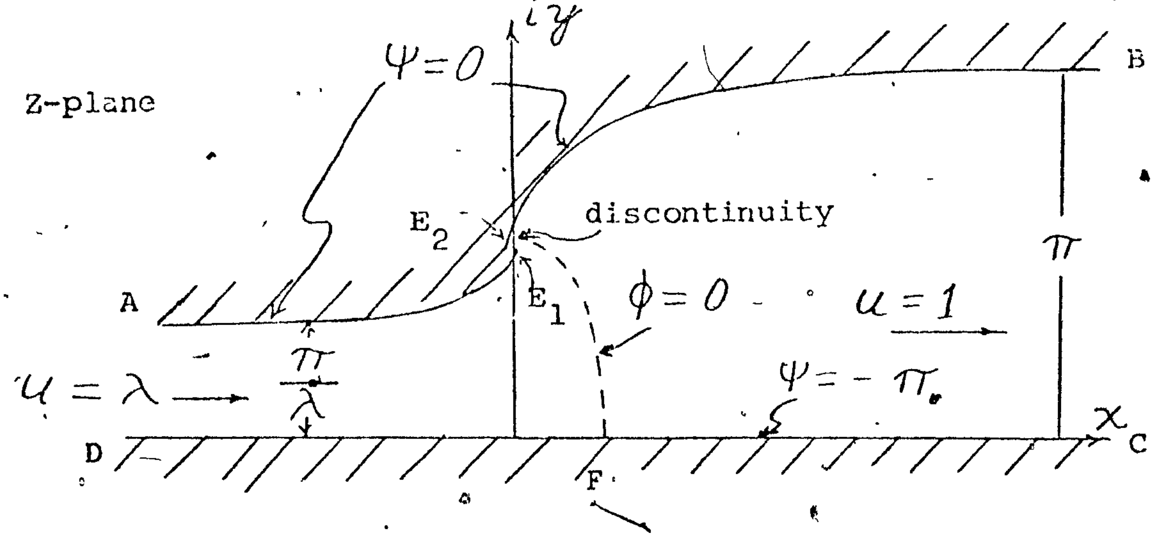

Fig. A2

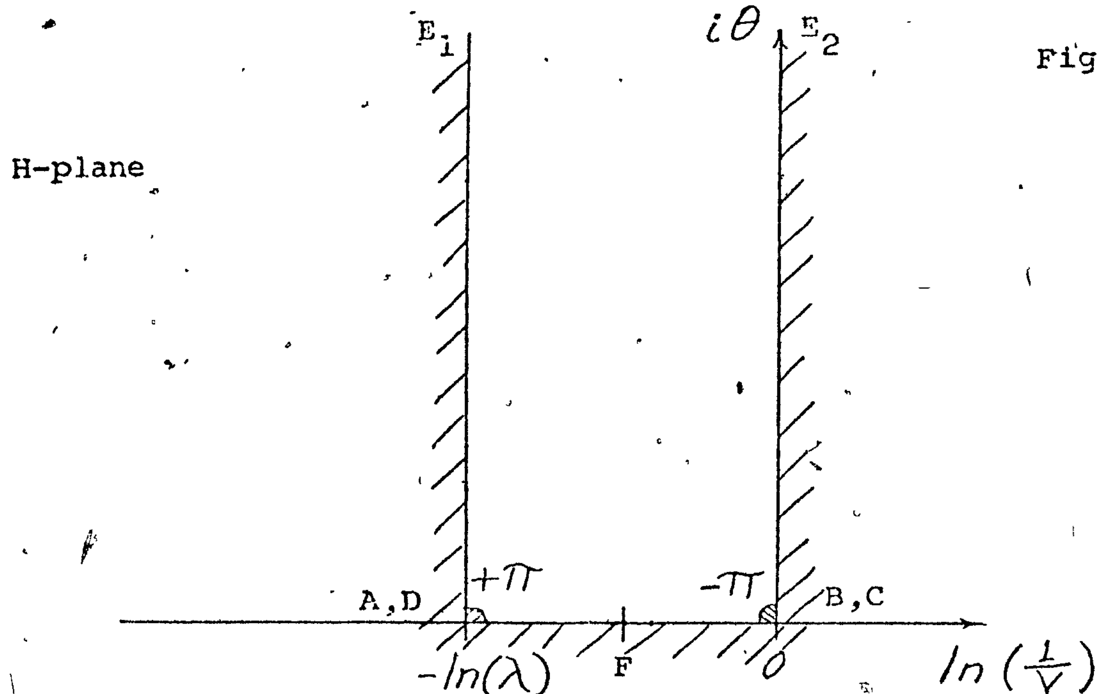

Fig. A3

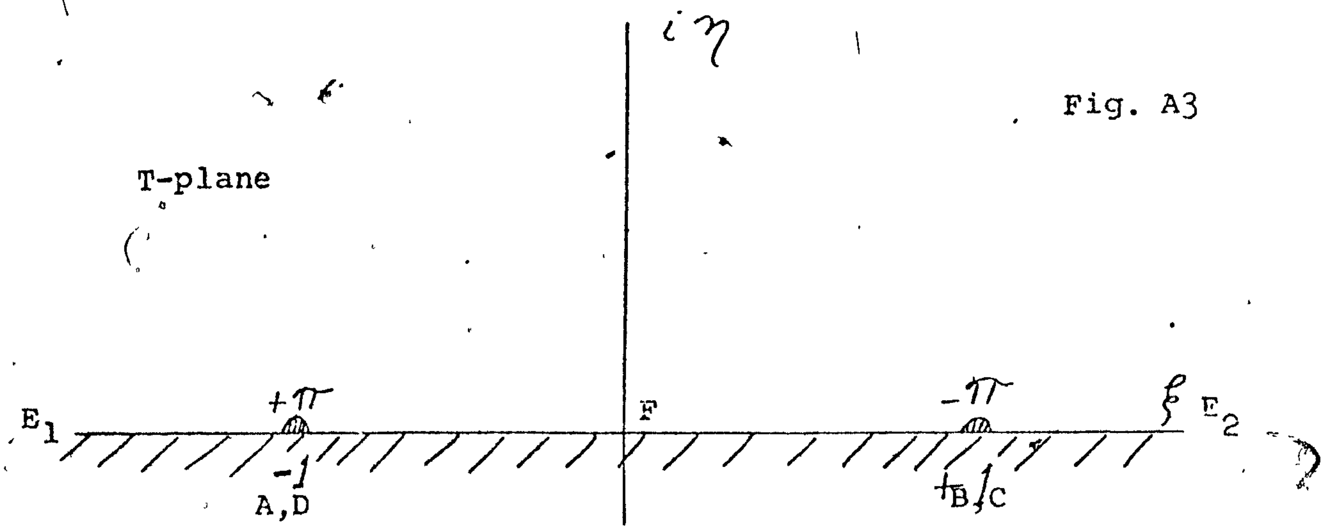

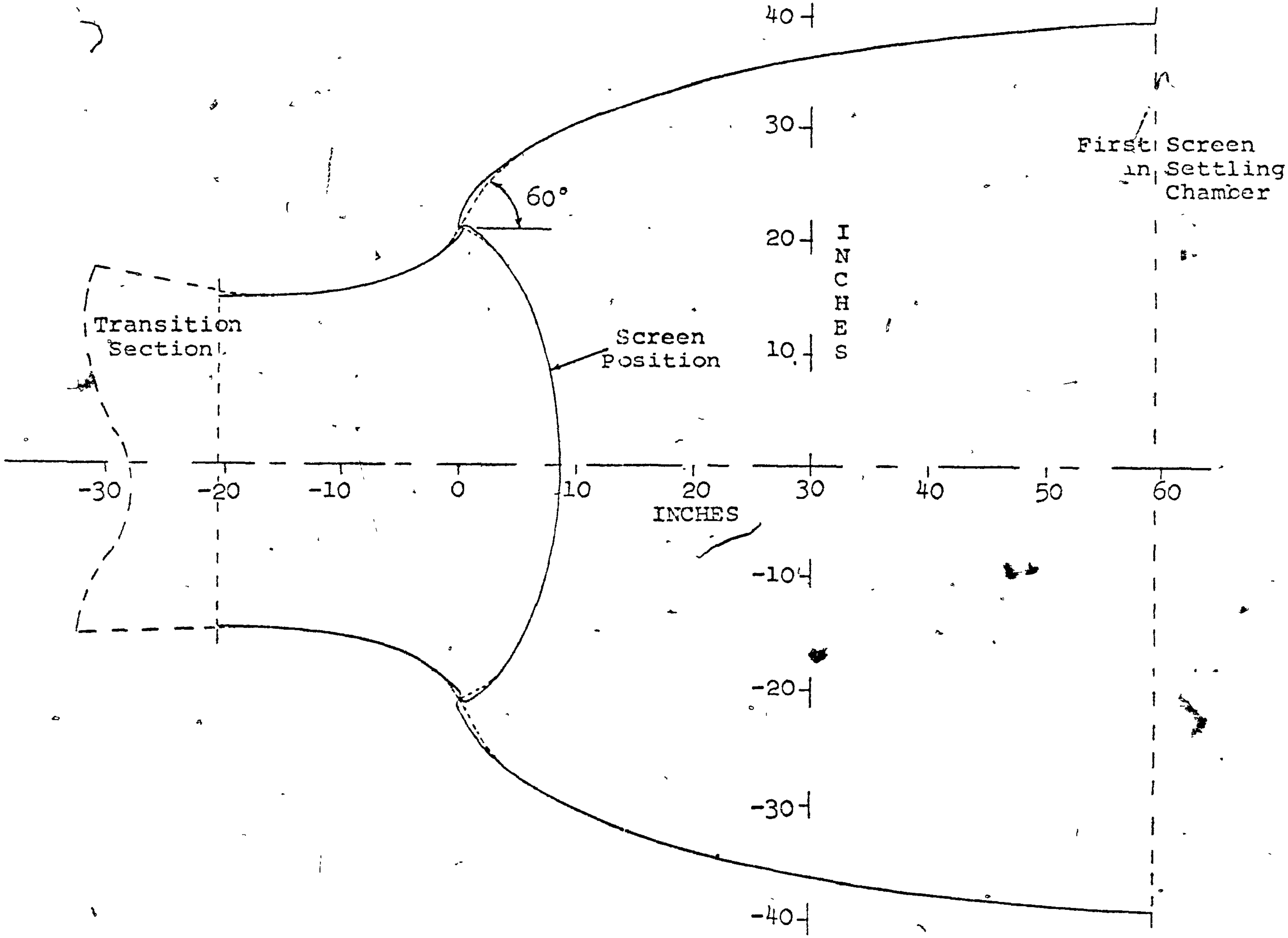

Profile of Two-Dimensional 'Diffuser'

Fig. A4

Appendix B

WARD-LEONARD CONTROL SYSTEM

INTRODUCTION

A Ward-Leonard control system was built to control the tunnel speed. A 40 H.P. 550 Volt 3 Ph. AC 1700 RPM electric motor drives a generator capable of delivering 240 Amps. of D.C. current at 125 Volts. This is connected to the 40 H.P. drive motor on the wind tunnel. The control unit mounted on the tunnel supplies 120 Volts, 2 Amps. D.C. to the fan motor field, and 0-120 Volts, 0-5 Amps. D.C. to the generator field windings to control the speed. Figure B1 is a block diagram of the complete circuit.

MOTOR-GENERATOR CIRCUIT

As can be seen from Figure B1 the motor-generator unit is used to power another wind tunnel drive. A 400 Amp. DPDT knife switch is used to transfer the high current D.C. between the two systems. Two DPST 120 Volt A.C. relays switch the field winding of the generator between the two control units of the tunnels, and these relays are in turn operated from micro-switches mounted under the high current knife switch. When this knife switch is completely closed it actuates one of the micro-switches.

In the high current D.C. line between the generator and the switch there is a hand reset overload relay set to trip at 260 Amps. When this relay trips it opens the stop line on the 40 H.P. A.C. motor control, and the motor-generator set stops. Figure B2 shows the circuitry for this section.

FAN MOTOR CIRCUIT

Figure B3 shows the fan-motor circuit. The 300 Amp. shunt for the motor-current meter is in the same box as the main disconnect switch. The motor field wiring also passes through this box.

The Klixon (Texas Instrument Co.) temperature sensors are four normally-open bi-metallic switches, one in each field winding, that will close if the motor overheats. They are connected in parallel.

MAIN CONTROL PANEL

The main control panel operates on 120 Volt A.C. which is obtained through a standard magnetic motor control switch. A green pilot light indicates when power is on. The A.C. current is fed to two autotransformers, and each transformer in turn feeds, a bridge rectifier to supply D.C. current to the fan-motor and generator fields. The autotransformer in the fan motor field circuit is a tapped transformer giving a range of output voltage of approximately 40 Volts. It is operated by a six position switch that is screwdriver adjusted from the front panel of the control box. In practice this switch is adjusted to give rated output voltage.

The autotransformer for the generator field current is continuously variable from 0-135 Volts by means of a front panel knob. It serves as the main speed control. An identical auto-transformer is also mounted in a separate portable box to serve as an extension speed control (Figure B4). It is connected to a four prong plug-in on the front panel of the main control box, and a switch on the main control box transfers control between the two autotransformers. There is also a green light on the portable box to indicate when it is switched into the circuit.

Four meters on the main panel monitor the electrical system. A 0-300 Amp. meter indicates the main motor current. In practice this is a most important meter, and it is monitored whenever the tunnel speed is increased to ensure that the rated amperage is not exceeded.

The other meters monitor the generator field current and voltage, and the main motor voltage.

A number of safety features are included in the circuit. In addition to fuses in the lines feeding each autotransformer, there are circuits that monitor both the motor field current and the motor temperature. A relay in series with the motor field current line is held in by the motor field current. If the field current falls significantly the relay opens and turns off the main control panel power. It does this by opening the stop line of the magnetic motor control switch. It should be noted that because of the inductance of the motor field windings, it takes approximately 2 seconds for the motor field current to build up sufficiently to activate this protective relay. Consequently, when switching on, the start button must be held down until this relay operates.

If the motor field windings should overheat at anytime one of the Klixon sensors will be activated, supplying 120 Volt A.C. to a second relay in the main control box, as well as to a red panel light. The contacts of this relay are also wired into the stop circuit of the magnetic motor control.

Figure B5 is the circuit for the main control box.

Although not connected to the electrical system, an aircraft airspeed indicator is mounted in the front panel of the control box, and indicates the approximate tunnel speed.

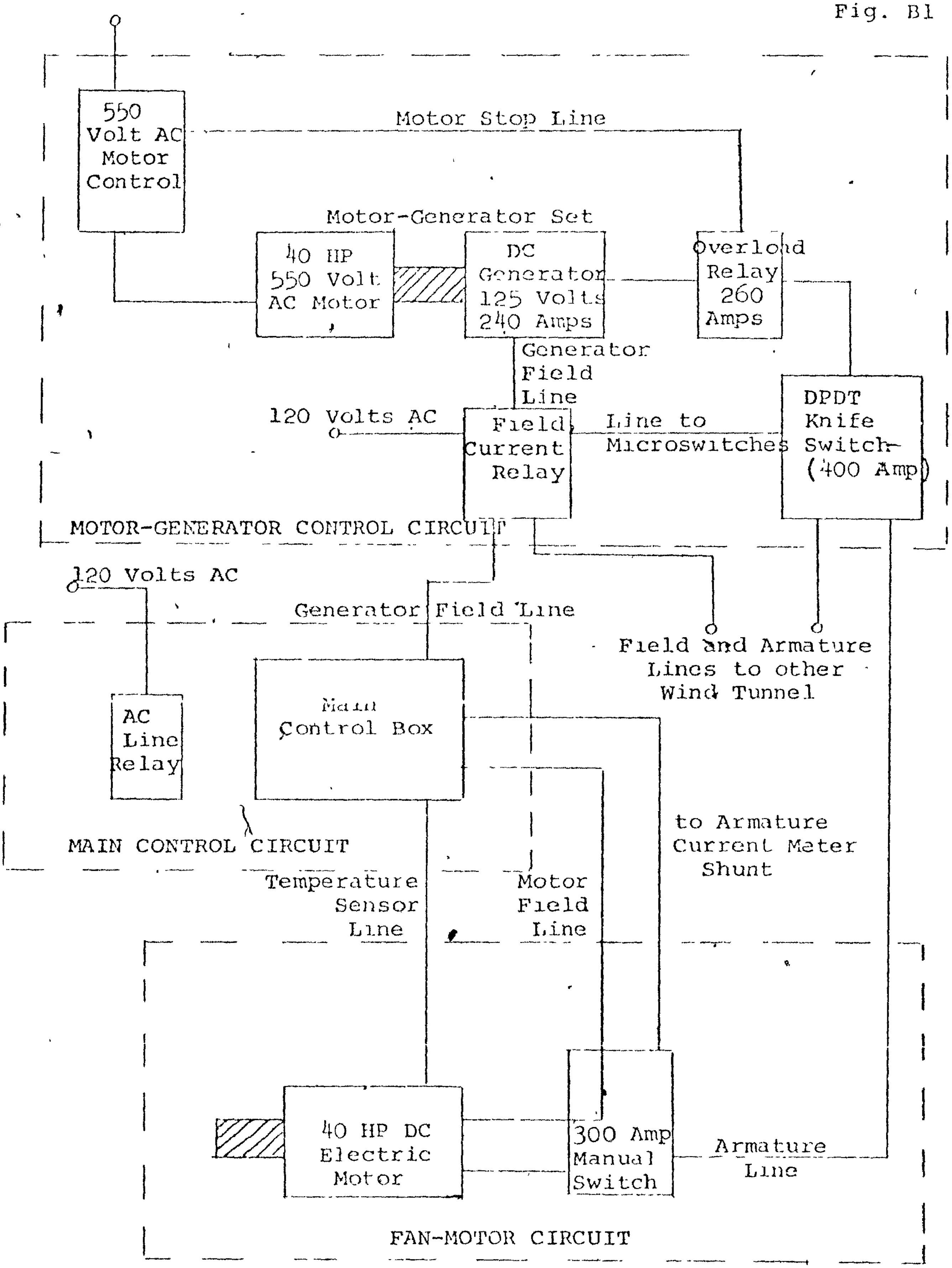

Block Diagram of Tunnel-Drive Circuit

Fig. B2

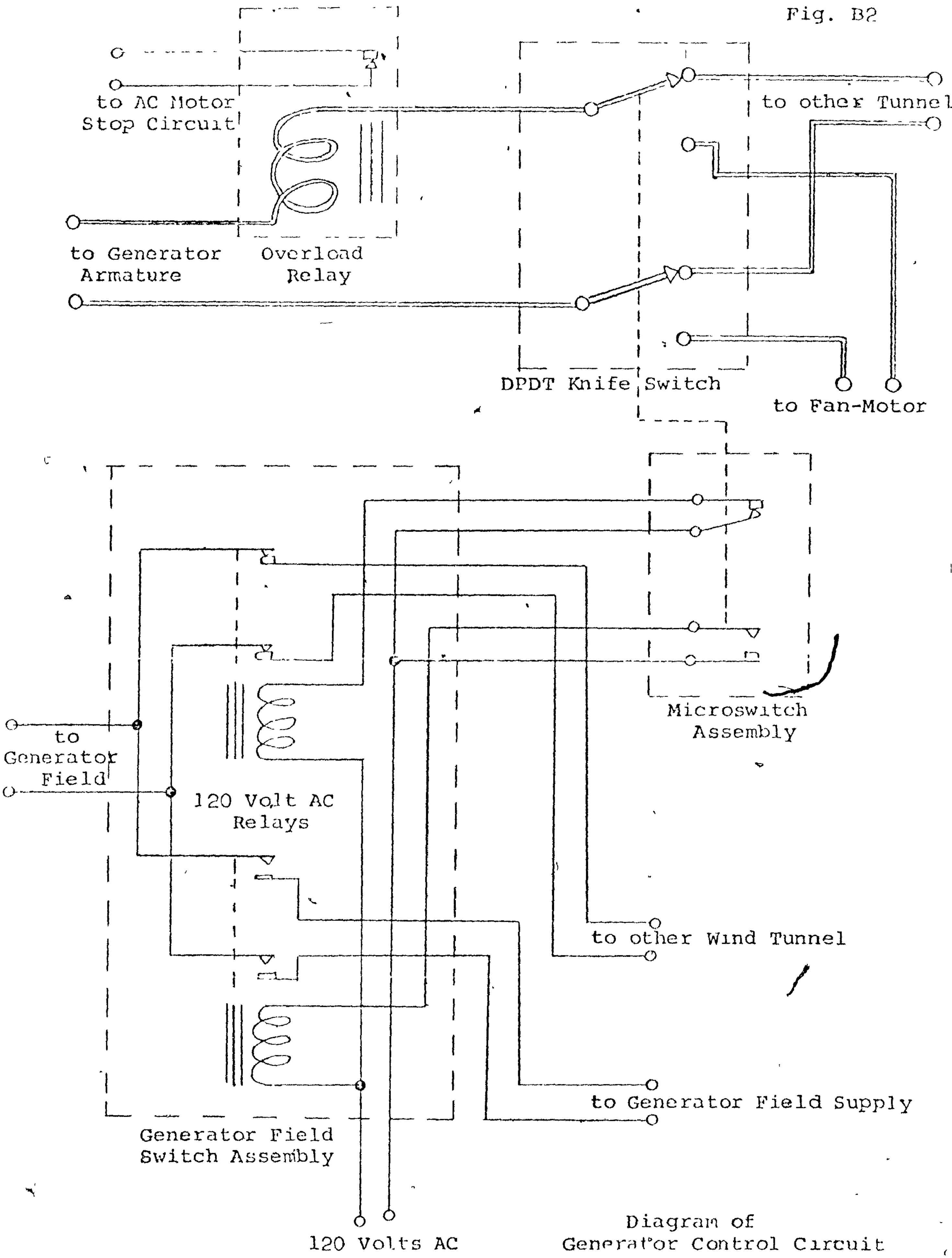

Diagram of
Generator Control Circuit

Fig. B3

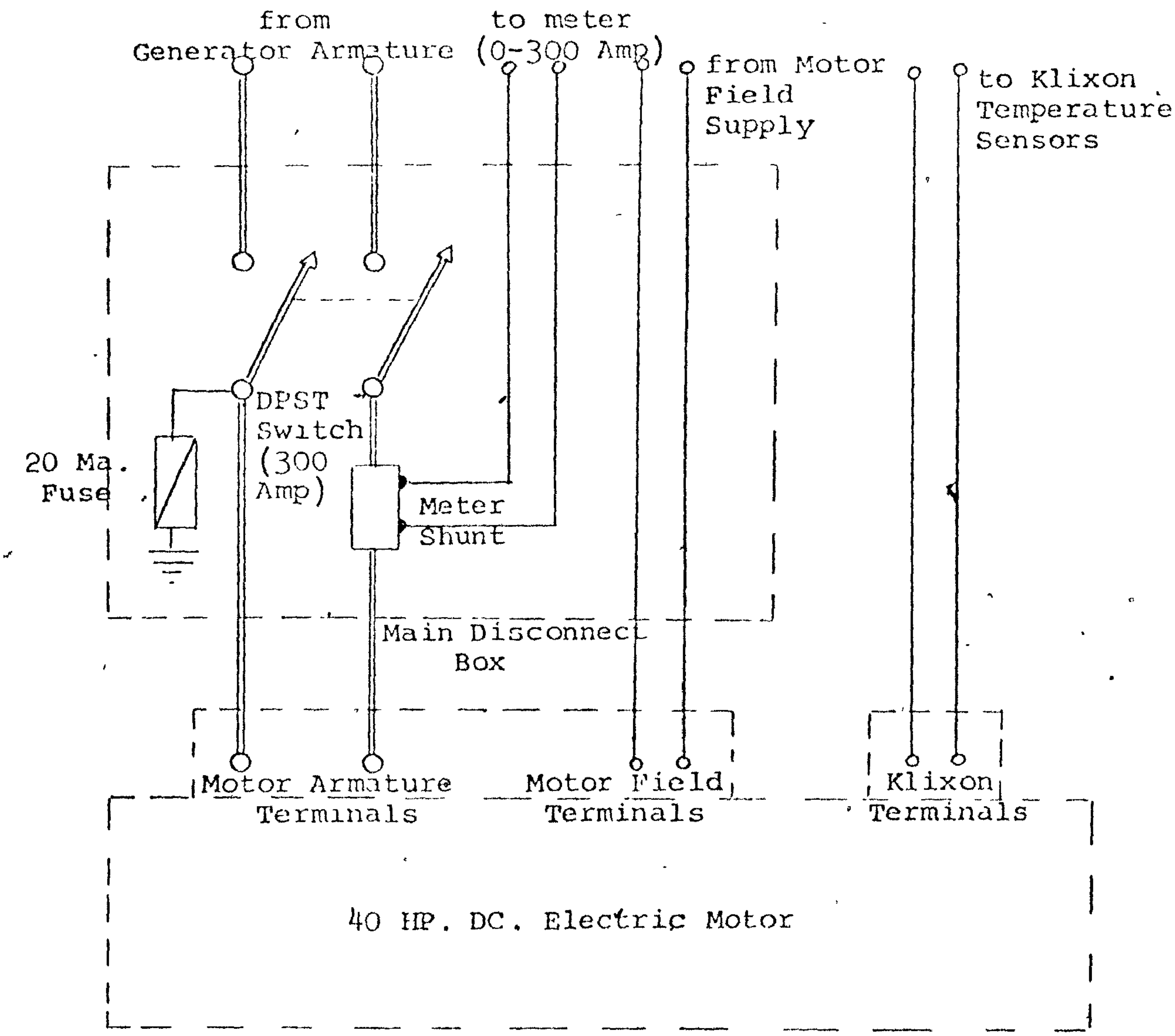

Diagram of Fan-Motor Circuit

Fig. B4

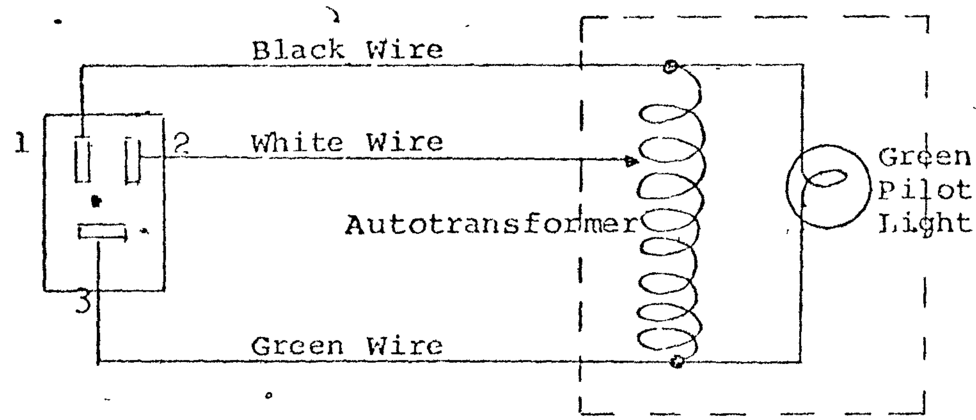

Diagram of External Speed Control

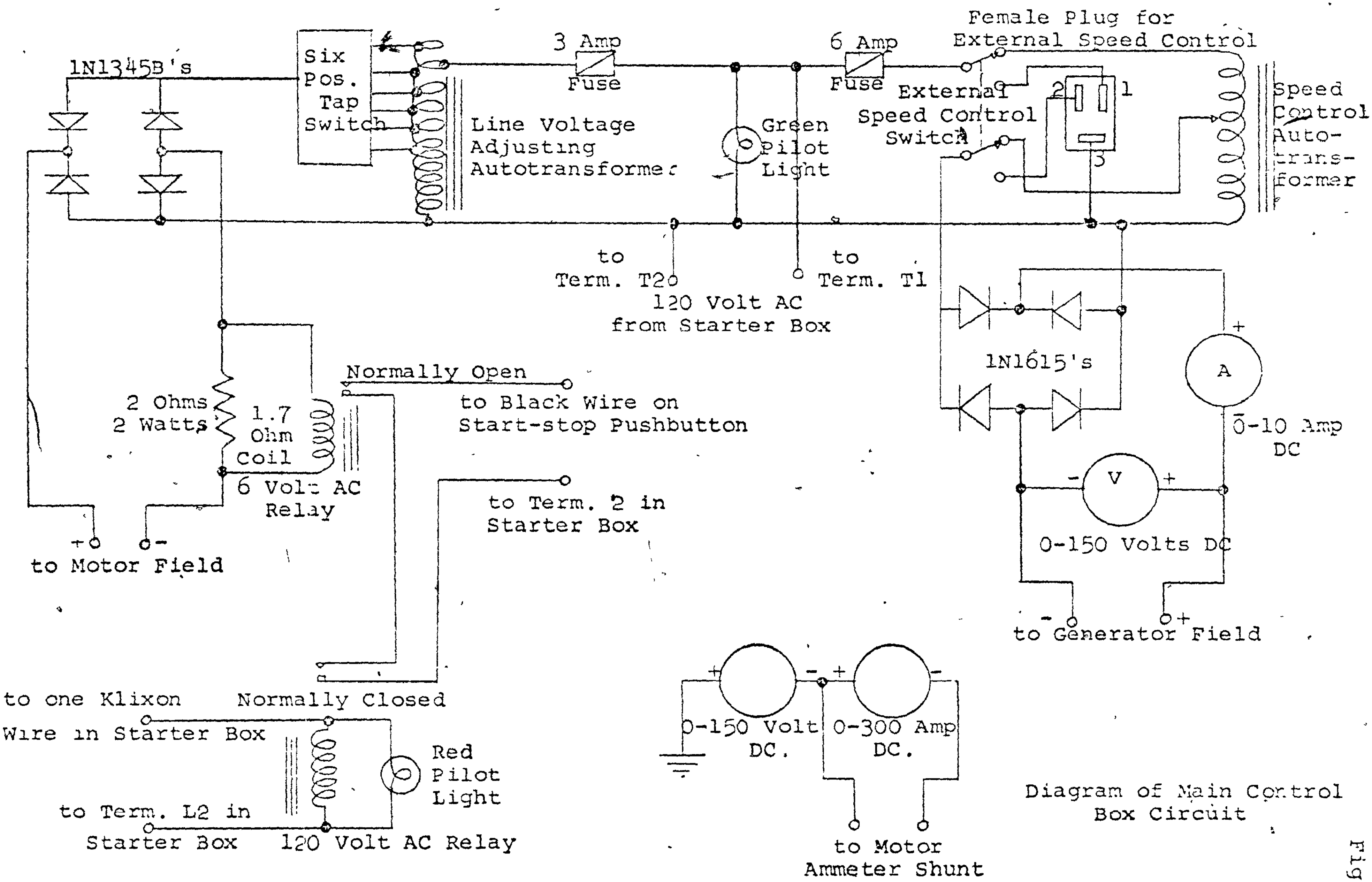

Diagram of Main Control Box Circuit

Fig. B5